

DELIVERY STRATEGIES FOR NUCLEIC ACIDS

by

Shayak Samaddar

A Dissertation

Submitted to the Faculty of Purdue University

In Partial Fulfillment of the Requirements for the degree of

Doctor of Philosophy



Department of Chemistry

West Lafayette, Indiana

August 2019

**THE PURDUE UNIVERSITY GRADUATE SCHOOL
STATEMENT OF COMMITTEE APPROVAL**

Dr. David H. Thompson, Chair

Department of Chemistry

Dr. Angeline Lyon

Department of Chemistry

Dr. Herman Sintim

Department of Chemistry

Dr. Yoon Yeo

Department of Industrial and Physical Pharmacy

Approved by:

Dr. Christine Hrycyna

Head of the Graduate Program

I would like to dedicate this thesis to my parents, Sri. Shankar Samaddar and Smt. Karabi Samaddar for their support, guidance, motivation and friendship through-out my life. Maa and Baba, it is impossible for me to put down in words how grateful I am to you. Thank you for always being there for me.

ACKNOWLEDGMENTS

It is my pleasure to express my deep sense of gratitude to my mentor, philosopher and guide, Prof. David H. Thompson. I am ineffably indebted to him for his conscientious guidance, support and encouragement to overcome research challenges. His timely advice and scientific approach have constantly motivated and inspired me, and has helped me grow as an independent researcher over past five year. Above all, I would like to thank him for guiding me through my curious scientific endeavors while making sure I stay on the accurate path which made my journey enjoyable and fruitful. I would also like to thank my thesis committee members: Prof. Herman Sintim, Prof. Angeline Lyon, and Prof. Yoon Yeo for their support, guidance and insightful comments.

This acknowledgement would not be complete without mentioning my gratefulness to my seniors Dr. Vivek Badwaik, Dr. Young Lee, Dr. Kyle Wright and Dr. Brad Loren for mentoring me during my early days in the Thompson research group. I would like to thank my wonderful colleagues Sam, Zinia, Craig, Reja, Zach, Shruti, Aayush, RJ and Kiera for making our laboratory a fun and enjoyable workplace. Additionally, I would like to thank my team of undergraduate researchers, especially Joshua Mazur and Devin Boehm, who have been instrumental in various of my research endeavors. It was a privilege learning, working and collaborating with all these great people.

I would also like to thank my family for their constant motivation, support, undying love and trust. My parent has always been my source of strength and endurance. Last but not the least, I would like to extend heartfelt gratitude to my very special friend Tamasree Majumder and extended Purdue family Arpita Pal, Ikjot Singh Sohal, Sayan Roy, Soumendu Majee and Mouli Modak who have been there of me and supported me when I need it the most. Thank You all.

TABLE OF CONTENTS

LIST OF TABLES	8
LIST OF FIGURES	9
ABSTRACT	15
CHAPTER 1. GENE THERAPY: AN INTRODUCTION	17
1.1 Introduction.....	17
1.2 Oligonucleotides targeting RNA.....	19
1.2.1 siRNA (Short interfering RNA).....	19
1.2.2 shRNA (Short Hairpin RNA)	21
1.2.3 microRNA (miRNA)	21
1.2.3.1 miRNA mimics.....	22
1.2.3.2 Antagomirs	22
1.2.3.3 miRNA sponges or ‘miRNA decoys’	23
1.2.4 Splice-switching ODNs (SSO).....	23
1.2.5 Gapmer	24
1.2.6 DNAzyme	25
1.3 Oligonucleotides targeting DNA	25
1.3.1 Triplex folding oligonucleotides (TFO)	25
1.4 Oligonucleotides targeting proteins	26
1.4.1 Oligonucleotides that stimulate the immune system	26
1.4.2 Aptamers.....	27
1.4.3 DNA decoys.....	28
1.5 Chemical modifications of nucleic acids to boost their <i>in vivo</i> efficacy	28
1.5.1 Carbohydrate modifications.....	29
1.5.2 Backbone modification.....	30
1.6 Summary.....	31
CHAPTER 2. DEVELOPMENT AND <i>IN VITRO</i> CHARACTERIZATION OF LIPID COATED POLYPLEX FOR DUAL DELIVERY OF GENE AND SMALL MOLECULES TO BLADDER TUMOR CELLS	32
2.1 Introduction.....	32

2.2	Materials and methods:	34
2.3	Results and discussion	39
2.3.1	Formulation and characterization of lipid coated polyplex	39
2.3.2	DNase protection assay.....	43
2.3.3	TEM Images	43
2.3.4	Quantifying plasmid and pyrene content.....	44
2.3.5	Quantifying cellular delivery of plasmid and pyrene:	45
2.4	Conclusion	48
CHAPTER 3. FAP TARGETED LIPID NANOPARTICLES FOR BLADDER CANCER IMMUNOTHERAPY		49
3.1	Introduction.....	49
3.2	Materials and methods	52
3.3	Results and discussion	55
3.3.1	Physicochemical characterization of LNPs	56
3.3.2	Cellular association studies.....	60
3.3.3	Enhanced immunostimulation by pH-sensitive targeted LNPs.....	61
3.3.4	Cellular localization studies.....	64
3.3.5	Human tumor association studies	65
3.4	Conclusion	66
CHAPTER 4. NON-VIRAL GENE DELIVERY VECTORS BASED ON CYCLODEXTRIN POLYMERS 67		
4.1	Introduction.....	67
4.2	CD-based polyrotaxanes.....	71
4.3	Polymers containing CDs in the backbone	89
4.4	Conclusions and perspectives	100
CHAPTER 5. EVALUATION OF POLYCARBONATE PENDANT POLYMER:β-CYCLODEXTRIN-BASED NUCLEIC ACID DELIVERY VECTORS.....		102
5.1	Introduction.....	102
5.2	Experimental methods	106
5.3	Results and discussion	107
5.3.1	Diblock Copolymer Synthesis and Characterization.....	107

5.3.2	Transfection Complex Formulation.....	107
5.3.3	Physico-chemical Charecterizations.....	107
5.3.4	In vitro Performance of Transfection Complex.....	109
5.4	Conclusions.....	110
CHAPTER 6. EVALUATION OF CHOLESTEROL EFFLUX POTENTIAL FOR HYDROXYPROPYL- β -CYCLODEXTRIN:POLY(DECAMETHYLENEPHOSPHATE) POLYROTAXANES IN NIEMANN-PICK C1 CELL.....		
		112
6.1	Introduction.....	112
6.2	Materials and methods	115
6.3	Results and discussion	116
6.3.1	Polymer Synthesis	116
6.3.2	Cholesterol efflux potential of developed polyrotaxanes	116
6.3.3	Confocal studies for cellular tracking of polyrotaxanes in NPC1 cells.....	119
6.3.4	FACS analysis Polyrotaxane cellular association with NPC1-deficient Cells	120
6.4	Conclusions.....	121
CHAPTER 7. STRUCTURE-FUNCTION RELATIONSHIPS OF CHOLESTEROL MOBILIZATION BY β -CD POLYROTAXANES IN NPC1-DEFICIENT HUMAN CELLS		
		122
7.1	Introduction.....	122
7.2	Materials and methods	124
7.3	Results and discussion	128
7.3.1	Effect of polyrotaxane structure on cellular cholesterol mobilization.....	129
7.3.2	Cellular localization of Decaarginine-endcapped PR by confocal microscopy	133
7.3.3	FACS analysis for cellular uptake of Fluorescently-labeled PR.	134
7.3.4	Cytotoxicity evaluation PR materials	135
7.4	Conclusions.....	137
REFERENCES		138
VITA.....		172
PUBLICATIONS		176

LIST OF TABLES

Table 1. Compositions Observed for TAEA-Pluronic Polyrotaxane Library Prepared by Hexane Solvent-Assistance. R ₁₀ = Decaarginine endcaps. Chol = Cholesteryl endcaps.....	128
Table 2. Compositions Observed for Cholesterol-endcapped TAEA-L81 Pluronic Polyrotaxane Library Prepared by Mechanochemical Synthesis.....	129

LIST OF FIGURES

Figure 1. Schematic representation of strategies involved in developing nucleic acid anti-cancer agents. (SSO = Splice switching oligonucleotides; TFO = Triple helix forming oligonucleotides; siRNA = small interfering ribonucleic acids; shRNA = short hairpin ribonucleic acids; miRNA = micro ribonucleic acids; TLRs = Toll-like receptors; RISC = RNA induced silencing complex) 18

Figure 2: Conceptual diagram of a single Lipid Coated Polyplex (LCP) in cross-section..... 34

Figure 3A Schematic representation of LCP formulation steps. Step 1: Cationic CD_{2.5kD}-PEI and plasmid are mixed at the desired N/P ratio within a microfluidic reactor. Step 2: Polyplex and a lipid mixture dissolved in 80% ethanol solution are mixed in the same microfluidic reactor. Step 3: The LCP are dialysed to remove ethanol and free pyrene from the formulation. A total flow rate of 10 mL/min and flow rate ratio of 1:1 was used for mixing..... 36

Figure 4 Effect of N/P ratio on polyplex properties. **A.** Hydrodynamic diameter (number mean); **B.** Polydispersity; **C.** Zeta Potential; **D.** Gel-shift assay for polyplex prepared by mixing 60 µg/mL plasmid with CD_{2.5kD}-PEI in 20mM HEPES buffer at different N/P ratios. The total flow rate was 10 ml/min and flow rate ratio was 1:1. Results are the mean ± SD (n=3)..... 40

Figure 5. Effect of total flow rate on polyplex properties. **A.** Hydrodynamic diameter (number mean); **B.** Polydispersity; and **C.** Zeta Potential. Polyplex were prepared by mixing 60 µg/mL plasmid with CD_{2.5kD}-PEI in 20mM HEPES buffer at a N/P ratio of 10. The flow rate ratio was kept constant at 1:1. Results are the mean ± SD (n=3)..... 42

Figure 6. Effect of lipid mixture concentration on LCP properties **A.** Hydrodynamic diameter (number mean); **B.** Polydispersity; and **C.** Zeta Potential. LCP were prepared by mixing 1 mL of polyplex solution with 1 mL of ethanolic lipid mixture (DOPE:CHEMS:DSPC:DSPE-mPEG_{2k} = 34:54:10:2) solution of varying concentration. The total flow rate was 10 mL/min and flow rate ratio was 1:1. Results are the mean ± SD (n=3). 42

Figure 7. Ability of LCP to protect loaded plasmid from DNAase degradation. LCPs were treated for 4 h with 2U DNase-I at 37 °C before quenching the enzymatic reaction with 2.5mM EDTA and heating at 65 °C for 10 mins. The entrapped pDNA was released using sequential treatment with 1% Triton X-100 and 0.15 mg/mL Heparin. The released pDNA was concentrated using vacuum centrifugation before agarose gel (1%) electrophoresis to analyze for plasmid integrity. 43

Figure 8. Negative stain TEM images of **A.** Polyplex and **B.** LCP. Polyplex were made using N/P ratio of 10; LCP were coated with 4 mM lipid solution (CHEMS:DOPE:DSPC:DSPE-mPEG_{2k} = 34:54:10:2)..... 44

Figure 9. Encapsulation and loading efficiency of (**A,B**) plasmid and (**C,D**) Pyrene. Plasmid content was measured via PicoGreenTM assay after decomplexing the LCP using 1% Triton-X100 to disrupt the lipid layer and 0.15 mg/mL heparin to release the plasmid from the polyplex. Pyrene content was measured by dissolving the LCP in 70% ACN solution to release pyrene, followed by HPLC separation and pyrene detection using absorbance at 338 ± 4 nm. Results are reported as mean ± S.D. (n=3)..... 45

Figure 10. **A.** EGFP-NLS plasmid transfection efficiency of the non-targeted, scrambled and targeted LCP. **B.** Histogram plot for GFP fluorescence distribution in MB49 cell population at 24 h. Cells were treated with LCP formulations for 4 h at 37 °C, followed by PBS washing to remove unbound complexes. The cells were further incubated for 4 h, 12 h or 24 h and then trypsinized, and resuspended in PBS for flow cytometry analysis. Error bars indicate the standard deviation of the mean (n=3). 47

Figure 11. **A.** Pyrene delivery of the non-targeted, scrambled and targeted LCP **B.** Histogram plot for pyrene fluorescence distribution in MB49 cell population at 4 h. MB49 cells were treated with LCPs for 4 h at 37 °C, followed by PBS washing to remove non-specific interactions. After further 4 hrs or 24 hrs incubation, cells were trypsinized, and resuspended in PBS for quantification of pyrene fluorescence using flow cytometer. Error bars indicate the standard deviation of the mean (n=3). 47

Figure 12. Cytotoxicity analysis of LCP formulations. MB49 cells were treated with different LCP formulations for 4 h followed by washing to remove uninternalized particles. The particles were incubated another 24 h before adding the MTS reagent. After incubating for 1 h, the absorbance of soluble formazan formed due to bio-reduction of MTS by live MB49 cells population was measure at 490 nm. All treatments for each formulation was performed in triplicates and error bars represents standard deviation of mean (n=3). 48

Figure 13. 35nm FAP targeted LNPs attaches to Fibronectin (FBN) on cell surfaces causing in dimerization of $\alpha 5$ and $\beta 1$ subunits of surface integrin followed by endocytosis via caveolar pathway. After endosomal acidification, the pH sensitive nature of the LNPs enables it to release CpG payload in close proximity to TLR9 receptors resulting in release of proinflammatory cytokines and an efficient immunostimulation. 51

Figure 14. Lipid nanoparticles characteristics. (a) hydrodynamic diameter (number mean), (b) Polydispersity (c) Zeta Potential (d) % Encapsulation for LNPs manufactured by Chemtrix 3221 reactor at a CpG concentration of 50 $\mu\text{g}/\text{ml}$ and lipid composition of DOTAP, DOPE, CHEMS, and DSPE-mPEG_{2K} (ratio 45:30:23:2). Aqueous to organic flow rate ratio was 3:1 whereas the total flow rate was 2 ml/min. Results are the mean \pm SD (n=3). 57

Figure 15. Physicochemical characterization of developed formulations at N/P of 5 (a) Size (b) PdI (c) Zeta Potential. Results are the mean \pm SD (n=3). 57

Figure 16. Proposed mechanism of LNP formation: The mixing of methanol phase with aqueous phase the cationic lipids are the first to interact with anionic CpG molecules forming inverted micelles. These micelles act as nuclei around which nanoprecipitation of lipids occur to form bilayer structures. These bilayer vesicles continue to fuse together forming larger vesicle with lamellar structures (A). At high N/P enhanced presence of cationic lipids on outer surface prevents membrane fusion by electrostatic repulsion and membrane rigidity due to faster recruitment of anionic CHEMS (B). 58

Figure 17. Cryo-TEM image of LNPs at (a) N/P 1 (b) N/P 5 (c) N/P 10 displaying a transition from electron dense system to vesicular system at high N/P ratios. Inset represents the Fast Fourier Transform (FFT) of respective images. LNPs were concentrated to 10-15mg/ml by ultracentrifugation using 100K MWCO centrifuge filter at 7,500 rpm for 2 hrs 59

Figure 18. Small Angle X-Ray scattering data for CpG LNPs at different N/P ratio showing characteristic q value peak at 1\AA^{-1} suggesting a scattering pattern associated with bilayer systems. LNPs were concentrated to 10-15mg/ml by ultra-centrifugation using 100K MWCO centrifuge filter at 7,500 rpm for 2 hrs. 59

Figure 19. Flow cytometric evaluation of Cy5.5 labelled targeted and non-targeted LNPs for cellular association with (a) MB49 cells and (b) RAW264.7 cells. Cells were treated with LNPs for 2 h at 37 °C, followed by PBS washing to remove non-specific interactions, trypsinization, and resuspension in PBS for flow cytometry analysis. Error bars indicate the standard deviation of the mean (n=3, t-test, ****p<0.0001, ***p<0.001) 61

Figure 20. ELISA data for TNF α release by RAW264.7 cells to compare immunostimulatory potential of FAP-targeted pH sensitive LNPs vs Non-targeted or pH non-sensitive formulation. Cells were treated with LNPs at CpG dose of 1 μ g/ml for 2 hrs at 37°C followed by PBS wash. Cells were further incubated for 12hrs in FBS supplemented media after which supernatant was collected for ELISA. Error bars indicate standard deviation of the mean (n=3, one-way ANOVA, ****p<0.0001)..... 63

Figure 21. Cytotoxicity analysis of LNPs on (A) RAW264.7 cells (B) MB49 cells. Cells were treated with LNP formulations at a CpG dose of 1 μ g/ml for 2 hrs at 37°C followed by PBS wash. Cells were further incubated for 12hrs in FBS supplemented media. Cytotoxicity was measure by MTS assay. Error bars indicate standard deviation of the mean (n=3, one-way ANOVA, p=ns) 63

Figure 22. LNP tracking analysis by confocal microscopy in RAW 264.7 cells showing enhanced cellular entry of FITC tagged CpG for targeted formulations(b,c) as compared to non-targeted LNPs(a) after 4 hrs. After 12 hrs, reduced FITC-CpG signal for pH sensitive formulation (e) vs pH non-sensitive LNPs (f) shows endosomal release capability of pH sensitive LNPs. Z-stack images showing endosomal localization of FITC-CpG for targeted formulations after 4 hrs (g,h). 65

Figure 23. Tumor samples from a cystectomy section were incubated with Cy5.5 labelled LNPs at a CpG concentration of 10 μ g/ml for 2 hrs at 37°C. Fluorescent images were taken with IVIS Lumina II optical imaging system (excitation: 640/25 nm; emission: 732.5/37.5 nm). 66

Figure 24 Viral and non-viral vectors 68

Figure 25. Types of cyclodextrin with cavity diameter 70

Figure 26. Diagrammatic representation of polyrotaxane with arrows showing degrees of freedom 71

Figure 27 Diagrammatic representation of cellular pathways involved in gene delivery via polyrotaxanes. 73

Figure 28. PRs with multiple oligoethylenimine(OEI)-grafted (a) α -CDs threaded on a PEO chain. K=15; x=1/5/9; y=5.2/4.9/2.3 (b) α -CDs threaded on a poly(EO-r-PO) random copolymer chain. K=12; x=1/5/9/14; y=4.4/4.8/2.6/3.1 (c) β -CDs threaded on a PEO-b-PPO-b-PEO triblock chain. K=13; x=1/5/9; y=6.7/5.3/3.4 (d) α -CDs threaded on a PPO-b-PEO-b-PPO triblock backbone K=8; x=1/5/9/14; y=5.3/5.0/2.3/3.5 75

Figure 29. (Reprint) PR based supramolecular hydrogels. Amphiphilic ECD forms micelles under aqueous environment with PCL core and mPEG/PDMAEMA corona. PDMAEMA at the corona is responsible for pDNA binding while MPEG serves both as stabilizing moiety for the resultant ECD/pDNA polyplex and hydrogel anchoring segment. Sustained release of pDNA polyplexes is achieved via hydrogel dissolution over time	77
Figure 30. (a) Anthryl grafted β -CD pseudopolyrotaxane. $m=4.5,5$ for $n=0,1$ respectively (b) 2-dimensional pseudopolyrotaxane. $a+b+c=24$	78
Figure 31. Fluorene capped DNA intercalating PR. $m=n/a$; ($n \sim 23$ or 230).....	78
Figure 32. Spermine grafted PR where $m=5.5$	79
Figure 33. Spermine modified α CD where $n = 2,3$ or 6	79
Figure 34. Diagrammatic representation of cyclodextrin delivery using pH sensitive polyrotaxane.	80
Figure 35. Disulfide linked PRs (DMAE-ss-PR).....	81
Figure 36. Gene delivery by tetra-lamellar multifunctional envelope-type nano-device (T-MEND)	82
Figure 37. pH sensitive PR with PEI backbone.....	82
Figure 38. α -CD:PEG cationic PRs grafted with DMAE groups	83
Figure 39. PRs with DMAE modified α -CD grafted onto multi-arm PEG	84
Figure 40. Folate targeted PRs.....	85
Figure 41. Polyaspartic acid endcapped PR.....	86
Figure 42. PAMAM G1 modified α CD PR	87
Figure 43. PR with hexacationic α -CD grafted on an ionene backbone	88
Figure 44. Formation of nucleic acid-containing particles with CDs embedded in cationic polymer backbone (A) Cyclodextrin oligomer chemical structure. (B) Schematic of particle assembly...	89
Figure 45. Thompson group pendent polymer system for plasmid delivery	93
Figure 46.(a) Hyaluronic acid -adamantane pendent polymer (b) β -CD PEI _{2.5k}	95
Figure 47. CDs developed for gene delivery by Fernandez and Mettel	97
Figure 48. Plasmid delivery strategy based on α CD conjugated to dendrimers	99

- Figure 49. Conceptual Diagram for Polycarbonate Pendant Polymer-Based Non-Viral Gene Delivery. (A) Polyplex formation (i) is accomplished via precomplexation of β -CD-PEI and pDNA. (ii) Polycarbonate diblock copolymers are used to coat the core β -CD-PEI:pDNA complex via host:guest interactions between the pendant groups and the surface-exposed β -CD cavities. (iii) Nanoparticles are targeted to cellular surfaces via electrostatic adsorption of the slightly positively charged particles prior to endocytosis (iv). Disassembly of the transfection complexes (v) is promoted by pendant group and polycarbonate block hydrolysis, thus leading to endolysosomal escape of the pDNA cargo. (B) Diblock copolymer structures derived from (i) homopolymerization of cyclic carbonate monomers, or (ii) copolymerization of cyclic carbonate monomers with trimethylene carbonate. The (iii) organocatalysts, (iv) pendant groups, and (v) β -cyclodextrin-poly(ethyleneimine) conjugate (β -CD-PEI) are also shown 105
- Figure 50. Gel Shift Analysis of Transfection Complexes at Various N/P Ratios. 108
- Figure 51. Size Analysis of Transfection Complexes at Various N/P Ratios by DLS 108
- Figure 52. Zeta (ζ) Potential Analysis of Transfection Complexes at Various N/P Ratios. 109
- Figure 53. Transfection performance of mPEG-b-PC coated polyplexes. (A) % GFP Positive HeLa Cells Treated with Transfection Complexes Containing AcGFP pDNA. (B) % Mean Fluorescence of HeLa Cells Treated with Transfection Complexes Containing AcGFP pDNA. 110
- Figure 54. Filipin staining of primary fibroblasts after treatment with α -CD, poly-(decamethylenephosphate) **1**, HP- β -CD and **6** for 24 h (25 μ M equivalent HP- β -CD dose, Filipin was used at 50 μ g/mL). 117
- Figure 55. Filipin staining of primary fibroblasts after treatment with α -CD, poly-(decamethylenephosphate) **1**, HP- β -CD and **6** for 24 h (25 μ M equivalent HP- β -CD dose. Nuclei were stained with Nuclear Red. Cells were imaged with a 5 x objective. 118
- Figure 56. Cytotoxicity of **6** evaluated via MTS assay after 24 h exposure to NPC1-deficient cells. 118
- Figure 57. Dose-response curve in NPC1 cells after a single 24 h treatment with **6** and HP- β -CD. 118
- Figure 58. Structures of FITC-tagged polyrotaxane **6a** and the fluorescent CD-derivative **7**.... 119
- Figure 59. NPC1-deficient cells treated with 25 μ M CD-equivalent FITC tagged polyrotaxane **6a** in Opti-MEM media. (A) untreated cells, (B) 4 h **6a** treatment (c) 24 h **6a** treatment, and (D) C + 24 h post-treatment. i : all fluorescence channel; ii : DAPI channel; iii : fluorescein channel, and iv : LysoTracker channel. Localization within acidic endosomes/lysosome (red, stained with LysoTracker) peaked at 24 h after addition of **6a**, after which the cells were washed to remove **6a** and incubated for another 24 h in complete MEM media. Confocal images acquired 24 h post treatment show a decrease in the FITC signal indicating either cyclodextrin escape from the acidic compartments or fluorescein degradation within them. The scale bar = 100 μ m. 120
- Figure 60. a) Histogram Plot for FITC intensity distribution among NPC1-deficient cell population. b) Cellular association of Polyrotaxane **6a** with NPC 1-deficient cells. 121

Figure 61. Cholesterol accumulation in NPC1-deficient cells as determined by filipin III staining after exposure to polyrotaxanes for 24 h at 25 μ M equivalent β -CD monomer concentration. **A.** Controls and polyrotaxanes **PR1 – PR8** prepared by the solvent-assisted method. **B.** Controls and polyrotaxanes **PR9 – PR20** prepared by solid state mechanochemical synthesis. Data are expressed relative to DMSO-treated controls and are an average \pm S.D. of two separate experiments with >25 cells imaged per condition in each experiment. 131

Figure 62. Cholesterol normalization as a function of polyrotaxane threading efficiency in NPC1 deficient cells. **A.** Cellular cholesterol content as a function of polyrotaxanes with Chol/PR > 1 . **B.** Cellular cholesterol content as a function of polyrotaxanes with Chol/PR < 1 . Cellular cholesterol levels are shown relative to untreated cells (100%)..... 133

Figure 63. Time course of FITC-conjugated PRs (**PR1*** and **PR2***) localization in NPC1-deficient fibroblasts. Cells were incubated with the compounds for the indicated times (h) and then washed and stained with lysotracker for an additional 45 min. The cells were fixed with paraformaldehyde, followed by staining of nuclei by DAPI. Cells were imaged by confocal microscopy as described in Methods. 134

Figure 64. Histogram plot for FITC fluorescence distribution following PR1* uptake within NPC1 deficient fibroblast cells. **B.** Cellular internalization of PR1* in the absence (2,8 and 24 h) and presence (24 h) of 30 μ g/mL of heparin. Cells were treated for 24 h at 25 μ M equivalent β -CD monomer concentration and analyzed by flow cytometry as described in the methods..... 135

Figure 65. Cytotoxicity analysis of compounds prepared by solid phase synthesis vs solvent-assisted synthesis. NPC1-deficient cells (1500 cells/well) were plated in a 96 well plate for 36 h before treatment with varying concentrations of PRs. Cells were incubated for a further 24 h before measuring toxicity of the compounds by MTS assay according to manufacturer's protocol..... 136

ABSTRACT

Author: Samaddar, Shayak. PhD
Institution: Purdue University
Degree Received: August 2019
Title: Delivery Strategies for Nucleic Acids
Committee Chair: David Thompson

Utilization of nucleic acids to manipulate genetic information within a cell is known as gene therapy. It has provided researchers with unprecedented opportunities in treatment and mitigation of several life-threatening diseases. Gene therapy is an attractive alternative to conventional chemotherapy or radiation therapy due to its high efficiency, minimal side effects, and potential to evade drug resistance. The versatility of gene therapy makes it useful for the treatment of diseases dangerous disease like cancer. However, delivery of nucleic acid payloads to the intended target has been the bottleneck in clinical translation of such therapies. Here, we have developed and evaluated three different delivery systems (lipid based, polymer based and lipid-polymer hybrid) which can complex nucleic acid payloads, able to target specific cell types and get disassembled on cellular internalization to release the therapeutic payload. Our lipid and lipid-polymer hybrid delivery systems utilize a novel bacterial peptide sequence which enables these vectors to “stick” to fibronectin present in tumor extracellular matrix making them attractive for intravesical administration in bladder cancer management. Additionally, these systems have pH responsive modalities which aids in vector disassemble under acidic endosomal pH conditions for efficient release of therapeutic cargos after internalization into target cells.

In our efforts to develop an ideal delivery system with a tunable the assembly/disassembly properties, we synthesized a library of pendent polymer with biodegradable polycarbonate backbone. The ability of the pendent groups to form host-guest interaction with hydrophobic core of cationic cyclodextrins determined the stability of the delivery system. We demonstrate the capability of such polymer systems to form nano-dimensional complexes with nucleic acid and transfect cancer cells. The above-mentioned property of cyclodextrins to form host-guest interaction with hydrophobic molecules also forms the basis of its utilization in the treatment of a rare metabolic disorder called Niemann Pick type C disease where there the cells loses the ability

to remove stored cholesterol from endo-lysosomal compartments. Cyclodextrin forms host-guest complexes with aberrantly stored cholesterol and helps normalization of cellular cholesterol level. However, the soluble nature and small size of the cyclodextrin causes very rapid clearance for the body necessitating dosage levels as high as 9000mg/kg for therapeutic benefit. We have also developed a library of polyrotaxanes, where multiple cyclodextrins are threaded onto linear polymer chains and end-capped with bulky groups to prevent slippage. This kind of assembly drastically increases the systemic circulation time by preventing rapid renal clearance. We evaluated the ability of these constructs to serve as a long circulation delivery system for delivery of β -cyclodextrins for potential treatment of Niemann Pick type C disease. Finally, we have studied the structure-function relationships of these supramolecular assemblies to aid in rational design of therapeutic polyrotaxanes.

CHAPTER 1. GENE THERAPY: AN INTRODUCTION

Adapted (Reprinted) from the book chapter titled “Nucleic acid is cancer therapeutics” authored by S.Samaddar and D.H.Thompson. Currently the chapter is under preparation for Biomaterials for cancer therapeutics (Elsevier group).

1.1 Introduction

Proteins are an essential part of any living organism and are associated with almost every function of the cell¹. All the proteins produced within the cells are coded by DNA². Human DNA contains about 19,000 to 20,000 protein coding genes³. The production of functional proteins from genetically encoded DNA sequences is referred to as central dogma of biology⁴⁻⁵. The first step in this process is called Transcription, wherein RNA polymerase and transcription factors bind to the promoter sequence on the DNA strand to initiate transcription of a downstream gene. The hydrogen bonding between base pairs in the DNA double helical structure is disrupted to form a transcription bubble. The RNA polymerase then recruits RNA nucleotides in a complimentary fashion to the DNA strand being transcribed to form a pre-mRNA strand. This pre-mRNA is then processed by addition of a polyadenosine tail⁶⁻⁷ and 5'-end capping⁸⁻⁹. These two structural features are essential for maturation of pre-mRNA to mature mRNA to enable transport outside the nucleus for protein synthesis in the ribosome. Additionally, another very important event called splicing occurs at this step. Splicing involves alterations where non-coding regions (introns) of the pre-mRNA are discarded or sometimes retained along with the coding regions (exons) to give mature-mRNA¹⁰. By altering the length of the retained exons and/or skipping intron sequences in the final mRNA sequence, the same pre-mRNA can be a precursor to a wide diversity of proteins produced by different cells under a variety of cellular conditions. This is a major mechanism underlying how ~20,000 protein coding sequences in the human genome can produce over 2 million different proteins.

Once the mRNA is exported outside the nucleus, the ribosomal machinery comprising of the 30s ribosomal subunit, tRNA carrying the amino acid methionine, and the 50s ribosomal subunit are recruited to the start codon of the mRNA. The methionine is then transferred to the tRNA of the neighboring codon before leaving the ribosomal machinery. The ribosome then shifts to the

following codon allowing the next codon to be occupied by the complimentary tRNA and amino acid for chain extension. This process continues sequentially until a stop codon is reached, wherein the polypeptide chain is released to fold into its active structure.

High-throughput phenotypic screening, gene silencing by RNA interference, time-lapse microscopy, and computational image processing efforts have shown that about 600 genes in the human genome are involved in cell division¹¹. Mutations in any of these genes can alter the expression profiles of a given protein. If this occurs for proteins involved in cell cycle control or apoptosis, uncontrolled cell division and proliferation – the hallmarks of cancer – can ensue. Thus, once the protein responsible for various aberrant cellular behaviors is identified, manipulation of the pathway at any of the above steps of the central dogma can theoretically be employed to alter the production of that protein from a therapeutic perspective. For the purposes of this chapter, we will categorize the nucleic acid therapies based on the cellular targets responsible for aberrant gene expression: (A) oligonucleotides targeting RNA; (B) oligonucleotides targeting DNA; and (C) oligonucleotides targeting protein.

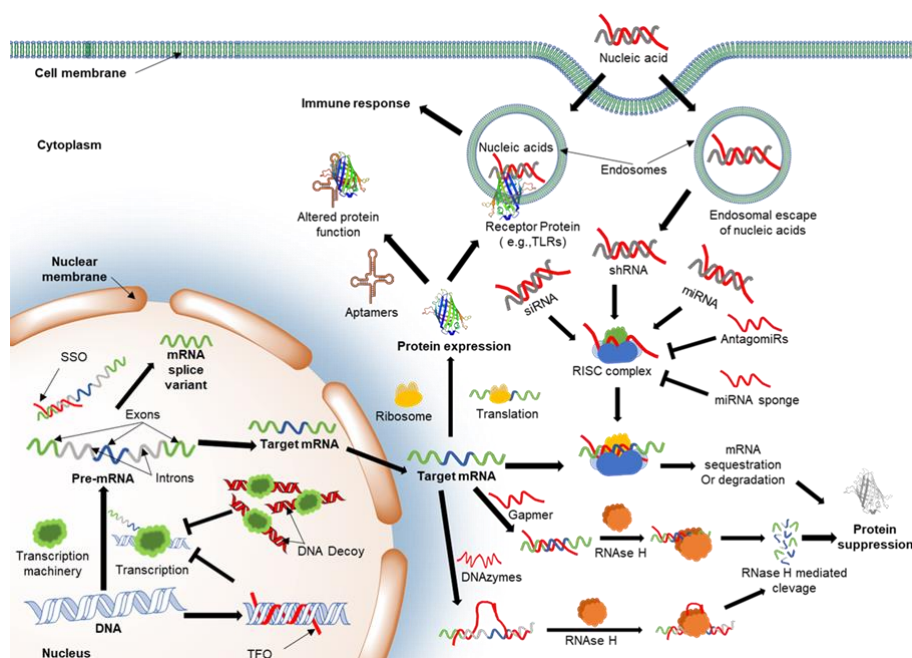


Figure 1. Schematic representation of strategies involved in developing nucleic acid anti-cancer agents. (SSO = Splice switching oligonucleotides; TFO = Triple helix forming oligonucleotides; siRNA = small interfering ribonucleic acids; shRNA = short hairpin ribonucleic acids; miRNA = micro ribonucleic acids; TLRs = Toll-like receptors; RISC = RNA induced silencing complex)

1.2 Oligonucleotides targeting RNA

1.2.1 siRNA (Short interfering RNA)

The first instance of gene silencing using a 742 base-pair long double stranded RNA to knock down an abundant myofilament protein was demonstrated by Fire and Mello in *C. elegans*¹². In 2006, they were awarded the Nobel Prize in Physiology or Medicine for their discovery¹³. Long double stranded RNA (dsRNA) are identified by endogenous RNase III endonuclease or Dicer in the cytoplasm of the cell. Dicer causes enzymatic cleavage of the dsRNA to form smaller 20 – 24 nucleotide long fragments with 3' two-nucleotide overhangs, known as short interfering RNA. siRNA becomes associated with the protein called Argonaut 2 prior to recruitment of other proteins involved in the silencing mechanism to form the RNA Induced Silencing Complex (RISC). Argonaut 2 unwinds the siRNA, leading to cleavage of one of the strands and leaving behind a single stand of guide RNA (anti-sense strand) bound to the RISC complex. This complex can identify specific mRNA target based on sequence complementarity and catalytic cleavage of the targeted mRNA mediated by Argonaut 2. Thus, if the sequence of the protein responsible for aberrant cellular behavior is identified (e.g. an overexpressed oncogene), appropriately designed siRNA can silence the gene via cleavage of the corresponding mRNA strands, thus making it a promising therapeutic strategy. Interestingly, it was observed that doubled stranded RNA (sense and anti-sense pair) cause much more potent gene silencing effects than the antisense strand alone. Unlike *C. elegans*, however, introduction of longer double stranded RNA (>30 bp) into the cytoplasm of mammalian cells can mimic a viral infection, thereby inducing an immune response characterized by activation of the protein kinase R (PKR) pathway and upregulation of pro-inflammatory cytokine genes like interferons that promote cell death by apoptosis¹⁴. Elbashir et al. demonstrated that introduction of synthetic short 21 nt long siRNA sequences, thus eliminating the need of DICER processing, avoided the immune response and showed potent gene silencing in mammalian cells¹⁵. The ability of RNA interference to cure multiple undruggable diseases attracted private investment and developmental siRNA therapeutic programs at many major pharmaceutical companies. Candidate siRNA molecules with little *in vivo* stabilization and/or targeting strategies were rushed to the clinic. These candidates required very high dosages and caused significant off-target effects, leading to failure of multiple late stage clinical trials of siRNA therapeutics and a disappointing start for RNAi technology field¹⁶.

The recent FDA approval of Alnylam's Onpatro (patisiran) in 2018 for treating hereditary transthyretin-mediated amyloidosis in liver, however, has rejuvenated interest in the field¹⁷. This was enabled by the development of novel and potent lipid-based delivery vehicles capable of delivering unmodified/minimally modified versions of nucleic acids to their target site without significant toxicity issues. A Phase I/II study of 43 patients with advanced hepatocellular carcinoma to evaluate safety and preliminary anti-tumor activity of TKM-080301, a lipid-based delivery of PLK1 siRNA, was conducted by Arbutus Biopharma¹⁸. Poor survival of hepatocellular carcinoma patients has been linked to enhanced expression of polo-like kinase 1 (PLK1) protein, therefore, silencing of PLK1 has attractive therapeutic potential. Although their results showed that the therapy was well tolerated (MTD of 0.6 mg/kg), a 46.2% stable disease rate (independent RECIST 1.1 criteria) and 23.1% of partial response (Choi's criteria) indicated that it had a limited antitumor effect as a single agent therapy¹⁹. A dual target knockdown strategy is currently undergoing clinical evaluation by Alnylam for advanced metastatic hepatocellular carcinoma²⁰⁻²¹. The candidate therapy, ALN-VSP, is a lipid nanoparticle containing siRNA for simultaneous knockdown of VEGF (Vascular Endothelial Growth Factor) and KSP (Kinesin spindle protein) involved in neo-angiogenesis and cell division, respectively. This Phase I study demonstrated the safety, RNAi mediated target mRNA cleavage products within tumor cells, and antitumor effectiveness of biweekly intravenous administration of the drug candidate²⁰. Atu-027, a lipoplex formulation of 23-mer chemically stabilized (alternating 2'-O-methyl) oligonucleotides which inhibits the expression of PKN3 protein, is another anti-cancer siRNA under Phase I clinical investigation by Silence Therapeutics²². PKN3 is a downstream effector of the phosphoinositide-3-kinase (PI3K) signaling pathway involved in endothelial cell migration control during tumor angiogenesis and metastasis²³⁻²⁴. This study in patients with advanced solid tumors showed that the therapy was efficacious and well tolerated up to a dose of 0.120 mg/kg, without cytokine activation²⁵. In a Phase Ib/IIa study with advanced pancreatic cancer patients, Atu-027 was tested at a dose of 0.253 mg/kg in combination with gemcitabine²⁶. Reports showed that the combination was safe and well tolerated. Disease control was observed in 58% of the patients receiving the therapy twice weekly and 36% of the patients who received a dose once per week²⁷. Unfortunately, both dosage regimens were associated with a very high percentage (92 and 82%, respectively) of Grade 3 adverse reactions²⁷.

1.2.2 shRNA (Short Hairpin RNA)

Although siRNA delivery can be an effective way to inhibit the expression of a target protein, the silencing effect is transient (days), especially in rapidly dividing cells (hours)²⁸⁻³¹. Although this can be advantageous in cases where short-term suppression of a gene is needed (e.g., viral infections), it could become a severe limitation when long term suppression of an oncogene is desired for cancer therapy. This challenge was overcome by Paddison *et al.* in 2002 who demonstrated that RNAi can be achieved by delivering a plasmid DNA which codes for the shRNA and integrates into the host cell genome to achieve heritable gene silencing³². These plasmids are transcribed into shRNA endogenously with help of a RNA polymerase III promoter in the nucleus. shRNA are about 70 nucleotides long, with a 19 – 29 base pair stem bearing 3' two-nucleotide overhangs and a short loop of 4 to 10 nucleotides. shRNA are exported from the nucleus via Exportin 5 to the cytoplasm. Alternatively, synthetically produced shRNA can also be delivered to the cytosol directly. In the cytoplasm, shRNA is recognized by DICER and the loop removed to form smaller 20 – 24 nucleotide long siRNA strands that perform RNAi as described above. Thus, shRNA results in sustained RNAi which cannot be achieved by synthetic siRNA. One of most advanced therapies in this class was developed by Gradalis Inc.³³. Their cationic liposome formulation encapsulates a plasmid coding for a bifunctional shRNA that silences stathmin 1 (STMN1) protein³³. STMN1 is a cytosolic protein with major pro-mitotic responsibility that is upregulated in tumors and aids in cancer cell survival and proliferation³³⁻³⁵. Their Phase I study in superficial advanced refractory cancer patients demonstrated the safety of intratumoral injections of the formulation over a 0.7 – 2 mg plasmid dose range³⁶. Additionally, they produced evidence of shRNA mediated silencing based on the detection of predicted targeted-sequence cleavage products using next generation sequencing (NGS) and RT-PCR techniques³³.

1.2.3 microRNA (miRNA)

miRNA was first identified in 1993 by Lee *et al.* who reported that two Lin4 non-coding gene products, one 22 and the other 61 nucleotides long, in *C. elegans*, had sequence complementarity to the 3'-untranslated region (UTR) of lin-14 mRNA. They suggested a post-transcriptional regulatory effect of the Lin4 transcripts on Lin14 protein expression via an antisense RNA interaction type mechanism³⁷. Since then, miRNA has established itself as an evolutionary conserved master regulator of multiple genes. miRNA precursors (pri-miRNA) are transcribed in

the nucleus by RNA polymerase II and further processed into ~70 nucleotide long pre-miRNA by DROSHA and its cofactor DGCR8. Pre-miRNA has a looped structure like shRNA and is also exported from the nucleus via the same Exportin 5 protein. These are then processed further by DICER in the cytoplasm to remove the loop domain and produce 20-22 nucleotide long mature miRNA that can then be loaded into the RISC complex. The miRNA within the RISC complex then guides the mRNA of the target gene to be regulated, typically via imperfect complementary to target mRNA's 3'-UTR region. Once bound, the target mRNA is either cleaved into two pieces, marked for early degradation by deadenylation of the polyA tail, or sterically prevented from translation into protein. Additionally, because of imperfect base pairing, this allows the same miRNA sequence to target multiple mRNA and the same mRNA to be targeted by multiple miRNA for silencing, unlike siRNA or shRNA where the targeting is very specific. This promiscuity adds another level of challenge for clinical translation of miRNA therapeutics since the chance for unintended off-target effects are high. Transcriptional downregulation of oncogenes recognizing miRNA or upregulation of tumor suppressors recognizing miRNA have been suggested in the pathogenesis of multiple cancers.

1.2.3.1 miRNA mimics

From a therapeutic perspective, cytosolic delivery of synthetic mimics of miRNA can be utilized to downregulate multiple cancer-causing genes at the same time. For example, miRNA-34a has been shown to downregulate expression of over 30 oncogenes as well as genes involved in immune evasion³⁸. Expression levels of miRNA34a are severely compromised in multiple solid tumors³⁹. A liposome incorporated synthetic mimic of miRNA-34a developed by Mirna Therapeutics, MRX34, was the first miRNA-based therapy to enter the clinic for patients with advanced stages of cancer including hepatocellular carcinoma⁴⁰. Although MRX34 showed evidence of antitumor activity in a subset of patients with refractory advanced solid tumors, the study had to be halted due to serious immune-related adverse events⁴¹.

1.2.3.2 Antagomirs

An alternative strategy would be to downregulate miRNAs responsible for suppressing genes that prevent tumor growth. Antagomirs are RNA strands having perfect complementarity to a miRNA sequence. It binds to guide miRNA strand within the RISC complex and prevents it from

downregulating other genes. Since it highly improbable that the exact same RNA sequence will be involved in different gene modulations, chances for off-target effect of antagomirs are limited. Antagomirs are often chemically engineered to improve its nuclease stability *in vivo*. For example, miR-100 promotes tumor metastasis and invasion capacity via a mTOR pathway mechanism⁴². Intratumorally injection of miR-100 antagomirs demonstrated significant reduction in tumor progression and lung metastasis in an orthoptic 4T1 mouse breast cancer model. Additionally, antitumor effects were enhanced when antagomir was used as a combination therapy with cisplatin⁴². Similarly, co-delivery of antagorR-21 and antagomir-10 in a systemic injection of RGD-targeted PLGA nanoparticle increased temozolomide chemosensitivity in a mouse xenograft tumor model of human glioblastoma multiforme cells⁴³.

1.2.3.3 miRNA sponges or ‘miRNA decoys’

These are long RNA sequences having multiple sites that can competitively bind to the seed regions of guide miRNA targets and thus block an entire miRNA seed family. This was first developed in 2007, as endogenously produced RNA from a vector plasmid utilizing RNA polymerase II promoter. It can be used for both transient expression or incorporated in chromosomal DNA for stable transfection⁴⁴. These transcripts have a bulge at the sites that are generally cleaved by the Argonaut proteins of RISC. This enables stable interaction of the construct with the target guide miRNA loaded within RISC without actually being cleaved. Recently, nuclease resistant miRNA sponge was developed by a group of researchers at John Hopkins, which could inhibit cancer cell proliferation and suppress activity of miR-21 in multiple gastric cancer cell lines *in vitro*⁴⁵. They demonstrated that miRNA sponges could be effectively used to suppress targeted miRNA functions *in vitro* and showed potential for treating diseases *in vivo*.

1.2.4 Splice-switching ODNs (SSO)

As mentioned earlier, splicing is a major mechanism for maintaining protein diversity. Over 90% of the proteins produced in cells undergo splicing⁴⁶⁻⁴⁷. Thus, splicing regulation provides an attractive therapeutic choice for aberrantly behaving proteins, especially those that arise from mutations causing an abnormal protein due to altered splicing events. Over 15,000 alternative splicing events have been associated with various forms of cancer and its pathogenesis⁴⁸. Splice-

switching ODNs are typically 15-30 nucleotides long. They can be directed towards splicing sites based on their sequence complementarity to mRNA regions involved in splicing and the introns that modulate the position of spliceosome recruitment. These ODNs can then correct an altered splicing event of a tumor suppressor protein or induce altered splicing to prevent formation of an aberrant protein. Already two SSO, nusinersen (Ionis Pharmaceuticals) and eteplirsen (Sarepta Therapeutics) received FDA approval in 2016 for treatment of muscular diseases showing the promise of this class of therapy in safely treating human disorders⁴⁹⁻⁵⁰. Multiple research efforts have already focused on regulating altered alternative splicing events using SSO in an attempt to enhance expression of tumor suppressor proteins or downregulate oncogenes. For example, alternative splicing of kinase MNK2 pre-mRNA could lead to production of Mnk2a or Mnk2b mRNA⁵¹. Mnk2a induces apoptosis through the p38-MAP kinase pathway and acts as tumor suppressor, whereas Mnk2b fails to activate the p38-MAP kinase pathway and acts as a protooncogene⁵¹. Mogilevsky *et al.* developed SSO to mask the 3' splice site of exon 14b of MNK2 pre-mRNA which resulted in upregulation of Mnk2a as the major spliced variant⁵². Treated cells showed inhibition of oncogenic properties in glioblastoma, hepatocellular carcinoma, and breast cancer cells and re-sensitized the glioblastoma cells to chemotherapeutic effects of doxorubicin, cisplatin, and temozolomide⁵². Additionally, the ability of the SSO to inhibit tumorigenesis was demonstrated in an orthotopic mouse xenograft model of human glioblastoma⁵².

1.2.5 Gapmer

These are chimeric oligonucleotides having a central region (known as the GAP) comprised of 6 – 10 nucleotide long deoxynucleotide sequences that are designed to induce RNase H cleavage, while the flanking regions are chemically modified to prevent nuclease degradation. The central region binds to the target mRNA or lncRNA by Watson-Crick complementarity and induces RNase H mediated cleavage to cause gene silencing. Amodio *et al.* provided the first pre-clinical demonstration of the effectiveness of a novel gapmers oligonucleotide in silencing an oncogenic lncRNA called metastasis-associated lung adenocarcinoma transcript 1 (MALAT1)⁵³. MALAT1 is responsible for abnormal proliferation of plasma cells within bone marrow, leading to the fatal B cell malignancy, multiple melanoma⁵⁴. The 16mer Gapmer was capable of inhibiting cell proliferation and inducing apoptosis in multiple melanoma and primary plasma cell lines from patients⁵³. The potent anti-tumor effectiveness was also translatable to a murine xenograft

model of human multiple melanoma⁵³. Custirsen and Apatorsen from OncoGenix, represent the most advanced therapeutic candidates in this class that have reached the clinic. Custirsen induces silencing of testosterone-repressed prostate message-2 (TRPM-2), an anti-apoptotic gene associated with chemoresistance⁵⁵. Currently, it is being evaluated as a combination therapy with docetaxel in a Phase III study in advanced metastatic (stage IV) non-small cell lung cancer⁵⁶. Apatorsen inhibits expression of Heat shock protein 27 (HSP27) gene⁵⁷. HSP27 is a chaperon protein that promotes cell survival under stress conditions⁵⁸. Silencing of HSP27 with Apatorsen has been shown to induce apoptosis and sensitize cancer cells towards chemotherapy⁵⁷. In a randomized Phase II study of Apatorsen in combination with docetaxel in advanced metastatic bladder cancer, patients showed significant survival benefits over docetaxel alone⁵⁹.

1.2.6 DNAzyme

DNAzymes are single stranded DNA molecules that bind to target mRNA by Watson-Crick base pairing and cause catalytic cleavage of target mRNA. A typical DNAzyme contains an active site for catalytic cleavage surrounded by two binding arms responsible for mRNA recognition. Joyce *et al.* pioneered the development of catalytic DNA strands using *in vitro* selection techniques⁶⁰. The first in class anticancer therapy using the DNAzyme called Dz13 was evaluated in a Phase I trial with nodular basal cell carcinoma patients⁶¹. Dz13 catalytically cleaves JUN mRNA, preventing its translation to c-JUN that contributes to cell growth and survival and is over expressed in cancer cells⁶²⁻⁶³. Intratumoral administration of the agent using a lipid based delivery system at all the administered doses produced no drug related adverse effects⁶¹. It was recently demonstrated that the intratumorally administered Dz13 lipid formulation reduced the sizes of satellite untreated tumors along with the primary treated tumors in a murine melanoma model, suggesting involvement of adaptive immunity⁶⁴.

1.3 Oligonucleotides targeting DNA

1.3.1 Triplex folding oligonucleotides (TFO)

TFO are strands of nucleic acids that bind to a DNA duplex along the major groove to form a triple helix, following the rules of Hoogsteen or reverse Hoogsteen base pairing⁶⁵. The bases of the TFO form hydrogen bonds with the matching base pair to create a complex, allowing for a high degree of selectivity with respect to its position along the DNA duplex. This class of oligonucleotides has

not yet entered clinical trials, however, several *in vitro* and *in vivo* studies suggest that they may have significant anti-cancer therapy potential. For example, Catapano et al. developed a TFO directed towards the P2 promoter region of the c-MYC gene to inhibit its transcription⁶⁶. Enhanced expression of the c-MYC gene product is associated with multiple human cancers. Protein binding studies showed that the TFO inhibited binding of nuclear transcription factors to the promoter sequence at a concentration of 1 μ M. TFO have also been used in combination with gemcitabine⁶⁷. In this case, the TFO activates the machinery that recognizes the triple helix as DNA damage and in the process of excision repair creates strand breaks⁶⁸. This initiates an unscheduled DNA repair synthesis (UDS) at the site of the human c-MYC gene and enhances the incorporation cytotoxic gemcitabine into the oncogene, resulting in tumor suppression. The tumor reduction efficacy of the TFO and gemcitabine combination therapy was also demonstrated in a mouse xenograft model of COLO 320DM human colon carcinoma. A 3'-propylamine modification was utilized to enhance the TFO stability for *in vivo* applications.

1.4 Oligonucleotides targeting proteins

1.4.1 Oligonucleotides that stimulate the immune system

Although an important strategy for designing oligonucleotides for DNA or RNA targets is to escape detection by the immune system, another paradigm for cancer therapy is based on the ability of nucleic acids to illicit an immune response by binding to protein receptors. This approach seeks to not only to kill cancer cells directly in the initial immune reaction, but also to develop an anti-cancer memory to prevent future tumorigenic outgrowths. The human immune system has developed a host of receptors called pattern recognition receptors (PRR) that can recognize exogenous nucleic acid sequences as pathogen associated molecular patterns (PAMPs)⁶⁹. These foreign nucleic acid patterns can trigger an immune response by activating a signaling cascade resulting in secretion of Type I and pro-inflammatory cytokines. This, in turn, results in enhanced tumor infiltration of activated immune cells (e.g., dendritic, macrophages, cytotoxic T lymphocytes, natural killer cells, and other immune cells) that contribute to tumor rejection. CpG motifs have served as the initial approach to this modality. Unmethylated CpG motifs are abundant in the microbial genome and are recognized as PAMPs by the endosomal PRR called Toll Like Receptor 9 (TLR9). Although multiple clinical studies failed to produce significant survival benefit

as monotherapy, the use of CpG in combination with other therapies are now undergoing clinical evaluation. One such example is a Phase I trial designed to evaluate the safety and efficacy of intratumorally injected SD101, (Dynavax Technologies) a CpG oligonucleotide candidate administered to patients with advanced metastatic solid tumors in combination with an anti-OX40 antibody that enhances T cell activation⁷⁰. Preliminary results from a Phase I/IIb evaluating the same SD101 candidate in combination with pembrolizumab (PD1 blocker) demonstrated that the therapy resulted in increased Type I IFN levels and CD8⁺ T-cell tumor infiltration⁷¹. The treatment showed an overall response rate (ORR) of 78% in patients without previous exposure to anti-PD1. The 12-month progression free survival rate was 88% in this study and the overall survival was 89%, whereas the ORR in patients with prior PD-1 therapy was only 15%⁷².

1.4.2 Aptamers

Aptamers are 15-100 nucleotide DNA or RNA sequences that can adopt complex tertiary or quadruplex structures due to hybridization of complementary sequences⁷³. Aptamers can be evolved to bind with high avidity and specificity to targets ranging from inorganic molecules, synthetic polymers, and large protein complexes. Their small size, manufacturability, high specificity, and low immunogenicity make them an attractive alternative to antibodies for targeted therapeutic applications. The first-in-class aptamer drug, pegaptanib (Macugen) from Eyetech Pharmaceuticals, was approved in 2004 for age related macular degeneration⁷⁴. Pegaptanib is an antagonist for VEGF that contributes to the aberrant neovascularization implicated in this ocular disease. Although the same strategy was targeted for inhibition of angiogenesis at tumor regions which allows metabolically active cancer cells to survive, this approach could not be substantiated in pre-clinical models⁷⁵. Since the route of administration for tumor treatment required I.V. administration, the short half-life of the aptamers in blood may account for the poor therapeutic outcome. Subsequent efforts have focused on stabilization strategies that improve the half-life of aptamers as in the case of AS1411, a nucleolin binding aptamer designed with G-rich quadruplex motifs to provide enhanced nuclease resistance and polyethylene glycol modification to provide extended blood circulation⁷⁶. Nucleolin is a multifunctional protein involved in remodeling of nucleolar chromatin, maturation of pre-RNA, rDNA transcription, and ribosome assembly that is overexpressed in multiple cancers⁷⁷. In a Phase II study in patients with relapsed acute myeloid leukemia, administration of AS1411 in combination with high dose of cytarabine demonstrated

good tolerability and better efficacy (overall response rate of 15%) at 10 or 40 mg/kg/day than cytarabine alone⁷⁸. Another Phase II study evaluating the effect of AS1411 as monotherapy in metastatic refractory renal carcinoma patients demonstrated a limited overall response rate of only 2.9%⁷⁶, however, the responding population had a dramatic response with over 84% reduction in tumor size and remained progression free even after 24 months without any requirement of additional therapy⁷⁶. Importantly, the responding patients had missense mutations in the mTOR and FGFR2 genes providing mechanistic insights into the mechanism of action and selection criteria of patients for future therapy.

1.4.3 DNA decoys

DNA decoys are short double stranded DNA oligonucleotides that mimic conserved genomic regulatory elements of the gene of interest and compete for the transcription protein machinery to downregulate its expression. Sen et al. performed the first-in-human trial of a STAT3 (a key mediator of oncogenic signaling) decoy oligonucleotide in head and neck cancer patients⁷⁹. The candidate oligonucleotide was a 15 base pair DNA with sequence homology to the conserved hSIE genomic element of the c-fos gene promoter⁷⁹. The sequence was modified with phosphorothioate modifications at the 5' and 3' nucleotides for nuclease resistance⁷⁹. In a phase 0 study involving 6 patients, intra-tumoral injection of STAT3 decoys demonstrated a significant pharmacodynamic signature of biologic activity such as decreased expression of STAT3 target genes, including cyclin D1 and Bcl-X_L as compared to pre-treated tumor biopsies⁷⁹.

1.5 Chemical modifications of nucleic acids to boost their *in vivo* efficacy

The major challenge of oligonucleotide-based therapies is their serum stability during systemic circulation while the agent seeks to engage the target site of action. Additionally, other important properties are high target binding affinity and avoidance of undesired immune system stimulation. Clinical applications of nucleic acid therapies heavily depend on the ability of these oligonucleotides to survive and function in such complex biological environments they encounter without producing off-target effects. Many different chemical modifications have been introduced into oligonucleotide constructs in an effort to address these challenges. The following summary of chemical modifications highlight the most frequently encountered strategies to enhance the bioactivity of oligonucleotide agents.

1.5.1 Carbohydrate modifications

Modifications to the furanose ring of the oligonucleotide sequence have been extensively used to modulate binding affinities, serum stability, and oligonucleotide activity. Multiple studies have shown that the interaction between nucleic acids can be arranged in the order of RNA-RNA > DNA-RNA > DNA-DNA⁸⁰⁻⁸¹. The inclusion of electron withdrawing “hydroxy” groups at the ribose 2' position shift the conformation of the RNA sugar towards a C3'-endo sugar pucker, resulting in a gauche conformation between 2' and 4'-oxygen atoms⁸²⁻⁸³. This results in a shorter distance between 3'- and 5'-phosphodiester moieties that increase the duplex stability⁸². On the basis of this understanding, multiple sugar modifications have been made to enhance their efficacy. An example of this effect is the naturally encountered, nontoxic 2'-methoxy (2'-OMe) ribose modification that can be effectively incorporated via chemical synthesis methods by alternating ribonucleotide bases with 2'-OMe-ribonucleotides. This strategy is believed to confer significant nuclease stabilization, enhanced binding affinity, and reduced off target effects⁸⁴⁻⁸⁷. Teprasiran (Quark Pharmaceuticals) is an example of an siRNA therapeutic containing alternate 2'-OMe modifications⁸⁸. Methoxyethyl incorporation at the 2' oxygen atom (MOE) of the ribose sugar locks the two oxygen atoms in a gauche conformation that is thought to sterically protect the 3' phosphodiester linkage from nuclease digestion. MOE modifications are found in the marketed antisense drugs mipomersen (Kynamro) and nusinersen (Spinraza). Substitution of the 2'-OH group with fluorine also confers nuclease resistance and thermal stability to the oligonucleotide^{87, 89}. Enhanced enthalpic stabilization of the Watson-Crick pairing to complementary RNA sequence (1 to 2°C per substitution) is aided by 2' fluoro polarization of the 2'-H atom involved in hydrogen bonding with complementary strand⁹⁰⁻⁹¹. Every uracil and cytosine nucleotide in pegaptanib (Macugen) has this modification⁹². Sulfur replacement of the 4' oxygen atom of the sugar ring has also been shown to form stable duplexes with complementary sequences and improved resistance to endonucleases, but not 3'-exonucleases⁹³⁻⁹⁴. Locked nucleic acids (LNA) and bridged nucleic acids (BNA), wherein the 2'-O and 4'-C are covalently linked using methylene bridges to lock the furanose conformation into the 3' endo sugar pucker, have greatly enhanced binding affinities (3 to 9 °C per substitution) due to improved base stacking and resistance to endo and exonucleases⁹⁵⁻⁹⁶. The antisense drug miravirsin, currently developed by Santaris Pharma and having completed Phase II clinical trials, uses this strategy to confer nuclease protection via methylene bridges that lock in 8 of its 15 nucleotides⁹⁷.

1.5.2 Backbone modification

The 3'- and 5'-phosphodiester linkages in the RNA and DNA backbone are the primary sites of nuclease digestion. Hence, multiple strategies have been employed to make this linkage resistant to endo or exonuclease exposure. One of the most common backbone modifications is substitution of an oxygen atom of phosphodiester bond with sulfur⁹⁸. Although this substitution greatly reduces the reactivity of oligonucleotides towards nuclease digestion and allows for RNase H functionality, significant loss in binding affinity (0.5°C per substitution) towards the target complementary sequence is associated with this modification⁹⁹. Additionally, the phosphorothioate backbone makes the sequence very “sticky”, leading to serum protein binding that can alter the pharmacokinetic properties of the oligonucleotide and increase cellular uptake¹⁰⁰. This increased stickiness, however, can also enhance non-specific immune detection due to increased interaction with immune receptors¹⁰¹⁻¹⁰². The first FDA approved antisense drug, Fomivirsen (Isis Pharmaceuticals), was a fully phosphorothioate linked 21 mer synthetic oligonucleotide. SD101, a nuclease resistant CpG oligonucleotide from Dynavax Technologies also belongs to this class. Substitution of the 3' oxygen atom with a nitrogen (e.g., N3'-phosphoramidates), also enhances nuclease stability and promotes greater binding affinity towards complementary sequences (2.5 °C per substitution)¹⁰³. Further modification of phosphoramidates to thiophosphoramidates also improves the acid stability of the oligonucleotide while retaining the binding affinity of the parent phosphoramidate construct¹⁰⁴. Modest improvements in the thermal stability of RNA duplexes (0.5°C per substitution) has also been demonstrated by replacing the phosphodiester linkage of the nucleic acid with amide linkages¹⁰⁵. Thermal stability can be further increased by incorporation of 2'-O-methyl groups on the ribose units¹⁰⁶. Replacement of the phosphodiester bonds with methylene-methylimino (MMI) linkages also renders the oligonucleotides resistant to nuclease activity. This alteration does not support RNase H activity and can lead to solubility issues when used at higher modification percentages, resulting in faster renal clearance¹⁰⁷.

Unlike backbone modifications that retain the anionic character of the oligonucleotide, morpholino phosphorodiamidate (PMO) and peptide nucleic acid (PNA) modifications results in a neutral backbone¹⁰⁸⁻¹⁰⁹. Although these neutral nucleic acids are not electrostatically repelled by negatively charged cell membranes as occurs with unmodified oligonucleotides, the cellular uptake of these uncharged constructs remains poor, thus necessitating novel cellular delivery

mechanisms for efficient internalization. In PMO, morpholino rings substitute the sugar moiety and link them with the phosphorodiamidate backbone¹⁰⁸. In PNA, the sugar moiety and the phosphodiester linkage are replaced by a peptide backbone¹⁰⁹. In spite of such drastic modification to the natural nucleic acid structure, PMO and PNA can form base pairs with complementary sequences and have very high nuclease resistance¹⁰⁸⁻¹⁰⁹. They typically form more stable duplexes as well since they lack the electrostatic repulsion between the phosphodiester linked strands of conventional oligonucleotides. Since they do not support RNase H activity, they are mainly used for mRNA silencing and splice switching functions^{108, 110-113}. Eteplirsen (Sarepta) is an FDA approved 30-mer phosphorodiamidate morpholino oligomer.

1.6 Summary

According to International Agency for Research on Cancer (IARC); there was an estimated 18.2 million new cases and 9.6 million deaths worldwide in 2018¹¹⁴. United States alone is predicted to have 1.7 million new cancer cases and over 0.6 million related cancer related deaths in 2019¹¹⁵. Although this number seems to be staggeringly high, deaths due to cancer in U.S. declined by 27% from 1991 to 2016¹¹⁵. With tremendous technological advancement in past century and rigorous experimentation to understand underlying molecular mechanism of cancer progression, multiple new therapies are coming to horizon and nucleic acid therapy has been a forerunner in this field. Nucleic acids offer the ability to manipulate expression of oncogenes in a highly specific and safe manner. The global market for nucleic acid therapies was \$2.3 billion in 2018¹¹⁶. It is expected to grow at a rate of 49.9% CAGR to a 17.4 billion dollar market by 2023¹¹⁶. Global revenue for gene therapies in cancer management is estimated to reach \$4.3 billion by 2024¹¹⁷. In United States, cancer gene therapy market is projected to grow at a steady rate of 20.9% over next seven years¹¹⁷. This rapid growth is fueled by recent rush of gene therapy approvals that has rejuvenated the interest of large pharmaceutical companies which are looking to expand drug pipeline and increase revenue inflow. This has also been aided by advancement of gene delivery strategies. On one hand viral delivery systems are becoming more and more biocompatible and on other hand, non-viral systems are overcoming its traditional limitation of limited *in vivo* transfection capabilities. Multiple gene therapies in late stage clinical trials have shown compelling evidence of safety and efficacy and are expected to gain market access in coming years. These therapies hold great promises in not only mitigation but complete cure of fatal disease like cancer in near future.

CHAPTER 2. DEVELOPMENT AND *IN VITRO* CHARACTERIZATION OF LIPID COATED POLYPLEX FOR DUAL DELIVERY OF GENE AND SMALL MOLECULES TO BLADDER TUMOR CELLS

Adapted from the research article titled “Development and *in vitro* characterization of lipid coated polyplex for dual delivery of plasmid and small molecules to bladder tumor cells” authored by S.Samaddar, J.K.Mazur, D.Boehm and D.H.Thompson. Currently the article is under consideration for publication in a peer-reviewed journal.

2.1 Introduction

The ability to co-deliver small molecule drugs and a therapeutic gene has attracted significant attention as a potential cancer treatment¹¹⁸. Since, delivery of single agent therapies often leads to development of multi-drug resistance (MDR), co-delivery of two pharmacologically active ingredients has the potential to overcome MDR by manipulating the expression profile of the MDR gene or activating synergistic pathways. Drug synergism can also lead to lower therapeutic doses that can also contribute to lower side effects. Zhang *et al.* reported a pH-responsive amphiphilic star polymer capable of co-delivering an immunostimulatory agent, imiquimod and green fluorescent protein (GFP) reporter plasmid for synergistic delivery of gene-based immunotherapeutics and vaccines¹¹⁹. The Li group has reported a folate targeted lipid-based carrier system to co-deliver docetaxel and an iSur plasmid (a suppressor of metastatic and resistance related gene called survivin). Their data showed an enhanced anti-tumor effect in a xenograft model of mouse hepatocellular carcinoma¹²⁰. Han *et al.* developed a transferrin receptor-targeted solid lipid nanoparticle (SLP) platform that co-delivered doxorubicin and a GFP reporter plasmid that displayed enhanced efficiency for the targeted SLP formulation relative to non-targeted SLP in A549 tumor bearing mice¹²¹.

Non-muscle invasive bladder carcinoma (NMIBC) has the highest recurrence rate among all types of cancer¹²². This requires constant monitoring and frequent hospitalization making NMIBC very expensive to manage on a cost-per-patient basis from diagnosis to death¹²³. Recently, there has been an increased appreciation regarding the role of MDR in poor prognosis of patients with recurring tumors after first-line chemotherapeutic therapy¹²⁴⁻¹²⁸. Kunze *et al.* reported that

silencing of genes like B-cell lymphoma 2 (BCL2), BCL2-like 1 (BCLXL), X-linked inhibitor of apoptosis (XIAP), and survivin using siRNA, led to sensitization of MDR expressing bladder carcinoma cells such as T24 and J82 cells towards mitomycin-C and cisplatin chemotherapy¹²⁹. In a similar study, it was shown that downregulation of the MDR-associated protein-1 (MRP1) by emodin, a natural anthraquinone analogue, increased cisplatin mediated apoptosis in cisplatin resistant T24 and J82 cells¹³⁰. However, the biggest challenge in successful co-therapy is availability of suitable carrier system that can load two therapeutic molecules with dramatically different physical properties¹³¹. Genes or nucleic acids are anionic and hydrophilic nature with large molecular weights, whereas chemotherapeutics are mostly hydrophobic molecules with much lower molecular weights.

An additional problem for urothelial carcinoma patients is that intravesical administration of therapeutics has poor retention within bladder due to constant urine influx and bladder voiding, resulting in sub-optimal therapeutic concentrations and clinical outcome¹³². Development of a bladder tumor-targeted dual delivery system which can ‘stick’ to cancerous sites and release dual payload may have advantages in treating urothelial carcinoma. We report a tumor-targeted dual delivery system as a potential model for delivery of small molecules and nucleic acids to bladder tumor cells. We used EGFP-NLS as our reporter gene and pyrene as a fluorescent small molecule for mimicking the properties of a hydrophobic drug to demonstrate the capability of this system for delivery of functional payloads to target cells¹³³⁻¹³⁴.

High molecular weight (M.W.; e.g. 10k and 25k) polyethyleneimine (PEI) has been widely used as a gene transfection agent *in vitro*¹³⁵. Unfortunately, these cationic polymers are highly cytotoxic, thereby limiting their *in vivo* applications¹³⁶⁻¹³⁷. On the contrary, low molecular weight PEI has a better toxicity profile, however, it lacks the high transfection efficiency of its high molecular weight counterparts¹³⁸. Conjugating β -CD to PEI has been shown to enhance luciferase gene transfection in HEK293 cells by almost 4 times relative to unmodified PEI and significantly decreases the toxicity of the polymer¹³⁹. Our formulation utilize β -CD and linear PEI (M.W. 2.5kD) as a conjugate (CD_{2.5kD}-PEI) to electrostatically condense the plasmid into a polyplex. The polyplex is then further coated with a layer of fusogenic lipid mixture to produce a lipid coated polyplex (LCP) that is also capable of encapsulating hydrophobic small molecules such as pyrene

(Figure 1). The exterior of the LCP is decorated with a lipopeptide that binds fibronectin attachment peptide (GNRQRWFV¹⁴⁰VWLGSTNDPV). The peptide mimics a fragment of the bacterial adhesive protein known as fibronectin attachment protein present on the surface of *Mycobacterium bovis*. This peptide sequence has been shown to be responsible for the functional activity of fibronectin attachment protein and the tetrapeptide RWFV within it is absolutely critical for fibronectin engagement¹⁴⁰. Our formulation approach uses a microfluidic mixing technique to form LCP with enhanced targeting to bladder tumor cells when the GNRQRWFV¹⁴⁰VWLGSTNDPV peptide is present on the particle surface.

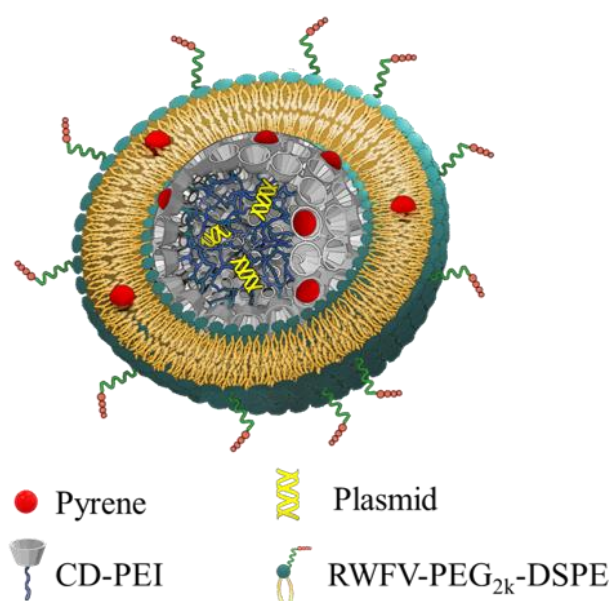


Figure 2: Conceptual diagram of a single Lipid Coated Polyplex (LCP) in cross-section

2.2 Materials and methods:

Materials. 1,2-Distearoyl-*sn*-glycero-3-phosphoethanolamine-N-[methoxy(polyethylene glycol)-2000] (DSPE-mPEG2k), 1,2-distearoyl-*sn*-glycero-3-phosphocholine (DSPC), 1,2-dioleoyl-*sn*-glycero-3-phosphoethanolamine (DOPE) and cholesterol hemisuccinate was purchased from Avanti Polar Lipids. Linear poly(ethyleneimine) (2.5kD) was purchased from Polysciences. β -Cyclodextrin and pyrene were purchased from Sigma. DNAase-I was purchased from New England Biolabs. EGFP-NLS was obtained as a gift from Prof. Rob Parton (Addgene plasmid# 67652). Slide-a-Lyzer dialysis cassettes (MWCO 20K, 3 mL) and cell culture reagents like

Dulbecco's modified Eagle medium (DMEM), Opti-MEM® reduced serum medium, 1X Phosphate buffered saline solution (PBS) and Gibco™ TrypLE express enzyme (1X) were purchased from Fisher Scientific. Fetal bovine serum (FBS), Penicillin-Streptomycin 10/10 (100X) and L-glutamine - 200mM (100X) were purchased from Atlanta Biologicals. Ultrapure water (18.2 MΩ) was used for preparation of 20 mM HEPES buffer (pH 7.4) and in all experiments. All solvents were of analytical grade, purchased from commercial sources. Buffers and solvents were filtered through 0.22 μm CA syringe filters (Macherey-Nagel Inc.) before use.

Synthesis of CD-PEI. Poly(ethylenimine) (2.5 kDa) was used to introduce a single modification onto the primary β-cyclodextrin rim as previously described¹⁴¹⁻¹⁴³.

Synthesis of lipopolymer conjugates. The FAP sequence (GNRQRWFVWVLGSTNDPV) with a propargylglycine modification at C termini was synthesized by solid phase peptide synthesis. Similarly, a control peptide sequence (scrambled peptide: (SCR) GNRQWVRFVWVLGSTNDPV) was also prepared where the order of the critical RWFV tetrapeptide was scrambled to WVRF. The alkyne modification on the peptide was utilized for a copper-catalyzed azide-alkyne cycloaddition (CuAAC) conjugation to DSPE-PEG2k-Azide. A detailed description of the method has been reported previously¹⁴⁴.

Formulation of polyplex and lipid coated polyplex (LCP). The formulation set-up comprised two syringes attached to a tube of 1/16" I.D. connected by a T-junction. The T junction was followed by 6' length tubing of the same I.D. wrapped around a plastic support 10 cm in length, 2.5 cm in width and 0.5 mm in height. Optimal conditions for polyplex formation were determined by mixing the HEPES solution (20 mM) of CD_{2.5kD}-PEI and 60 μg/mL EGFP-NLS at different N/P ratios of 5,10,15 and 20. Flow rates were varied from 10 μL/min to 5 mL/min.

The polyplex formed above were then mixed with an 80% ethanolic solution of 0.5 mM, 1 mM, 2 mM, 4 mM or 8 mM mixture of lipids (CHEMS:DOPE:DSPC:DSPE-mPEG-RWFV = 34:54:10:2). The flowrate was kept constant in this step at 5mL/min for each syringe. The resulting LCP were immediately diluted in HEPES buffer to < 16% ethanol after collection. The diluted particles were then dialyzed using 20K MWCO dialysis cassettes against 500 volumes of 20mM HEPES for 24 h. The collected particles were then analyzed for size, polydispersity and zeta potential. For loading

pyrene, 5 mol% of pyrene was mixed with the ethanolic lipid solution. Non-targeted and scrambled LCP were prepared as controls using the method described above except that the DSPE-mPEG-RWFV was replaced by DSPE-mPEG (non-targeted control) or DSPE-mPEG-SCR (scrambled control). A schematic representation of the formulation steps are shown in Figure 2.

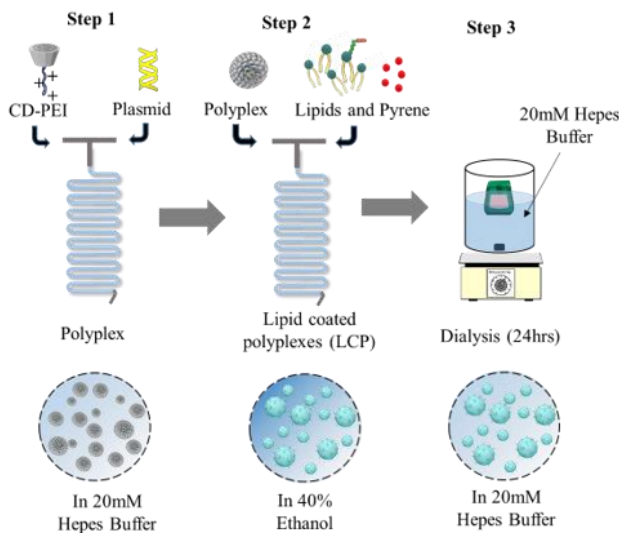


Figure 3A Schematic representation of LCP formulation steps. Step 1: Cationic CD_{2.5kD}-PEI and plasmid are mixed at the desired N/P ratio within a microfluidic reactor. Step 2: Polyplex and a lipid mixture dissolved in 80% ethanol solution are mixed in the same microfluidic reactor. Step 3: The LCP are dialysed to remove ethanol and free pyrene from the formulation. A total flow rate of 10 mL/min and flow rate ratio of 1:1 was used for mixing.

Dynamic light scattering (DLS) measurements. The hydrodynamic diameters (Number mean), polydispersity index (PdI) and zeta potentials (ζ) of the materials were evaluated using a particle size analyzer (Zetasizer Nano ZS, Malvern Instruments Ltd.) at 25 °C with a scattering angle of 173°. 30 μ L Particle solutions were diluted to 1 mL with sterile filtered NanoPure water before analysis.

Gel-shift assay. The pDNA complexation ability of polymers mixed within the flow channel was determined by 1% agarose gel electrophoresis. The agarose gels were precast in 1X TBE buffer with GelRed dye (Biotium Inc.) at 1:10,000 dilution. Polyplex containing 0.1 μ g of pDNA at different N/P ratios was added to loading dye (5:1 dilution) and loaded onto the gel, prior to initializing electrophoresis at a constant voltage of 55 V for 1.5 h in 1X TBE buffer. The pDNA bands were then visualized under a UV transilluminator at 365 nm.

TEM images. Transmission Electron Microscopy images of LCP were collected using a Tecnai G2 20 microscope equipped with a 200 kV LaB₆ filament and fitted with a bottom mount 2k X 2k Gatan US1000 CCD camera. Samples were deposited onto Formvar/carbon-coated Cu 400-mesh grids and stained with 2% uranyl acetate prior to visualization. Further image analysis was performed using ImageJ software (NIH).

Quantifying plasmid content. Encapsulation efficiencies and loading efficiencies of plasmid DNA in LCP were determined using the membrane impermeable dye PicoGreen (Molecular Probes, Eugene, OR, USA) that binds specifically to double-stranded DNA and fluoresces only when bound. PicoGreen fluorescence was measured with a spectrofluorometer (Biotek Synergy) using excitation and emission wavelengths of 490 and 525 nm, respectively. Plasmid content was determined by measuring the PicoGreen fluorescence after treating the LCP for 30 min at 25 °C with 1% Triton X-100 for disrupting the lipid coat, followed by another 30 min treatment with 0.15 mg/mL of heparin sulphate solution for decomplexing the polyplex¹⁴⁵⁻¹⁴⁶. Plasmid concentration was calculated by comparing PicoGreen fluorescence values to the calibration curve prepared using plasmid standards. The encapsulation efficiency (EE) and loading efficiencies (LE) were calculated using the following formula:

$$EE = \frac{\mu\text{g of plasmid in formulation}}{\mu\text{g of plasmid added}} \times 100$$

$$LE = \frac{\mu\text{g of plasmid in formulation}}{\mu\text{g of LCP}} \times 100$$

Quantifying pyrene content. HPLC technique was used to measure the amount of pyrene that was encapsulated within the LCP. Briefly, 50 μL of the LCP was dried using a VacufugeTM (Eppendorf) at 40 °C for 2 h. NanoPure water (30 μL) was added to the dried pellet, followed by addition of 70 μL of acetonitrile to dissolve the LCP. An Agilent 1200 HPLC system equipped with a XBridgeTM C18 column (2.1 mm X 100 mm, pore size 3.5 μm) and employing Mobile phase A (water with 10 mM NH₄OAc) and mobile phase B (75% acetonitrile:25% methanol with 10 mM NH₄OAc) was used for analysis. A gradient elution was used from 95% A to 95% B over 4 min at a flow rate of 250 $\mu\text{L}/\text{min}$, with pyrene absorbance monitored at 338 ± 4 nm using a diode array detector. Pyrene concentrations was calculated by comparing the pyrene absorbance for LCP to a calibration curve prepared using absorbance values obtained from standard pyrene concentration.

The encapsulation efficiency (EE) and loading efficiencies (LE) were calculated using the following formula:

$$EE = \frac{\mu\text{g of pyrene in formulation}}{\mu\text{g of pyrene added}} \times 100$$

$$LE = \frac{\mu\text{g of pyrene in formulation}}{\mu\text{g of LCP}} \times 100$$

DNAase protection assay. The ability of the LCP to protect the complexed DNA against nucleases was evaluated by incubation with DNase-I¹⁴⁷. In brief, LCP formed at N/P = 10 were incubated at 37 °C in 20 mM HEPES buffer containing 2U DNase I. The reaction was quenched by addition of 10 mM EDTA solution to a final EDTA concentration of 2.5 mM and heating at 65 °C for 10 mins using a heat block. The particle solutions were then treated with 1% Triton X-100 for 30 min at 25 °C to strip the lipid coating followed by another 30 min treatment at 25 °C with 0.15 mg/mL heparin to decomplex the polyplex and release the pDNA. Next, CHCl₃ was added at a 1:1 ratio, the mixture vortexed and incubated for 15 min to effect phase separation. The aqueous layer containing pDNA was collected and concentrated using an Eppendorf vacufuge under reduced pressure at 20 °C. The extracted pDNA was analyzed using 1% agarose gel electrophoresis.

Quantifying transfection efficiency. MB49 cells were seeded in 96-well plates at a density of 15,000 cells per well in 100 µL of complete medium (DMEM containing 10% FBS, supplemented with 1% penicillin-streptomycin and 1% L-glutamine) and incubated for 24 h prior to transfection. The medium was replaced, and naked plasmid, non-targeted LCP, scrambled LCP, or targeted LCP were added at 0.1 µg DNA per well in 100 µL in Opti-MEM® media for 4 h. Then, the cells were rinsed with PBS and incubated at 37 °C for an additional 4 h, 12 h or 24 h in complete media. Next, the cells were trypsinized and analyzed using a FC500 (Beckman Coulter) flow cytometer equipped with a 488 nm laser and 525 ± 20 nm detector. As positive control, Lipofectamine™ LTX was used according to the manufacturer's protocol. All transfection experiments were performed in triplicate.

Quantifying pyrene delivery. MB49 cells were seeded in 24-well plates at a density of 2 x 10⁵ cells per well in 500 µL of complete medium and incubated for 24 h prior to transfection. Media was replaced with either non-targeted LCP, scrambled LCP or targeted LCP at an equivalent dose of 0.05 µg/mL pyrene in 500 µL opti-MEM® media for 4 h. Opti-MEM® media without LCP was

used as a negative control. Next, the cells were rinsed with PBS and incubated at 37 °C for an additional 4 h or 24 h in complete media. Cells were trypsinized and analyzed using a BD Fortessa flow cytometer equipped with a 355 nm UV laser and 379 ± 14 nm detector.

Cytotoxicity evaluation. Cell viability was measured using CellTiter 96® AQueous One Solution Cell Proliferation Assay (Promega). MB49 cells were seeded at 15,000 cells per well in 96-well plates in growth medium and allowed to adhere overnight at 37 °C. Cells were washed with PBS and incubated with LCP samples in Opti-mem media for 4 h. The cells were then washed with PBS and incubated overnight in complete DMEM media. Next, 20 μ L of the MTS reagent was added into each well and incubated for another 1 h at 37 °C before recording the absorbance at 490 nm using a Synergy Biotek plate reader. The absorbance of the wells without any cells was subtracted from the untreated controls and treated sample wells for background correction. The cell viability (%) relative to untreated cells was calculated as $[A]_{\text{sample}} / [A]_{\text{untreated}} \times 100\%$, where $[A]_{\text{untreated}}$ is the absorbance of the wells without LCP and $[A]_{\text{sample}}$ is the absorbance of the wells treated with LCP. All experiments were performed in triplicates and the cytotoxicity values reported are the mean from three different measurements.

2.3 Results and discussion

2.3.1 Formulation and characterization of lipid coated polyplex

A sonication- and extrusion- free technique for formulating dual loaded LCP was developed. First, we studied the N/P ratio needed for complete complexation of CD_{2.5kD}-PEI and the 5.2 kB plasmid. For all the N/P ratios studied, the flow rate was kept constant at 5mL/min for each syringe. The positively charged polymer was mixed with the anionic plasmid to produce electrostatically condensed polyplex. The hydrodynamic diameter of the polyplex were 133 ± 9 nm, 97 ± 3 , 87 ± 8 and 78 ± 10 nm at N/P of 5, 10, 15 and 20, respectively (Figure 3a). At N/P ratios of 5 and 10, the polydispersities were 0.26 ± 0.01 and 0.27 ± 0.03 respectively which increased to 0.32 ± 0.03 and 0.33 ± 0.06 for N/P of 15 and 20, respectively (Figure 3b). At a low N/P of 5, the measured ζ of the polyplex was -18.2 ± 1.1 mV, suggesting that the plasmid was incompletely complexed by the polymer. At an N/P of 10, the polyplex displayed a positive $\zeta = 14.8 \pm 2.9$ mV, suggesting complete complexation of the plasmid cargo. For higher N/P ratios, we did not observe any significant

increase in surface charge, such that $\zeta = 12.6 \pm 3.0$ mV and 16.3 ± 0.8 mV at N/P 15 and 20, respectively (Figure 3c). These findings are consistent with our gel-shift assay results (Figure 3d). At N/P 5, there was a significant amount of uncomplexed plasmid as revealed by the migrated electrophoretic bands visible on the agarose gel. At N/P ≥ 10 , however, no bands were visible due to the absence of free plasmids. Thus, all subsequent lipid coated polyplex formulations employed N/P = 10.

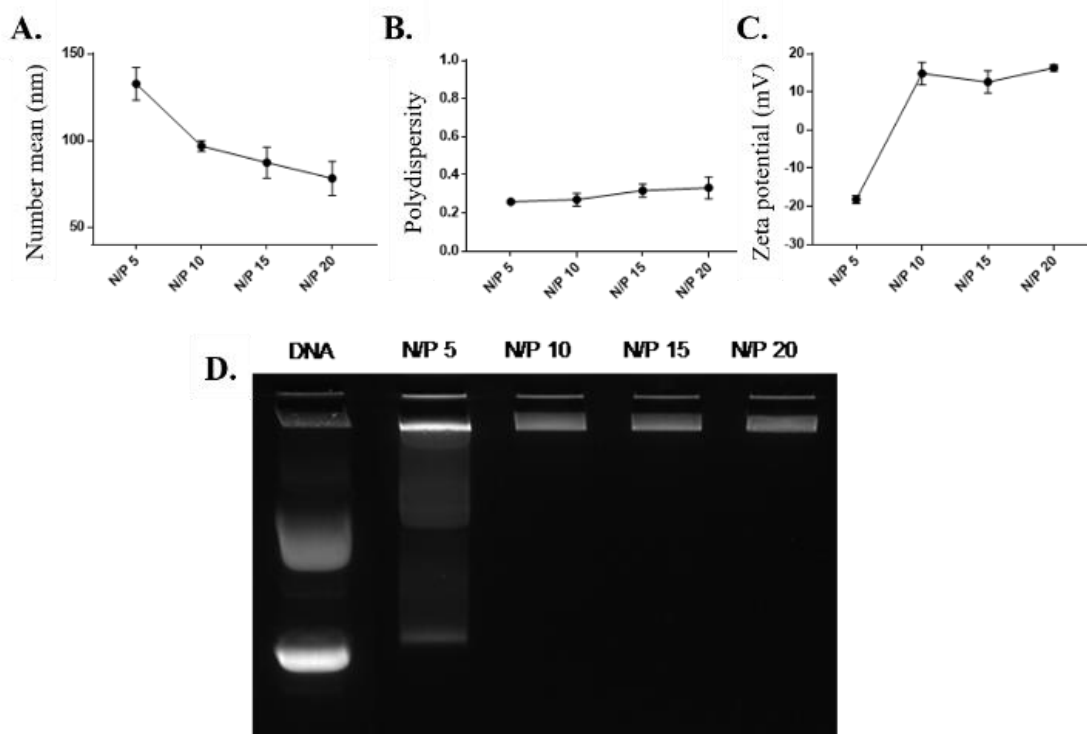


Figure 4 Effect of N/P ratio on polyplex properties. **A.** Hydrodynamic diameter (number mean); **B.** Polydispersity; **C.** Zeta Potential; **D.** Gel-shift assay for polyplex prepared by mixing 60 µg/mL plasmid with CD_{2.5kD}-PEI in 20mM HEPES buffer at different N/P ratios. The total flow rate was 10 ml/min and flow rate ratio was 1:1. Results are the mean \pm SD (n=3).

When T junctions are used in flow reactor systems, mixing occurs primarily due to diffusion at the contact surface between the two fluid streams, thereby necessitating the use of long mixing channels¹⁴⁸. Alternatively, higher flow rates can be utilized to promote the formation of eddies and vortices within the fluidic channels to aid in efficient mixing¹⁴⁹⁻¹⁵⁰. We evaluate the effect of flow rate on polyplex formation at N/P = 10 by increasing the total flow rate (TFR) from 0.02 mL/mins to 10 mL/min while maintaining a flow rate ratio of 1:1. Increasing the TFR produced a polyplex size decrease from 234 ± 57 nm at lowest flow rate to 97 ± 3 nm at the highest flow rate of 10

mL/min (Figure 4a). Improvement in polyplex polydispersity was also observed from 0.66 at the lowest TFR to 0.28 at a TFR of 10 mL/min (Figure 4b). Additionally, the ζ of the polyplex increased from 8.6 ± 1.5 mV to 14.8 ± 2.9 mV (Figure 4c). These results confirm that higher flow rates ensure efficient mixing between the cationic polymer and the pDNA streams, resulting in smaller and more highly condensed polyplex of greater homogeneity. All subsequent formulation experiments used a TFR of 10 mL/min.

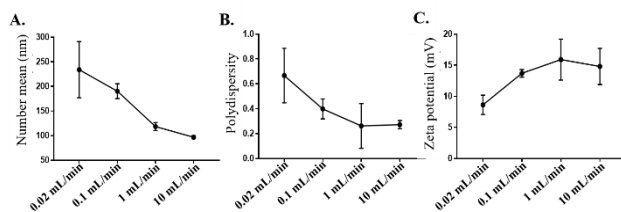


Figure 5. Effect of total flow rate on polyplex properties. **A.** Hydrodynamic diameter (number mean); **B.** Polydispersity; and **C.** Zeta Potential. Polyplex were prepared by mixing 60 $\mu\text{g/mL}$ plasmid with CD_{2.5kD}-PEI in 20mM HEPES buffer at a N/P ratio of 10. The flow rate ratio was kept constant at 1:1. Results are the mean \pm SD (n=3).

Next, we studied the concentration of lipid needed for efficient coating of the polyplex (N/P = 10). The effects of 0.5 mM, 1 mM, 2 mM, 4 mM and 8 mM lipid on the size, surface charge and polydispersity of the LCP was evaluated. At a concentration of 0.5 mM lipid, the LCP diameters were 259 ± 68 nm, a larger diameter than expected that we attribute to LCP aggregation. At 1, 2, 4 or 8 mM lipid concentrations, the LCP sizes decreased to an essentially uniform size of 108 ± 10 nm, 118 ± 40 nm, 110 ± 10 nm and 127 ± 20 nm, respectively (Figure 5a). Polydispersities were found to follow a similar trend wherein the LCP had high polydispersity (0.67 ± 0.15) at 0.5 mM, that became similar above 1mM lipid concentration (0.16 ± 0.01 at 1 mM, 0.18 ± 0.01 at 2mM, 0.15 ± 0.01 at 4mM and 0.19 ± 0.01 at 8 mM) (Figure 5b). In contrast, ζ were found to display a significant decrease from -14.8 ± 2.2 mV at 0.5 mM to -26.8 ± 1.0 at 4 mM (Figure 5c). Increasing lipid concentration to 8 mM did not result in any significant change in surface charge in the zeta potential. Thus, we conclude that 4 mM lipids were sufficient to produce a complete coating of the polyplex, such that further increases in lipid concentration would only result in depositing multiple lipid coats onto the polyplex core.

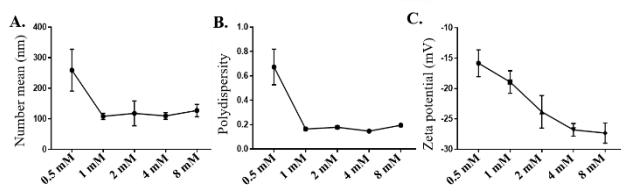


Figure 6. Effect of lipid mixture concentration on LCP properties **A.** Hydrodynamic diameter (number mean); **B.** Polydispersity; and **C.** Zeta Potential. LCP were prepared by mixing 1 mL of polyplex solution with 1 mL of ethanolic lipid mixture (DOPE:CHEMS:DSPC:DSPE-mPEG_{2k} = 34:54:10:2) solution of varying concentration. The total flow rate was 10 mL/min and flow rate ratio was 1:1. Results are the mean \pm SD (n=3).

2.3.2 DNase protection assay

Next, we evaluated the ability of the delivery system to protect the plasmid from nuclease degradation. The LCP containing pDNA at its core were treated with and without 2U DNase-I at 37 °C for 4 h. After exposure to the enzyme, the DNase was inactivated using EDTA before extracting the plasmid from the LCPs. Plasmid extracted from DNase treated and untreated LCPs showed identical band plasmid patterns on agarose gels, indicating that the plasmid inside the LCP was protected from enzymatic degradation. In contrast, the naked plasmid treated with same amount of DNAase did not show any electrophoretic bands on the gel, indicating that the DNAase enzyme was active and completely digested the naked plasmid (Figure 6).

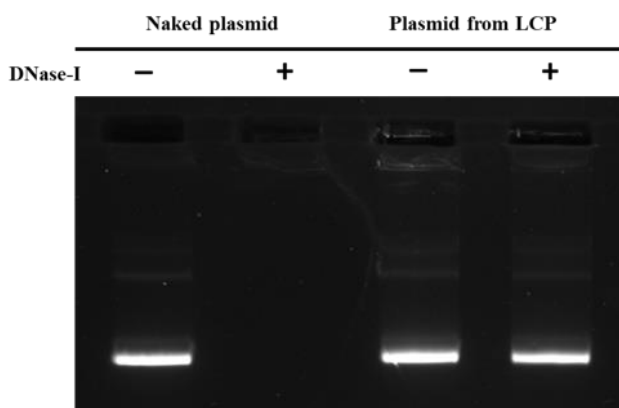


Figure 7. Ability of LCP to protect loaded plasmid from DNAase degradation. LCPs were treated for 4 h with 2U DNase-I at 37 °C before quenching the enzymatic reaction with 2.5mM EDTA and heating at 65 °C for 10 mins. The entrapped pDNA was released using sequential treatment with 1% Triton X-100 and 0.15 mg/mL Heparin. The released pDNA was concentrated using vacuum centrifugation before agarose gel (1%) electrophoresis to analyze for plasmid integrity.

2.3.3 TEM Images

The morphology of the polyplex and LCP was evaluated using negative stain transmission electron microscopy. TEM images showed that polyplex formed at N/P = 10 were smaller than 100 nm in diameter (Figure 7a), in good agreement with our DLS data. Lipid coating of the polyplex increased the particle diameter (Figure 7b). Size analysis of the TEM images using ImageJ revealed that the LCP are made up of about 90 nm diameter polyplex that are coated with a 12 nm lipid layer around the polyplex core, resulting in LCPs that are about 114 nm in diameter. Since a

single bilayer of lipid is approximately 5 nm in thickness, we can expect that there are about 2 bilayers around each polyplex at 4 mM concentration¹⁵¹.

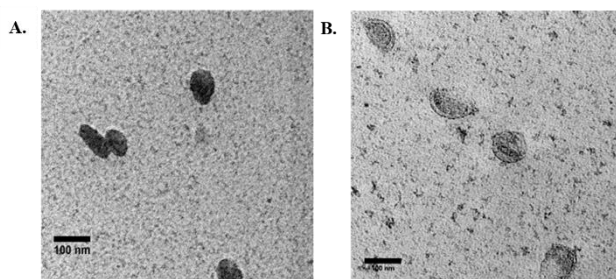


Figure 8. Negative stain TEM images of **A.** Polyplex and **B.** LCP. Polyplex were made using N/P ratio of 10; LCP were coated with 4 mM lipid solution (CHEMS:DOPE:DSPC:DSPE-mPEG_{2k} = 34:54:10:2)

2.3.4 Quantifying plasmid and pyrene content

Plasmid and pyrene content analysis showed that there was no significant difference between the encapsulation and loading of the payload amongst the targeted, scrambled and non-targeted controls. The plasmid encapsulation efficiencies for non-targeted, scrambled, and targeted formulations were $48.5 \pm 0.1\%$, $50.0 \pm 0.4\%$, $48.7 \pm 2.9\%$, respectively (Figure 8a). To determine the % mass of plasmid within the LCP, loading efficiencies were calculated and was found to be $0.33 \pm 0.01\%$ for all the different formulations (Figure 8b). Similarly, the encapsulation efficiencies of pyrene were found to be $17.9 \pm 1.3\%$, $15.2 \pm 0.6\%$ and $15.7 \pm 0.4\%$ for the non-targeted, scrambled, and targeted LCPs, respectively (Figure 8c) indicating that the different formulations were each composed of $0.15 \pm 0.01\%$ of pyrene by mass. (Figure 8d). These findings indicate a 1:2 pyrene:plasmid mass ratio within the LCP. Considering that the 5.2 kB EGFP-NLS plasmid molecular weight is ~ 3380 kD (650 da/bp), it can be calculated that for every molecule of plasmid there are approximately 8300 pyrene molecules loaded within the LCP particles.

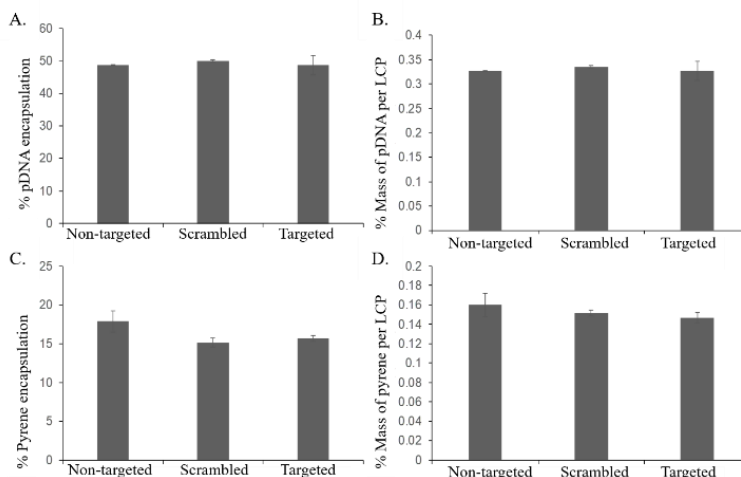


Figure 9. Encapsulation and loading efficiency of (A,B) plasmid and (C,D) Pyrene. Plasmid content was measured via PicoGreenTM assay after decomplexing the LCP using 1% Triton-X100 to disrupt the lipid layer and 0.15 mg/mL heparin to release the plasmid from the polyplex. Pyrene content was measured by dissolving the LCP in 70% ACN solution to release pyrene, followed by HPLC separation and pyrene detection using absorbance at 338 ± 4 nm. Results are reported as mean \pm S.D. (n=3).

2.3.5 Quantifying cellular delivery of plasmid and pyrene:

The developed delivery system utilizes a novel bacterial adhesin peptide that enables the delivery system to engage exposed fibronectin matrix at the tumor site¹⁵². We anticipate that this interaction will prevent loss of vehicle from the bladder tumor sites due to the urine influx and bladder voiding. Previously, we have reported the empty Cy5.5 labelled liposomes displaying the RWFV targeting peptide was able to associate with murine bladder cancer cells (MB49) in a sequence specific manner¹⁴⁴. Unfortunately, those dispersions were prepared using sonication and extrusion techniques, making it impossible to effect the delivery of fragile nucleic acid payloads in a functional manner. The formulation technique used here avoids both sonication and extrusion to enable the encapsulation and delivery of functional plasmid. Interestingly, weak transfection activity was observed for CD2.5kD-PEI polyplex alone (i.e., no lipid coating or targeting peptide) (Figure 9). This can be attributed to the fact that the polyplex associates with cells electrostatically in a non-specific manner due to its positive zeta potential, however the transfection efficiency is low because it lacks endosomal escape properties such that the cargo is degraded within the lysosomal compartment. To facilitate endosomal escape, we utilized CHEMS and DOPE to coat the polyplex. At acidic endosomal pH, CHEMS becomes protonated and loses its ability to stabilize bilayers such that the inverted hexagonal phase forming lipid, DOPE, promotes fusion

with the endosomal membrane¹⁵³⁻¹⁵⁴. Since coating of the positively charged polyplex with a lipid mixture containing anionic CHEMS introduces a negative surface charge on the LCP, non-targeted LCP are electrostatically repelled from the cell surface, thus limiting entry of the LCP into the target cell population. Introduction of RWFV peptide onto the LCP particle surface, however, overcomes this barrier. To examine the impact of sequence specificity of the targeting peptide on transfection efficiency, we synthesized two versions of the targeting peptide-lipopolymer construct. One contained the critical RWFV tetrapeptide sequence and other contained WVRF (a scrambled version of the key RWFV binding motif) in the targeting peptide. Scrambled peptides are often used as negative controls to show that a specific sequence is critical for function¹⁵⁵⁻¹⁵⁶. Naked DNA and Lipofectamine LTX were used as negative and positive controls, respectively. Cellular internalization of FAP-FBN-integrin complexes, the pathway by which RWFV constructs enter the cells via the caveolar uptake pathway, are known to occur with very slow kinetics in MB49 cells¹⁵². Our results show that at 4 h and 12 h time points, transfection by targeted LCPs are significantly lower than the transfection achieved by Lipofectamine LTX. However, after 24 h, the presence of the targeting ligand resulted in four times greater GFP expression as compared to the scrambled peptide and comparable to positive controls. These results demonstrate that the RWFV tetrapeptide sequence is crucial for boosting the plasmid expression profile. Similar results were observed for pyrene delivery (Figure 10 a,b). After 4 h incubation, targeted LCP resulted in 2-fold enhancement in pyrene delivery to cells relative to scrambled LCP and 4-fold relative to non-targeted LCP. After 24 h, the pyrene fluorescence decrease, possibly due to metabolism by the cellular polycyclic aromatic hydrocarbon (PAH) metabolizing enzymes¹⁵⁷⁻¹⁵⁸. Secondly, these data show that although the internalization of the FAP targeted LCP-FBN-integrin complex occurs via slow uptake kinetics compared to cationic LipofectamineTM LTX, the endocytosed targeted LCPs can efficiently decomplex and deliver similar quantity of functional payload to the nucleus for translation to occur. Additionally, to make sure that the developed formulation was non-toxic to MB49 cells, we performed MTS assays. Our toxicity data suggests that all the developed formulations resulted in similar cellular viability as compared to untreated cells showing that the LCPs were non-toxic to cells at concentrations used (Figure 11).

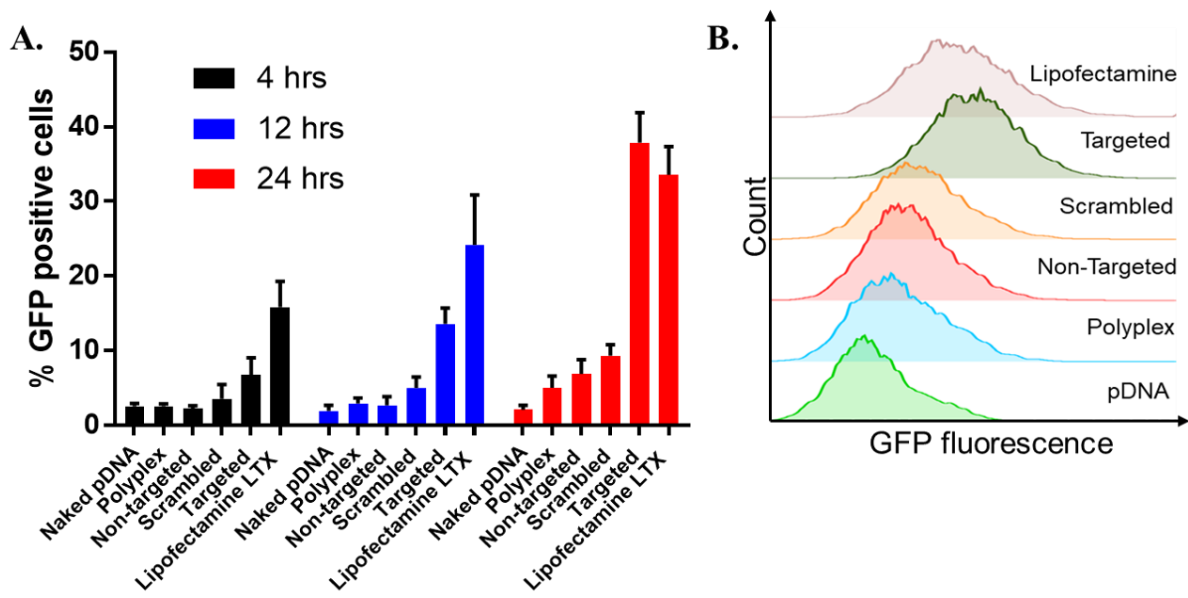


Figure 10. **A.** EGFP-NLS plasmid transfection efficiency of the non-targeted, scrambled and targeted LCP. **B.** Histogram plot for GFP fluorescence distribution in MB49 cell population at 24 h. Cells were treated with LCP formulations for 4 h at 37 °C, followed by PBS washing to remove unbound complexes. The cells were further incubated for 4 h, 12 h or 24 h and then trypsinized, and resuspended in PBS for flow cytometry analysis. Error bars indicate the standard deviation of the mean (n=3).

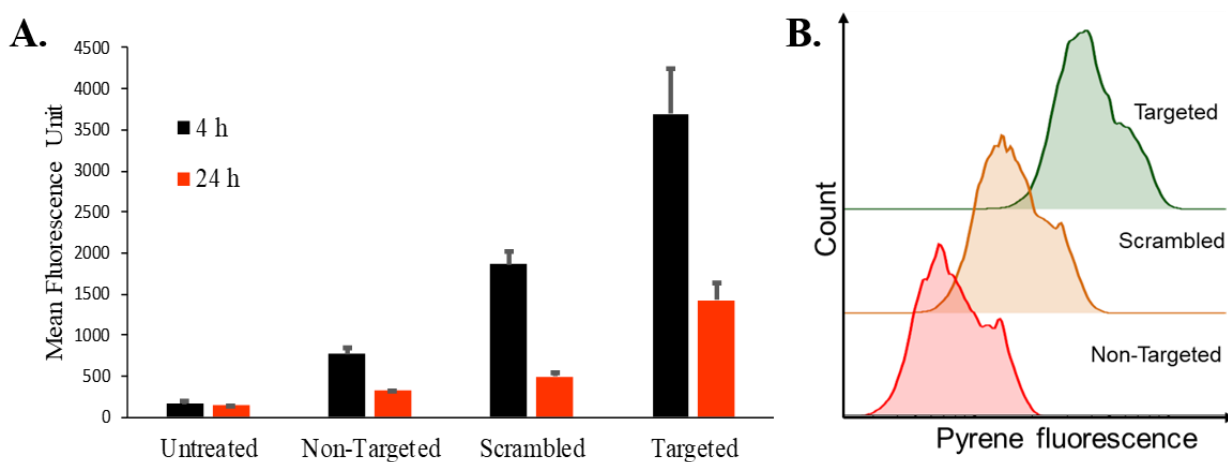


Figure 11. **A.** Pyrene delivery of the non-targeted, scrambled and targeted LCP. **B.** Histogram plot for pyrene fluorescence distribution in MB49 cell population at 4 h. MB49 cells were treated with LCPs for 4 h at 37 °C, followed by PBS washing to remove non-specific interactions. After further 4 hrs or 24 hrs incubation, cells were trypsinized, and resuspended in PBS for quantification of pyrene fluorescence using flow cytometer. Error bars indicate the standard deviation of the mean (n=3).

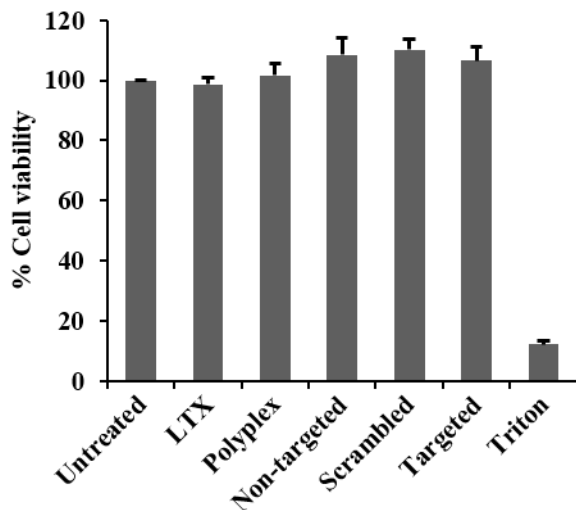


Figure 12. Cytotoxicity analysis of LCP formulations. MB49 cells were treated with different LCP formulations for 4 h followed by washing to remove uninternalized particles. The particles were incubated another 24 h before adding the MTS reagent. After incubating for 1 h, the absorbance of soluble formazan formed due to bio-reduction of MTS by live MB49 cells population was measure at 490 nm. All treatments for each formulation was performed in triplicates and error bars represents standard deviation of mean (n=3).

2.4 Conclusion

In conclusion, we have developed a carrier system for co-delivery of plasmid DNA and small, hydrophobic molecules to MB49 bladder cancer cells in a targeted manner. The fabrication utilizes an easy microfluidic mixing approach that can be readily scaled-up^{145, 159}. The inner cationic and outer hydrophobic character of the LCP allows for simultaneous entrapment of nucleic acids and small molecules, suggesting that these formulations may be useful for dual delivery approaches. The use of a lipid shell conveniently allowed the incorporation of the RWFV-lipopeptide, that confers tumor-targeting and internalization properties for the LCP formulations. The non-toxic nature of the RWFV targeted LCP combined with the efficient transfection and small molecule delivery characteristics of these formulations warrants further investigation.

CHAPTER 3. FAP TARGETED LIPID NANOPARTICLES FOR BLADDER CANCER IMMUNOTHERAPY

Adapted (Reprinted) from the research article titled “FAP targeted Lipid nanoparticle for bladder cancer immunotherapy” authored by S.Samaddar, J.K.Mazur, J.Sargent and D.H.Thompson. Currently the article manuscript is under preparation.

3.1 Introduction

Bladder cancer is the 9th most common form of cancer worldwide. In US alone, 81,190 new cases and 17,240 deaths are expected in 2018¹⁶⁰. Projected economic burden of bladder cancer on U.S. economy has risen from \$3.98 billion in 2010 to \$5.25 billion in 2020¹⁶¹. Nearly 80% of the cases are classified as non-muscle invasive bladder cancer (NMIBC) and most are treated with surgery. After surgery; however, disease frequently recurs, making NMIBC, the most expensive type of cancers to treat due to the need for long-term patient follow-up and repeat procedures^{2,3}. Thus, effective new therapeutic countermeasures against bladder cancer are urgently needed.

The bladder displays unique structures and challenges as a therapeutic target. Epithelial cells lining the luminal surface (i.e., umbrella cells) are engaged in tight junctions that prevent access to the lower transitional cell layers.¹⁶²⁻¹⁶³ Umbrella cells also express extracellular uroplakin proteins that assemble into semi-rigid plaques that shield the apical surface. The urothelium is further isolated from the bladder lumen by a glucosaminoglycan (GAG) layer that is produced and assembled on the apical surface of the umbrella cells.¹⁶⁴ In addition, well-differentiated umbrella cells have limited secretory and endocytic capacity.¹⁶² In contrast, malignant bladder cells are usually less differentiated, less polarized, and exhibit diminished levels of uroplakin expression and GAG layer synthesis.¹⁶⁵ Consequently, neoplastic cells are exposed to the lumen of the bladder, leading to increased accessibility of tumor lesions to instilled therapeutic agents compared to the well-protected normal regions of the bladder. Unfortunately, constant urine influx and bladder voiding limits the impact of direct instillation of drugs on these tumors.

In 1976, Morales et.al. first demonstrated the effectiveness of BCG in treating NMIBC¹⁶⁶. Intravesicular instillation of live BCG has remained the adjuvant therapy of choice for the post-

operative treatment of NMIBC since its FDA approval in 1990. Multiple meta-analysis and large scale randomized studies comparing BCG with intravesical chemotherapy with small molecule drugs such as mitomycin C, doxorubicin, epirubicin, thiotepa has concluded the inability of these small molecule drugs to match the reduction in recurrence rates and disease progression that is achieved by BCG¹⁶⁷⁻¹⁷⁶. Unfortunately, intravesical BCG is associated with high local morbidity and significant risk of systemic mycobacterial infection. Additionally, multiple instillations also leads to increased toxicity, thus limiting patient tolerance for the treatment regimen required for effective anti-cancer activity¹⁷⁷. To overcome adverse effect associated with BCG, Morales et.al; developed a Mycobacterium phlei cell wall nucleic acid complex to mimic therapeutic benefits of BCG. Two international multi centered clinical trials have demonstrated the safety and efficacy of this approach as compared to BCG¹⁷⁸⁻¹⁷⁹. Unfortunately, the heterogenous population of the trials and lack of clear study endpoints led to its FDA failure.

Recent studies have led to the identification of Fibronectin attachment protein (FAP) as the adhesin protein in mycobacterial cell wall used by BCG for binding to fibronectin rich tumor microenvironment of bladder tumor preventing easy removal form the cancerous sites. FAP-fibronectin interaction provides a novel and potentially powerful approach for the high local delivery of therapeutic agents to tumor area greatly enhance therapeutic outcome which is a current drawback for intravascular delivery of drugs. Since full length FAP is prone to aggregation, we have developed a robust synthetic peptide, derived from full length FAP, that is presented at the distal terminus of a lipopolymer¹⁸⁰⁻¹⁸¹. The key binding motif of FAP 'RWFV' has been encoded within this synthetic peptide sequence. The amino acid sequence (GNRQRWFVVWLGSTNDPV) from FAP has been used as the key binding motif that promotes site specific binding to the FBN network surrounding the bladder tumor cells⁵, as well as additional flanking sequences that enhance FBN affinity. Previously we have shown the sequence specific targeting capabilities of FAP lipopolymer incorporated liposomes in *in vitro* and orthotopic bladder tumor models proving that carriers displaying FAP as a targeting moiety may serve as an effective delivery system for immunostimulatory nucleic acid for triggering an immunotherapeutic response for bladder cancer treatment and a potential replacement for BCG therapy.

Here we formulated a pH sensitive FAP targeted lipid nanoparticles (LNP) for delivery of CpG, a well known immunostimulatory agent using a scalable Chemtrix®3321 flow reactor. The developed size-controlled lipid/CpG complexes from a mixture of lipids that promote cellular targeting and membrane fusion within target cell membrane (**Figure. 1**). We used a cationic lipid 1,2-dioleoyl-3-trimethylammonium-propane (DOTAP) for efficient complexation of anionic CpG¹⁸². The presence of 1,2-dioleoyl-*sn*-glycero-3-phosphoethanolamine (DOPE) provides fusogenic properties to the LNP so that it can fuse with cellular membranes¹⁸³. Cholesterol hemisuccinate (CHEMS) under neutral conditions stabilizes DOPE in lamellar phase. However, within acidic endosomal pH conditions, protonation of CHEMS causes it to lose its stabilizing property and DOPE transitions into inverted hexagonal phase releasing the cargo¹⁵⁴. The novel FAP-mPEG_{2K}-DSPE ligand was incorporated into the lipid mixture for targeting bladder tumor. We show that FAP targeted LNPs produced using flow reactor shows enhanced association with fibronectin secreting cells and a greater immunostimulatory potential.

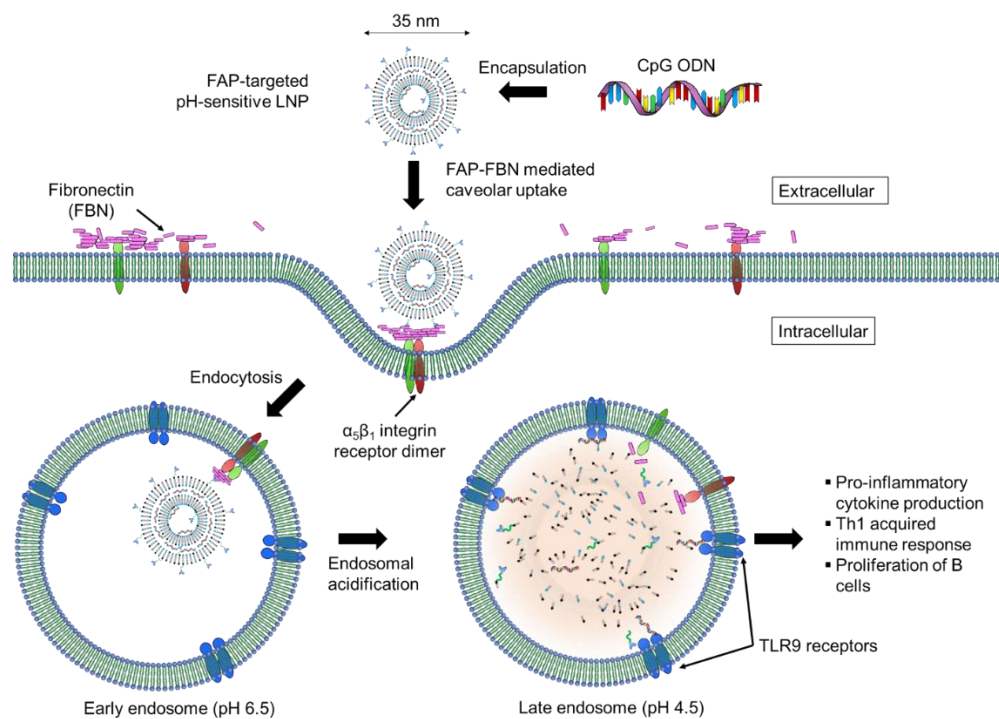


Figure 13. 35nm FAP targeted LNPs attaches to Fibronectin (FBN) on cell surfaces causing in dimerization of α_5 and β_1 subunits of surface integrin followed by endocytosis via caveolar pathway. After endosomal acidification, the pH sensitive nature of the LNPs enables it to release CpG payload in close proximity to TLR9 receptors resulting in release of proinflammatory cytokines and an efficient immunostimulation.

3.2 Materials and methods

Reagents. 1,2-dioleoyl-3-trimethylammonium-propane (DOTAP), 1,2-dioleoyl-sn-glycero-3-phosphoethanolamine (DOPE), 1,2-distearoyl-sn-glycero-3-phosphoethanolamine-PEG2000 (PEG_{2K}-DSPE), 1,2-dioleoyl-sn-glycero-3-phosphoethanolamine-N-Cyanine 5.5 (Cy5.5-DSPE), Cholesterol hemisuccinate (CHEMS) and cholesterol (CHOL) were purchased from Avanti Polar Lipids. Cellulose acetate (CA) syringe filters were purchased from Macherey Nagel Inc. FITC-CpG 1826 was purchased from Invivogen. CpG 1826 having the sequence “TCCATGACGTTCTGACGTT” was synthesized by Integrated DNA Technology, Iowa. LysoTracker Red DND-99 and Hoechst 33342 were purchased from Life Technologies. Slide-a-lyzer dialysis cassettes (MWCO 20K, 3ml), Amicon™ ultracentrifugation filters (100K MWCO) as well as cell culture reagents such as Dulbecco’s modified eagle medium (DMEM), Opti-MEM® reduced serum medium, 1X Phosphate buffered saline solution (PBS) and Gibco™ TrypLE express enzyme (1X) was purchased from Fisher Scientific. Fetal bovine serum (FBS), Penicillin-Streptomycin 10/10 (100X) and L-Glutamine - 200mM (100X) were purchased from Atlanta Biologicals. Ultrapure water (18 MΩ) was used for preparation of all buffers and in all experiments. All solvents were of analytical grade, purchased from commercial sources. Buffers and solvents were filtered through 0.22 μm CA syringe filters before use.

Synthesis of FAP Peptide-Lipopolymer. The alkyne terminated FAP was synthesized on wang resin using standard solid phase peptide synthesis methods following its conjugation with N₃-PEG_{2K}-DSPE lipid via copper-catalyzed azide-alkyne cycloaddition as previously reported¹⁸⁰.

LNP formulation. The CpG solution was prepared at 50μg/ml concentration in 20 mM HEPES buffer (pH 7.4). Lipids DOTAP, DOPE, CHEMS, and DSPE-mPEG_{2K} were dissolved in methanol at a molar ratio of respectively 45:30:23:2 to produce LNPs at a N/P of 1, 5, 10 and 15. For tumor-targeted formulations, equimolar FAP- mPEG_{2K}-DSPE was used in place of DSPE-mPEG_{2K}. For pH non-sensitive formulation, CHOL was used in place of CHEMS. These aqueous and organic solutions were then mixed in a Chemtrix 3221 SOR chip at a 3:1 flow rate ratio (v/v; respectively) and total flow rate 2 mL/min. The LNP solution is immediately diluted to ~15% methanol before being dialyzed against a 500-fold volume of 20mM HEPES (pH 7.4) using a 20K MWCO cassette to remove methanol and unencapsulated CpG.

Size, Zeta potential and encapsulation. Particle sizes, size distributions, and ζ -potentials of the different preparations were determined using a Malvern Zetasizer Nano ZS dynamic light scattering device. All measurements were conducted at 25°C in triplicate and reported as the number mean \pm SD. For encapsulation efficiency, LNP samples were incubated with 1% Triton X-100 dissolved in HEPES buffer for 1hrs following addition of Quant-iT™ OliGreen ssDNA dye. Fluorescence generated by the intercalation of single-stranded oligonucleotide to dye was measured using the Synergy Biotek plate reader (excitation/emission wavelength 485/535 nm). Encapsulation efficiency was calculated as the fraction of fluorescence generated after dialysis compared to the fluorescence generated before dialysis.

Cryo-Transmission Electron Microscopy. Cryo-TEM experiments were conducted following the general procedures reported previously, except that C-Flat lacey carbon film on 400-mesh copper grids were used as sample substrates¹⁸⁴⁻¹⁸⁵. Images were obtained using a Talos F200C cryo-electron microscope operating at 200 kV under low-dose conditions at a nominal magnification of 120,000 or 150,000X and using different degrees of defocus (-3 to -7 nm) to obtain adequate phase contrast. Images were recorded using a Ceta 16 Mpixel CMOS camera. Image processing and analysis was performed with TIA (FEI, Inc). Image were acquired for LNP prepared at N/P of 1,5 and 10. Prior to freezing samples for cryo-TEM analysis, LNPs were concentrated to 10-15mg/ml using Amicon™ ultra centrifugation filters (100K MWCO) at 7,500 rcf for 2hrs.

Small Angle X-ray Scattering (SAXS). Small-angle X-ray scattering (SAXS) experiments were carried out utilizing a SAXSpoint 2.0 (Anton Paar) with a copper K α source ($\lambda = 1.54 \text{ \AA}$). An incident beam, fixed at 8.05 keV and collimated under vacuum using an advanced scatterless beam collimation (Anton Paar), was employed using a sample to detector distance of 350 mm. An EIGER R series Hybrid Photon Counting detector was used for data collection. Particles were concentrated to 10-15 mg/ml using Amicon™ ultra centrifugation filters (100K MWCO) at 7,500 rcf for 2hrs and placed in 1mm quartz capillaries (Anton Paar). Each data set was collected by averaging three frames of 5-minute exposures per frame. Data reduction was performed using SAXS analysis Version 2.50 (Anton Paar). Further background subtraction was performed using

Igor Pro 8.00 with Irena macros (Jan Ilavsky). Experiments were carried out at N/P ratio of 1,5 and 10.

Cell Viability Assay. Cell viability was measured using CellTiter 96® AQueous One Solution Cell Proliferation Assay from Promega. RAW 264.7 cells were seeded at 30,000 cells per well in 96-well plates in complete DMEM medium (supplemented with 10%FBS, 1% Penicillin-Streptomycin, 1% L-Glutamine) and allowed to adhere overnight at 37 °C, 5% CO₂, and 95% relative humidity. Cells were washed with PBS and incubated with LNP samples in Opti-MEM® media for 2 h. The cells were then washed with PBS and incubated overnight in complete DMEM media. Next, 20 µl of CellTiter 96® AQueous One Solution Reagent was added into each well and incubated for another 1 hr at 37°C before recording the absorbance at 490nm using a Synergy Biotek plate reader.

LNP cellular association studies. Cellular association with RAW 264.7 cells and MB49 cells was studied by seeding 30, 000 cells per well in 96-well plates and culturing them at 37 °C, 5% CO₂, and 95% relative humidity in complete DMEM media for 24 h to reach 80–90% confluency. Various Cy5.5 labelled LNP formulations were incubated with the cells for 2 h at 37 °C in Opti-MEM® media. The unbound LNPs were removed by aspirating the spent medium and washing the cells with 100 µl PBS thrice. The attached cells were detached by trypsinization and diluted with 160 µl PBS for flow cytometric analysis using a BD LSRFortessa equipped with a robotic high throughput sampler. The Cy5.5-tagged LNPs were excited with a 627nm red laser and emission was monitored using 670/14 filter.

Cellular localization studies in RAW264.7 cells. Spatio-temporal tracking analysis FITC-tagged CpG containing LNPs was performed using multiphoton confocal microscopy. RAW264.7 cells were cultured at 37 °C, 5% CO₂, and 95% relative humidity in complete DMEM at a cell density of 100,000 cells/well in 4 chambered slides. After 24 hrs, the culture media was replaced with Opti-MEM® media containing the non-targeted, targeted and targeted pH non-sensitive LNPs. Cells were treated for 2 h at 37 °C, followed by removal of the LNP suspension and rinsing of the cells three times with PBS. Next, the cells were incubated for 4 or 12 h in complete DMEM media. For imaging, nucleus was stained with Hoechst 33342 and acidic endosomal and lysosomal

compartments were stained with lysotracker red DND 99. Confocal images were acquired using Nikon A1R multiphoton confocal microscope with a 60X oil objective equipped with 405nm, 488nm and 561nm lasers for Hoechst 33342, FITC and Lysotracker red DND 99 respectively.

Release of TNF- α from Macrophage. RAW 264.7 cells were seeded at 30,000 cells per well in 96-well plates in DMEM medium and allowed to adhere overnight in a 37 °C incubator. Cells were washed with PBS and incubated with LNP samples in Opti-MEM® media for 2 hrs. The cells were then washed with PBS and incubated for 24 hrs in complete DMEM media. The spent media was collected and centrifuged at 10,000 rcf for 5 mins to remove any cellular debris. The supernatant was used to quantify the amount of TNF- α released using an ELISA kit from Invitrogen Inc according to manufacturer's protocol.

Human bladder tumor association studies. Bladder tumors obtained from a cystectomy section of 85-year-old white female suffering from papillary urothelial carcinoma was used to monitor the ability of FAP targeted LNPs to associated human tumors. Post-surgery the tumors were isolated and stored overnight in DMEM media at 4°C prior to treatment. Obtained tumor was washed extensively to remove any blood or serum stains. Then, tumors were incubated with Cy5.5 labelled targeted or non-targeted LNPs at a CpG dose of 10 μ g/ml for 2 hrs at 37°C in 20mM Hepes buffer. Next, the tumor chips were washed three times with 15 ml of 1X PBS. The tumors were imaged for LNP associated fluorescence using an IVIS Lumina II optical imaging system from Perkin Elmer equipped with Andor ikon CCD camera. Acquisition parameters for the epi-illumination image were as follows: Field of view: 5 cm; object height: 5 cm; excitation: 640/25 nm; emission: 732.5/37.5 nm; exposure time: 1 s; f/stop: 2; Binning: 2.

3.3 Results and discussion

Utilizing FAP as a targeting strategy to delivery drugs at bladder tumor sites has shown lot of promise for an enhanced therapeutic outcome. It leverages on the ability of BCG to “stick” to tumor sites without the adverse effects associated with bladder instillation of live bacterium. Previous studies show that FAP mediated uptake occurs via a caveolae mediated pathway with a strict 70nm cutoff. Liposomes represent one of the most clinically successful delivery system capable of delivering therapeutic molecules to target site¹⁸⁶. However, traditional methods of

downsizing liposomes to fit the 70nm cutoff involves extensive extrusion and sonication procedures which are not amenable for fragile immunostimulatory nucleic acids¹⁸⁷. Recently, another type of lipid-based delivery system, LNPs, formulated using microfluidic devices has shown unprecedented control over size, encapsulation of nucleic acid, therapeutic integrity of payload as well as scalability¹⁸⁸. Here we hypothesize that utilizing microfluidics approach to develop sub 70nm FAP targeted pH sensitive LNPs will significantly improve the therapeutic response of CpG oligonucleotide which is a well-studied nucleic acid for bladder cancer immunotherapy.

3.3.1 Physicochemical characterization of LNPs

Chemtrix microfluidic reactors used here consists of microfluidic channels ($300\ \mu\text{m} \times 120\ \mu\text{m}$) itched on to glass surfaces having a total reactor volume of $1\ \mu\text{l}$. Two static micromixers, called staggered oriented ridge (SOR) are employed where the two phases meet to increase the mixing efficiency ($T_{\text{mix}} < 0.3\text{s}$)¹⁸⁹. Self-assembly of dissolved lipids into LNPs occur as the lipids in organic solvent is rapidly diluted with the aqueous stream containing CpG oligonucleotides. The positively charged lipids interact with the anionic oligonucleotides to form nuclei around which further nanoprecipitation of lipid molecules can occur as the polarity is increase (**Figure 2**). Faster the mixing of aqueous and organic phase, faster is the increase in polarity and smaller is the size of LNPs produced. We have employed a fractional flowrate of 3:1 (aqueous: methanol) and a total flow rate of 2ml/min for formulation. LNPs were made at N/P of 1,5,10 and 15 to optimize for size, polydispersity and encapsulation. As seen in the Figure1. the size of LNPs reduces significantly from 40 nm N/P 1 to 13nm at N/P of 15. Surface charge of LNPs increase from -10mV at N/P of 1 to 16mV. This is because, at lower N/P ratio, as polarity increase, the fusion of metastable vesicles gives rise to larger LNPs with lamellar arrangement of CpG and lipids (**Figure 2, inset A**) The fusion will continue unless outer surface is stability sterically by PEGylation or prevented by membrane rigidity due to presence of CHEMS. However, higher N/P ratios leads to formation of more positively charged particles which gets primarily stabilized owing to its positive surface potential by electrostatic repulsion. These positive charged vesicles can easily recruit anionic CHEMS leading to membrane rigidity with further prevents fusion (**Figure 2, inset B**). Stabilization of LNPs at a much earlier stage of formation is the main reason for the marked difference in particle size and lamellarity. It should also be noted that at same N/P ratio of 5,

CHEMS leads to 37nm LNPs (Targeted pH sensitive LNPs) which is slightly larger particles as compared to CHOL (Targeted pH non-sensitive LNPs) which gives 30nm LNPs (Supplementary Figure 1). This is because recruitment of anionic CHEMS leads to decrease in cationic surface potential and subsequent membrane fusion. This is not in case of neutral CHOL, whose recruitment is albeit, slower due to lack of electrostatic attraction.

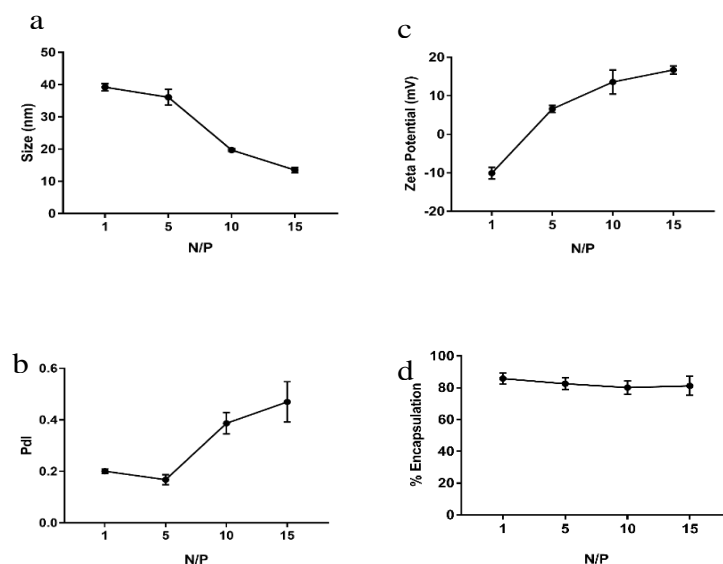


Figure 14. Lipid nanoparticles characteristics. (a) hydrodynamic diameter (number mean), (b) Polydispersity (c) Zeta Potential (d) % Encapsulation for LNPs manufactured by Chemtrix 3221 reactor at a CpG concentration of 50 $\mu\text{g/ml}$ and lipid composition of DOTAP, DOPE, CHEMS, and DSPE-mPEG_{2K} (ratio 45:30:23:2). Aqueous to organic flow rate ratio was 3:1 whereas the total flow rate was 2 ml/min. Results are the mean \pm SD (n=3).

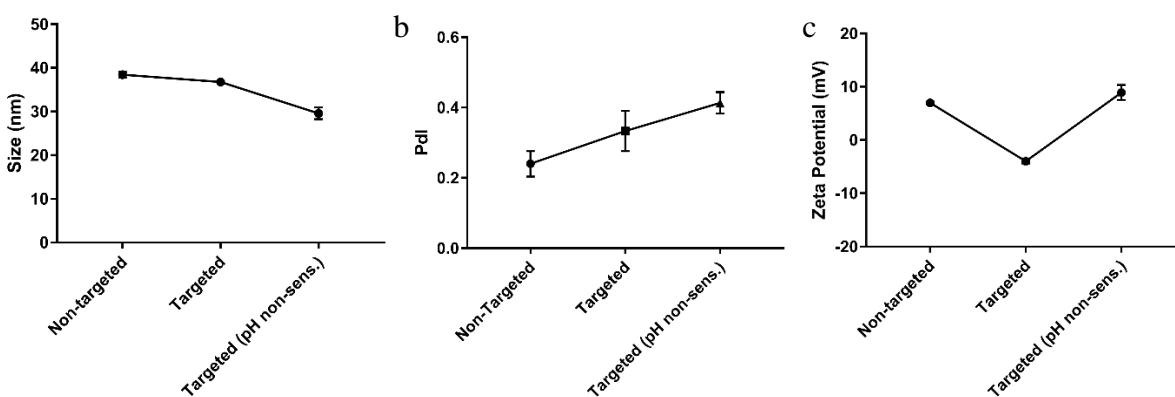


Figure 15. Physicochemical characterization of developed formulations at N/P of 5 (a) Size (b) Pdl (c) Zeta Potential. Results are the mean \pm SD (n=3).

We also find an increase in polydispersity as N/P ratio increases. One probable reason for this at higher N/P ratios formation of empty lipid vesicle is encouraged due to presence of more lipids. These empty vesicles undergo lipid exchange (Oswald ripening) increasing the polydispersity. Additionally, because of the smaller size the particles at high N/P ratio, the curvature on the surface of particles increases exposing hydrophobic acyl chains of the lipids to aqueous environment introducing thermodynamic instability in the system.

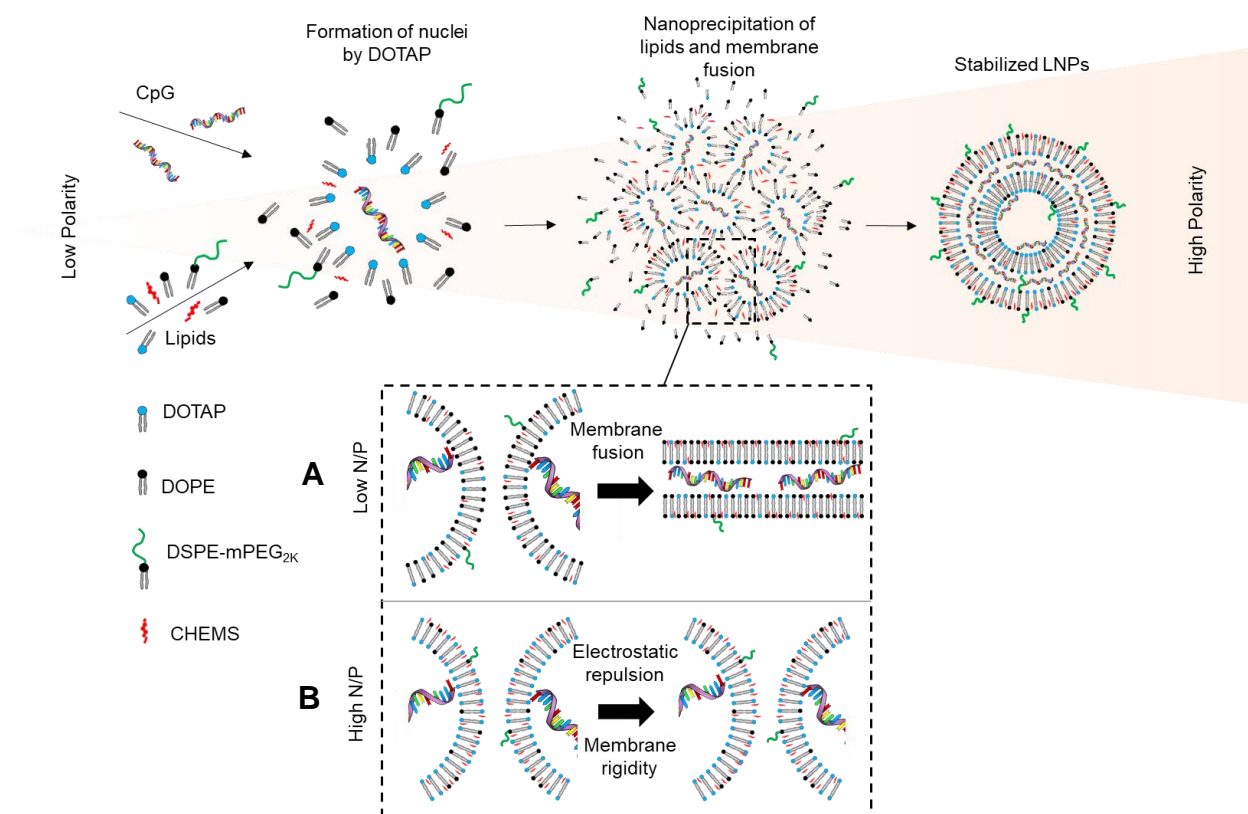


Figure 16. Proposed mechanism of LNP formation: The mixing of methanol phase with aqueous phase the cationic lipids are the first to interact with anionic CpG molecules forming inverted micelles. These micelles act as nuclei around which nanoprecipitation of lipids occur to form bilayer structures. These bilayer vesicles continue to fuse together forming larger vesicle with lamellar structures (A). At high N/P enhanced presence of cationic lipids on outer surface prevents membrane fusion by electrostatic repulsion and membrane rigidity due to faster recruitment of anionic CHEMS (B).

This was further supported by our Cryo-TEM data. At N/P 1 particles exhibit a very small interior core which is surrounded by electron dense layer. However, as N/P increases we find increase size of the interior core to almost a vesicular system of empty LNPs at N/P of 10. To understand if the

electron dense outer layer arises from stacking of oligonucleotides and lipid molecules we performed SAXS studies on developed LNPs. It is seen that SAXS produces scattering patterns suggestive of a stacked layer of lipids and oligonucleotide at a repetitive distance of 6.04 nm. It closely relates to the arrangement of siRNA and lipids (distance repeat of 5.8nm) in LNP formulation which recently completed phase 3 clinical trial to treat transthyretin (TTR)-induced amyloidosis¹⁹⁰. Also, it is worthwhile to mention here that multiple studies have shown that cationic lipids and plasmid DNA show characteristic peaks at $q=0.1\text{\AA}^{-1}$.¹⁹¹⁻¹⁹² At N/P of 5 and 10 the peak reduced in intensity and broadened indicating a transition from primarily lamellar structure to a vesicular formulation of amorphous nature.

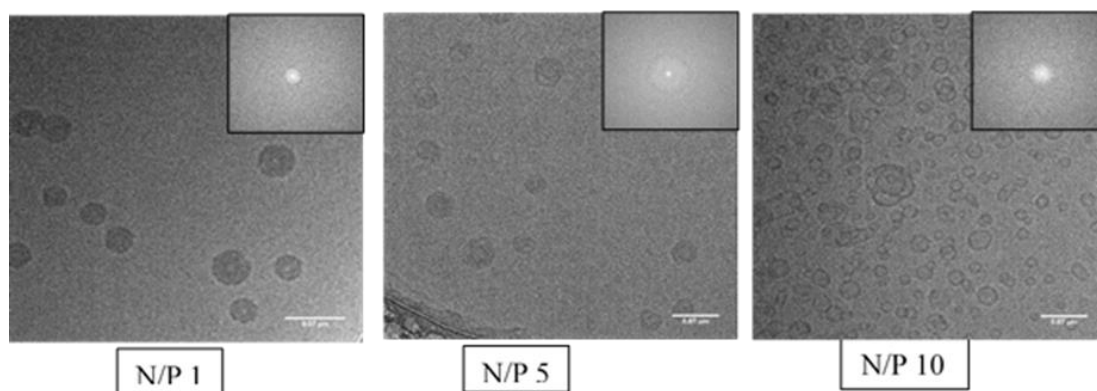


Figure 17. Cryo-TEM image of LNPs at (a) N/P 1 (b) N/P 5 (c) N/P 10 displaying a transition from electron dense system to vesicular system at high N/P ratios. Inset represents the Fast Fourier Transform (FFT) of respective images. LNPs were concentrated to 10-15mg/ml by ultra-centrifugation using 100K MWCO centrifuge filter at 7,500 rpm for 2 hrs

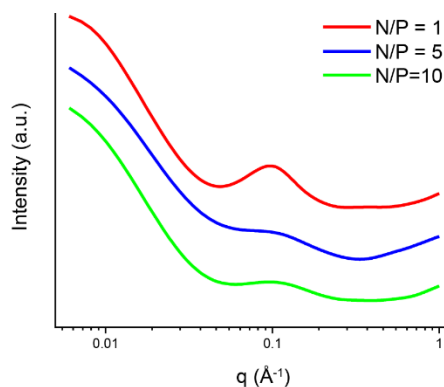


Figure 18. Small Angle X-Ray scattering data for CpG LNPs at different N/P ratio showing characteristic q value peak at 1\AA^{-1} suggesting a scattering pattern associated with bilayer systems. LNPs were concentrated to 10-15mg/ml by ultra-centrifugation using 100K MWCO centrifuge filter at 7,500 rpm for 2 hrs.

Next, we evaluated the effect of N/P ratio on encapsulation efficiency of developed LNPs. Interestingly we found similar encapsulation efficiency as we go from N/P 1 to 15. Increase in cationic lipids did not result in a significant increase in encapsulation of payload. Since N/P of 5 gave the optimum balance between size, polydispersity and surface potential we use this ratio for development of FAP-targeted pH sensitive for further biological evaluation.

3.3.2 Cellular association studies

Numerous studies have taken the advantage of utilizing peptide sequences to enhance cellular targetability of delivery systems. For e.g., Zhao et.al. utilized arginine-glycine-aspartic acid tripeptide (RGD) functionalized sterically stabilized liposomes to deliver paclitaxel to ovarian cancer cells expressing integrin receptors¹⁹³. Dai et.al. utilized N-acetyl-proline-histidine-serine-cysteine-asparagine-lysine (PHSCNK) sequence to functionalize pegylated liposomes to deliver doxorubicin to cells of tumor neovascular overexpressing $\alpha_5\beta_1$ integrin receptors¹⁹⁴. More recently, Sakurai et.al. utilized a non-standard macrocyclic peptide to deliver siRNA to epithelial cell adhesion molecule (EpCAM) overexpressing cancer cells¹⁹⁵.

Previously we have established that “GNRQRWFVWVLGSTNDPV” peptide displaying liposomes show sequence specific cellular association with MB49 cells both *in vitro* and in orthotopic bladder cancer model¹⁸⁰. Altering the critical “RWVF” to a scrambled sequence of “WVRF” resulted in suboptimal association¹⁸⁰. Additionally, lipopeptide was optimized at 2 mol% of lipids for liposomal formulations¹⁸⁰. However, self-assembly of lipids in microfluidic reactors poses challenge where by the targeting ligand could get buried inside the core of the LNPs during self-assembly process of LNP formation.

Thus, we evaluate the ability of FAP targeted LNPs formulated using microfluidics reactor to associate with fibronectin secreting cells of bladder tumor microenvironment. We used two cells lines, first MB49 and second a macrophagic cell line RAW264.7, also known to secrete fibronectin in extracellular matrix¹⁹⁶⁻²⁰⁰. Our flow cytometry data (**figure 4**) suggest an enhanced cellular association of our targeted formulation as compared to our non-targeted formulation or untreated (no LNPs) in both cell lines. Thus, proving that FAP targeting ligands are still exposed on the surface and available to bind to the fibronectin rich cellular surfaces. It is also important to mention

here, recent literature suggests a preferential accumulation of saturated lipid towards the periphery of LNPs for stabilization of outer shell during self-assembly process using microfluidics chip reactors^{190, 201}. Computer stimulation data also predicts distribution of PEG-lipid on the surface of LNPs²⁰². These studies indicate the advantage of conjugating targeting moieties to a PEG-saturated lipid construct for surface modifications of LNPs formulated using microfluidic devices.

Additionally, in comparison to non-targeted formulations, we observed 200% higher LNP associated fluorescence of targeted formulations in MB49 cells as compared to 75% in case of RAW264.7 cells which is suggestive of relative higher presence of fibronectin in extracellular surface of MB49 cells. Further, for non-targeted LNPs, nominal cellular association was also seen in both cell lines due to cationic nature of the LNPs.

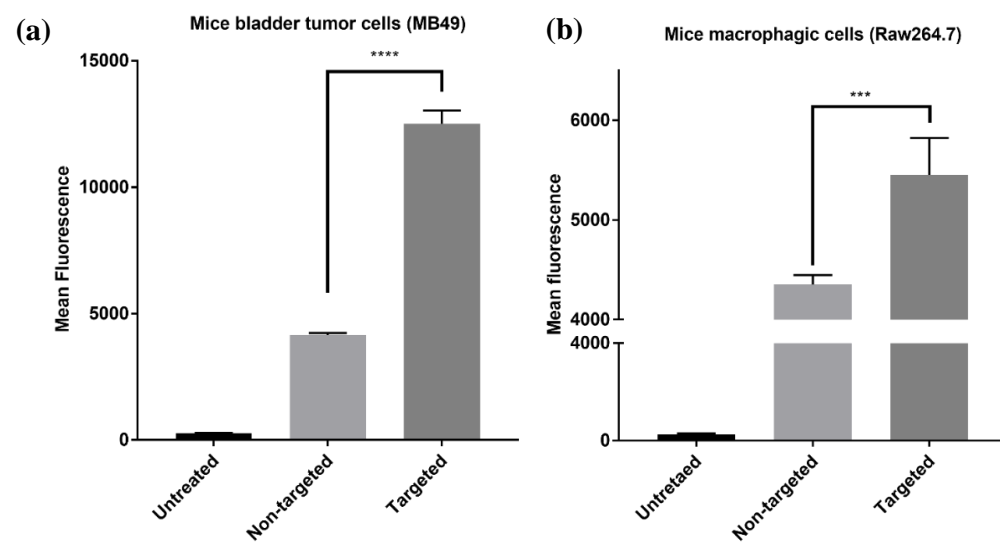


Figure 19. Flow cytometric evaluation of Cy5.5 labelled targeted and non-targeted LNPs for cellular association with (a) MB49 cells and (b) RAW264.7 cells. Cells were treated with LNPs for 2 h at 37 °C, followed by PBS washing to remove non-specific interactions, trypsinization, and resuspension in PBS for flow cytometry analysis. Error bars indicate the standard deviation of the mean (n=3, t-test, ****p<0.0001, ***p<0.001)

3.3.3 Enhanced immunostimulation by pH-sensitive targeted LNPs

For enhanced therapeutic outcome achieving a high delivery efficiency of payload to target cell is very important²⁰³. But, equally important is the ability of the delivery system to release the payload near the target effector within the cell²⁰⁴⁻²⁰⁶. A failure to do so, causes the delivery system to get degraded in lysosomal compartment and hence produces a sub optimal immunostimulatory

response. The presence of CHEMS and DOPE in our LNP formulation ensures efficient release of the payload within the acidic endosomal/lysosomal compartments where the target receptors (TLR9) responsible for CpG detection are present. Cholesterol hemisuccinate (CHEMS) under neutral conditions stabilizes DOPE in lamellar phase. However, within acidic endocytic membranes, protonation of CHEMS causes it to lose its stabilizing property and DOPE transitions into inverted hexagonal phase releasing the cargo^{154, 207}. Although CpG is a well-studied immunostimulatory oligonucleotides using orthotopic bladder cancer models of MB49 cells²⁰⁸⁻²¹⁰, there is no reports on positive immunostimulatory effects of CpG on MB49 cells in *in vitro* setting. This is due to the lack of TLR9 expression in these cells²¹¹. So, it can be concluded that the established therapeutic benefits of CpG in bladder tumors is mainly due to stimulation of infiltrating immune cells. Here, we used macrophagic RAW 264.7 cells, also capable of secreting fibronectin, to monitor the ability of CpG LNPs to elicit a therapeutic immune response by quantifying the release of TNF α under *in vitro* conditions. The cells were treated at a CpG dose of 1 μ g/ml for 2 hours. 12 hrs post-treatment, our targeted pH sensitive formulation showed the highest release of TNF α . However, both the non-targeted and pH non-sensitive formulation resulted in lower immunostimulation. This proves that both enhanced cellular association and endosomal release properties is essential for a successful therapeutics outcome. To ensure that the treatment did not result in cytotoxicity for cells we performed cellular viability by MTS assay. MTS assay is based on bio-reduction of MTS tetrazolium compound by living cells to colored formazan which is soluble in cell culture medium. As shown in **supplementary figure 2**, all treatment conditions were non-toxic to cells proving that the developed LNPs were biocompatible.

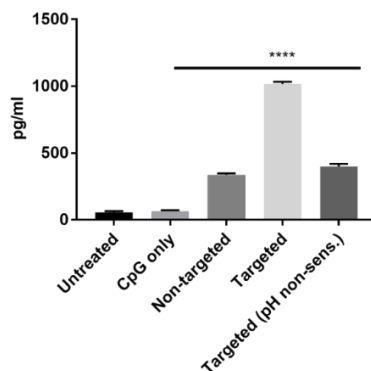


Figure 20. ELISA data for TNF α release by RAW264.7 cells to compare immunostimulatory potential of FAP-targeted pH sensitive LNPs vs Non-targeted or pH non-sensitive formulation. Cells were treated with LNPs at CpG dose of 1 μ g/ml for 2 hrs at 37°C followed by PBS wash. Cells were further incubated for 12hrs in FBS supplemented media after which supernatant was collected for ELISA. Error bars indicate standard deviation of the mean (n=3, one-way ANOVA, ****p<0.0001)

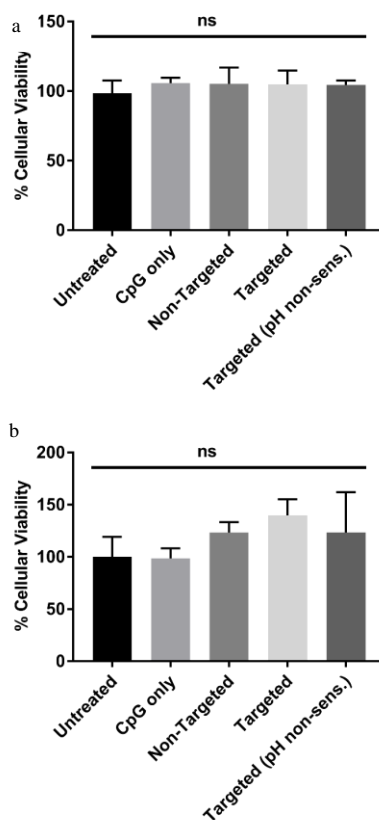


Figure 21. Cytotoxicity analysis of LNPs on (A) RAW264.7 cells (B) MB49 cells. Cells were treated with LNP formulations at a CpG dose of 1 μ g/ml for 2 hrs at 37°C followed by PBS wash. Cells were further incubated for 12hrs in FBS supplemented media. Cytotoxicity was measure by MTS assay. Error bars indicate standard deviation of the mean (n=3, one-way ANOVA, p=ns)

3.3.4 Cellular localization studies

Therapeutic outcome is function of the delivery system's ability to provide entry of the payload into the cell as well as it releases within the endosomes²¹²⁻²¹³. To track the efficiency of our pH sensitive targeted LNPs in delivering payload we used a FITC labelled CpG oligonucleotide and treated cells with non-targeted, targeted and targeted (pH non-sensitive) formulations. As seen in **figure 8**, we find minimal cellular entry, demonstrated by low FITC channel signal, for non-targeted CpG formulation (**figure 8a**) as compared to targeted formulations (**figure 8 b, c**) after 4hrs post-treatment. At this point, the Z-stack images of cells demonstrate that for targeted formulations (both pH sensitive and non-sensitive), FITC-tagged CpG gets colocalization within endosomal/lysosomal compartments stained with LysoTracker Red and visualized as yellow overlap (**figure 8 g, h**). However, after 12 h post-treatment, we find that for pH non-sensitive LNPs (**figure 8 f**) much higher amounts of FITC labelled CpG remaining within the endosomal/lysosomal compartments as compare to the pH sensitive formulation (**figure 8 e**) showing the capability of pH sensitive LNPs to release the therapeutic payload. This perfectly supports our ELISA results which show lower immunostimulation for targeted pH non-sensitive LNPs due inability to release the payload effectively under endosomal pH conditions.

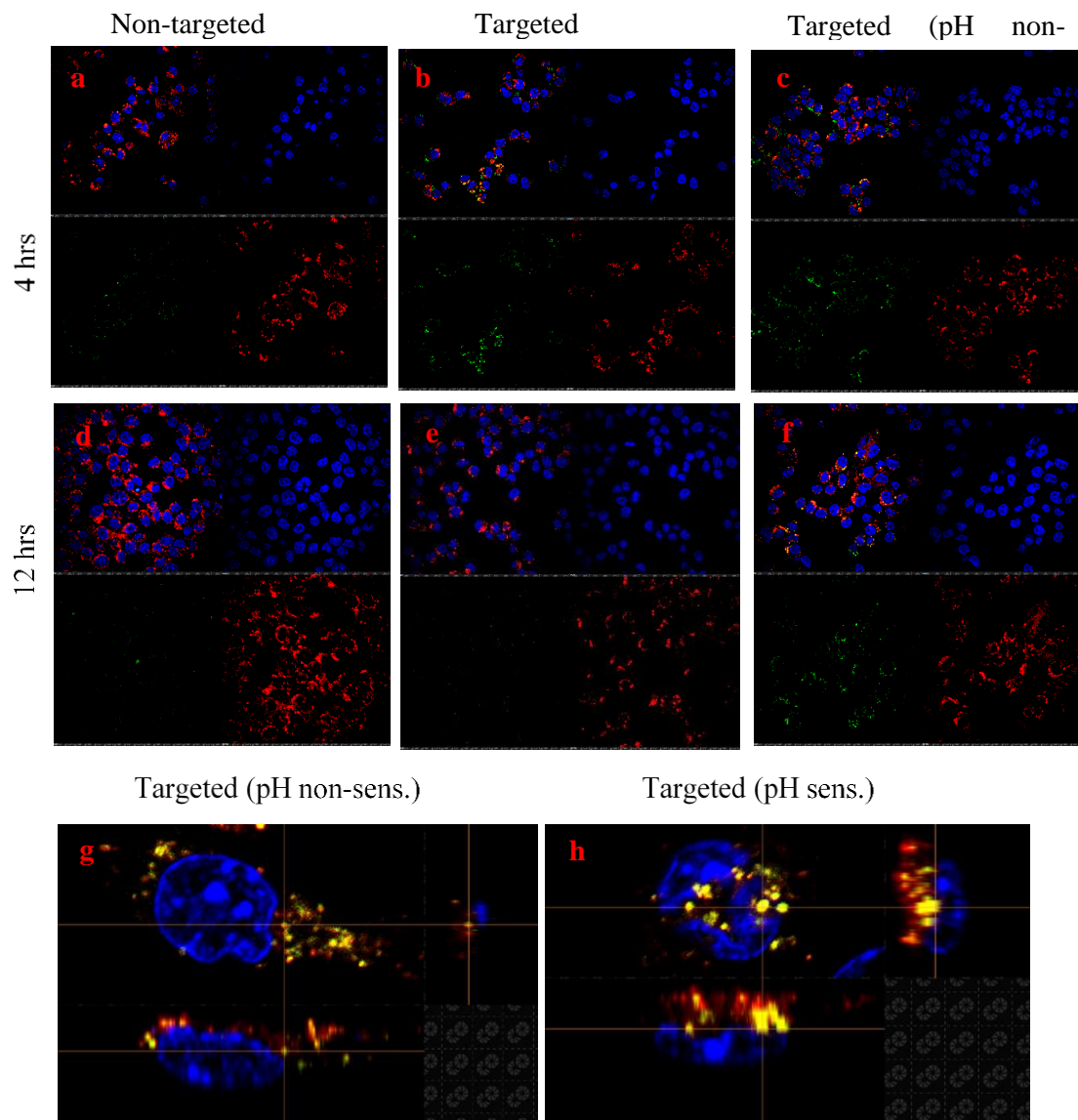


Figure 22. LNP tracking analysis by confocal microscopy in RAW 264.7 cells showing enhanced cellular entry of FITC tagged CpG for targeted formulations(b,c) as compared to non-targeted LNPs(a) after 4 hrs. After 12 hrs, reduced FITC-CpG signal for pH sensitive formulation (e) vs pH non-sensitive LNPs (f) shows endosomal release capability of pH sensitive LNPs. Z-stack images showing endosomal localization of FITC-CpG for targeted formulations after 4 hrs (g,h).

3.3.5 Human tumor association studies

Finally, to demonstrate the translational potential of FAP targeting we have performed preliminary association studies with human bladder tumor samples. Incubation was performed for 2 hrs at 37°C which the recommended retention time for intra-vesicular BCG therapy in clinics. Enhanced fluorescence of tumor sample treated with targeted formulation shows the ability of developed

targeting ligand to achieve higher association with human bladder tumor. Although we find a 34% increase fluorescence signal with our targeted formulation as compared to non-targeted formulations, further studies are underway to optimize formulation for enhanced penetration in clinically relevant tumors.

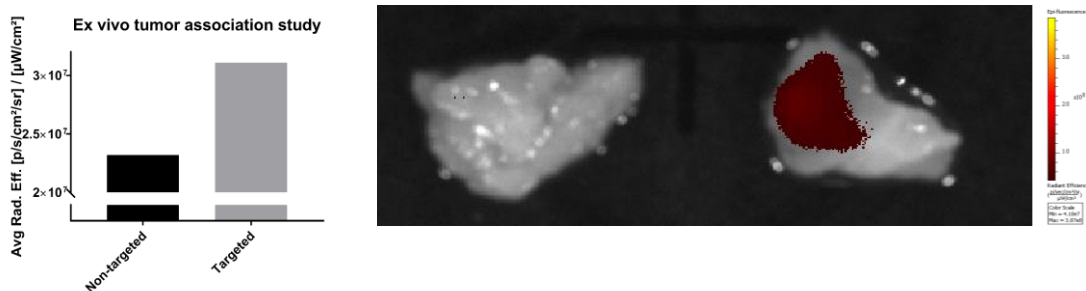


Figure 23. Tumor samples from a cystectomy section were incubated with Cy5.5 labelled LNPs at a CpG concentration of 10 $\mu\text{g/ml}$ for 2 hrs at 37°C. Fluorescent images were taken with IVIS Lumina II optical imaging system (excitation: 640/25 nm; emission: 732.5/37.5 nm).

3.4 Conclusion

We have developed a biocompatible pH sensitive targeted lipid nanoparticle system capable of delivering immunotherapeutic oligonucleotides to cells in bladder tumor microenvironment. The presence of FAP targeting ligand enables enhanced cellular association followed by internalization within endosomal compartments. The inherent pH sensitive nature of the LNPs enable release of the incorporated payload with the acidic endosomal compartments where they interact with TLR9 receptors to initiate a potent immune stimulatory response. Absence of either the targeting moiety or pH sensitive nature of the LNPs results in a sub optimal therapeutic response showing the importance of both FAP-targeting ligand and pH sensitivity of LNPs in developing a delivery system for bladder cancer immunotherapy.

CHAPTER 4. NON-VIRAL GENE DELIVERY VECTORS BASED ON CYCLODEXTRIN POLYMERS

Adapted (Reprinted) from the review article titled “Non-viral gene delivery vectors based on cyclodextrin polymers” co-authored by S.Samaddar, A.Kulkarni, and D.H.Thompson. Currently, the article manuscript is under preparation.

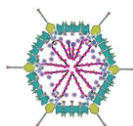
4.1 Introduction

Gene therapy is the utilization of nucleic acids to manipulate genetic information within a cell. It has provided researchers with unprecedented opportunities in treatment and mitigation of several life-threatening diseases. Gene therapy is an attractive alternative to conventional chemotherapy or radiation therapy due to its high efficiency, minimal side effects, and potential to evade drug resistance. The versatility of gene therapy makes it useful for the treatment of diseases as varied as cancer, viral, cardiovascular, neurological and production of DNA vaccines²¹⁴⁻²¹⁵. These genetic interventions can be broadly categorized into two different sub-genres. First, is the introduction of a new gene or transcript into the cell to help in production of a functional protein. Second, is down regulating the expression of mutated protein which is functioning improperly. An additional genetic intervention category is genome editing via Zinc finger nucleases (ZFNs), Transcription Activator Like Effector Nucleases (TALENs) or more recently discovered CRISPR/Cas9 system. Introduction of new gene involves the delivery of pDNA to augment naturally occurring proteins, produce cytotoxic proteins, prodrug-activating enzymes, or expression of viral genes that can result in immune responses.²¹⁵⁻²¹⁷ Downregulation or “knocking down” the expression of a mutated protein is achieved by introducing 21 – 23 nucleotides long fragments of RNA known as small interfering RNA (siRNA). On delivery, siRNA gets incorporated into the RNA-interference silencing complex (RISC) in the cytoplasm of the cell. The antisense strand is retained within the multi-functional protein present inside the RISC known as Argonaut 2 then unwinds the siRNA, leading to cleavage of the sense strand. activated RISC where it helps to selectively bind and degrade its complementary mRNA target. Due to its catalytic nature, appropriately designed siRNA can theoretically silence any gene in the body via cleavage of multiple mRNA strands, thus making it much more effective than antisense therapy and a promising therapeutic strategy.²¹⁸⁻²¹⁹. Administration of naked nucleic acids has been shown to have extremely poor efficacy due to poor

serum stability and their anionic nature, which results in low cellular uptake. The successful clinical translation of gene therapy is hence limited due to the absence of a controllable and safe method for gene delivery. Extensive research is being carried out in the development of efficient vectors for gene delivery that can circumvent the aforementioned barriers, however very few of them have achieved clinical success. Gene delivery vectors can be broadly classified into viral vectors and non-viral vectors.

Viral Delivery Systems

- Adenovirus,
- Adeno associated virus
- Retrovirus
- Lentivirus
- Epstein-Barr virus etc.



Advantages

- High transfection efficiency
- Stable transfection

Disadvantages

- Possibility to revert back to original infectious form
- Extremely Immunogenic-restricting
- repeated administration
- Safety concerns
- Large scale production challenges

Non-viral Delivery Systems

Physical Approaches:

- Needle Injection
- Gene gun
- Electroporation
- Ultrasound

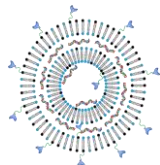


Limitations

- Invasive/Tissue damage
- Acute Immune / Inflammatory Responses
- Complicated procedure with costly instruments
- Difficulty in reaching deep tissues
- Low efficiency

Chemical Approaches

- Cationic Polymers
- Cationic lipids
- Lipid- Polymer hybrid



Advantages

- Easily tunable to specific needs
- Less immunogenic
- Less invasive
- Potentially targetable (Both at tissue level and cellular level)
- Large scale production

Disadvantages

- Toxicity Issues
- Lack of target specificity
- Poor *In-vivo* efficacy
- Non-Biodegradability

Figure 24 Viral and non-viral vectors

Viruses were a natural choice for delivery vectors due to their innate ability to infect specific cells. Viruses such as lentivirus, retrovirus, and adenovirus have been previously transformed into vectors for gene delivery by replacing the infectious part of the genome with a therapeutic gene. Despite advantages such as high efficiency and stable transfection, viral vectors received a major setback due to safety concerns such as toxicity and immunogenicity and difficulties with large-scale production. Viruses have a possibility to revert back to its original infectious form hence

making them unsafe for human therapy. They are also extremely immunogenic restricting their repeat administration due to possible dangers of severe immune reactions. Due to these reasons non-viral vectors are gaining prominence over viral vectors.²²⁰⁻²²² In December 2017, the FDA approval of first ever gene therapy, LUXTURNA®, an adeno associated virus based gene delivery strategy for patients suffering from hereditary biallelic RPE65 mutation associated retinal dystrophy. Although the approval has invigorated the enthusiasm in viral community, the treatment comes at a hefty price tag of \$850,000 for a single dose. Additionally, eye being an immuno-privileged region has advantage of less exposure to human immune system. Translation to systemic delivery without significant toxicity issues is still a major challenge yet to be overcome by viral delivery systems. Another milestone achievement in field of gene therapy came in August 2018 with the FDA approval of first ever gene silencing therapy. Onpattro®, a lipid-based siRNA nanodelivery system to treat hereditary transthyretin mediated amyloidosis showed that non-viral systems are now starting to break the low transfection barrier. However, additional challenges are now needed to be met to target organs beyond liver since systemic delivery for nanoparticles naturally tends to be cleared by liver. Additionally, at an annual price tag of \$345,000 it is still very expensive treatment.

Non-viral vectors are relatively less immunogenic when compared to viral vectors, safer, and highly scalable. However, most non-viral vectors suffer from issues such as low efficacy and transient transfection²²³. Most commonly, non-viral vectors are cationic materials that can electrostatically complex with the nucleic acid and condense it into positively charged nanoparticles that can protect the cargo and internalize into cells. The most commonly used non-viral vectors include cationic lipids²²⁴. Cationic polymers such as poly(ethylene imine) (PEI)²²⁵, or polypeptides such as polylysine (PLL) (Fig. 1)²²⁶. Other materials that are being studied and developed for gene delivery include PAMAM dendrimers²²⁷⁻²²⁸ Polyaminoesters²²⁹⁻²³⁰, polyamidoamines²³¹, polyphosphoesters²³², chitosans²³³, and gold nanoparticles²³⁴. All these vectors are capable of condensing nucleic acids into stable positively charged nanoparticles that enter cells via non-specific uptake mechanisms. While these materials can successfully protect the nucleic acid from degradation and increase their cell permeability, most of them suffer from significant cytotoxicity, lack of specificity, and low circulation times in the body²³⁵⁻²³⁶. The barrier for clinical translation is to create non-viral vectors that have high transfection efficiencies while

maintaining high specificity, *in vivo* stability, low toxicity. This requires an integration of various factors such as serum stability, specific binding to target cells, and efficient un-packaging and release of the cargo upon cellular internalization.

The use of low-cost materials that are considered as GRAS (Generally Regarded As Safe) in the formulation of vectors is a promising strategy to ensure low-toxicity and minimal off-target effects. Several formulations have employed carbohydrate vehicles such as chitosan¹⁹, hyaluronic acid²³⁷, and cyclodextrins (CDs). Cyclodextrin based materials were first used for gene delivery in 1999²³⁸. Since that time several, CD containing polymers have been developed and studied as vectors for gene delivery. This review focuses on CD based materials that have been developed and used for nucleic acid delivery between the period of 2012 till 2018.

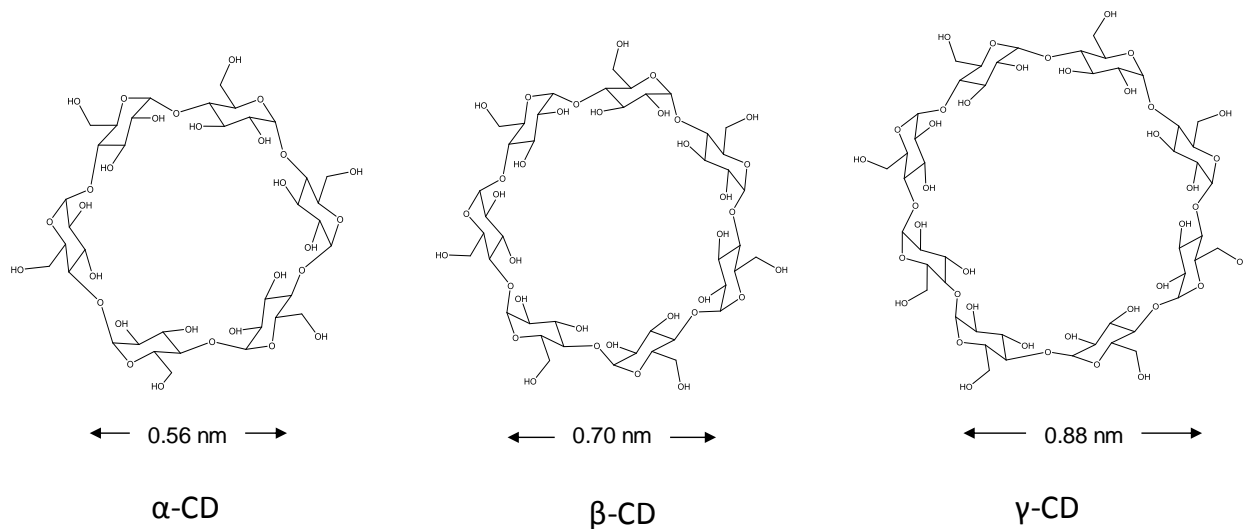


Figure 25. Types of cyclodextrin with cavity diameter

CDs are a family of cyclic oligosaccharides that have extensive applications in the food, agrochemical, and pharmaceutical industries. The three main types of CDs that exist are α , β , and γ , which are oligosaccharides of 5, 6 or 7, glucose units (Fig. 2)²³⁹. There are numerous variations of these CDs that are used for different applications. CDs have a large number of hydroxyl groups hence making them extremely water-soluble. The water solubilities of α -, β - and γ -CD at ambient conditions are approximately 13%, 2% and 26% (w/w), respectively²⁴⁰. Despite the high solubility of the CDs, the interior of the cup is relatively less polar making it a hydrophobic microenvironment. CDs hence have a hydrophilic exterior and a hydrophobic interior allowing

them to encapsulate and solubilize hydrophobic “guest” molecules.²⁵ This ability to form host:guest complexes with hydrophobic moieties makes them extremely attractive in the pharmaceutical industry for solubilization of hydrophobic drug molecules (Figure 3)^{241 242} .

Due to their biocompatibility and non-toxic nature, CDs are Generally Regarded As Safe materials by the FDA and hence are commonly used in the pharmaceutical industry for improving the solubility, bioavailability and stability of drugs. There are more than 45 approved CD based formulations of drugs in world markets²³⁹. Due to their unique structures and host:guest complexation abilities, CDs are also used extensively in constructing nanoparticle based drug delivery vehicles²⁶. The most successful example is the design and development of IT-101 by Davis and coworkers for the encapsulation and delivery of camptothecin to tumors²⁴³. The biocompatibility, water solubility, and binding affinity of CDs for a wide range of compounds can hence be exploited for the construction of novel and effective vectors for gene delivery. The unique property of CDs to act as nanometric containers²⁴⁴, their ability to improve drug bioavailability, their ability to enhance membrane absorption, and most importantly their ability to stabilize biomolecules in physiological media by shielding them from non-specific interactions²⁴⁵, makes them extremely attractive for the construction of gene delivery vectors.

4.2 CD-based polyrotaxanes

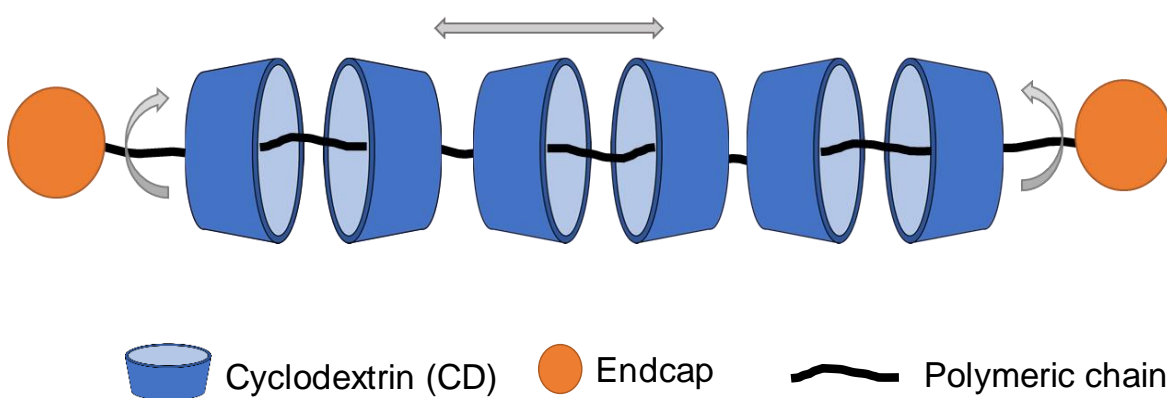


Figure 26. Diagrammatic representation of polyrotaxane with arrows showing degrees of freedom

Polyrotaxanes (PRs) are self-assembled structures consisting of a molecular macrocycle(s) threaded onto a polymeric chain. These structures are then entrapped by bulky blocking groups

(also referred to as endcaps) attached to the polymer terminus, which prevent the macrocycles from dethreading (Fig 4). The efficacy of the threading is governed by the non-covalent interactions between the polymer and the macrocycle(s) and the adjacent macrocycles. If the polymer lack endgroups or if the size of the endgroups is not large enough to prevent the dethreading of the macrocycles, the complex is termed as a pseudopolyrotaxane (i.e., false wheel and axle)²⁴⁶⁻²⁴⁹.

The construction of PRs from FDA approved materials such as CDs for the macrocyclic moiety and PEG/Pluronics based polymers as the polymeric axle make them highly attractive for biomedical applications. Attachment of cationic groups to the CDs gives them the ability to complex nucleic acids. The facile rotation and translational motion of the CDs across the polymeric axle make the PRs highly effective agents for complexing genes at lower N/P ratios (ratio of +ve charges on polymer to -ve charges on nucleic acid). This hence results in a lower overall positive charge resulting in a significantly lower toxicity profile and higher stability *in vivo*²⁵⁰.

Cellular entry of cationic PR polyplexes occurs primarily by two pathways, at least in absence of serum. First is the non-specific electrostatic interactions between the cationic complexes and anionic cellular membrane. Second, if the polyplex presents a ligand for a receptor at its surface, receptor mediated endocytosis can be the predominant mode of cellular internalization. However, in presence of serum, one must be aware that the cationic polyplex can bind to serum proteins (protein corona) which then bind to cells through their specific receptors. Once internalized within the cells, inability to release nucleic acid payload in the cytoplasm can mark the endosomal content for lysosomal degradation, resulting in sub-optimal biological outcome. Cationic polyplex (e.g., polyplexes with amine containing polycations) are thought to rupture endosomes by creating osmotic pressure (proton sponge effect), thereby enabling the carrier system to escape the endosomal compartment. However, the exact location of release of payload from delivery system is ambiguous. In the case of siRNA payloads, cytoplasmic release is sufficient for the nucleotide to engage RISC complex and cause gene suppression. But for gene expression using plasmid DNA, the payload must be able to translocate to the nucleus for the transcription mechanism to happen. Under such situations, release of pDNA far away from the peri-nuclear space can lead to loss of protection and cytosolic degradation. Multiple studies have underscored the importance of

cytoskeletal motor proteins to transport genetic materials along microtubules from periphery of cytoplasm to the perinuclear regions^{39, 251-252}. However, whether the transport occurs as endosomes containing polyplex, polyplexes themselves or naked pDNA is not clear. Once delivered to perinuclear space, the pDNA must get past the nuclear membrane to express the coded protein. For this, it can rely on either of nuclear localization sequences which can be tethered to the pDNA to enable its energy dependent transport into the nucleus or it should wait (which depending on its cellular life time) for mitosis for nuclear membrane to break down to gain access by an energy independent mechanism²⁵³⁻²⁵⁴.

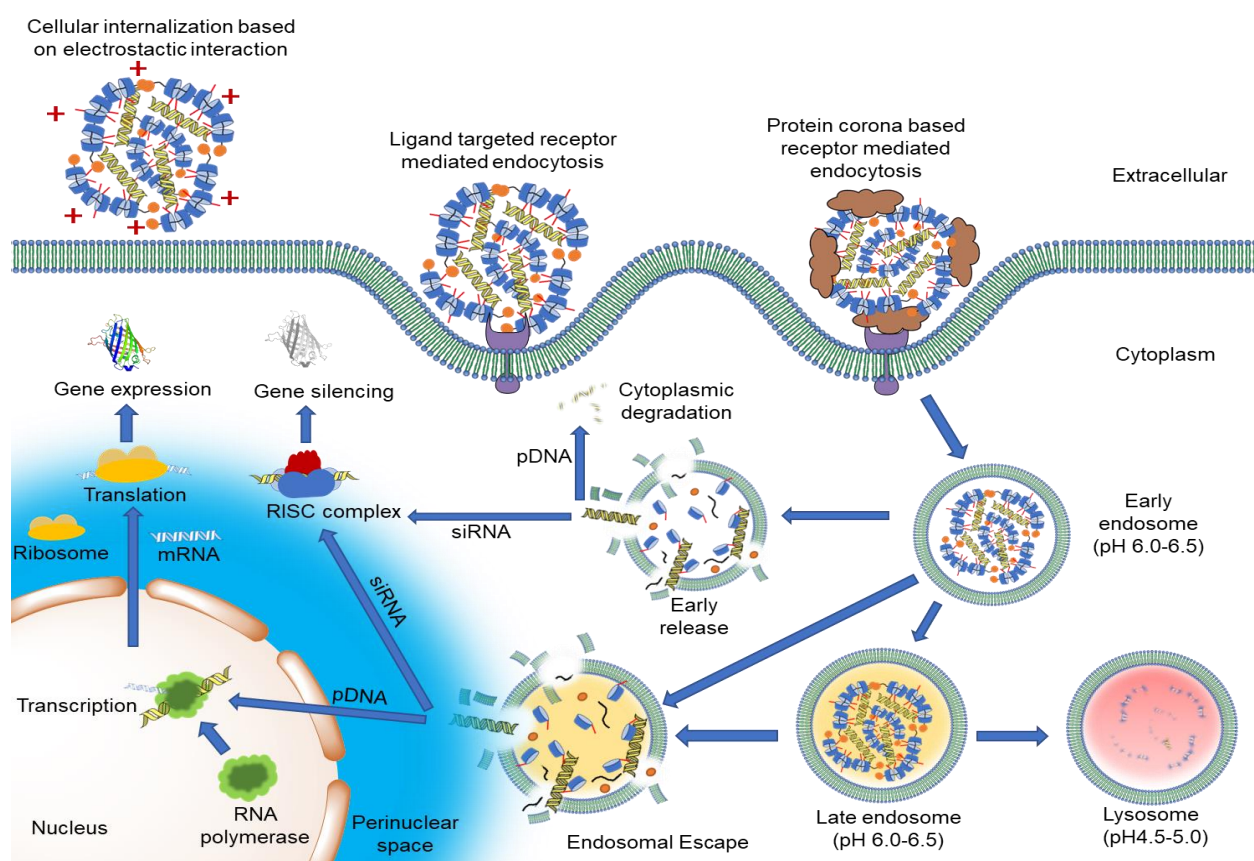


Figure 27 Diagrammatic representation of cellular pathways involved in gene delivery via polyrotaxanes.

The most common type of CD-PR gene delivery vehicle consists of CDs threaded on a single polymeric block. The resulting PRs are then post-modified by grafting the surface with cationic groups in order to enhance the overall PR solubility and ability to condense nucleic acids. Li and

coworkers have reported the synthesis of a series of cationic PRs with multiple oligoethylenimine(OEI)-grafted α -CDs threaded on a PEO chain as gene delivery vectors (Fig 6a)^{255 256}. The PRs were able to compact pDNA efficiently into nanoparticles of 100-200 nm in size and demonstrated low cytotoxicity with comparable or higher transfection efficiency as branched PEI (25K) in BHK-21 and MES-SA kidney cell lines. The authors showed that higher concentrations of cations in the PRs promoted better transfection performance. Interestingly, in some cases the presence of serum produced higher transfection efficiency than without serum when compared to PEI at N/P ratio of 10²⁵⁷. The authors further expanded the scope of their study by synthesizing PRs wherein the α -CDs were threaded onto a poly[(ethylene oxide)-ran-(propylene oxide)] (P(EO-r-PO)) random copolymer chain²⁵⁸. The authors demonstrated that their synthesized cationic PRs had a molecular weight of 2370 Da and an EO/PO molar ratio of 4:1, while the cationic α -CDs that were grafted with linear or branched oligoethylenimine (OEI) of various chain lengths had molecular weights up to 600 Da. The OEI-grafted alpha-CD rings were located selectively on the EO segments of the polymer while the PO segments had no CDs complexed onto them. This in turn resulted in increased mobility of the α -CDs and greater flexibility of the PRs. It was anticipated that this increased flexibility would enhance the interaction of the cationic groups with the nucleic acid and/or the cellular membrane resulting in higher transfection efficiency. The authors studied the biological activity of these PRs in a range of cell lines such as HEK293, COS7, BHK-21, SKOV-3, and MES-SA. Cytotoxicity studies revealed that the PRs with linear OEI chains of molecular weights up to 423 Da exhibited much less cytotoxicity than the branched PEI (25 kDa) in both HEK293 and COS7 cell lines. The cationic PRs also displayed high transfection efficiencies in all the cell lines with significantly higher transfection efficiency than branched PEI (25 kDa) in HEK 293 cells.

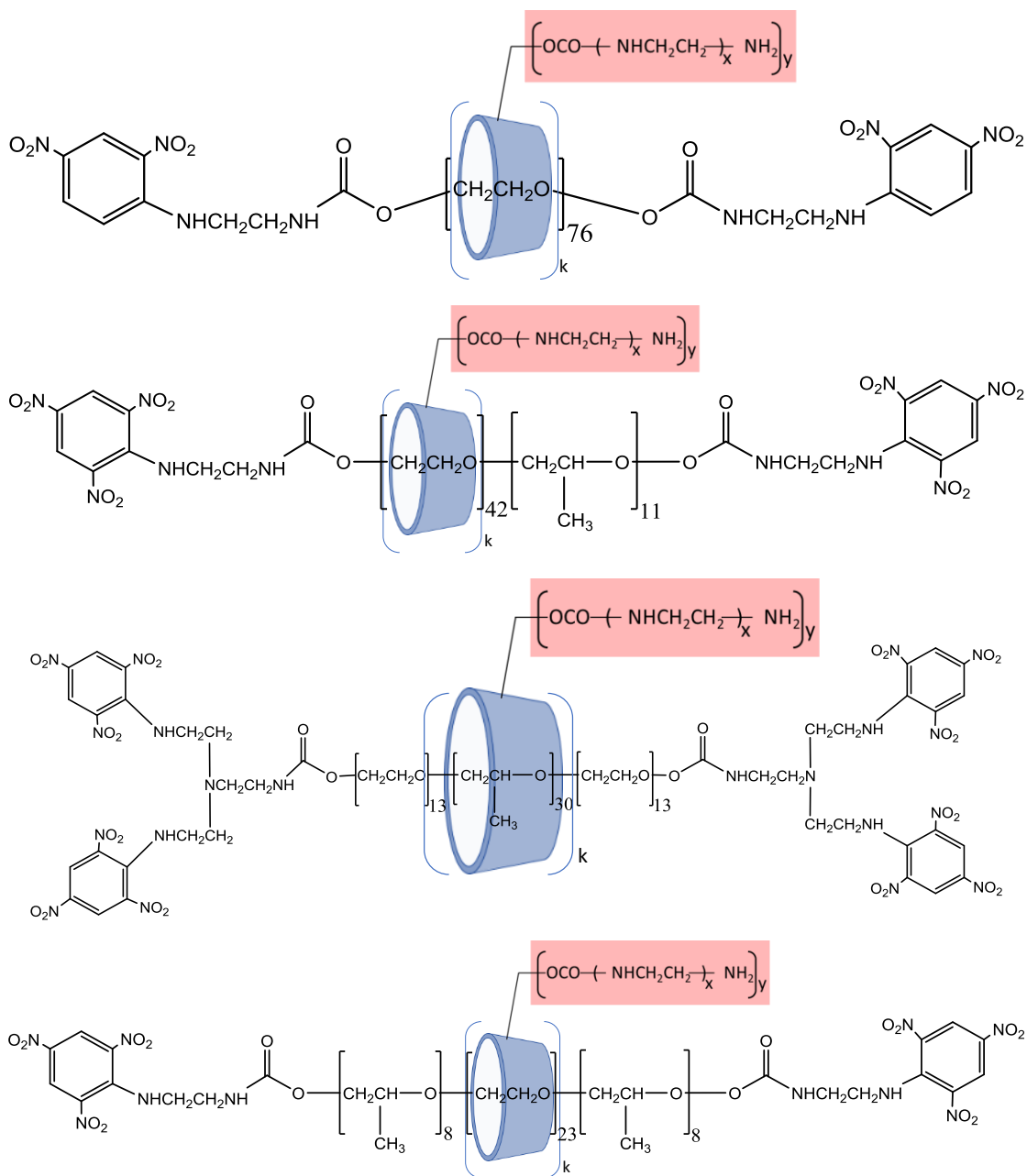


Figure 28. PRs with multiple oligoethylenimine(OEI)-grafted (a) α -CDs threaded on a PEO chain. $K=15$; $x=1/5/9$; $y=5.2/4.9/2.3$ (b) α -CDs threaded on a poly(EO-r-PO) random copolymer chain. $K=12$; $x=1/5/9/14$; $y=4.4/4.8/2.6/3.1$ (c) β -CDs threaded on a PEO-b-PPO-b-PEO triblock chain. $K=13$; $x=1/5/9$; $y=6.7/5.3/3.4$ (d) α -CDs threaded on a PPO-b-PEO-b-PPO triblock backbone $K=8$; $x=1/5/9/14$; $y=5.3/5.0/2.3/3.5$

Li and coworkers also synthesized cationic PRs consisting of multiple OEI-grafted β -CD rings threaded on a PEO-b-PPO-b-PEO triblock copolymer chain(Fig 6b)²⁵⁹. In this case, β -CD was

complexed selectively on the PPO block followed by endcapping with TNB-endcaps. Fluorescence titration assay confirmed the ability of the cationic PR to condense pDNA at N/P ratios higher than 2. *In vitro* studies of the cationic PRs in SKOV-3 and PC3 cancer cells lines revealed low cytotoxicity and high transfection efficiency of the PRs comparable or significantly higher than that of the PEI (25 kDa) standard. While PEI transfection efficiency is known to decrease with increasing N/P ratio, the cationic PRs display a sustained gene delivery capability in PC3 cell, both in presence and absence of serum.

Similarly, this group has also explored the triblock polymers based on PPO-*b*-PEO-*b*-PPO for the synthesis of amphiphilic cationic PRs as potential gene delivery carriers (Fig 6c). They have synthesized cationic PRs consisting of α -CD rings grafted with OEI chains threaded on PPO-*b*-PEO-*b*-PPO amphiphilic triblock polymers²⁵⁵. These novel amphiphilic supramolecules have very low cytotoxicity in both HEK293 and COS7 cells in comparison with PEI (25K) due to the low positive charge density of the cationic PRs/pDNA complexes. Studies revealed that the PRs had very high transfection efficiency as much as 7 to 10-fold higher than PEI (25k) in HEK293 cells lines. Moreover, the cationic PRs displayed sustained gene delivery capabilities in both serum and serum free conditions while the PEI efficiency decreased with increased expression duration.

As a further development, this group also explored the use of polyrotaxane as a hydrogel-based gene delivery system. They prepared a few biodegradable triblock copolymers of methoxy-poly(ethylene glycol)-*b*-poly(ϵ -caprolactone)-*b*-poly-[2-(dimethylamino)ethyl methacrylate] (MPEG-PCL-PDMAEMA) with well-defined cationic block lengths to condense pDNA²⁶⁰. The mPEG-PCL-PDMAEMA copolymers exhibit good ability to condense pDNA into 275–405 nm polyplexes with hydrophilic mPEG in the outer corona. The mPEG corona imparted greater stability to the pDNA polyplexes and also served as an anchoring segment when the pDNA polyplexes were encapsulated in α -CD-based supramolecular pseudopolyrotaxane hydrogels. More interestingly, the resultant hydrogels were able to sustain release of pDNA up to 6 days. The pDNA was released in the form of polyplex nanoparticles as it was bound electrostatically to the cationic segment of the mPEG-PCL-PDMAEMA copolymers. The overall results showed protein expression levels that were comparable to PEI. These materials also displayed thixotropic properties and were easily prepared without using organic solvent, suggesting that they may be useful as injectable materials for sustained gene delivery.

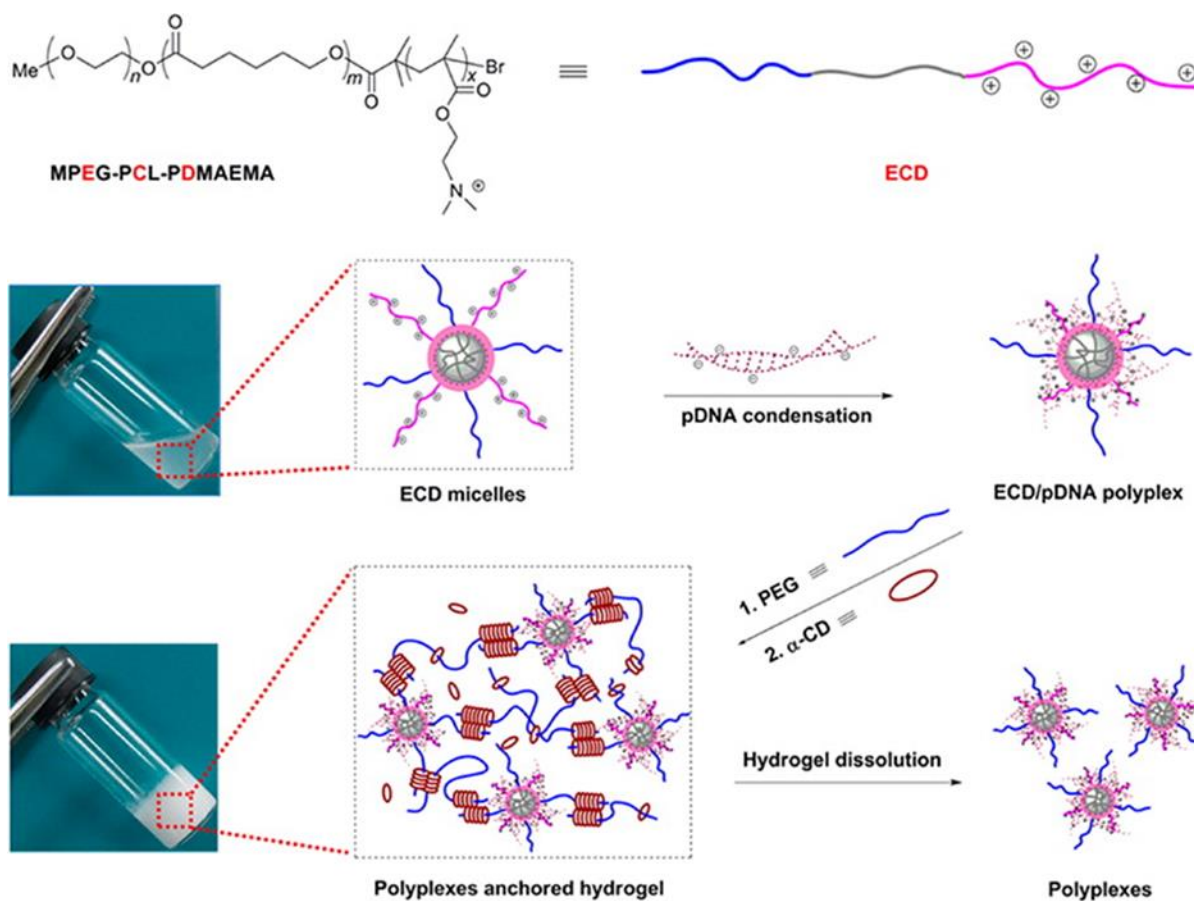


Figure 29. (Reprint) PR based supramolecular hydrogels. Amphiphilic ECD forms micelles under aqueous environment with PCL core and mPEG/PDMAEMA corona. PDMAEMA at the corona is responsible for pDNA binding while MPEG serves both as stabilizing moiety for the resultant ECD/pDNA polyplex and hydrogel anchoring segment. Sustained release of pDNA polyplexes is achieved via hydrogel dissolution over time

Liu and coworkers have also synthesized two pseudoPRs based on anthryl-grafted β -CDs threaded on PPG chain²⁶¹. Addition of the pseudoPRs to calf thymus DNA in solution promoted the formation of spherical nanoparticles with an average diameter of 100 nm. The group findings confirm the ability of the anthryl-grafted pseudoPRs as intercalators for condensing DNA again suggesting potential applications for gene delivery. An improved design utilized a 2-dimensional pseudopolyrotaxane constructed by threading ω -aminohexylamino β CD on a PPG4000 polymer

backbone, followed by complexing cucurbit[6]uril units (20) on the branches of the modified CDs (Fig.)²⁶²⁻²⁶³.

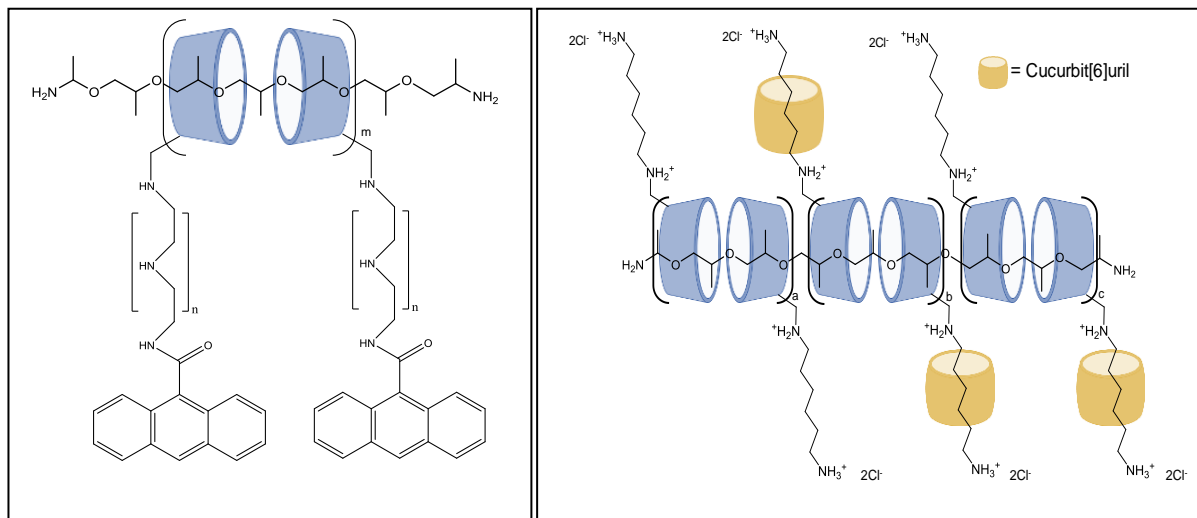


Figure 30. (a) Anthryl grafted β -CD pseudopolyrotaxane. $m=4.5,5$ for $n=0,1$ respectively (b) 2-dimensional pseudopolyrotaxane. $a+b+c=24$

A related intercalation strategy was adopted by Sakurai *et al* who synthesized PRs with groups for binding and condensing DNA into nanocomplexes. They have developed α -CD PRs threaded on a PEG chain (M.W. 2 or 20 kDa) endcapped with fluorene groups, a known DNA intercalator with a high binding constants (10^6 M^{-1})²⁶⁴. AFM imaging revealed that only the PR with 20 kDa PEG chain when mixed with DNA was able to act as a bridge between the DNA strands by holding them with fluorene end groups. This work demonstrated that DNA intercalators could be used for complexation and manipulation of DNA.

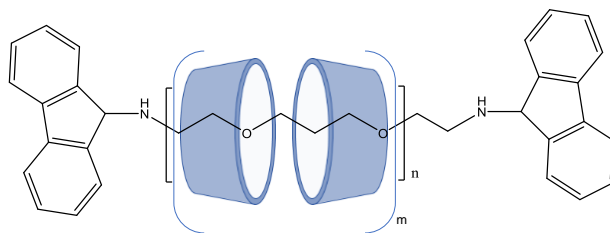


Figure 31. Fluorene capped DNA intercalating PR. $m=n/a$; ($n \sim 23$ or 230)

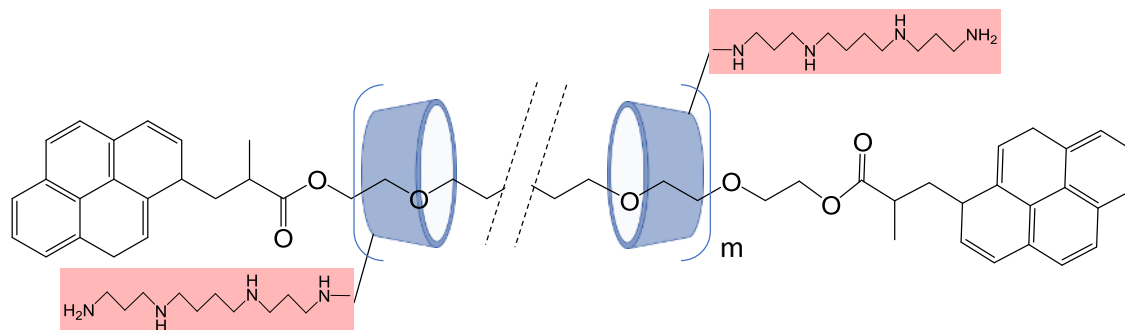


Figure 32. Spermine grafted PR where $m=5.5$

A unique approach, developed by Pérès and coworkers involves two hydrolysable cationic PRs spermine grafted α -CD synthesized by two distinct pathways²⁶⁵. They used polyethylene oxide (M.W 1100) as their backbone and pyrene molecule as endcaps. Their first strategy consisted of post modifying α -CD PRs with spermine moieties by first selectively oxidizing all the secondary alcohols of the CDs following by the addition of spermine groups via reductive amination. To improve their control in the CD grafting reaction, a second strategy was designed in which the α -CDs were first modified by the same oxidation reductive amination sequence, followed by the synthesis of the PR. This strategy provided better control over the degree of substitution on the α -CDs hydroxyl groups and the amount of threading. Small Angle Neutron Scattering (SANS) analysis of the developed PRs showed a rod-like asymptotic behavior. These novel cationic PRs showed rapid degradation at cytoplasmic pH 6.5 and were proposed as a biodegradable gene delivery vehicle.

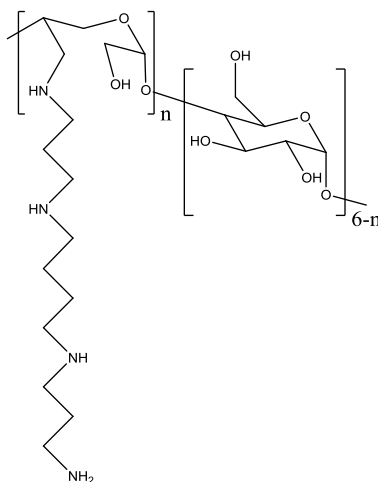


Figure 33. Spermine modified α CD where $n = 2,3$ or 6

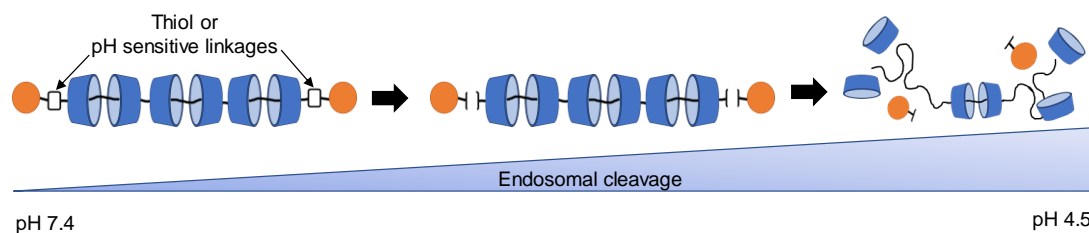


Figure 34. Diagrammatic representation of cyclodextrin delivery using pH sensitive polyrotaxane.

Yui and coworkers have developed a library of bio-cleavable PRs for enhanced gene transfection consisting of modified α -cyclodextrins with dimethylaminoethyl groups (DMAE- α -CDs) threaded on PEO chain and capped with benzyloxycarbonyl-L-tyrosine via disulfide linkages (DMAE-SS-PRX) (FIG 13).²⁶⁶⁻²⁶⁸ # # # All the synthesized DMAE-SS-PRXs were able to form stable polyplex with pDNA at low N/P ratios. Remarkably, most of the DMAE-SS-PRX/pDNA complexes were stable even after exposure to dextran sulfate as a pDNA binding competitor, indicating a stable complex. In contrast, most of the supramolecular complexes dissociate in the presence of DTT (10 mM) and dextran sulfate to release the pDNA. These observations were attributed to the cleavage of the disulfide bond by the DTT, thereby promoting dethreading of the PR and disassembly of the complex. Most of the DMAE-SS-PRX complexes resulted in high gene transfection efficiency independent of the N/P ratios above 2. The transfection was significantly enhanced with those PRs having the lowest number of α -CDs and amino groups with the exception of the lowest threaded α -CDs PR with the lowest amount of amino group. These findings suggest that premature pDNA release in the cytosol may cause pDNA degradation by cytosolic nucleases. Hence, the transfection efficiency is strongly dependent on the time of pDNA release within cells. This group has further demonstrated the application of the bio-cleavable PRs for siRNA complexation²⁶⁹ # and delivery²⁷⁰ # , as well as their use in PR:DNA complexes within lipid nanoparticles for improved bioavailability. Yui and coworkers demonstrated that the bio-cleavable PRs had gene silencing efficiency comparable to linear PEI (25 kDa) and superior to non-cleavable PRs hence emphasizing the importance of the degradability of the PR²⁷¹ # . Moreover, in attempt to achieve targetability, functionalized PRs were utilized to investigate the relation to multivalent interactions between the mannose moiety and Con A immobilized surfaces. The SPR spectroscopy results showed a higher response of the mannose-conjugated PRs than any other mannose conjugate on both surfaces of high- and low-density Con A. A further investigation using FRET

studies revealed that the mobility of α -cyclodextrins in the PR more efficiently contributes to their binding interactions in a multivalent manner. The studied system was shown to have control over ligand density, ligand mobility, and gives an efficient response to the biological interaction receptor, which has not been easy to achieve in covalently bound polymeric systems²⁷².

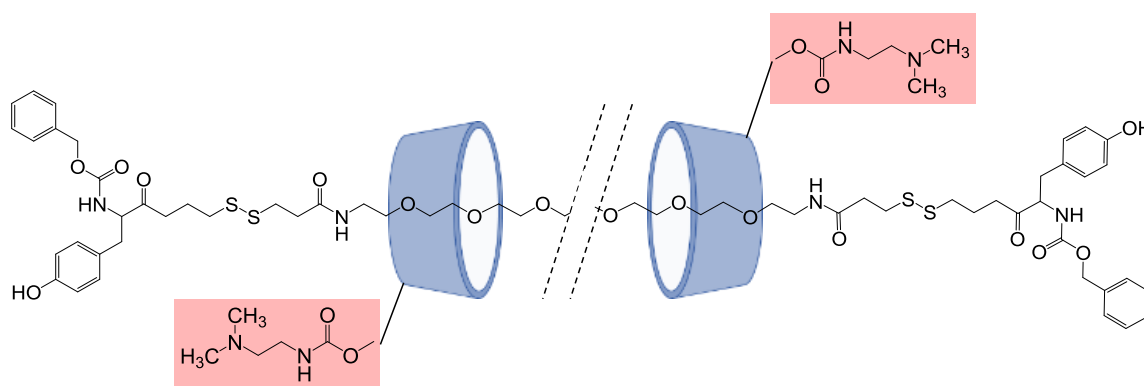


Figure 35. Disulfide linked PRs (DMAE-ss-PR)

The Harashima and Yui groups have performed a detailed mechanistic study into the PR mediated nucleic acid delivery. The study was aimed at imaging the nuclear condensation/decondensation status of pDNA in nuclear subdomains using fluorescence resonance energy transfer (FRET) between quantum dot (QD)-labeled pDNA as donor, and rhodamine-labeled polycations as acceptor. This pDNA/polycation nanoparticle assembly was encapsulated in a nuclear delivery system - a tetra-lamellar multifunctional envelope-type nano-device (T-MEND), designed to overcome the endosomal membrane and nuclear membrane via stepwise fusion. They used DOPE and Cardiolipin (1:1) as inner envelope composition for nuclear entry and an outer layer of octa-arginine decorated DOPE/PA (7:2) layer for endosomal escape. Nuclear subdomains (i.e. heterochromatin and euchromatin) were revealed by difference in fluorescence intensity peaks for Hoechst 33342 staining. Thereafter, a Z-series of confocal images were captured by confocal laser scanning microscopy. The pDNA condensation/decondensation status in heterochromatin or euchromatin was quantified based on the pixel area of the signals derived from the QD and rhodamine fluorescence. The results obtained indicate that modulation of the supra-molecular structure of PR (DMAE-ss-PRX), a condenser that is cleaved in a reductive environment, conferred euchromatin- preferred decondensation²⁷³.

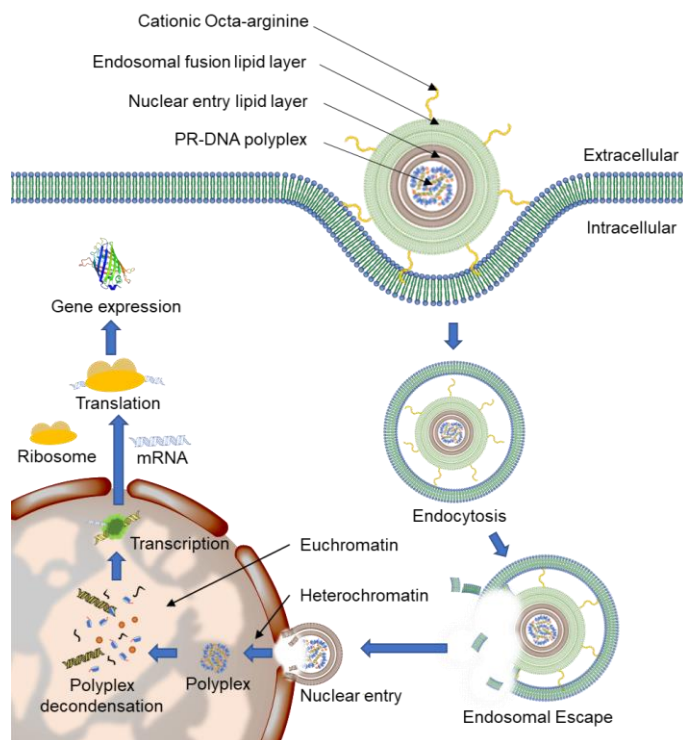


Figure 36. Gene delivery by tetra-lamellar multifunctional envelope-type nano-device (T-MEND)

Another example of pH sensitive polyrotaxane was recently developed by Hu et.al.²⁷⁴ They threaded α -CDs onto a linear 2.5k PEI backbone and endcapped it with 2, 4-dinitrobenzene formaldehyde via acid stimuli responsive $-C=N-$ moiety. For acid non-sensitive PRs, endcapping was done via $-C-NH-$ linkage. When compared to the acid non-sensitive PRs, *in vitro* on HEK293T (human embryonic kidney cell lines) using EGFP as a reported plasmid, the acid cleavable PRs showed higher transfected cell percentage and mean fluorescence intensity at N/P of 10, 20 and 30.

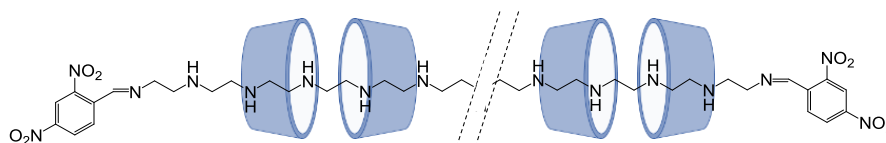


Figure 37. pH sensitive PR with PEI backbone

Thompson and coworkers synthesized and screened a family of α -CD:PEG cationic PRs grafted with DMAE groups constructed from PEGs of different molecular weights (2000, 3400, and 10000

Da) for siRNA delivery²⁷⁵. Their study revealed that the PRs demonstrated a size-activity relationship wherein the PRs constructed from higher molecular weight PEGs (3400 and 10000 Da) had superior gene silencing efficiency compared to the PR constructed from the lower molecular weight PEG (2000 Da). The authors demonstrated that these PRs can condense siRNA into positively charged particles that are <200 nm in diameter, enabling their facile internalization into mammalian cells. The cationic PRs displayed cytotoxicity profiles that were >10²-fold lower than the commercial standard branched PEI (25 kDa) and gene silencing efficiencies that are comparable to Lipofectamine 2000 and branched PEI (25 kDa) standards.

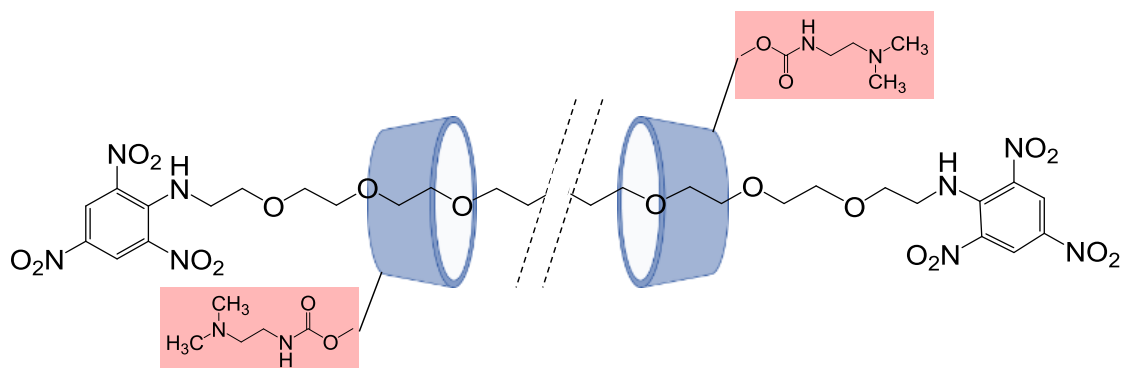


Figure 38. α -CD:PEG cationic PRs grafted with DMAE groups

Thompson and coworkers also developed a family of novel multi-armed cationic PRs for siRNA delivery²⁷⁶. They synthesized the multi-armed PRs by threading multiple cationic α -CDs onto a multi-armed poly(ethylene glycol) (PEG) core followed by endcapping with TNBS. The studies revealed that the multi-armed PRs formed stable, positively charged complexes with diameters of 150-250 nm at N/P ratios as low as 2.5. While the materials were shown to have gene-silencing efficiencies comparable to those of Lipofectamine 2000 and branched PEI (25 kDa), toxicity profiles were also in the same range as the commercial standards.

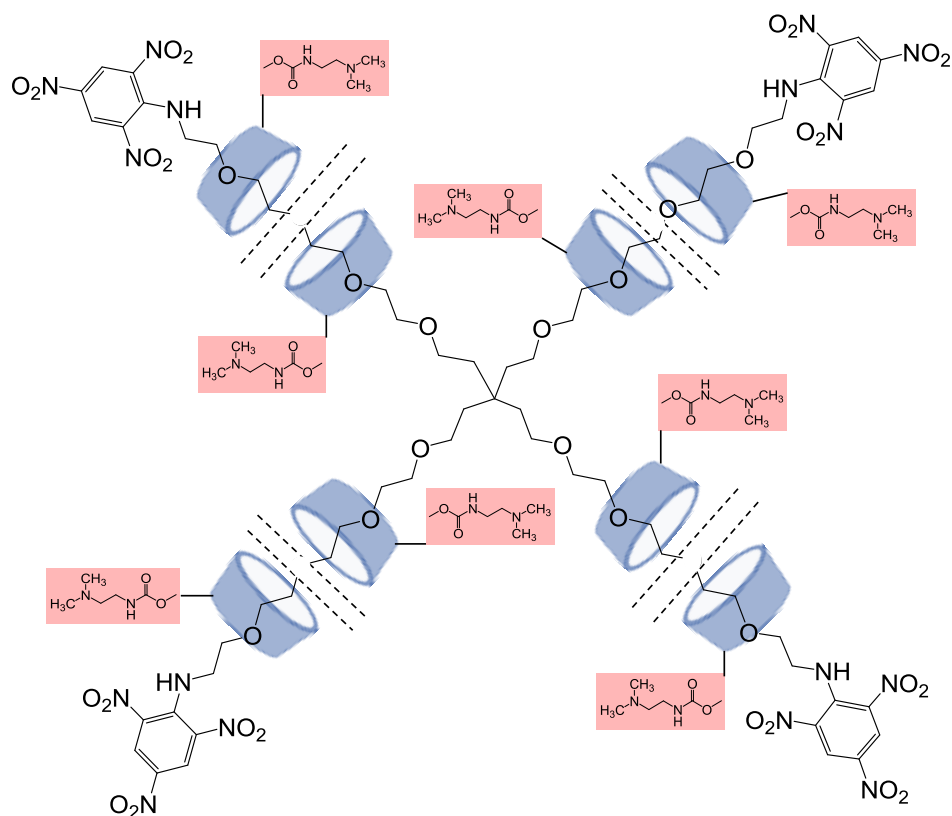


Figure 39. PRs with DMAE modified α -CD grafted onto multi-arm PEG

Badwaik et al.²⁷⁷ developed a family of cationic Pluronic-based PRs (PR(+)), threaded with 2-hydroxypropyl- β -cyclodextrin (HPCD), for pDNA delivery into multiple cell lines. All PR(+) formed highly stable, positively charged pDNA complexes that were < 250 nm in diameter. The cellular uptake and pDNA transfection efficiencies of the PR(+):pDNA complexes was enhanced relative to the commercial transfection standards L2K and bPEI, while displaying similar or lower toxicity profiles. Charge density and threading efficiency of the PR(+) agent significantly influenced the colloidal stability and physical properties of the complexes, which impacted their intracellular transfection efficiencies.

This family of PRs was also evaluated for siRNA delivery into multiple cell lines. Moreover, this group studied the relationship between molecular structure, supramolecular assembly, and polyplex structure on toxicity, siRNA loading, complexation behavior, stability and cellular localization on gene silencing efficiency²⁷⁸. The biological data showed that PR(+):siRNA complexes were well tolerated (~90% cell viability) and produced efficient silencing (>80%) in

HeLa-GFP and NIH 3T3-GFP cell lines. A multi-parametric approach was used to identify relationships between the PR(+) structure, PR(+):siRNA complex physical properties, and biological activity. Small angle X-ray scattering and cryoelectron microscopy studies revealed periodicity and lamellar architectures for PR(+):siRNA complexes, whereas the biological assays, ζ potential measurements, and imaging studies suggested that silencing efficiency was influenced by the effective charge ratio (peff), polypropylene oxide (PO) block length, and central PO block coverage (i.e., rigidity) of the PR(+) core. Their findings suggested that more compact PR(+):siRNA nanostructures arise from lower molecular weight, rigid rod-like PR(+) polymer cores that produced improved silencing efficiency relative to higher molecular weight, more flexible PR(+) vectors of similar effective charge. This study revealed that PR(+):siRNA complex formulations can be produced having higher performance than Lipofectamine(®) 2000, while maintaining good cell viability and siRNA sequence protection in cell culture.

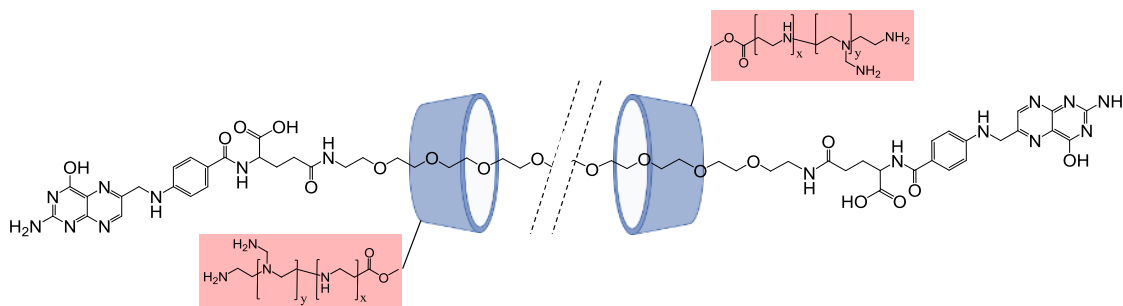


Figure 40. Folate targeted PRs

Chen and coworkers developed the first of its kind targeted PRs by using folic acid (FA) as endcaps for the PR²⁷⁹. The authors synthesized PRs composed of PEI (600 kda; branched chain) grafted α -CD threaded onto PEG which were endcapped with folic acid that can target folic acid receptors that are overexpressed on the surface of cancer cells. The PRs exhibited a lower cytotoxicity, strong specificity to folate receptors, and higher efficiency of delivering p53 tumor suppressor gene to target cells in vitro and in vivo. Interestingly, their in vitro data showed an enhanced transfection in presence of serum. The authors proposed electrostatic interaction between cationic complexes and anionic serum protein may reduce the cytotoxicity associated with the PRs and increase the endocytosis of the complex. Therefore, it was unclear if the enhancement in endocytosis was folate mediated or not. The intravenous tail vein injection of folate end-capped

PR:DNA complexes showed an enhanced antitumor effect in a KB melanoma bearing nude mice model when compared with non-targeted complexes or PEI-25K, hence suggesting that the FA targeted PRs maybe a promising targeted delivery vehicle for cancer gene therapy.

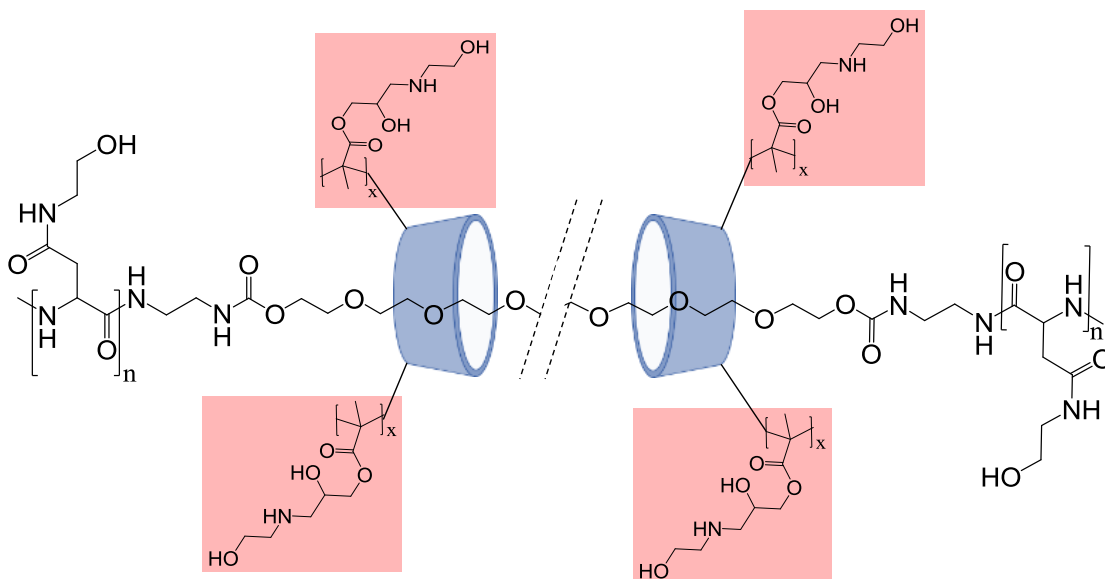


Figure 41. Polyaspartic acid endcapped PR

More recently, Xu and coworkers, developed a high-performance cationic PR with polypeptide endcaps²⁸⁰. They threaded α -CDs modified with three ethanolamine (EA) arms functionalized with poly (glycidyl methacrylate) onto a polyethylene glycol backbone. Poly aspartic acid was used as the biodegradable peptide endcaps where degradation of peptide would allow the α -CDs to slide off the backbone, disassembling the complex and release the nucleic acid payload. Multiple hydroxyl and secondary amine groups within the branched arm of CDs allowed complexation of nucleic acids to sub-250 nm particles for efficient transfection and low cytotoxicity. The synthesized PRs showed significantly improved cellular uptake and transfection capabilities in C6 glioma and HepG2 cell lines *in vitro* compared to the monomeric assembly units of functionalized α -CDs or standard PEI-25k. Further, the PRs were evaluated *in vivo* in a C6 glioma tumor model via intra-tumoral delivery. Cationic PRs and p53 anti-oncogene polyplex demonstrated slower growth of the tumor, resulting in the lower weights and volumes at the end of study as compared to modified α -CDs polyplex treatment or PBS control.

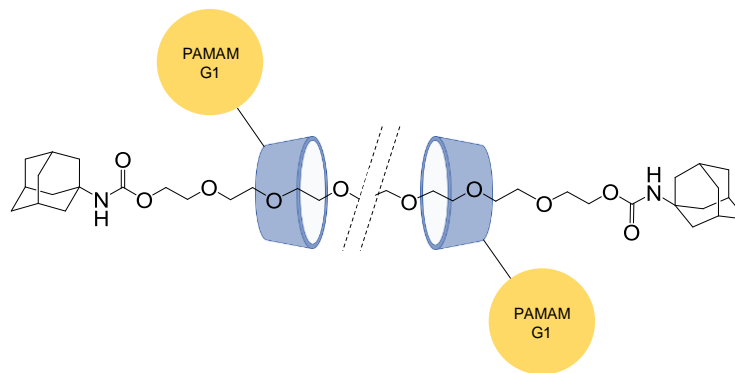


Figure 42. PAMAM G1 modified α CD PR

To overcome the instability of polyplex while undergoing dilution in the body, Huang et al developed the dilution-stable PAMAM G1-grafted PR (PPG1) supramolecular assemblies in which PAMAM G1-grafted α -cyclodextrins are threaded onto a PEG chain capped with hydrophobic adamantanamine. The PPG1/pDNA polyplex ~ 100 nm was very stable and kept its initial particle size and a uniform size distribution at ultrahigh dilution, whereas DNA/PEI 25K polyplex was above three times larger after at a 16-fold dilution than their initial size. Particle size distribution analysis revealed multiple peaks, mainly due to the formation of loose and noncompacted aggregates. They also found that the PPG1 assemblies delivered DNA into HEK293A through a caveolae-dependent pathway but not a clathrin-dependent pathway as occurs with PEI 25K. These findings suggest that the caveolae-dependent pathway of PPG1/pDNA polyplex avoid lysosomal degradation to produce high transfection efficiency. The dilution-stable PPG1 polyplex that undergoes caveolae-dependent internalization has the potential to surmount the challenges of high dilution in the body and lysosomal degradation that limit the utility of many non-viral delivery vehicles²⁸¹.

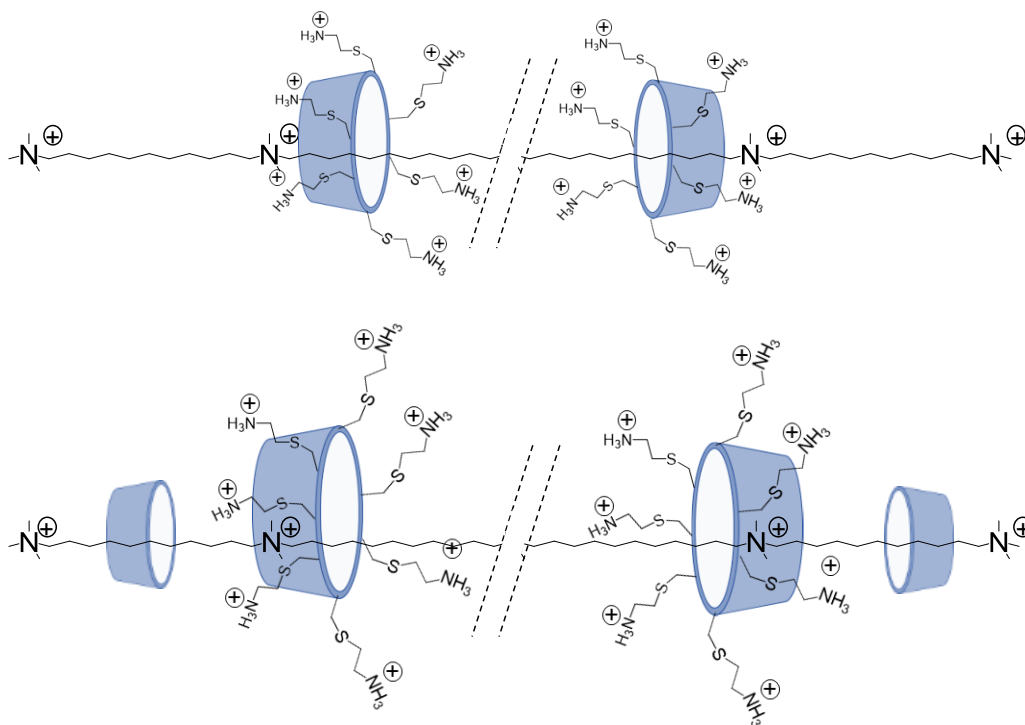


Figure 43. PR with hexacationic α -CD grafted on an ionene backbone

The Wenz group developed an endcap free PRs produced by the temperature activated threading of hexacationic α -CD onto a cationic ionene polymer.²⁸² The cationic α CD threaded the polymer very slowly at 70°C due to steric hindrance from the bulky dimethylammonium groups of the ionene backbone. These endcap free PRs were stable at room temperatures for up to 10 days. At N/P of 2, these endcap free PRs formed sub-100 nm complexes with pDNA. When compared with PEI standards, these polyplexes showed 10-30 times higher transfection efficiency of luciferase gene in A549 (human alveolar basal epithelial cells) and C2C12 (mouse myoblasts) with lower toxicity profile. For siRNA delivery the same group developed a more labile PR by threading heptacationic β -CDs on to ionene backbone and used unmodified α -CD as supramolecular stoppers²⁸³. At N/P of 2, these PRs formed stable 140 nm particles when used at a pDNA and siRNA combination of 1:3 wt/wt. These polyplexes achieved a luciferase gene knockdown efficiency 60% in A549 cells. The ease of synthesis of these PRs unlike most others that require post-modification of the PRs with cationic groups make them highly attractive for further development as gene carriers.

4.3 Polymers containing CDs in the backbone

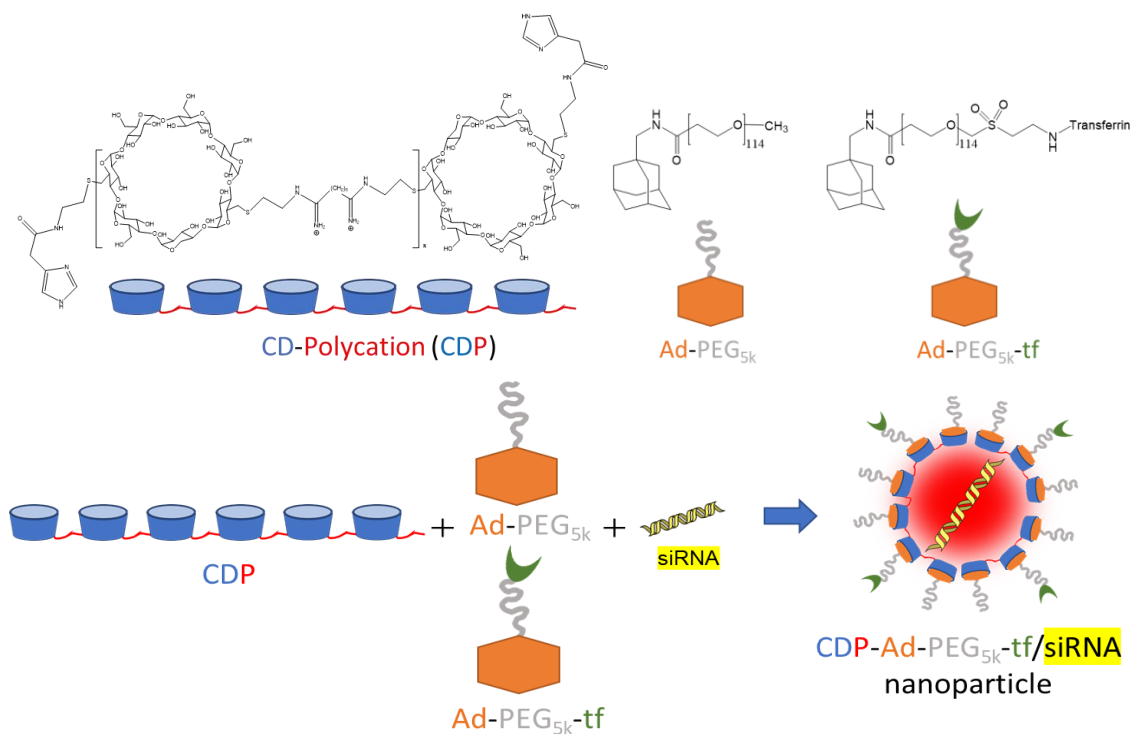


Figure 44. Formation of nucleic acid-containing particles with CDs embedded in cationic polymer backbone (A) Cyclodextrin oligomer chemical structure. (B) Schematic of particle assembly

Mark E. Davis and coworkers pioneered the development of CD containing polymers for gene delivery applications.^{238, 284-286} Linear, cationic, β -cyclodextrin (β -CD)-containing polycation (CDP) were synthesized by copolymerizing difunctionalized β -CD monomers (AA) with other difunctionalized comonomers (BB) such that an AABBAABB product is formed. The β -CD polymers were able to bind ~ 5 kbp pDNA above N/P ratios of 1.5. The pDNA complexes were 100–150 nm in size at N/P above 5, and transfect cultured cells at N/P above 10. *In vitro* transfections with these vectors were comparable to the best results obtained with PEI and Lipofectamine. Although some of these compositions exhibited toxicity *in vitro*, no toxicity was apparent at charge ratios as high as 70 for transfections conducted in 10% serum. Moreover, single IV and IP doses as high as 200 mg/kg in mice showed no mortalities.

This group also developed cyclodextrin polymer:adamantane based host:guest system for delivering nucleic acids.^{284, 286-290} They demonstrated that the CDP based materials could efficiently complex DNA and deliver it systemically to the target site. Extensive studies were performed to understand the impact of structural parameters such as carbohydrate size²⁸⁹, charge center type²⁹⁰, and cyclodextrin type²⁸⁸ on their performances. Furthermore, the detailed in vitro and in vivo behavior of these materials²⁹¹⁻²⁹² was studied in a gene delivery for cutaneous wound healing model²⁹³.

Based on the mechanistic understanding of how the CDP materials performed, Davis and coworkers designed a 3 component formulation that included a short β -CD polycation to condense the nucleic acid cargo, a therapeutic siRNA for knockdown of M2 subunit of ribonucleotide reductase protein (RRM2), and a combination of adamantane modified PEG (Ad-PEG) and adamantane modified PEG conjugated transferrin (Ad-PEG-Tf) (Fig. 21). This CDP material was the first targeted siRNA delivery system to be tested in human patients with solid tumors as summarized below²⁹⁴.

The CDP component was able to condense siRNA into nanoparticles and was designed to escape endosome on cellular internalization. The CDP system exhibited the “proton sponge” effect due to the presence of titratable amine groups. The proton sponge effect involves the buffering of the endosome by amines, which in turn results in the swelling of the vesicle due to osmotic pressure and eventual rupture. The Ad-PEG component was able to complex with the CD cavity in the polymer chain, with the PEG conferring steric stabilization, serum stability and prolonging circulation time of the nanoparticles. The PEG corona also reduces the apparent zeta potential of the particles making them closer to neutral. The Ad-PEG-Tf provided the nanoparticle with targeting capabilities for tumors. The final formulated nanoparticles were found to have sizes in the range of 50 – 70nm and zeta potentials between 15 – 25 mV. MicroPET/CT experiments to study the effects of targeting on the biodistribution and clearance rates of the particles revealed that the presence of Tf did not affect the clearance rate significantly with both non-targeted and targeted particles having identical clearance profiles.²⁹⁵ Multimodal imaging indicated that while the distribution profiles and clearance rates of the targeted and non-targeted particles were very similar, the targeted particles showed a higher knockdown of the luciferase gene compared to the

non-targeted particles. This indicated that a larger amount of functional siRNA was delivered to the tumors in case of the targeted nanoparticles²⁹⁵.

The authors then conducted the first in-human phase I clinical trial for the systemic administration of the targeted siRNA nanoparticle^{294, 296}. The tumor biopsies further revealed that there was a dose-dependent tumor localization of the nanoparticles which was a first for any kind of nanoparticles administered IV. Their qRT-PCR and western blot studies revealed RRM2 knockdown both at mRNA and protein level respectively. Additionally, 5'-RNA ligand-mediated rapid amplification of cDNA ends (5'-RLM-RACE) PCR technique was used to identify cleavage products of RRM2 mRNAs proving that the delivered siRNA was able to engage the siRNA machinery and cause the gene knockdown. These studies strongly suggested that the CDP materials were promising candidates for human siRNA therapy.

Although the particles were designed to avoid rapid renal clearance, PET imaging studies indicated that a majority of the dose is cleared from the kidney within the first 10 minutes. To further investigate the clearance mechanism, the authors performed a combination of confocal microscopy, PET/CT, and TEM experiments. The experiments revealed that one of the major reasons for renal filtration of the polycationic CDP:siRNA nanoparticles was their disassembly at the glomerular basement membrane (GBM)²⁹⁶. The results from the electron microscopy demonstrated that the CDP:siRNA nanoparticles accumulated and disassembled in the GBM but not in blood. This could be attributed to the high concentration of heparin sulfate at the GBM, which competitively binds to the complexes resulting in their disassembly. The authors also generalized that this kind of decomplexation can be extended to any kind electrostatically self-assembled nanoparticles.

Few recent reports including the above results have demonstrate feasibility of nanoparticle therapeutic delivery to the glomerulus with reduced off-target effects and toxicities²⁹⁷⁻³⁰⁰. Based on these findings, Davis group has recently explored the hypothesis that intravenously administered polycationic cyclodextrin nanoparticles containing siRNA (siRNA/CDP-NPs) can be used for delivery of siRNA to the GBM³⁰¹. They demonstrated that siRNA/CDP-NPs localize to GBM with limited deposition in other areas of the kidney after intravenous injection. Additionally, it was found that both mouse and human mesangial cells rapidly internalize

siRNA/CDP-NPs *in vitro* and that nanoparticle uptake can be enhanced by attaching the targeting ligands mannose or transferrin to the nanoparticle surface. Efficient knockdown of mesangial enhanced green fluorescent protein expression in a reporter mouse strain following *i.v.* treatment with siRNA/CDP-NPs was reported.

Based on these experiments, it can be concluded that the CDP materials are effective vectors for siRNA delivery. The Davis group showed the ability of these nanoparticles to mediate RNAi in mouse xenograft model of head and neck squamous cell carcinoma (HNSCC)³⁰². Additionally, they also showed the ability of transferrin targeted gold nanoparticles to cross blood brain barrier via a receptor mediated transcytosis. However, these strategies met with limited clinical success.³⁰³ A major reason for this could be the fast renal excretion rates and stability of the particles *in vivo* which limits its ability to accumulate at target site beyond GBM. The relatively low stability and the easy disassembly of the particles at the GBM can be attributed to the oligomeric nature of the CDP materials and the relatively weak individual host:guest binding affinities (e.g. β -CD: adamantane $K_d \sim 10^5$). Increasing the multivalency of the host:guest interactions could be a possible strategy to avoid this issue.

Thompson and coworkers designed a pendant polymer:CD guest: system based on the inclusion complex formation of Ad:CD (Fig. 6).³⁰⁴ This system employed cationic β -CD derivatives with a pendant polymer comprised of adamantane-modified (Ad) poly(vinyl alcohol)-poly(ethylene glycol) (PVA-PEG), whose Ad units were linked through an acid-labile acetal motif. It was anticipated that pDNA compaction could be achieved via complexation with self-assembled amino- β -CD:Ad-PVA-PEG host:guest pendant polymer complexes via multivalent electrostatic interactions between the cationic β -CD derivatives and the nucleic acid cargo. The amino- β -CD units were then held into place via multivalent hydrophobic interactions between the β -CD host cavities and the pendant benzylidene acetal-linked Ad groups on the PVA backbone. This design enabled the compaction of nucleic acid cargo into stable nanometer-size particles that could then be internalized and degraded within the acidic endosomes of target cells by acid-catalyzed cleavage of the acetal linkage. Their initial study utilized a poly(vinyl alcohol) MW 27kDa (PVA) main chain polymer bearing poly(ethylene glycol) MW750 (PEG) or MW2000 PEG and acid-labile adamantane-modified (Ad) grafts appended via an acid-sensitive benzylidene acetal linkage.

Two different complexation methods were used to formulate the pDNA complexes with the aforementioned pendant polymers and cationic β -CD: either precomplexation of the pendant Ad-PVA-PEG polymer with the cationic β -CD derivatives before pDNA condensation (Method A) or pDNA condensation with the cationic β -CD derivatives prior to addition of Ad-PVA-PEG to engage host:guest complexation (Method B). The pendant polymers were observed to degrade under acidic conditions, while remaining intact for more than 5 d at pH 7. HeLa cell culture data showed that these materials had over 10^3 -fold lower cytotoxicity than 25 kDa branched PEI, while maintaining transfection efficiencies that were superior to those observed for PEI when the Method A assembly scheme is employed. These results suggested that the pendant polymer:cationic CD system has potential as a safe and effective gene delivery vector.

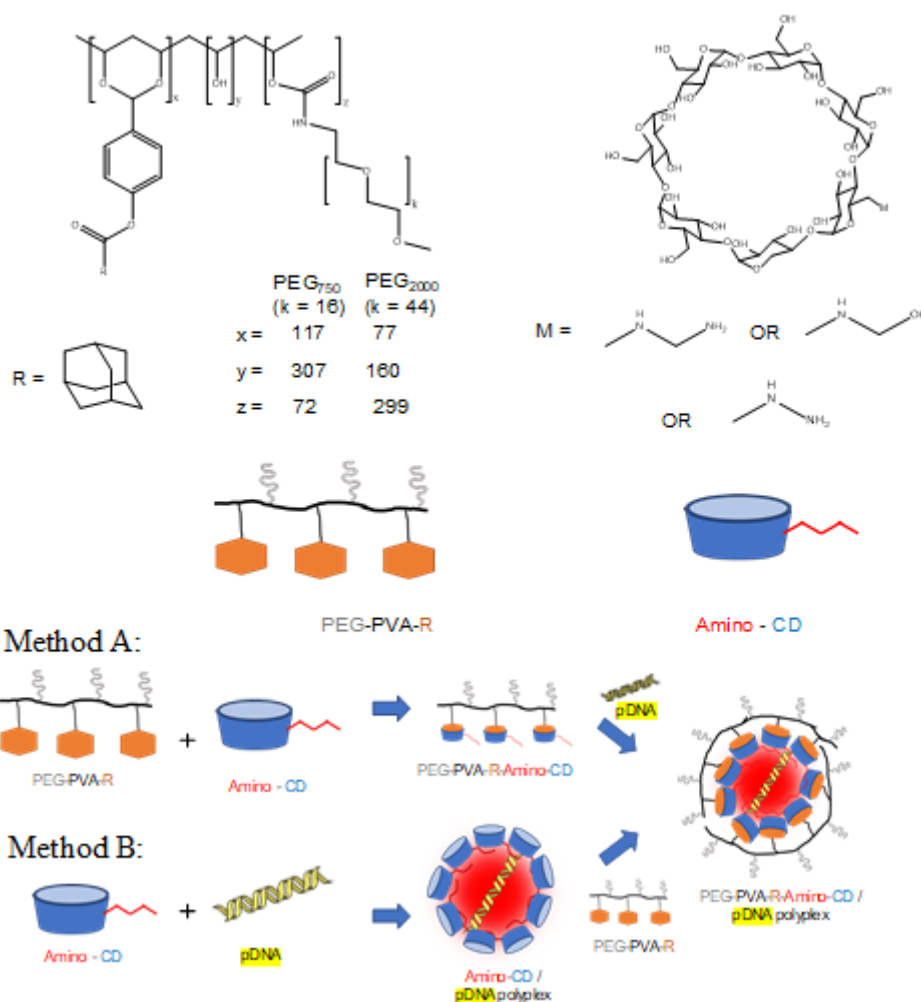


Figure 45. Thompson group pendant polymer system for plasmid delivery

This group explored the mechanistic details of this system by synthesizing a family of pendant polymers whose pendant groups had a wide range of binding affinities for the β -CD cavity.³⁰⁵ This study was performed to elucidate the effect of the binding group affinity for the CD cavity on the stability of the complexes formed and their biological performance. Cytotoxicity studies revealed that all of the cationic- β -CD:pendant polymer host:guest complexes have 10^2 to 10^3 -fold lower toxicity than bPEI, with pDNA transfection efficiencies that are comparable to branched polyethylenimine (bPEI) and Lipofectamine 2000 (L2K). Complexes formed with pDNA at N/P ratios greater than 5 produced particles with diameters in the 100 – 170 nm range and ζ -potentials of 15 – 35 mV. To elucidate the stability of the complexes in presence of high concentrations of heparin which are present in the glomerular basement membrane of the kidney, the authors performed competitive binding studies with the complexes. These studies revealed that adamantyl- and noradamantyl-modified complexes displayed the best resistance toward heparin-induced decomplexation, which were corroborated by in vitro FRET studies. These findings suggest the high affinity host:guest binding constant between the pendant polymers and the β -CD cavity are needed to confer excellent colloidal stability to the complexes. Indeed, pendant groups with lower binding affinities were shown to have lower colloidal stability. Their work further showed that pDNA delivery occurred via acid catalyzed hydrolysis of the acetal linked pendent groups. The authors concluded that the host:guest binding constant had a significant impact on the colloidal stability in the presence of serum, cellular uptake efficiency, endosomal disassembly, and transfection performance of cationic- β -CD:pendant polymer complexes, with the Ad pendant polymer demonstrating optimal stability and performance.

The pendant polymer concept was further extended for applications in siRNA delivery wherein cholesterol was used as a pendant group on PVA instead of adamantane. The authors demonstrated that the pendant polymer system had 10^3 -fold lower toxicity than commercial branched PEI (25 kDa) while having gene silencing efficiencies comparable to PEI and Lipofectamine 2000 in CHO-GFP cells.

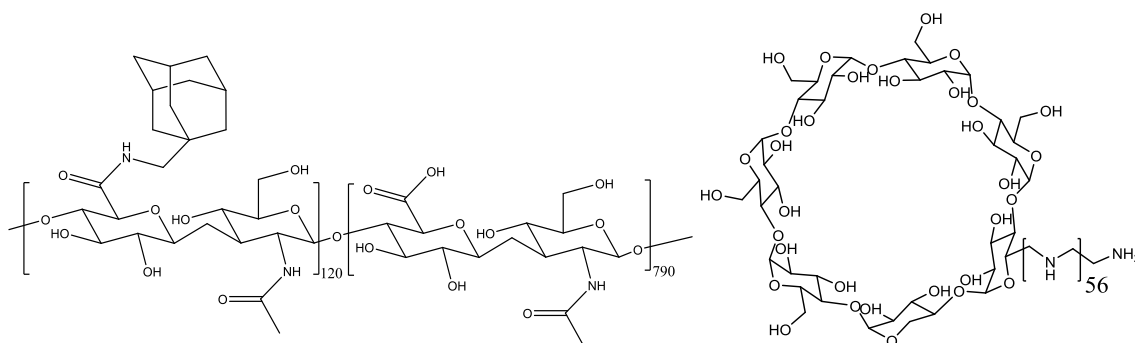


Figure 46.(a) Hyaluronic acid -adamantane pendent polymer (b) β -CD PEI_{2.5k}

Thompson and coworkers have also used a commercial micro-reactor to assemble cationic- β -cyclodextrin: hyaluronic acid-adamantane host:guest pDNA nanoparticles using a layer-by-layer approach.³⁰⁶ These studies reveal that the particles formulated via microfluidic assembly have much smaller sizes, lower polydispersity, lower ζ -potentials, and comparable cell viability and transfection profiles in HeLa cells than bulk mixed particles. The complexes also showed a flow rate-dependent stability, with particles formed at slower flow rates giving rise to more stable complexes as determined by heparin challenge. These findings suggest that microfluidic reactors offer an attractive method for assembling reproducible, size-controlled complexes from multi-component transfection complex assemblies. Moreover, this system provides a targeting element to the pendant polymer family towards CD44 positive cells lines.

Spatial and dynamic tracking of the cationic- β -cyclodextrin:hyaluronic acid-adamantane host:guest pDNA transfection complexes was reported by Badwaik et.al.³⁰⁷ Confocal microscopy and multicolor flow cytometric techniques was used to evaluate the target specificity, subcellular localization, and endosomal escape process in an effort to gain better mechanistic insights into the performance of these materials. The results showed that only the cells expressing CD44 undergo enhanced cellular uptake and transfection efficiency with HA-Ad:CD-PEI:pDNA complexes. This transfection system, comprised noncovalent assembly of cyclodextrin:adamantamethamidyl-modified hyaluronic acid via host:guest interactions to condense pDNA, is a potentially useful tool for targeted delivery of nucleic acid therapeutics.

Most recently, to overcome reproducibility issues of the PVA- and HA-based material syntheses and nonbiodegradability vinyllic polymers backbone (e.g., PVA), the Thompson group designed of a new generation of biocompatible pendant polymers with a backbone made of well-defined mPEG–polycarbonate diblock copolymers.¹⁴² Polycarbonate were chosen as backbone material because they have controlled degradation rates as well as yields nonacidic and nontoxic cellular degradation byproducts. The synthesized materials were able to form stable 100 to 250 nm pDNA complexes with β -CD-PEI_{2.5k} via host guest interaction. *In vitro* studies in HeLa cells showed that these complexes had transfection efficiencies similar to L2k at N:P \geq 30. However, the transfection efficiencies did not vary significantly with change in backbone molecular weight or difference in pendant groups. The authors attributed these findings to acid-catalyzed ester hydrolysis of the pendant group that led to subsequent disassembly of the complex within the acidic endosomal compartment after internalization, yielding a plasmid complex of similar bioavailability regardless of the initial pendant group type.

O’Driscoll *et al.* pioneered the use of polycationic CDs to complex pDNA. They modified 6 hydroxy position of β -cyclodextrins with pyridylamino, alkylimidazole, methoxyethylamino or primary amine groups to show that the constructs form stable nanocomplexes with nucleic acids³⁰⁸. On evaluating transfection efficiency in COS-7 cells, it was shown that CDs with amino, pyridylamino or butylimidazole group at the 6-positions along with unmodified 2- and 3-hydroxyl groups were efficient in delivering the pCMVluc gene. However, chloroquine (an endosomolytic agent) treatment resulted in a 10-400 fold increase in transfection efficiency suggesting that the complexes were not able to the escape endosome efficiently. The group also showed that amphiphilic cyclodextrin molecules bearing acyl chains on the primary OH groups and short oligo(ethylene glycol) chains on the 2-OH groups were capable of forming bilayer vesicles in water with a diameter of 30–35 nm (when acyl chain was 16 carbons long) or nanoparticles with a diameter of 120 nm (when acyl chain was 6 carbon long).³⁰⁹ Incorporation of oligo(ethylene) chains also helped in reducing immunogenicity and improving water solubility. Addition of primary amine groups to the polar chains enabled the amphiphilic molecules to form complex with nucleic acids³¹⁰. Transfection efficiency was governed by length of the alkyl chain where C16 was superior to C12, C6 or C2 in delivering pCMVluc gene to HepG2 cells and comparable to the commercially available transfecting agent DOTAP.³¹¹

They further expanded their system by conjugating galactose targeting ligands to the termini of the oligo(ethylene glycol) chains to effect targeting to asialoglycoprotein receptors (AGPR) of hepatocytes. The delivery system was a co-formulation of targeted and cationic amphiphilic CDs along with helper lipid, DOPE, to enable efficient endosomal escape. Their results demonstrated galactose-specific targeting via lecithin and resulted in enhanced transfection of HepG2 cells expressing AGPR. Addition of DOPE to the formulation resulted in a 8-fold enhancement in gene expression³¹². Recently, this group has used dilysine modified CDs to complex siRNA. PEGylated adamantane derivatives with anisamide were synthesized to form inclusion complexes with CDs to produce sub-300nm complexes which showed sigma receptor mediated cellular uptake in prostate cancer cells and substantial PLK1 gene knockdown³¹³. They have also utilized targeting ligand conjugated with phospholipids via a polyethylene glycol spacer(DSPE-PEG-folate / DSPE-PEG-Fab / DSPE-PEG-anisamide) in co-formulations with amphiphilic CDs to achieve receptor specific gene delivery³¹⁴⁻³¹⁶.

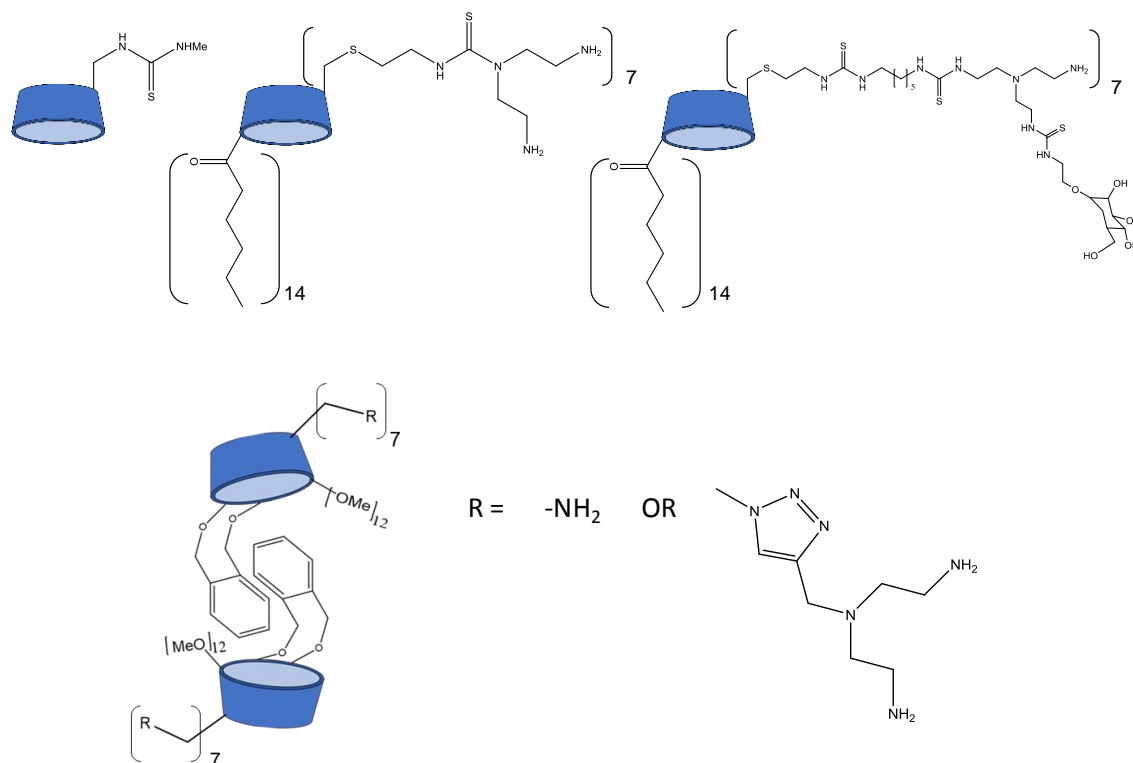


Figure 47. CDs developed for gene delivery by Fernandez and Mettel

Fernandez and Mettel *et al.* described the use of glycosyl and glycopeptidyl derivatives of thioureido- β -CDs as molecular carriers with higher solubility and reduced hemolytic properties as

compared to parent β -CDs.³¹⁷ The further modification of their CDs to produce amphiphilic constructs by incorporating a multivalent cationic group (aminoethyl, 7 copies) at the primary rim and hydrophobic chains (hexanoyl, 14 copies) at the secondary 2,3-hydroxyl groups formed species there were capable of self-assembly into nanometric complexes (40-110 nm) in presence of pDNA and mediate efficient transfection.³¹⁸ Next, they included a bio-recognizable glycosyl moiety, mannose, on the hydrophilic rim in the CD scaffold.³¹⁹ The mannosylated cationic amphiphilic CDs complexed pDNA into optimal complexes at N/P of 5. These glyco-CD complexes were shown to be recognized by mannose specific lectins like Concanavalin A and human macrophage mannose receptors. Their capacity to transfect in a mannose specific manner was demonstrated *in vitro* using mannose-fucose receptor expressing RAW 264.7 cells.

Biophysical analysis of the amphiphilic CD-plexes by SAXS and Cryo-EM revealed multilamellar lyotropic liquid crystal phases which is characterized by a layer-by-layer arrangement of amphiphilic CDs and pDNA sandwiched between them.³²⁰ Additionally, they showed that in biological milieu, cationic CD-plexes adsorb serum protein to form a protein corona where by their hydrodynamic diameter increases from 114 nm to 153 nm and surface potential decreases from +30 mV to -17 mV.³²⁰ LC/MS/MS analysis showed that the corona was mainly comprised of complement factors, lipoproteins and coagulation proteins. Minor amount of immunoglobulins, tissue leakage and acute phase proteins were also detected. In depth analysis into the mechanism of cellular uptake of the CD-plexes showed that chlorpromazine (inhibitor of clathrin mediated endocytosis) reduced internalization by 76% without significantly inhibiting transfection.³²¹ On other hand, genistein (a inhibitor of caveolae mediated endocytosis) resulted in only partial decrease in internalization but complete abolition of transfection. The authors concluded that transfection by CD-plexes with pDNA cargo was mediated primarily by the caveolar uptake. The authors also suggested that the lack of release of the payload at endosomal pH may occur in the case of clathrin mediated endocytosed particles. Since this represents the majority of the internalized CD-plexes, the bulk of these complexes are degraded within the lysosome. To overcome this challenge, the authors replaced the hydrophobic hexanoyl chains on the secondary hydroxyl face of the CD with hydrophobic xylylene moieties.³²² Xylylene was linked to a single glucopyranosyl unit via a hinge-type diether linkage to prevent self-inclusion into the CD cavity. The hydrophobic interaction between xylylene groups promotes dimerization

The developed particles were nontoxic and showed effective hepatocyte specific gene silencing effect in vitro and low RNAi at a dose of 9mg/kg upon I.V administration. The authors concluded that on systemic administration the complexes faced serum stability issue which led to low RNAi efficiency. To overcome this problem, the author utilized a polyanion, sacran (M.W. 100), to coat their cationic particles³²⁶. They developed a ternary complexes that were approximately 180 nm in diameter (which was drastically more than the 20 nm binary complex) and had a moderate polydispersity of ~0.3 at N/P of 50. Unexpectedly, there was an increase in zeta potential from ~+7 mV to ~+14mV after incorporation of the polyanion. These data may suggest that multiple particles aggregated to form larger particles in presence of sacran. Nevertheless, these complexes showed high serum stability and endosomal escaping properties in HepG2 cells. The sacran coated particles also had higher liver accumulation as compared to uncoated particles after I.V. administration. Subsequently, there was a significant improvement in gene silencing efficiency of the delivery system in vivo at a dosage of 5mg/kg. The authors concluded that these ternary complexes made of AGPR targeted α CDE, siRNA and sacran is promising as a gene silencing system for hepatocytes.

4.4 Conclusions and perspectives

We have briefly summarized the findings from recent studies demonstrating the application of CD-based polymers as gene delivery vectors. Most reports have shown the ability of CDs to improve the transfection efficiency of existing cationic polymers, lipids, or dendrimers. These reported materials take advantage of the ability of CDs to permeate cell membranes, as well as their enhanced solubilizing properties to improve the cellular uptake and transfection efficiency of existing non-viral vectors while keeping the toxicity profile low. The innate anisotropy of the CDs and their ability to encapsulate hydrophobic molecules in their cavity confers the CDs with capabilities to form several interesting self-organizing supramolecular structures. Additionally, the commercial availability, ease, and relatively inexpensive synthesis of the target materials, as well as their stability, biocompatibility, lack of immunogenicity, and safety, make CDs an extremely attractive platform for development of non-viral vectors.

While there have been several reports of CD-polymer based non-viral vectors, the CDP materials developed by Davis and coworkers have met with the greatest success. These materials have taken advantage of the inclusion properties, solubility, and cell permeation capability of the CDs to

construct a system that can form a targeted self-assembling nanoparticle that can encapsulate siRNA and deliver the therapeutic cargo to the target tumor site. The CDP materials were clinically translated for therapy against melanoma and were the first in-human targeted nanoparticle based gene delivery vectors to be tested. Despite their clinical success and efficacy, detailed mechanistic studies revealed an extremely low residence time ($< 5\text{min}$) of the materials in blood hence potentially requiring larger doses to elicit a therapeutic response.

Hence there still is an unmet need for development of an effective delivery vector that can not only have high delivery efficiency and low toxicity, but also be stable in vivo for effective clinical translation. Finally, with two gene therapy getting FDA approval within a year has shown that novel development in delivery system is the key for success of the field.

CHAPTER 5. EVALUATION OF POLYCARBONATE PENDANT POLYMER:β-CYCLODEXTRIN-BASED NUCLEIC ACID DELIVERY VECTORS

Reprinted (adapted) from the journal article titled “Organocatalytic Synthesis and Evaluation of Polycarbonate Pendant Polymer:β-Cyclodextrin-Based Nucleic Acid Delivery Vectors”, authored by Kyle J. Wright, Vivek D. Badwaik, Shayak Samaddar, Seok-Hee Hyun, Kristof Glauninger, Taeyoon Eom, and David H. Thompson. Shayak Samaddar was involved in physicochemical and biological characterization of transfection complexes which includes particle formulation, gel-shift assay, dynamic light scattering and transfection experiments. Published: *Macromolecules*, 2018,5,13,670-678.

5.1 Introduction

There has been considerable recent interest in the development of non-viral nanoparticle-based nucleic acid delivery systems.³²⁷⁻³³¹ These agents typically load the cargo via coacervation, physical entrapment, or covalent conjugation to alter the pharmacokinetic and pharmacodynamic properties of the nucleic acid agent.³³²⁻³³⁶ Amphiphilic block copolymers have been one of the most extensively studied delivery platforms owing to their synthetic accessibility, modular properties, and the variety of nanoparticle types that can be formulated using these materials.³³⁷ These agents are used to effect gene delivery wherein the transfer of nucleic acids to knock-in, knock-out, or repair the genetic composition of target cells. Non-viral gene therapy offers the potential for improved safety, greater flexibility in accommodating large cargo, and more facile and robust design and production strategies relative to viral vectors. Non-viral vectors typically bind their nucleic acid cargo via electrostatic interactions that condense the cargo into particles, protect the cargo from degradation, and mediate cellular entry. Many different material strategies, including cationic lipids and polymers, have been proposed as non-viral gene-delivery vectors.^{332, 338-340} A particularly promising class of cationic polymers that have recently been developed for this application are the biocompatible and degradable polycarbonates bearing amidine modifications that promote nucleic acid complexation via the arginine fork motif.^{330, 341-342}

In recent years, organic catalysis has become an increasingly attractive and powerful alternative for the synthesis of functional amphiphilic copolymers compared to traditional metal-based catalysis.³⁴³ Ring-opening polymerization (ROP) is the most common method for synthesis of

well-defined biodegradable block copolymers. Most organocatalysts used in ROP are relatively inexpensive commercially-available chemicals, generally easily purified, have long shelf lives, and are well-suited for a range of reaction conditions, solvents and monomers. Traditional metal-based catalysts generally function via the coordination-insertion mechanism as in the case of the polymerization of L-lactide by tin(II) 2-ethylhexanoate. These catalysts have generated concerns related to trace contamination of the polymer with toxic Sn containing byproducts arising from the ROP catalyst.

Common organocatalysts for ROP include N-heterocyclic carbenes, organic “super base” catalysts³⁴⁴⁻³⁴⁵ and bifunctional catalysts. Bifunctional thiourea-amine catalysts were first applied to the polymerization of lactide.³⁴⁶ These systems involve simultaneous activation of monomer by the thiourea (a Lewis acid) and the initiator (an alcohol) by the amine-component. This strategy was applied to two-component systems of thiourea and organic base and bifunctional thiourea-amine (TU/A) catalysts.³⁴⁶ The most common super-base catalysts include 1,8-diazabicyclo[5.4.0]undec-7-ene (DBU), 1,4,5-triazabicyclo[4.4.0]dec-5-ene (TBD), 7-methyl-3,5,7-triazabicyclo[4.4.0]dec-5-ene (MTBD), and other phosphazene-based compounds.³⁴³ These catalysts are more active than the TU/A system, display different activities (TBD > MTBD > DBU) and have been applied for the polymerization of many different cyclic monomers.^{341, 347} TBD, in particular has been shown to exhibit very high reactivity for monomers with low ring strain or which exhibit low conversion with other catalysts. TBD functions via dual activation of the monomer and initiator in an analogous fashion to the TU/A-based catalysts. Alternatively, TBD has been shown to polymerize L-lactide via an H-bonding mechanism which does not involve acyl transfer.³⁴⁸ Urea anions have also recently been reported as rapid and selective ring opening polymerization catalysts.³⁴⁹

Kulkarni *et al.* first introduced the concept of pendant polymer-based nucleic acid delivery with a system composed of poly(vinyl alcohol) (PVA) main chain polymer that was modified with methoxypoly(ethylene oxide) (mPEG) and acid-sensitive cholesteryl benzylidene acetal linkages.^{339, 350} This polymer was used in combination with amine-modified- β -cyclodextrin derivatives, wherein the latter were used to condense the nucleic acid cargo and the former served as a consolidating agent that created a passivating layer via host:guest complexation. These

materials effectively formed transfection complexes in the 120-170 nm range by engaging multiple host-guest interactions between the cationic β -CD:nucleic acid core via binding affinities in the $10^{0.5}$ - 10^5 M⁻¹ range in aqueous media.³⁵¹ The pendant polymer concept was further applied to microfluidic assembly of transfection complexes composed of siRNA, β -CD-PEI2.5kDa conjugate (β -CD-PEI), and hyaluronic acid (HA)-modified with adamantyl substituents.³⁵²

Although these materials showed good performance, several issues related to the reproducibility of the PVA and HA-based material syntheses, and the limitations associated with non-biodegradable vinylic polymers (e.g., PVA), prompted the design of a new generation of biocompatible pendant polymers that would improve on this concept by utilizing organocatalytic ROP to synthesize a library of well-defined block-copolymers. This approach could allow for a more tunable synthesis and enable the incorporation of guest moieties of varying density within a biodegradable platform.

An oligocarbonate-based non-viral gene delivery system described by Hedrick, Waymouth, Wender and coworkers³⁴¹⁻³⁴² suggested an approach using a novel family of pendant polymers derived from PEG-polycarbonate diblock copolymers (**Figure 1**). This library of mPEG-b-PC diblock copolymers bearing hydrophobic pendant moieties of varying affinity for the β -CD cavity was sought to evaluate the effects of overall molecular weight, relative block length, and pendant group densities along the linear polycarbonate backbone on their transfection performance. TBD and the DBU/thiourea organocatalysts³⁴⁶ were utilized due to their high activities and ability to generate well-defined copolymers with low polydispersity.³⁴⁴ Polycarbonate diblocks were chosen due to their controlled degradation rates, yielding non-acidic and non-toxic degradation by-products within the transfected cell. In addition to homopolymerization of cyclic carbonate monomers initiated by mPEG,³⁵³ copolymers where the cyclic carbonate monomer is blended with trimethylene carbonate (TMC, **12**) are also included in the library to evaluate the effect of pendant group density on nanoparticle formation and efficacy of transfection complexes derived from mPEG-b-PC and β -CD-PEI materials.^{339, 352} We found that the performance of the materials was highest for pendants having the weakest β -CD association, yielding transfection efficiencies at N:P ≥ 30 that were modestly higher than the commercial agent, Lipofectamine 2000 (L2k), as benchmark.

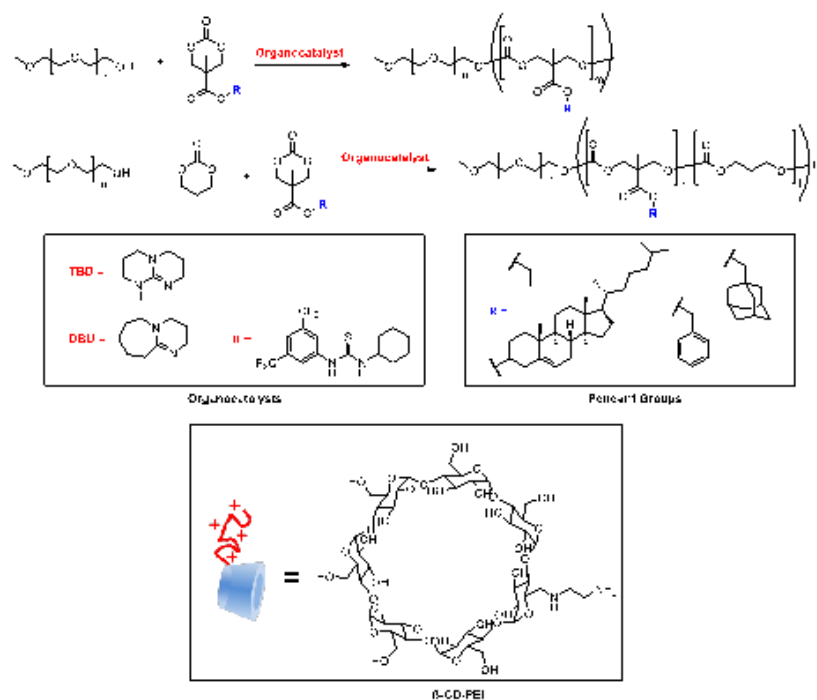
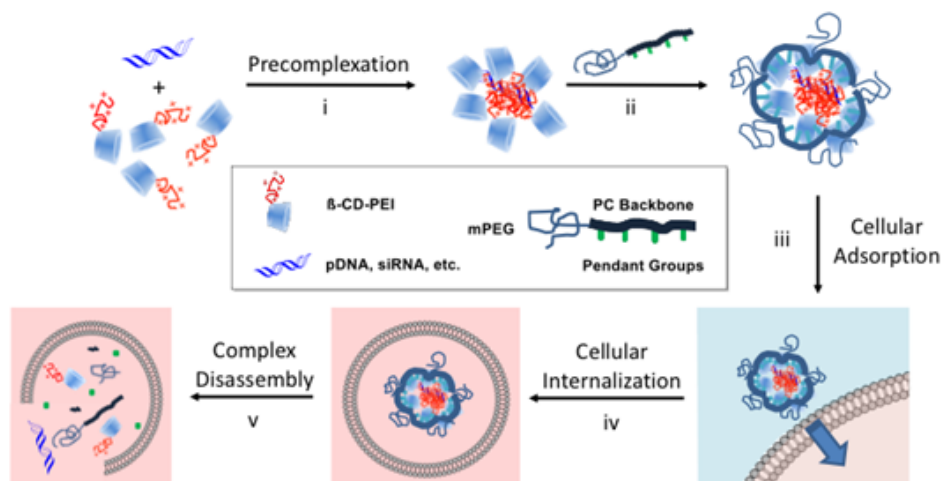


Figure 49. Conceptual Diagram for Polycarbonate Pendant Polymer-Based Non-Viral Gene Delivery. (A) Polyplex formation (i) is accomplished via precomplexation of β -CD-PEI and pDNA. (ii) Polycarbonate diblock copolymers are used to coat the core β -CD-PEI:pDNA complex via host:guest interactions between the pendant groups and the surface-exposed β -CD cavities. (iii) Nanoparticles are targeted to cellular surfaces via electrostatic adsorption of the slightly positively charged particles prior to endocytosis (iv). Disassembly of the transfection complexes (v) is promoted by pendant group and polycarbonate block hydrolysis, thus leading to endolysosomal escape of the pDNA cargo. (B) Diblock copolymer structures derived from (i) homopolymerization of cyclic carbonate monomers, or (ii) copolymerization of cyclic carbonate monomers with trimethylene carbonate. The (iii) organocatalysts, (iv) pendant groups, and (v) β -cyclodextrin-poly(ethyleneimine) conjugate (β -CD-PEI) are also shown

5.2 Experimental methods

Synthesis of Pendant polymer systems. Materials, methods and synthetic procedures for cyclic carbonate monomer synthesis are detailed in the publication.

pDNA-Pendant Polymer Transfection Complex Formation. mPEG-b-PC pendant polymers solutions (1 mM equivalent of pendant groups) were vortex mixed with equal volumes of β -CD-PEI (1mM equivalent of PEI cyclodextrin units) solution in water to form mPEG-b-PC: β -CD-PEI complexes. Transfection complexes were formed by adding appropriate amount of mPEG-b-PC: β -CD-PEI complexes to the 1 μ g of pDNA (unmodified or FITC-labelled) dissolved in 30 μ L of TE buffer in 1.5 mL centrifuge tubes. The amount of mPEG-b-PC: β -CD-PEI added to DNA varied from 1-3 μ L to produce the desired N/P ratios of 5, 10, 20 & 30. These solutions were then incubated at 4 °C for 1 h before use in transfection experiments.

Particle Size and Zeta (ζ) Potential Measurements. The diameters, size distributions, and ζ -potentials of the materials were evaluated by dynamic light scattering (DLS) using a Zetasizer Nano S (Malvern Instruments Ltd.) at 20 °C with a scattering angle of 90°. At least 40 measurements were made and averaged for each sample. The particles were diluted to 1 mL with HEPES buffer (20 mM, pH 7.4) prior to analysis.

Gel Shift Assay. The complexation ability of mPEG-b-PC: β -CD-PEI with pDNA was determined by low melting point 1% agarose gel electrophoresis. The agarose gels were precast in TBE buffer with GelRed[®] dye at 1:10,000 dilution. mPEG-b-PC: β -CD-PEI:pDNA complexes containing 0.2 μ g of pDNA at different N/P ratios were loaded onto the gel before addition of loading dye (1:5 dilution) to each well and electrophoresis at a constant voltage of 55 V for 2 h in TBE buffer. The pDNA bands were then visualized under a UV transilluminator at $\lambda = 365$ nm.

In Vitro Transfection Assay in HeLa Cells. HeLa cells were cultured in complete DMEM medium with 10% FBS. All cells were incubated at 37 °C, 5% CO₂, and 95% relative humidity, respectively, at a cell density of 10,000cells/well in a 96-well plate. After 24 h, the culture media was replaced with Opti-MEM[®] media, with addition of mPEG-b-PC: β -CD-PEI:pDNA complexes containing 0.1 μ g of AcGFP, at N/P ratios of 10, 20,30 and 60. The cells were incubated with the

complexes for 24 h, after which the spent media was aspirated. Then the cells were washed with PBS, trypsinized, and analyzed by flow cytometry using a FC500 flow cytometer. The %GFP mean fluorescence intensity was calculated relative to L2k controls, considered as 100%. All treatment conditions were performed at n=4.

5.3 Results and discussion

5.3.1 Diblock Copolymer Synthesis and Characterization.

Please refer to attached publication.

5.3.2 Transfection Complex Formulation.

Next, select members the homopolymer library generated via TBD-catalyzed ROP were tested for their abilities to effectively form nanoparticulate transfection complexes upon bulk mixing with β -CD-PEI^{339, 352} and pDNA. β -CD-PEI and pDNA were pre-complexed before addition of the diblock copolymer, yielding a layer-by-layer type of transfection complex that is stabilized by multiple host:guest interactions between the pendant groups in the polycarbonate block with the cavities of the β -cyclodextrin units in a manner described by Thompson and coworkers.^{339, 350}

5.3.3 Physico-chemical Characterizations.

Next, a gel retardation assay was performed to determine the ability of the mPEG-b-PC: β -CD-PEI-based materials to condense pDNA at various N/P ratios (**Figure 2**). Higher molecular weight diblock copolymers (e.g., **15e-g**) required N/P ratios >20 to effectively condense pDNA, whereas lower molecular weight diblock copolymers (e.g., **15j-l**) effectively condensed pDNA at N/P = 5, likely due to lower entanglement/steric interference of the mPEG block during the initiation of host:guest interactions between the β -CD-rich core and the polycarbonate pendant groups.

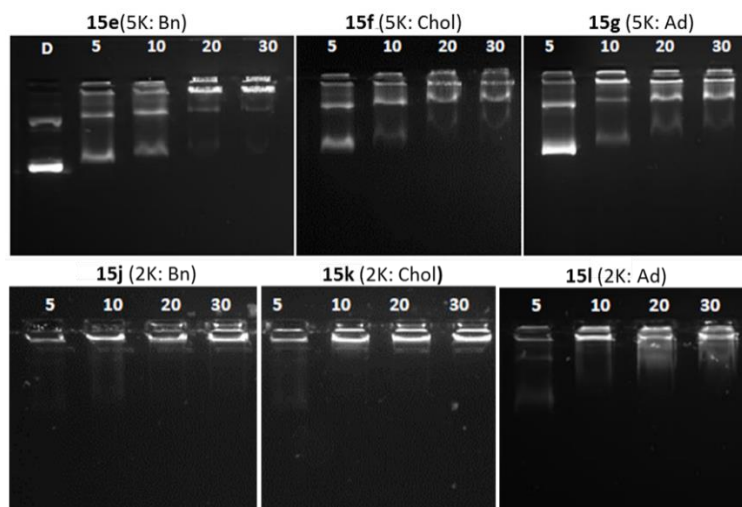


Figure 50. Gel Shift Analysis of Transfection Complexes at Various N/P Ratios.

Dynamic light scattering (DLS) was used to determine size and polydispersity of the transfection complexes generated using **15e-g** and **15j-l** (Figure 3). These complexes ranged between 100 - 250 nm in diameter, a size regime that is capable of cellular internalization.³⁵⁴ Transfection complexes formed from lower molecular weight diblock copolymers showed relatively larger sizes compared to those of higher molecular weight polymers at $N/P = 10$; however, they were of comparable size and polydispersity at $N/P \geq 20$. There was no apparent correlation between particle size or polydispersity and pendant group identity observed.

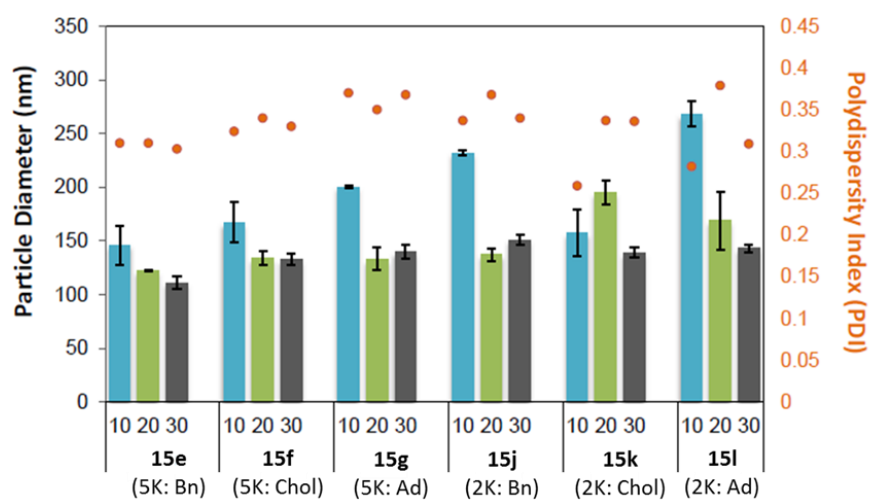


Figure 51. Size Analysis of Transfection Complexes at Various N/P Ratios by DLS

Zeta potential (ζ) analysis of transfection complexes formed by 15e-f and 15j-l revealed values in the range of +5-10 mV (Figure 4). These modestly positive ζ are generally preferred in order to promote internalization via electrostatic interaction of the positively-charged nanoparticle surface with the negatively-charged cellular surface. Transfection complexes formed at N/P = 10, 20, and 30 resulted in particles with similar ζ . β -CD-PEI alone exhibited an elevated ζ = +24 mV. Copolymers 15e and 15j both exhibited a neutral charge in solution, whereas mixtures of these copolymers with β -CD-PEI resulted in positive ζ that were lower in magnitude than β -CD-PEI. We infer from these findings that the diblock copolymers effectively screen the positive charge of β -CD-PEI both in the host:guest complex form and in the final transfection complex. Furthermore, since the β -CD-PEI:diblock copolymer complexes showed zeta potentials similar to the transfection complexes, we conclude that the plasmid is likely not surface exposed and, thus, may be protected from nuclease degradation.

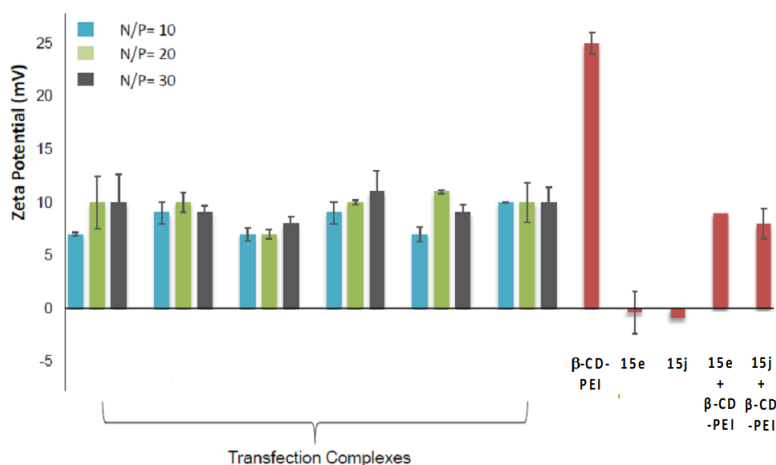


Figure 52. Zeta (ζ) Potential Analysis of Transfection Complexes at Various N/P Ratios.

5.3.4 In vitro Performance of Transfection Complex.

Transfection complexes prepared from mPEG-b-PC **15e**, **15f**, **15j**, or **15l** as mentioned earlier, and were evaluated for their transfection efficiencies in HeLa cells (**Figure 5**). Transfection complexes made of benzyl modified materials showed similar efficiency relative to L2k as benchmark (**Figure 5A**). Block copolymer molecular weight also seemed to have little impact on transfection efficiency, although higher N/P tended to give higher transfection efficiencies. We attribute these

findings to acid-catalyzed ester hydrolysis of the pendant group and subsequent disassembly of the complex within the acidic endolysosomal compartment after internalization, yielding a plasmid complex of similar bioavailability regardless of the initial pendant group type. The modest boost in transfection performance for the benzyl derivatives is attributed to pendant exchange between the endosomal membrane and the weaker host:guest interactions of these species with the β -CD-PEI:pDNA core. When transfection efficiency is evaluated in terms of % mean fluorescence (**Figure 5B**), similar trends were apparent, with no clear correlation between transfection efficiency and polymer molecular weight, or pendant group.

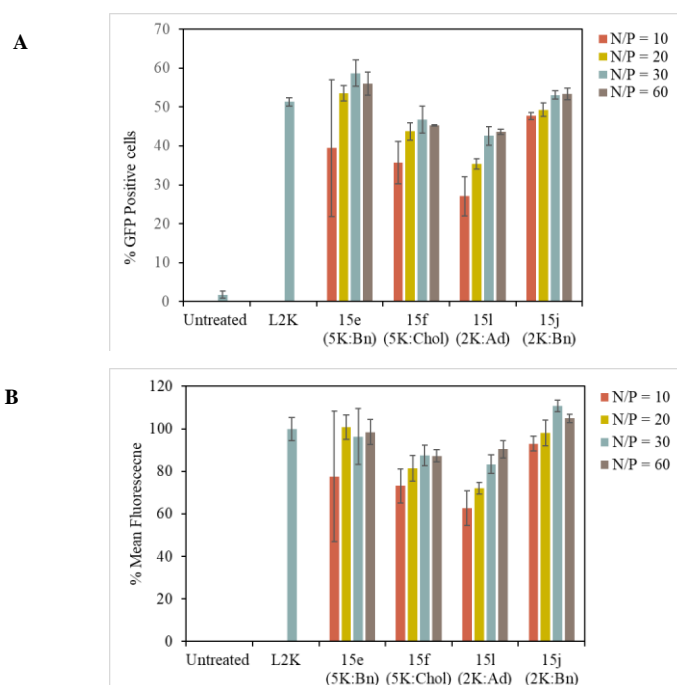


Figure 53. Transfection performance of mPEG-b-PC coated polyplexes. (A) % GFP Positive HeLa Cells Treated with Transfection Complexes Containing AcGFP pDNA. (B) % Mean Fluorescence of HeLa Cells Treated with Transfection Complexes Containing AcGFP pDNA.

5.4 Conclusions

The pendant polymer-based gene delivery concept has shown significant potential as a novel non-viral gene delivery strategy. We sought to address material-specific limitations of previously reported pendant polymer materials by using organocatalytic ROP to develop a more well-defined new generation of degradable pendant diblock copolymers. A family of mPEG-b-PC pendant polymers was successfully synthesized from several novel and previously reported cyclic

carbonate monomers via organocatalytic ROP using either TBD or the DBU/TU co-catalyst system. Several copolymerizations of the cyclic carbonate monomers were performed to generate materials having tunable pendant group density along the polymer backbone and polydispersities of ~ 1.2 . These diblock copolymers formed nanoparticles in the 100 - 250 nm size range, with slightly positive ζ , when compared with β -CD-PEI and β -CD-PEI:pDNA complexes at N/P ratios > 10 . The favorable transfection performance of these complexes relative to Lipofectamine 2000 suggests that these materials may be useful agents for *in vivo* gene delivery applications.

CHAPTER 6. EVALUATION OF CHOLESTEROL EFFLUX POTENTIAL FOR HYDROXYPROPYL- β - CYCLODEXTRIN:POLY(DECAMETHYLENEPHOSPHATE) POLYROTAXANES IN NIEMANN-PICK C1 CELL

Reprinted (adapted) from the journal article titled “Synthesis of Hydroxypropyl- β -cyclodextrin:Poly(decamethylenephosphate) Polyrotaxane and Evaluation of its Cholesterol Efflux Potential in Niemann-Pick C1 Cells”, authored by Kerstin Egele, Shayak Samaddar, Nina Baudendistel, David Thompson, Gerhard Wenz. Shayak Samaddar performed *in vitro* biological characterization of polyrotaxanes which includes fillipin staining, high content imaging, cytotoxicity evaluations, confocal microscopy and flow cytometry experiments. Published: J. Mater. Chem. B, 2019,7, 528-537

6.1 Introduction

Cyclodextrins (CDs) are cyclic oligomers of glucose known to complex hydrophobic or amphiphilic guest molecules in aqueous environments due to hydrophobic interactions³⁵⁵⁻³⁵⁶. This binding ability has been widely exploited for the solubilization of active pharmaceutical ingredients (APIs) for improvement of their bio-availability and reduction of undesirable side effects³⁵⁷⁻³⁵⁸. Hydroxypropyl- β -CD (HP- β -CD), a highly water-soluble derivate of β -CD, is already commercially used for several drug formulations, for example for itraconazole (“Sporanox”)³⁵⁹, hydrocortisone (“Dexocort”)³⁶⁰, and indomethacin (“Indocid”)³⁶¹. Furthermore, HP- β -CD itself can exhibit pharmacological action due to solubilization and transport of cholesterol as well as influencing the lipid rafts of cells³⁶²⁻³⁶³. HP- β -CD forms a water-soluble 2 : 1 complex with cholesterol as demonstrated by solubility measurements³⁶⁴⁻³⁶⁵, thus offering therapeutic potential for the treatment of lysosomal metabolic disorders such as Niemann-Pick Type C (NPC)³⁶⁶⁻³⁶⁸. This rare genetic disease (incidence $\sim 1 : 120\,000$) leads to an accumulation of cholesterol and sphingolipids in the lysosome because of mutations in either the NPC1 or NPC2 proteins. Aberrant accumulation of cholesterol as microcrystalline deposits leads to damage of liver, spleen and brain, causing progressive degeneration of the patient³⁶⁹. Administration of HP- β -CD promotes cholesterol normalization within late endosomal/lysosomal compartments to enable its metabolism and excretion³⁷⁰. Subcutaneous administration of 4000 mg kg⁻¹ body weight of HP- β -CD 4 days a week produced a 72% reduction of total cholesterol content in the liver of npc^{-/-} mice after treatment for 77 d³⁷¹. Despite this success, the poor pharmacokinetics of HP- β -

CD require frequent administrations that are cumbersome and potentially toxic (*e.g.*, lung damage)³⁷²⁻³⁷³. These side effects can be mitigated by intracisternal administration; however there is still a risk of ototoxicity³⁷⁴⁻³⁷⁵. Therefore, alternative methods for a safer administration of HP- β -CD are desirable. We report a new material for cyclodextrin delivery based on a water-soluble polyphosphate HP- β -CD polyrotaxane.

In general, polymers are attractive as potential carriers for the controlled delivery of APIs. Polymeric delivery vehicles have been employed to improve both the solubility and bioavailability of drugs to improve their efficacy and/or diminish their toxicity³⁷⁶⁻³⁷⁷. These vehicles can improve the retention of the drug in the human body due to reduced renal clearance^{212, 378}. Targeting is also possible through incorporation of ligands that promote active transport into specific cells *via* receptor-mediated endocytosis³⁷⁹.

Covalent linkage of APIs to degradable polymers produces polymeric pro-drugs that are new molecular entities, thus requiring extensive toxicity and efficacy testing³⁸⁰. More commonly, a strategy of physically mixing small molecules and polymeric carriers, such as PLGA or modified starch, is employed to produce vehicles with improved delivery characteristics, although burst release of the API due to weak intermolecular interactions is often observed for these formulations. Polyrotaxanes, molecules where many macrocyclic rings are strung onto a polymer chain, are interesting alternative carrier entities since they are kinetically less stable than polymeric prodrugs, but by far more stable than physical mixtures due to the topological bond between the threaded rings and the polymeric backbone³⁸¹⁻³⁸². The dissociation rate of a polyrotaxane can be controlled by the type of stopper groups attached along the polymer or at the chain ends to allow slow release of the threaded rings^{381, 383}.

Polyrotaxanes have been synthesized from various ring shaped molecules, such as crown ethers, cucurbiturils and cyclodextrins³⁸⁴. Among these macrocyclic precursors, cyclodextrins have been the most widely explored since they are produced on an industrial scale, display very low toxicity under physiological conditions, and have been widely used as excipients in FDA-approved small molecule drug formulations^{359, 385}. Amphiphilic polymers are suited best for the formation of CD polyrotaxanes since CDs spontaneously thread onto hydrophobic chain segments in water driven

by hydrophobic interactions^{381, 386}. So far, neutral and cationic polymers like polyethylene glycol³⁸⁷, polypropylene glycol^{70, 388}, poly(oligomethylenimine)s³⁸¹ and derivatives of them, as well as polyamides³⁸⁹ and polyesters have been complexed by CDs to form polyrotaxanes. Among them, the neutral CD polyrotaxanes show very low water solubilities and require further derivatization³⁵⁶. Rapid normalization of cholesterol levels in NPC cells³⁷⁰ and the mouse model of NPC disease³⁸² has been reported for polyrotaxanes composed from HP- β -CD (or 2-(2-hydroxyethoxy)ethyl carbamate-modified β -CD) and PEG-PPG-PEG block polymers^{36, 370, 382, 390}. Although the PEG backbone provides modest improvements in polyrotaxane solubility, it could potentially contribute to immune responses, liver accumulation, and poor bio-degradability. Cationic CD polyrotaxanes³⁹¹⁻³⁹² are known to be highly water-soluble; however, these materials are often accompanied by significant toxicity^{266, 282}. These potential shortcomings in the development of an effective CD polyrotaxane-based NPC therapy led us to explore the synthesis and performance testing of anionic polyrotaxanes derived from poly(decamethylenephosphate), a nontoxic water-soluble polymer that is degradable by hydrolysis in aqueous media. Polymeric phosphoric acid diesters are synthetic analogs of polynucleotides that are known to be degradable by nucleases to generate non-toxic byproducts³⁹³. They can be readily prepared by oxidation of polymeric phosphorous acid diesters. The latter are typically prepared by transesterification of diphenyl phosphite with α,ω -diols³⁹⁴. Polymeric phosphodiester have already been used as prodrugs, hydrogels and drug carriers³⁹⁵⁻³⁹⁷. A pseudopolyrotaxane based on biodegradable polyphosphoester ionomers obtained by ring opening polymerization has been described by Tamura *et al.*³⁹⁸ Polyrotaxane formation was only observed with α and γ -CD and the resulting polyrotaxanes formed precipitates in aqueous solution. No inclusion complexes were obtained with β -CD.

We herein describe for the first time the homogenous assembly of a water-soluble polyrotaxane from HP- β -CD and an anionic polymeric phosphodiester. The resulting HP- β -CD polyrotaxane displays cholesterol normalization activity in NPC cells.

6.2 Materials and methods

Synthesis and TNS assay. Please refer to published manuscript.

Filipin Staining of NPC1 cells. NPC1-deficient cells (Coriell Institute) were seeded in 96 well tissue culture dishes at a density of 1600 cells/well in Eagle's minimum essential medium, supplemented with 10% fetal bovine serum and 1% penicillin/streptomycin. The cells were incubated for 24 h at 37 °C in 5% CO₂ before treatment with **6** or free HP-β-CD solution in triplicate. A 100 μL solution containing 0.24 mg of **6** to give a HP-β-CD equivalent concentration of 800 μM in the cell culture media was used per well as the highest concentration. HP-β-CD equivalent concentrations of 400, 200, 100, 25, 12.5 μM and untreated control were used to evaluate the dose-response relationship of **6** in NPC1-deficient cells. α-CD (0.4 μg) and 3.4 μg polydecamethylene phosphate **1** per well (amount of **1** present in 25 μM HP-β-CD equivalent of **6**) were additional controls. After 24 h, the cells were washed with PBS and fixed using 3.7% paraformaldehyde solution. Total unesterified cholesterol content within the cells was determined by staining with 50 μg/mL Filipin III in PBS for 1.5 h. Next, the cells were washed and the nuclei were stained with a solution of 16 μM Nuclear Red DCS1 (AAT Bioquest) in PBS. Cells were imaged using the 5× objective on an Opera Phenix High-Content Imaging System (Perkin Elmer). Harmony Software (v4.1, Perkin Elmer) was used to quantify the data collected from one field per well while excluding border cells. Nuclei were identified in the Cy5.5 channel and unesterified cholesterol content was evaluated using the mean filipin intensity above the background in the DAPI channel. Mean filipin intensity in treated cells were compared to that of untreated cells and expressed as % Fillipin stain ± SEM. One-way ANOVA analysis was performed in GraphPad Prism (v7.03, GraphPad Software). MTS assays were performed as per manufacture's protocol to evaluate the apparent toxicities of **6** at the concentrations used.

Cellular Tracking of α-CD End-capped Polyrotaxanes. NPC1-deficient cells were treated with 25 μM CD equivalent FITC-tagged polyrotaxane **6a** in Opti-MEM media and incubated for either 4 h or 24 h at 37 °C, 5% CO₂ and 95% relative humidity. After 24 h treatment, the polyrotaxane solution was removed and the cells washed with 1X PBS to remove non-internalized polyrotaxane **6a** and incubated for another 24 h under the same conditions. For imaging, the nuclei were stained with Hoechst 33342 and the acidic endosomal and lysosomal compartments were stained with

Lysotracker Red DND 99. Confocal images were acquired using a Nikon A1R multiphoton confocal microscope with a 60X oil objective equipped with 405 nm, 488 nm and 561 nm lasers for Hoechst 33342, FITC and Lysotracker Red DND 99, respectively.

FACS Analysis. NPC1-deficient cells treated with 25 μM CD equivalent FITC tagged PR **6a** in Opti-MEM media and incubated for 4 h or 24 h at 37 $^{\circ}\text{C}$, 5% CO_2 and 95% relative humidity. After 24 h treatment, the PR solution was removed by aspiration and washing the cells with 1X PBS to remove non-internalized **6a** and incubated for another 24 h under the same conditions. FACS analysis for cellular association was performed using a BD LSR Fortessa flow cytometer equipped with a 488 nm laser to quantify mean fluorescence of 5000 NPC1 cells (n=3, one-way ANOVA, ****p<0.0001)

6.3 Results and discussion

6.3.1 Polymer Synthesis

Refer to Publication

6.3.2 Cholesterol efflux potential of developed polyrotaxanes

The therapeutic potential of polyrotaxane **6** was evaluated in primary NPC1 fibroblasts. In brief, NPC1-deficient cells (1600 cells/well in 96-well plates) were incubated with **6** for 24 h at 37 $^{\circ}\text{C}$ with different equivalent concentrations of free HP- β -CD in the cell media. The cells were then rinsed, fixed, stained with filipin, and the relative degree of cholesterol accumulation in the treated cells compared with untreated controls. Filipin staining correlates with the relative cholesterol accumulation in cells. A significant decrease in filipin staining (~10%) was observed in treated NPC1 cells relative to untreated cells upon incubation for 24 h with a single dose of polyrotaxane **6** at an equivalent HP- β -CD concentration of 25 μM (i.e., polyrotaxane **6** concentration = 25 μM HP- β -CD \div 14 HP- β -CD/PR = 1.825 μM **6**). Additionally, treatment monomeric α -CD (at a concentration present in 1.825 μM **6**) did not result in any cholesterol efflux. This is most likely because the hydrophobic cavity of α -CD is too small of accommodate cholesterol molecule as reported by Davidson *et al.*⁶³ Increasing the concentration of **6** results in enhanced cholesterol efflux with about 20% and 40% decrease in fillipin staining at 200 μM and 800 μM HP- β -CD

equivalent concentrations, respectively. The observed smaller effect of polyrotaxane **6** compared to free HP- β -CD was attributed to the slow release of the threaded rings leading to a much lower bioavailability of the polyrotaxane-borne HP- β -CD. A cytotoxicity profile evaluation of **6** using MTS assay (**Figure 7**), however, reveals a sharp increase in toxicity of **6** above 200 μ M HP- β -CD equivalent dose. We infer from these findings that **6** is dethreaded after internalization by the cells to release the HP- β -CD payload to effectively mobilize the aberrantly stored cholesterol deposits in NPC1-deficient cells as previously reported by Mondjinou *et al.*³⁷⁰ Although monomeric dose of HP- β -CD performs better in cholesterol efflux from the cells after a single 24 hours treatment in comparison of **6** (**Figure 8**), the potential of **6** as a long circulating and slow HP- β -CD releasing platform makes them an attractive candidate for NPC therapeutics.

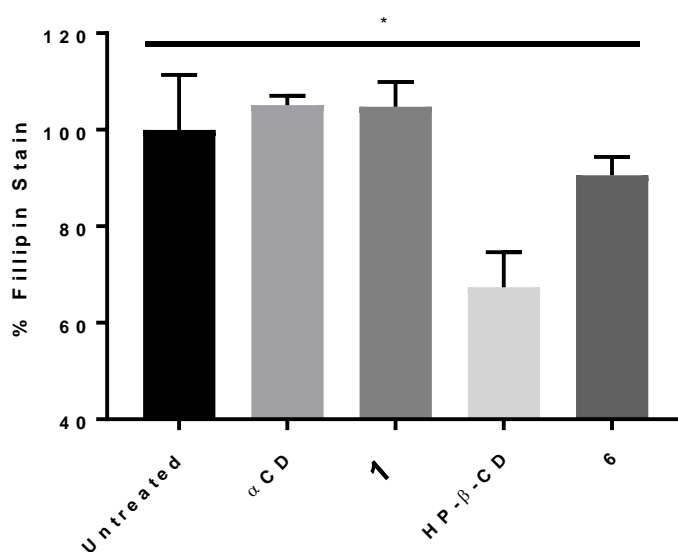


Figure 54. Filipin staining of primary fibroblasts after treatment with α -CD, poly-(decamethylenephosphate) **1**, HP- β -CD and **6** for 24 h (25 μ M equivalent HP- β -CD dose, Filipin was used at 50 μ g/mL).

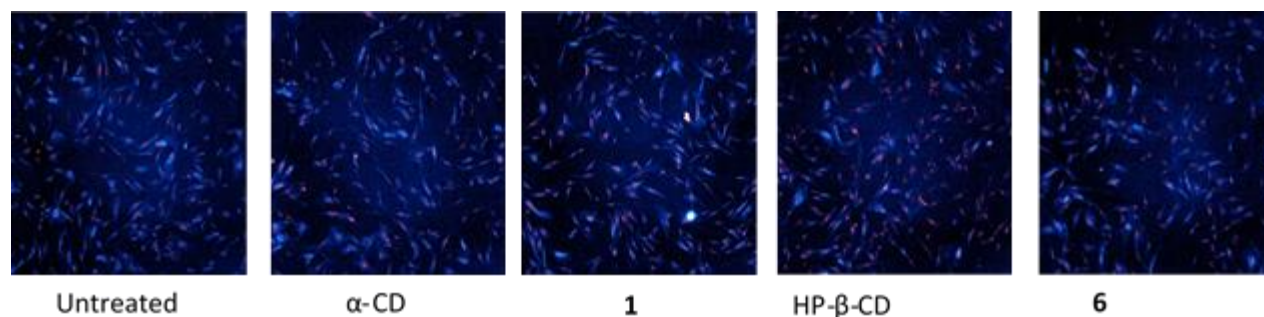


Figure 55. Filipin staining of primary fibroblasts after treatment with α -CD, poly-(decamethylenephosphate) **1**, HP- β -CD and **6** for 24 h (25 μ M equivalent HP-*b*-CD dose. Nuclei were stained with Nuclear Red. Cells were imaged with a 5 x objective.

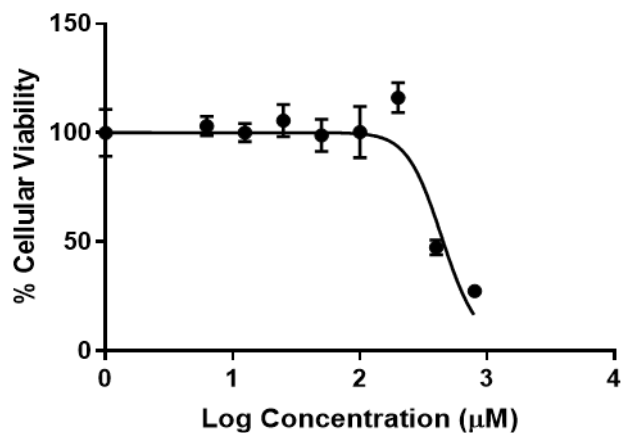


Figure 56. Cytotoxicity of **6** evaluated via MTS assay after 24 h exposure to NPC1-deficient cells.

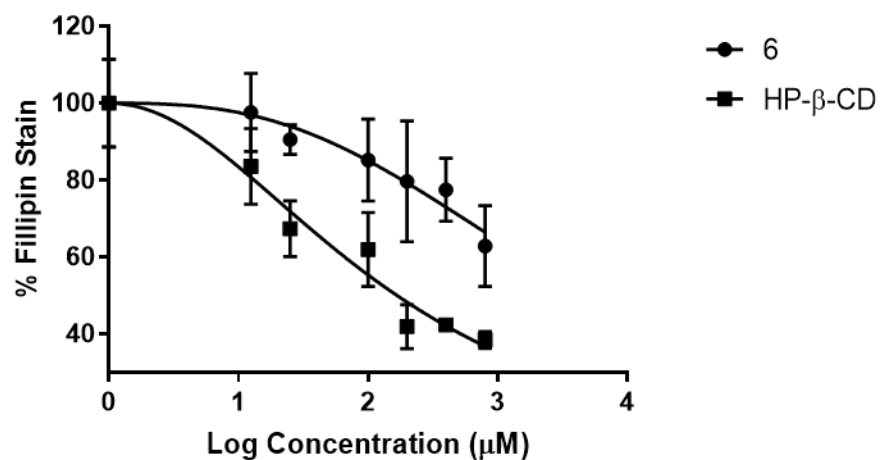


Figure 57. Dose-response curve in NPC1 cells after a single 24 h treatment with **6** and HP- β -CD.

6.3.3 Confocal studies for cellular tracking of polyrotaxanes in NPC1 cells

A FITC tagged polyrotaxane **6a** was prepared for cellular tracking studies by co-threading a small amount of fluorescein-labeled β -CD **7** (shown in **Figure 9**, synthesis described in Supporting Information) with HP- β -CD and subsequently stoppered by α -CD.

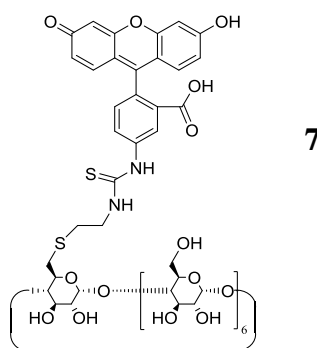


Figure 58. Structures of FITC-tagged polyrotaxane **6a** and the fluorescent CD-derivative **7**.

NPC1-deficient cells begin to internalize polyrotaxane **6a** within 4 h, however, the polyrotaxane appears only within non-acidic vesicles (i.e, compartments that are not stained by LysoTracker). These are most likely to be endosomes at an earlier stage of maturation.^{65,66} Extensive association of the polyrotaxane with the extracellular matrix of NPC1-deficient cells was also observed as indicated by prominent extracellular staining. Significant cellular uptake and localization within the acidic late endosomal/lysosomal compartment was observed after 24 h of treatment (**Figure 10C**) Next, the non-internalized polyrotaxane was removed and cells were washed to prevent further uptake of **6a** before incubating for another 24 h to monitor the cellular fate of the already internalized polyrotaxane (**Figure 10D**). The latter images show decreased fluorescein signal intensity indicating that the cyclodextrins escape the endosomal/lysosomal compartments of the cell or are degraded within them.

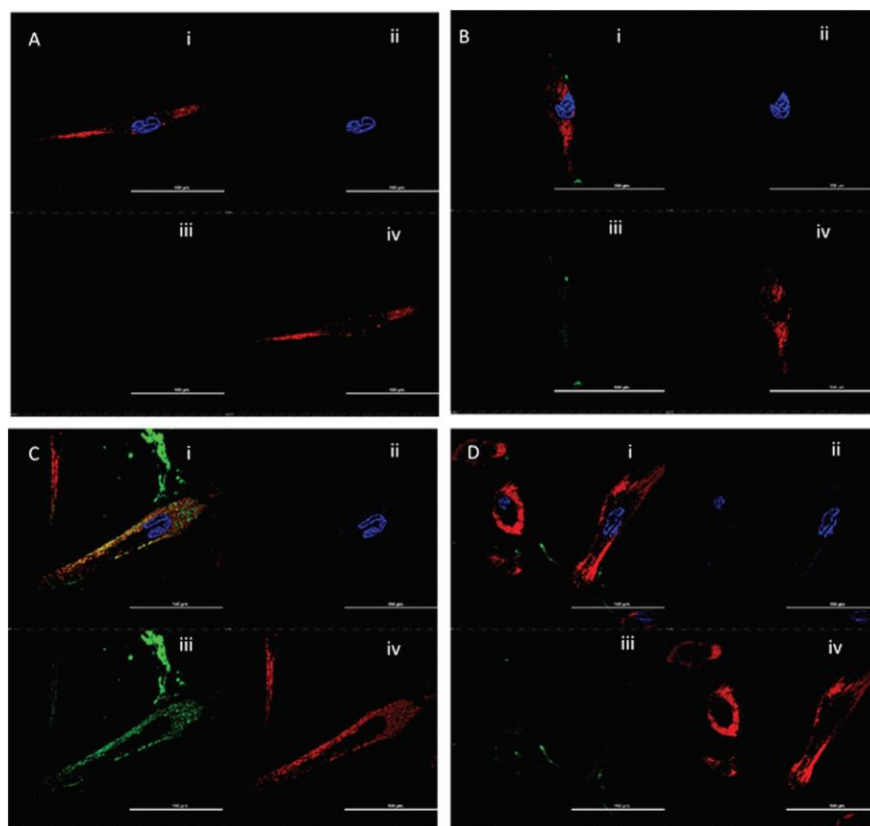


Figure 59. NPC1-deficient cells treated with 25 μ M CD-equivalent FITC tagged polyrotaxane **6a** in Opti-MEM media. (A) untreated cells, (B) 4 h **6a** treatment (c) 24 h **6a** treatment, and (D) C + 24 h post-treatment. i : all fluorescence channel; ii : DAPI channel; iii : fluorescein channel, and iv : LysoTracker channel. Localization within acidic endosomes/lysosome (red, stained with LysoTracker) peaked at 24 h after addition of **6a**, after which the cells were washed to remove **6a** and incubated for another 24 h in complete MEM media. Confocal images acquired 24 h post treatment show a decrease in the FITC signal indicating either cyclodextrin escape from the acidic compartments or fluorescein degradation within them. The scale bar = 100 μ m.

6.3.4 FACS analysis Polyrotaxane cellular association with NPC1-deficient Cells

As suggested by our confocal data, NPC1-deficient cells show cellular association by 4 h. Mean fluorescence intensities peaked at 24 h after treatment. The cells were washed to remove non-internalized PR and prevent further uptake of PR before incubating for another 24 h to monitor the cellular fate of the already internalized PR. This is referred to as the 48 h timepoint. The 48 h time point images show decreased mean FITC intensity, indicating that all cells internalize the PR. The data also suggest that the PR are capable of escaping from the endosomal/lysosomal compartments of the cell or are degraded within them (**Figure 11**).

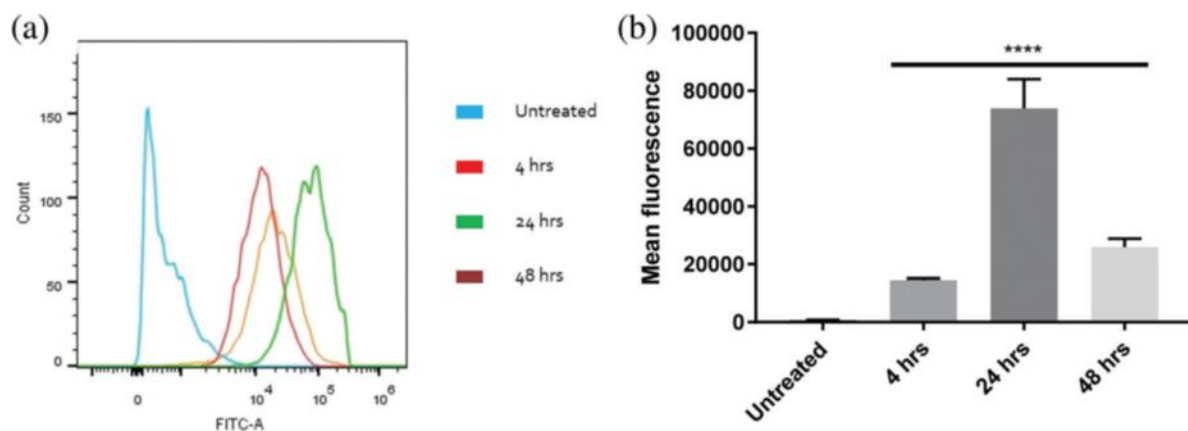


Figure 60. a) Histogram Plot for FITC intensity distribution among NPC1-deficient cell population. b) Cellular association of Polyrotaxane **6a** with NPC 1-deficient cells.

6.4 Conclusions

A new HP- β -CD polyrotaxane containing a decamethylenephosphate core has been synthesized and its cholesterol normalization capacity evaluated in NPC1-deficient cells. The degree of polymerization in preparation of the decamethylenephosphate polymeric precursor was determined to be 76. The degree of α -CD threading to produce 5 was estimated to be 48.5% after 2.9 d, whereas the HP- β -CD coverage was 18% and α -CD endcapping was approximately 3% in polyrotaxane 6. Reduction in filipin staining, indicative of cholesterol depletion, was found to be approximately 20% at a polyrotaxane concentration of 0.3 g/L after 24 h incubation, similar in magnitude to the reductions observed by Mondjinou *et al.*³⁹⁹ with mixed HP- β -CD:SBE- β -CD Pluronic polyrotaxanes that were used in 6 h exposures to NPC1 cells. Taken together, the findings shown in Figures 5, 6 and 8, suggest that polyrotaxane 6 may be a useful tool for the delivery of HP- β -CD as a therapeutic payload for normalizing cholesterol levels in Niemann-Pick Type C cells. The main advantages of our system is the simple release of HP- β -CD from the polymer by slippage³⁹⁷ and the expected slow renal clearance due to the high molecular weight of the polyrotaxane 6 of around 35 kDa. There is no need for any cleaving enzymes to release the drug in the cells.

CHAPTER 7. STRUCTURE-FUNCTION RELATIONSHIPS OF CHOLESTEROL MOBILIZATION BY β -CD POLYROTAXANES IN NPC1-DEFICIENT HUMAN CELLS

Adapted (Reprinted) from the research article titled “Structure-function relationships of cholesterol mobilization by β -CD polyrotaxanes in NPC1-deficient human cells” authored by Shayak Samaddar, Debosreeta Bose, Bradley P. Loren, Joseph L. Skulsky, Olga Ilynytska, Zachary J. Struzik, Judith Storch and David H. Thompson^a. Shayak Samaddar was involved in cholesterol efflux, flow cytometry and cytotoxicity studies. Currently the article is under consideration for publication in a peer reviewed journal.

7.1 Introduction

Niemann-Pick Type C disease (NPC) is a fatal, neurodegenerative, lysosomal lipid trafficking disorder resulting from aberrant accumulation of unesterified cholesterol and glycosphingolipids in the late endosomal/lysosomal (LE/LY) compartment in many organs including brain, liver, lungs, and spleen⁴⁰⁰. This rare autosomal recessive disease has a broad spectrum of clinical phenotypes, including severe liver disease, breathing difficulties, developmental delay, seizures, decreased muscle tone, lack of coordination, feeding problems, and vertical gaze palsy⁴⁰¹. Life expectancy for NPC patients is generally below 20 years of age, although later onset cases have also been reported⁴⁰². Its prevalence in Western countries has been reported to be as low as 1:120,000 to 1:150,000 live births⁴⁰². The genetic cause of the disease has been traced to loss of function mutations in the genes encoding for Niemann-Pick Type C1 (NPC1) or Niemann-Pick Type C2 (NPC2) proteins⁴⁰³⁻⁴⁰⁴. Most patients (90-95%) diagnosed with NPC have mutations in the NPC1 gene⁴⁰³. At present, there is no FDA approved therapy for this rare genetic disorder, making it a serious unmet medical need.

2-Hydroxypropyl- β -cyclodextrin (HP- β -CD) has shown efficacy in reducing cellular cholesterol levels in both the mouse and cat models of NPC⁴⁰⁵⁻⁴⁰⁶. Weekly *s.c.* administration of HP- β -CD in NPC mice reduced cholesterol levels in most organs except lungs and brain⁴⁰⁵. Notably, its poor pharmacokinetic properties due to rapid renal excretion necessitated the use of high doses (4000 mg/kg) administered at frequent intervals to achieve the therapeutic effect⁴⁰⁵. The severity of the disease and the apparent inability of HP- β -CD to cross the blood-brain barrier efficiently has led the FDA to approve two clinical trials for HP- β -CD derivatives, one where the drug is administered by the intrathecal route (VTS-270)⁴⁰⁷ and the other where it is administered intravenously

(Trappsol)⁴⁰⁸. Phase 1 clinical trials with VTS-270 showed encouraging safety and effectiveness data when administered via monthly *i.t.* injection at a 900 mg dose.⁴⁰⁹ VTS-270 was evaluated in a Phase IIb/III prospective, randomized, double-blind, sham-controlled study to further probe its safety and efficacy via *i.t.* injections every 2 weeks at doses of either 900, 1200, or 1800 mg⁴⁰⁷. Although the clinical data are encouraging, high doses of HP- β -CD have been reported to cause lung damage and ototoxicity⁴⁰⁷. Consequently, a safer formulation that improves the pharmacokinetic profile and avoids off-target toxicity of this promising drug candidate is highly desirable.

We have previously reported the synthesis and cellular cholesterol normalization performance of β -cyclodextrin (β -CD)-based polyrotaxanes (PR) as potential NPC therapeutics;⁴¹⁰⁻⁴¹³ findings that were subsequently corroborated using compounds of similar structure⁴¹⁴⁻⁴¹⁵. Polyrotaxanes are non-covalent self-assemblies derived from macrocycles that are threaded onto a polymer core followed by the attachment of a bulky molecule (or endcap) to prevent dethreading of the macrocycle. Our efforts have focused on threading various β -CD derivatives onto Pluronic triblock copolymers. The hydrophobic central polypropylene glycol (PPG) block of these copolymers provides a driving force for interaction with the hydrophobic central core of the β -CD molecules. The number of β -CD molecules threaded onto the polymer impacts not only the molecular weight of the assembly, but also the rigidity of the PR structure. This, in turn, has an impact on the pharmacokinetics and pharmacodynamics of the PR *in vivo*, with highly threaded variants exhibiting longer blood residence times and depositing primarily in the liver⁴¹². Variants with lower threading efficiencies, however, are more rapidly cleared through the kidneys.⁴¹²

In an effort to more thoroughly explore how PR structure impacts its ability to clear cholesterol from NPC1-deficient cells, we now report the synthesis and testing of two different PR libraries. The first compound collection was synthesized using a previously reported solvent-assisted threading protocol,⁴¹⁰ wherein both the polymer core structure and β -CD type were varied. A simplified solvent-free mechanochemical synthesis approach was also developed and used to produce the second compound library. This solid phase method, conceptually related to the method of Tanaka and coworkers,⁴¹⁶ was used to fabricate PR containing a nominal 7:3 molar ratio of 2-hydroxypropyl- β -cyclodextrin (HP- β -CD) and 4-sulfobutylether- β -cyclodextrin (SBE- β -CD) with similar polymer cores to evaluate the effect of threading efficiency on the ability of these PR to normalize cholesterol levels in NPC1 patient fibroblasts.⁴¹⁷

7.2 Materials and methods

Materials. Pluronic triblock copolymers L35 (EO 22, PO 16) and L81 (EO 6, PO 43), HP- β -CD (DS 7-8), methyl- β -cyclodextrin, carbonyldiimidazole (CDI), triethylamine (TEA), and tris(2-aminoethyl)amine (TAEA) were purchased from Sigma-Aldrich. SBE- β -CD (DS 6.5) was a gift from Ligand Pharmaceuticals (San Diego, CA). Toluene, dichloromethane (DCM), and acetonitrile (ACN) were dried using a PPT Solvent Drying Apparatus (Nashua, NH) prior to use. Slide-A-Lyzer™ cellulose dialysis cassettes (2 kDa molecular weight cutoff (MWCO)) were obtained from Thermo Fisher Scientific and immersed in deionized water for at least 30 min prior to use. Ultrapure water (resistivity $\approx 18.2 \text{ M}\Omega/\text{cm}^{-1}$) was generated from a Barnstead *MicroPure* water purification system. Human fibroblasts from an NPC1 disease patient (GM03123) were obtained from Coriell Institute of Medical Research (Camden, NJ). Filipin III and Heparin sodium salt (from porcine intestinal mucosa) were purchased from Sigma.

Nuclear Magnetic Resonance Spectroscopy. ^1H NMR spectra were collected using a Bruker AV-III-500-HD spectrometer fitted with a cryoprobe. Spectra were recorded at 25 °C at a concentration of approximately 10 mg PR/1 mL in DMSO- d_6 .

General Procedure for Preparation of EDA-modified Pluronics. (Procedure conducted by Brad Loren) The Pluronic precursor (5 g) was azeotropically dried four times from toluene and evaporated overnight under a $< 100 \text{ }\mu\text{m Hg}$ vacuum. The Pluronic was then suspended in dry ACN (95 mL) before addition of CDI (10.67 g) with stirring for 5 h. Water was then added (4 mL) to quench unreacted CDI, followed by addition of ethylenediamine (EDA, 8.8 mL) and stirring at 20 °C overnight. Partial solvent removal by rotary evaporation to reduce the volume by approximately two thirds was performed before adding water (37.5 mL) and dialyzing the mixture for 3 d against 30% ethanol in water using 2 kD MWCO dialysis cassettes. The dialysate was then subjected to rotary evaporation to remove as much solvent as possible before azeotropically drying the product three times from toluene.

General Method for Decaarginine Endcapping of EDA-modified Pluronics (PR1 & PR2). (Procedure conducted by Joseph Skulsky) EDA-modified Pluronic (0.62 g) was suspended in 38 mL hexanes and stirred overnight at 20 °C before adding 6.37 g of HP- β -CD. The resulting

suspension was bath sonicated for 1 h, probe sonicated for 30 min, and then stirred at 20 °C for 3 d. The solvent was removed by rotary evaporation, followed by addition of 20 mL of dry ACN and CDI (67 mg) with stirring of the mixture for 5 h at 20 °C under Ar. Solid decaarginine (0.992 g) was added to the reaction mixture with stirring at 20 °C under Ar. After stirring for 12 h, triethylamine (0.59 mL) was added and the mixture stirred for an additional 24 h at 20 °C under Ar. The mixture was then processed by rotary evaporation of the solvent, dissolution of the solid in ~25 mL deionized water, and dialysis of the aqueous solution against deionized water using 6-8 kD MWCO dialysis cassettes.

General Method for Preparation of α,ω -Bis-tris(2-aminoethyl)amine-modified Pluronics.

(Procedure conducted by Brad Loren) The method used for the synthesis of all TAEA modified Pluronics in this study generally followed the approach described by Mondjinou *et al.*⁴¹⁰ Pluronic L81 (3.64 mmol) was azeotropically dried with toluene and placed under a < 100 μm Hg vacuum overnight before dissolving in dry ACN (200 mL) and adding CDI (37.5 mmol). The solution was stirred under an Ar atmosphere overnight. DI water (8 mL) was then added to quench the unreacted CDI and the reactor vented to air to enable CO₂ gas evolution for 20 min. Tris(2-aminoethyl)amine (181.8 mmol) was then added and the solution stirred at 20 °C overnight. Roughly one third of the ACN was removed by rotary evaporation before addition of 30% EtOH and transfer of the solution to 2 kDa MWCO dialysis cassettes. The product was dialyzed over 3 d against 30% EtOH. The solvent was then removed and dried under vacuum to yield α,ω -bis-tris(2-aminoethyl)amine Pluronic intermediate (Pluronic-TAEA) as a viscous liquid.

Solvent-Assisted Synthesis of Cholesterol-endcapped HP-/SBE-/Me- β -CD Polyrotaxanes

(PR3 – PR8). (Procedure conducted by Brad Loren) These compounds were prepared as previously described.^{410, 417} In brief, the β -CD derivative(s), at a total CD equivalency of one CD unit per two PPG monomer repeats in the Pluronic, was added to a solution of TAEA-Pluronic in hexanes and the slurry briefly bath and probe sonicated before stirring vigorously for 3 d. Cholesteryl chloroformate in DCM was then added and the mixture stirred for 1 d before purification by dialysis (6-8 kDa MWCO membranes) against DMSO for 1 d and deionized H₂O for 4 d. Lyophilization yielded the product as a white powder. Threading efficiencies were determined by integration of the protons on the cyclodextrin derivatives relative to the CH₃ group

of the PPG block of the Pluronic polymer, wherein 100% threading efficiency occurs at a 2:1 ratio of PPG monomer units:CD. ¹H NMR (500 MHz, DMSO-d₆): $\delta = 4.1 - 5.1$ (*b*, C₁-H and C₆-OH of CDs), 3.5-3.8 (*m*, C_{3,5,6}-H of CD), 1.6 (*b*, (CH₂)-SO₃⁻), 1.0 (*d*, CH₃ of PPG).

Mechanochemical Synthesis of Cholesterol-endcapped HP-/SBE- β -CD Polyrotaxanes (PR9

– PR 20). (Procedure conducted by Brad Loren) A mixture of solid TAEA-Pluronic and the desired β -CD variants (500 mg of Pluronic + β -CD mixture at varying ratios) were loaded into agate jars with agate balls and processed in a planetary ball mill (PQN04, Across International) at 350 rpm for varying periods of time (24 – 96 h). For each sample, the number of 6 mm (30-35) and 10 mm (0-5) balls varied. Endcapping with cholesteryl chloroformate and TEA was performed in DCM as previously described.⁴¹⁷ In all cases, purification was accomplished by multiple ether washes and the product collected by centrifugation, followed by dialysis against deionized H₂O using 6-8 kDa MWCO dialysis cassettes. Each sample was lyophilized to obtain the PR as a white powder. Threading efficiencies were determined as described above. ¹H NMR (500 MHz, DMSO-d₆): $\delta = 4.5 - 5.1$ (*b*, C₁-H and C₆-OH of CD), 3.5-3.8 (*m*, C_{3,5,6}-H of CD), 1.6 (*b*, (CH₂)-SO₃⁻), 1.0 (*d*, CH₃ of PPG).

Evaluation of Cholesterol Mobilization by β -CD and PR Derivatives in NPC1 Cells.

Cell culture was performed as previously described¹¹ with minor modification. Briefly, NPC1-deficient cells were seeded in 12 well cell culture plates with cover slips using Eagle's minimum essential medium with Earle's salts supplemented with 15% FBS, 1% PenStrep and 1% L-glutamine. Cells were seeded at a density of 2 X 10⁴ cells per well and incubated at 37 °C with 5% CO₂ for 36 – 48 h until they reached 85 – 90% confluency. The compounds were solubilized in DMSO (with sonication if needed) and diluted in culture medium to yield a final concentration equivalent to 25 μ M β -CD monomer. The final DMSO concentration was $\leq 0.01\%$ v/v. Cells were treated with these solutions for 24 h at 37 °C with 5% CO₂. Following the incubation period, cells were washed with PBS and fixed with 4% paraformaldehyde solution for 30 min. After fixation, cells were washed with chilled PBS and stained twice with 0.05 mg/mL filipin III for 1 h at 37 °C, with PBS washing after each staining period. The cover slips with filipin-stained cells were mounted on glass slides with Fluoromount G and sealed with clear nail polish. Images were taken at 40x magnification on an Olympus FSX microscope equipped with a DAPI filter set. Filipin

accumulation in cells was determined using NIS-Elements selection tools as previously described¹¹. The results in treated cells were normalized to filipin accumulation in untreated NPC1-deficient fibroblasts. MTS assays were performed as per the manufacturer's protocol (Promega®) to evaluate the apparent toxicities of the polyrotaxanes at the concentrations used.

Synthesis of Fluorophore-labeled PR Derivatives (PR1* and PR2*). (Procedure conducted by Zach Struzik) Fluorescently labeled PRs (PR1* and PR2*) were synthesized according to the following procedure. The polyrotaxane (1 equivalent) was placed in a septum sealed 2-neck round bottom flask equipped with a magnetic stir bar. Dry DMF (5 mL) was added under Ar and the mixture stirred before adding CDI (3 equivalents) to the solution from a 9 mg/mL stock solution in dry DMF. This mixture was stirred for 3 h before adding 2,2'-(ethylenedioxy)bis(ethylamine) (3 equivalents) to the reaction from a 2.5% stock solution in dry DMF and stirring for an additional 16 h. Fluorescein isothiocyanate (3 equivalents) was then added to the reaction mixture with stirring for another 12 h. The solution was then diluted with 15 mL of DI water and dialyzed against DI water using 6-8 kDa MWCO regenerated cellulose dialysis membranes over 3 d. The dialyzed polyrotaxane was then centrifuged to remove any water insoluble particles and the final product lyophilized to yield 29 mg of an orange powder.

Localization of Fluorescently-labeled PR Derivatives. NPC1-deficient cells were grown on glass coverslips. FITC-conjugated PRs were reconstituted in DMSO; the final polymer concentration used for the treatment yielded the equivalent of 25 μ M free HP- β -CD. Compounds were added to NPC1-deficient fibroblasts for 1, 2, 6, 16 and 24 h. After incubation, the cells were rinsed with PBS and incubated with 75 nM Lyotracker Red DND 99 (Thermo Fisher Scientific, Waltham, MA) for 45 min in complete medium. Cells were rinsed with PBS, fixed in 4% paraformaldehyde (Electron Microscopy Sci., Halfield, PA) for 10 min, stained with DAPI to visualize nuclei (Thermo Fisher Scientific) and mounted using Fluoromount-G Slide Mounting Medium (Electron Microscopy Sci). Images were acquired using a Zeiss LSM710 confocal microscope (Carl Zeiss Inc., Thornwood, NY) equipped with a 63x, 1.4-numerical-aperture Zeiss Plan Apochromat oil objective.

FACS Analysis for cellular uptake of Fluorescently-labeled PR. NPC1-deficient cells were grown in 12 well plates as described above. At 80% confluency, cells were treated with 25 μM HP- β -CD equivalent PR1* and incubated for 2, 8 or 24 h under 37 $^{\circ}\text{C}$, 5% CO_2 and 95% relative humidity. Additionally, to inhibit heparan sulfate proteoglycans (HSPG) receptor mediated uptake of PR1*, cells were incubated in the presence of 30 $\mu\text{g}/\text{mL}$ heparin for 24 h. After incubation, cells were thoroughly rinsed with 1X PBS before trypsinization. Trypsinized cells were resuspended in 1 mL 1X PBS for flow cytometric analysis with BD LSR Fortessa equipped with a 488nm laser to quantify FITC fluorescence. Mean fluorescence from at least 500 cells were quantified. The experiment was performed in triplicate.

7.3 Results and discussion

Two libraries of compounds were prepared for this study, one using hexane-assisted synthesis and the other using a solid state mechanochemical synthesis approach. The materials were characterized by ^1H NMR to determine the relative ratios of β -CD, threading efficiency, cholesteryl endcapping extent, and molecular weight. The results are summarized in Tables 1 (solvent-assisted) and 2 (solid state).

Table 1. Compositions Observed for TAEA-Pluronic Polyrotaxane Library Prepared by Hexane Solvent-Assistance. R₁₀ = Decaarginine endcaps. Chol = Cholesteryl endcaps.

	Pluronic core	Ave. # HP- β -CD/PR	Ave. # SBE- β -CD/PR	Ave. # Me- β -CD/PR	Total # CD/PR	Endcap (# & Type)	Threading Efficiency (%)	MW (kDa)
PR1	L81	18	0	0	18	2, R ₁₀	82	31.9
PR2	L35	4	0	0	4	2, R ₁₀	50	11.4
PR3	L81	17	0	0	17	4, Chol	75	32.6
PR4	L35	6	0	0	6	4, Chol	77	17.3
PR5	L35	4	0	0	4	4, Chol	50	9.6
PR6	L35	4	2	0	6	4, Chol	75	13.6
PR7	L81	0	0	10	10	4, Chol	47	17.7
PR8	L81	12	6	0	18	4, Chol	82	34.0

Table 2. Compositions Observed for Cholesterol-endcapped TAEA-L81 Pluronic Polyrotaxane Library Prepared by Mechanochemical Synthesis.

	Pluronic Core	Ave. # HP- β -CD/PR	Ave. # SBE- β -CD/PR	Total # CD/PR	Endcap (# & Type)	Threading Efficiency (%)	MW (kDa)
PR9	L81	7	3	10	1.4, Chol	46	20.1
PR10	L81	2	3	5	0.1, Chol	23	12.4
PR11	L81	0	4	4	0.44, Chol	18	11.5
PR12	L81	6	4	10	1.6, Chol	46	20.7
PR13	L81	7	9	16	3.8, Chol	73	32.8
PR14	L81	4	3	7	1.6, Chol	30	15.8
PR15	L81	2	4	6	0.5, Chol	27	14.4
PR16	L81	12	6	18	1.3, Chol	81	33.0
PR17	L81	2	3	5	0.3, Chol	23	12.4
PR18	L81	6	4	10	0.8, Chol	46	20.2
PR19	L81	5	3	8	0.6, Chol	36	16.8
PR20	L81	3	4	7	0.9, Chol	32	15.9

7.3.1 Effect of polyrotaxane structure on cellular cholesterol mobilization

We have previously shown that PR with cholesterol endcaps recruit a variety of serum proteins, particularly apolipoproteins A-I, A-II, A-IV, C-I, C-II, C-III, and E lipoproteins.⁴¹² The cholesterol endcapped polyrotaxane derivatives were designed with this association in mind to serve as a potential Trojan Horse strategy by promoting their delivery to the LE/LY of NPC cells via LDL receptor mediated endocytosis. Satisfyingly, we found that incubation with these PR compounds led to cholesterol clearance from the LE/LY compartment, presumably via receptor mediated endocytosis since a fluorescent analogue of these compounds was shown to colocalize with LysoTracker,¹⁰ although bulk phase endocytosis may also be contributing to some of the PR delivery observed⁴¹⁸.

Cell-penetrating peptides are known to efficiently transport a variety of molecular and macromolecular cargo across plasma membranes⁴¹⁹⁻⁴²⁰ via energy-dependent and/or energy-independent pathways depending on the nature of the construct⁴²¹. We therefore sought to evaluate the effect of a positively charged decaarginine PR endcap on cholesterol normalization. Multiple studies have suggested that oligoarginine sequences do not cross the plasma membrane of live cells directly (i.e., by electrostatic interaction with negatively charged lipid of cell membrane);

rather, they bind to heparan sulfate proteoglycans (HSPG) present on the cell surface, resulting in heparan sulfate-mediated endocytosis⁴²²⁻⁴²⁶. Once inside this compartment, HSPG is cleaved by heparinase into oligosaccharide fragments. In the event that the oligoarginine endcapped PR materials follow this pathway, these constructs would be released into the cytosol. Although oligoarginine constructs can also escape into cytoplasm by endosomal leakage, this phenomenon has not been reported at the low micromolar concentrations used in our study⁴²¹. Under these conditions, the PR containing endosomes are likely to mature into lysosomes, where the carbamate bonds linking the decaarginine endcaps to the PR core are enzymatically cleaved to enable HP- β -CD dethreading⁴¹¹. Once the HP- β -CD units have been dethreaded, they are then available to mobilize accumulated cholesterol. Our Filipin III staining data suggest that PR1 and PR2, HP- β -CD polyrotaxanes with decaarginine endcaps led to cholesterol mobilization from cells, reducing cholesterol accumulation by 35 – 40% relative to untreated controls (Figure 1A). LDL receptor mediated endocytosis of LDL occurs predominantly by caveolar uptake⁴²⁷, whereas HSPG mediated endocytosis is a clathrin- and caveolin-independent, but dynamin- and flotillin-dependent, pathway⁴²⁸. Since both L81- and L35-based polyrotaxanes resulted in similar internalization kinetics and localizations, these findings reveal that cellular uptake is independent of the polymer backbone length. Interestingly, PR3 and PR4, species having similar HP- β -CD content, but with cholesterol endcaps and internalized via LDL receptor mediated pathways, were less effective than the decaarginine-endcapped PR1 and PR2, although this difference may also reflect the comparatively poor solubility of PR3 and PR4 relative to PR1 and PR2.

Inclusion of SBE- β -CD in the HP- β -CD polyrotaxane formulation was intended to boost the PR solubility in physiological saline solutions⁴¹⁷. Cholesterol mobilization improved when SBE- β -CD was included in the polyrotaxane scaffold. Our results show that PR6 and PR8 produced cholesterol mobilization levels that were almost as effective as the monomeric β -CD controls. Direct comparison of PR4 (6 HP- β -CD) and PR6 (4 HP- β -CD and 2 SBE- β -CD), both having the same total number of β -CD threaded onto a Pluronic L35 core, shows that inclusion of SBE- β -CD boosted sterol efflux to approximately 60% of control, while the compound with HP- β -CD alone led to efflux of only about 25%. The same trend is apparent for PR3 and PR8 with Pluronic L81 cores, where threading of HP- β -CD along with SBE- β -CD lowers the accumulated cholesterol by 70% compared to untreated NPC1 deficient cells, while the compound with HP- β -CD alone

reduced sterol by 40%. We infer from these findings that, as intended, the solubility enhancement provided by inclusion of SBE- β -CD units can substantially improve the performance of the polyrotaxanes⁴²⁹⁻⁴³⁰. Interestingly, the length of the polymer chain and number of CDs threaded on it did not result in a significant difference in cholesterol mobilization effectiveness, as had been expected; for example, between PR3 and PR4, or between PR1 and PR2, two groups of compounds with the same endcaps and Pluronic cores and 3-fold differences in β -CD units per molecule, similar cholesterol efflux levels were found. Our observations suggest that solubility of the PRs is a critical determinant of therapeutic outcome at a fixed dose of CD units.

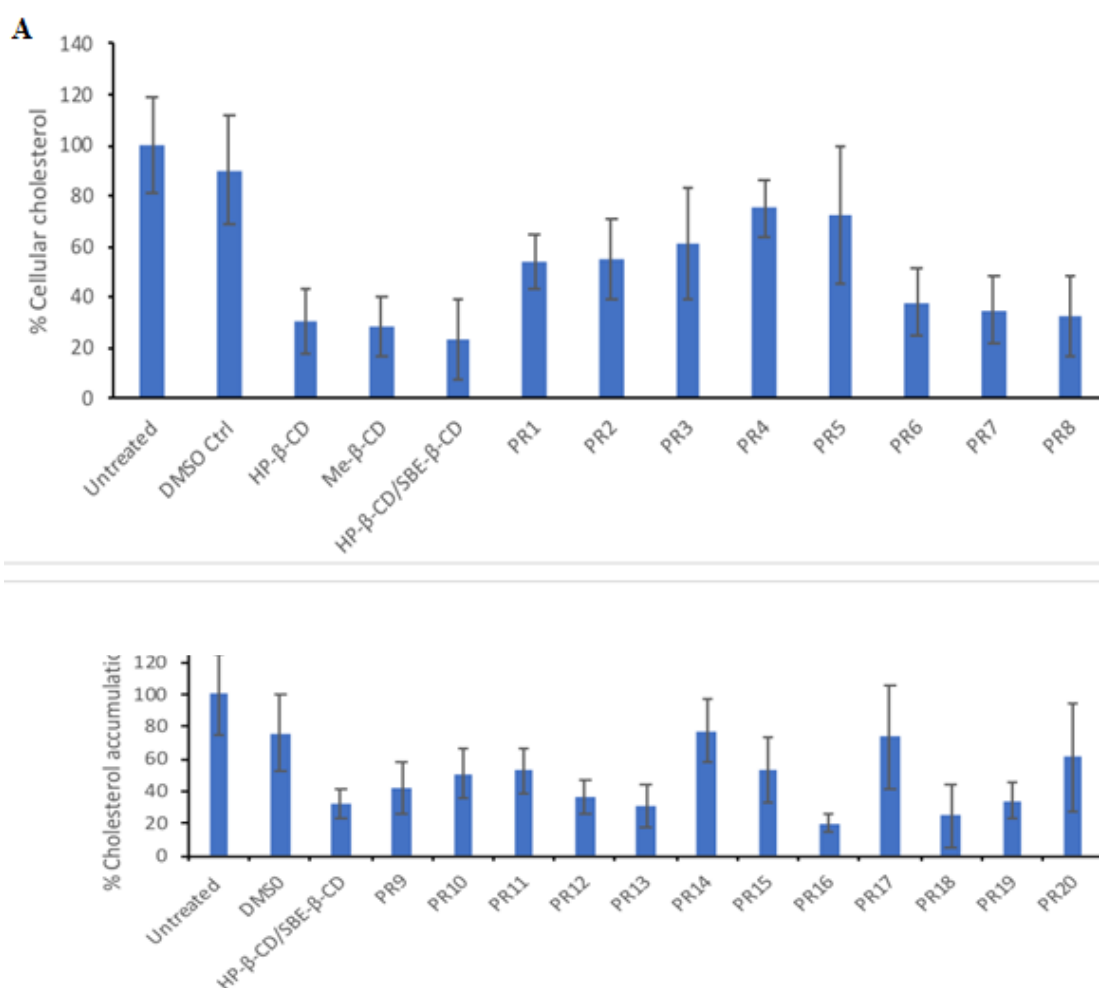


Figure 61. Cholesterol accumulation in NPC1-deficient cells as determined by filipin III staining after exposure to polyrotaxanes for 24 h at 25 μ M equivalent β -CD monomer concentration. **A.** Controls and polyrotaxanes **PR1 – PR8** prepared by the solvent-assisted method. **B.** Controls and polyrotaxanes **PR9 – PR20** prepared by solid state mechanochemical synthesis. Data are expressed relative to DMSO-treated controls and are an average \pm S.D. of two separate experiments with >25 cells imaged per condition in each experiment.

We also evaluated the cholesterol efflux efficacy of the materials made via solid state mechanochemical synthesis (**Figure 1B**). Since previous results suggested L81 as the best Pluronic core for cholesterol mobilization activity and long circulation *in vivo*, we utilized this polymer core in these preparations.⁴¹² Additionally, we also incorporated SBE- β -CD in all the PRs of mechanochemical synthesis as the PRs made in the hexane phase demonstrated the therapeutic benefit of its inclusion. Highly threaded PR such as **PR13** (7 HP- β -CD, 9 SBE- β -CD) and **PR16** (12 HP- β -CD, 6 SBE- β -CD), with threading efficiencies of 73% and 81%, showed the greatest ability to lower cholesterol accumulation, with reductions of approximately 70% and 80%, respectively, compared to untreated NPC1 cells. **PR9** and **PR12**, which had only 46% threading efficiency, reduced cholesterol levels by approximately 40% relative to untreated controls. **PR18**, with a similar CD loading and threading efficiency, showed somewhat increased effectiveness in cholesterol clearance; this may be attributed to the lower cholesterol endcap content in this PR, thereby enabling the β -CD rings to dethread more easily once inside the LE/LY compartment. It should be noted that the higher threading efficiency would lead to more rigid rod like structure compared to PR with low threading efficiencies that have greater flexibility. Previously, we have analyzed in depth the effect of PR rigidity on the pharmacokinetics of the PR in mice. These studies showed that rigid PR circulate longer and preferentially accumulate in liver⁴¹² relative to their more flexible congeners. The data in Table 1 suggests that PR rigidity is linked with increased cholesterol efflux. This is consistent with the recent finding that high aspect ratio rod-like particles have an enhanced ability to enter cells⁴³¹. Consistent with this interpretation, PR having threading efficiencies below 32% (e.g., **PR10**, **PR11**, **PR14**, **PR15**, **PR17**, and **PR20**) were not as effective in cholesterol clearance, reducing sterol accumulation by 50% or less relative to untreated cells. (Fig.2).

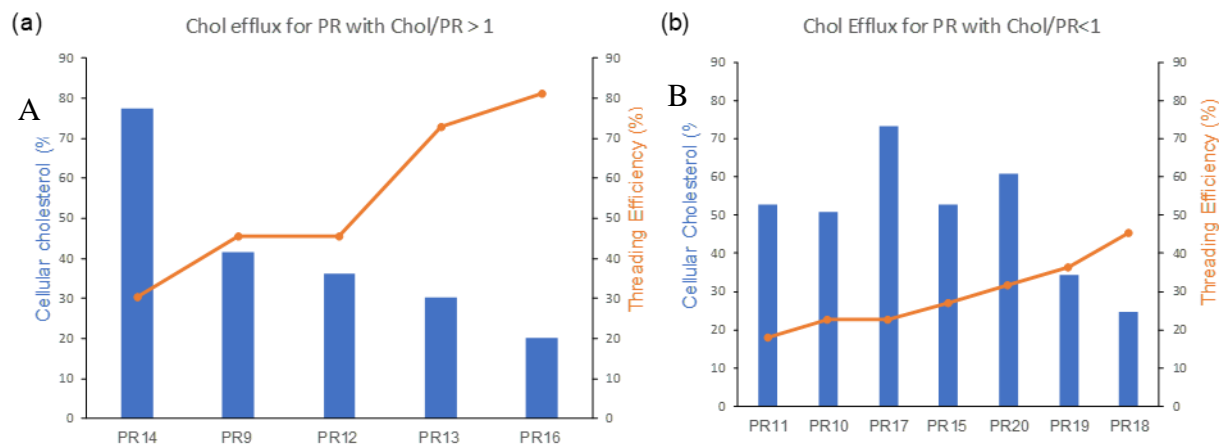


Figure 62. Cholesterol normalization as a function of polyrotaxane threading efficiency in NPC1 deficient cells. A. Cellular cholesterol content as a function of polyrotaxanes with Chol/PR > 1. B. Cellular cholesterol content as a function of polyrotaxanes with Chol/PR < 1. Cellular cholesterol levels are shown relative to untreated cells (100%).

We further explored the role of endcapping extent in the PR library to evaluate the impact of dethreading on cholesterol clearance efficiency. Our findings reveal some important trends that can guide subsequent polyrotaxane designs. First, at a Chol/PR ratio of >1, it can be clearly seen that the cellular cholesterol percentage decreases (i.e. efficacy increases) as the threading efficiency increases ($R^2=0.87$). Second, for polyrotaxanes with low end capping extent (Chol/PR ratio of <1), no trends in polyrotaxane composition were evident ($R^2 = 0.16$). Third, as was observed for the polyrotaxane materials derived from solvent-assisted synthesis, more extensive cholesterol endcapping is essential for producing highly threaded PRs.

7.3.2 Cellular localization of Decaarginine-endcapped PR by confocal microscopy

The effectiveness of the PR compounds in cholesterol mobilization likely requires their localization within the lysosomal compartment where sterol accumulates. To directly examine the subcellular localization of these compounds, two fluorescent-tagged PR (PR1* and PR2*) were generated as described above. Fluorescence microscopic imaging demonstrated that partial co-localization of HP- β -CD with a lysosomal marker was detected at 6h, and more prominent co-localization was detected after 16 h treatment, indicating that over time the fluorescent PR compounds accumulate in the lysosomes (Figure 3). These data suggest that the decaarginine

endcapped PR were efficiently endocytosed possibly via a receptor mediated endocytosis and were thus able to mobilize cholesterol from their late endosomal/lysosomal sites of accumulation.

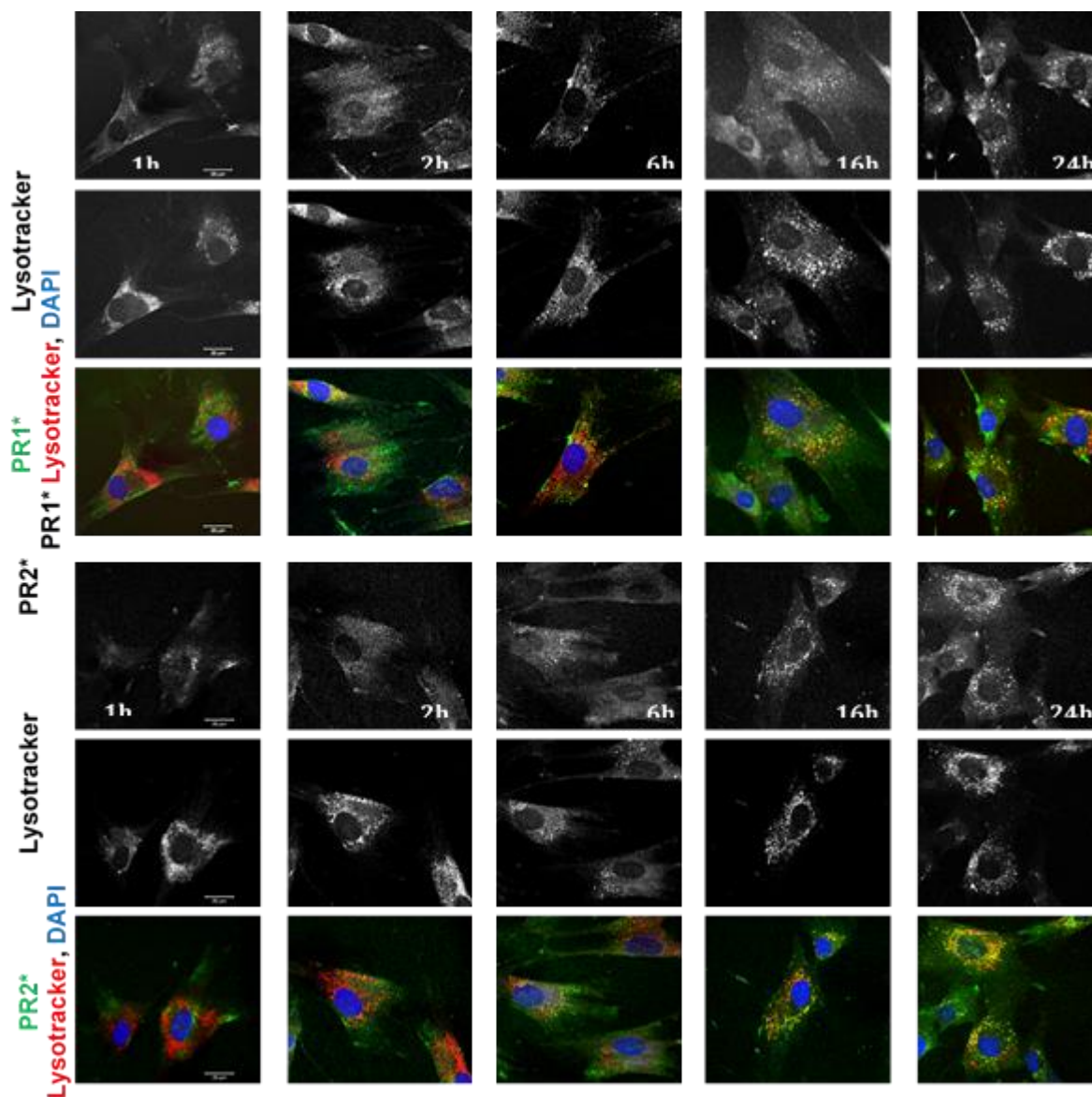


Figure 63. Time course of FITC-conjugated PRs (**PR1*** and **PR2***) localization in NPC1-deficient fibroblasts. Cells were incubated with the compounds for the indicated times (h) and then washed and stained with lysotracker for an additional 45 min. The cells were fixed with paraformaldehyde, followed by staining of nuclei by DAPI. Cells were imaged by confocal microscopy as described in Methods.

7.3.3 FACS analysis for cellular uptake of Fluorescently-labeled PR.

Flow cytometry analysis with FITC-labelled PR (PR1*) confirms our confocal data, and shows that internalization of oligoarginine end-capped PRs begins within 2 h of incubation resulting in

enhanced FITC associated fluorescence of NPC1 deficient cells (Figure 4). The cellular fluorescence is maximum after 24 h of incubation with PR1*. Mani *et al.* reported the presence of HSPG receptors in NPC1 fibroblast cells⁴³². To probe whether the oligoarginine end-capped PRs utilize the HSPG receptor for cellular internalization, we antagonized the HSPG receptor with 30 $\mu\text{g}/\text{mL}$ heparin and monitored its effect on PR1* uptake⁴³³⁻⁴³⁵. Our results show that after 24 h of incubation, only ~7% of cells internalized PR1* (FITC positive) in the presence of heparin in comparison to ~62% cells that internalized the oligoarginine end-capped PR in the absence of heparin. These findings suggest that the oligoarginine endcapped PRs are most likely internalized via an energy dependent HSPG pathway.

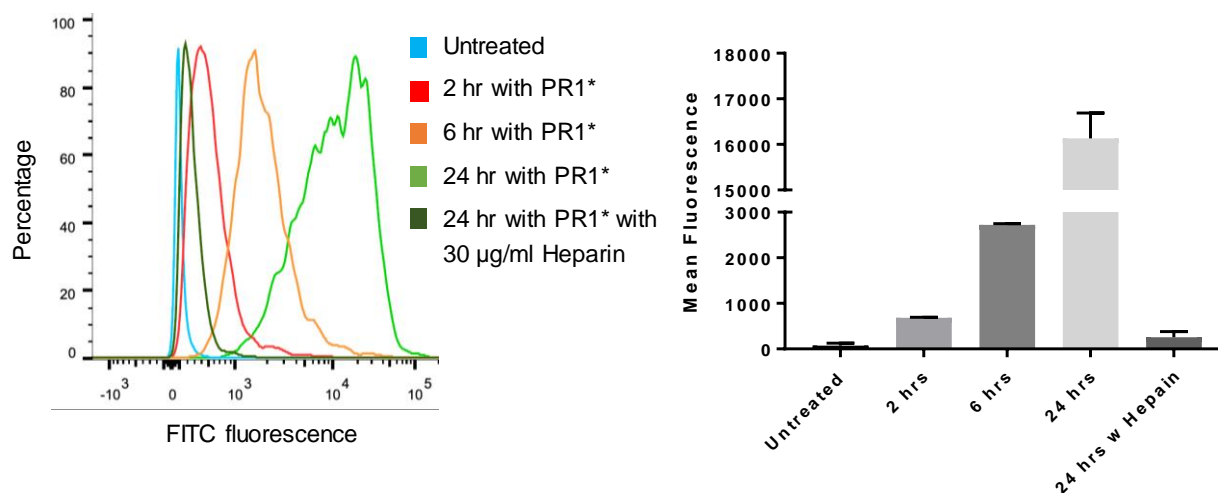


Figure 64. Histogram plot for FITC fluorescence distribution following PR1* uptake within NPC1 deficient fibroblast cells. **B.** Cellular internalization of PR1* in the absence (2,8 and 24 h) and presence (24 h) of 30 $\mu\text{g}/\text{mL}$ of heparin. Cells were treated for 24 h at 25 μM equivalent $\beta\text{-CD}$ monomer concentration and analyzed by flow cytometry as described in the methods.

7.3.4 Cytotoxicity evaluation PR materials

The clinical success of any drug delivery strategy depends on the ability of system to elicit therapeutic benefit without significant toxic effects. In fact, our design approach was devised to use only precursors found in FDA approved materials to obtain the final PR products that would have an “FDA-friendly” toxicity profile. Here, PR9, PR13, PR16 and PR18 were used as representative of materials prepared by the solid phase method, while PR1 and PR8 were used as representative of compounds prepared by the solvent-assisted route. Our cytotoxicity evaluations

revealed that the materials synthesized by the solvent-assisted method were much less cytotoxic than the compounds prepared by solid phase synthesis. As shown in Figure 5, MTS assay results revealed that the solvent-assisted materials PR1 and PR8 did not display significant cytotoxicity at the concentrations tested. By contrast, over this same concentration range, the enhanced toxicity of the compounds prepared by solid phase synthesis was clearly evident. At a concentration of 100 μM , compounds prepared by solid phase synthesis (PR9, PR13, PR16, PR18) were significantly more toxic than those prepared by the solvent-assisted method (PR1 and PR8). Further analysis using GraphPad Prism revealed that PR9, PR13, PR16 and PR18 had IC_{50} values of 34 μM , 24 μM , 48 μM and 56 μM , respectively, which severely limits their therapeutic potential. Since both synthesis methods did not contain materials that could contribute to their toxicity and were analytically similar by ^1H NMR, we attribute the toxicity to a side reaction of the ball milling process that may produce a difficult-to-detect crosslinked PR structures that are cytotoxic. Additional studies to understand the source of this toxicity are needed before further pursuing the solid phase synthesis approach for biological experimentation.

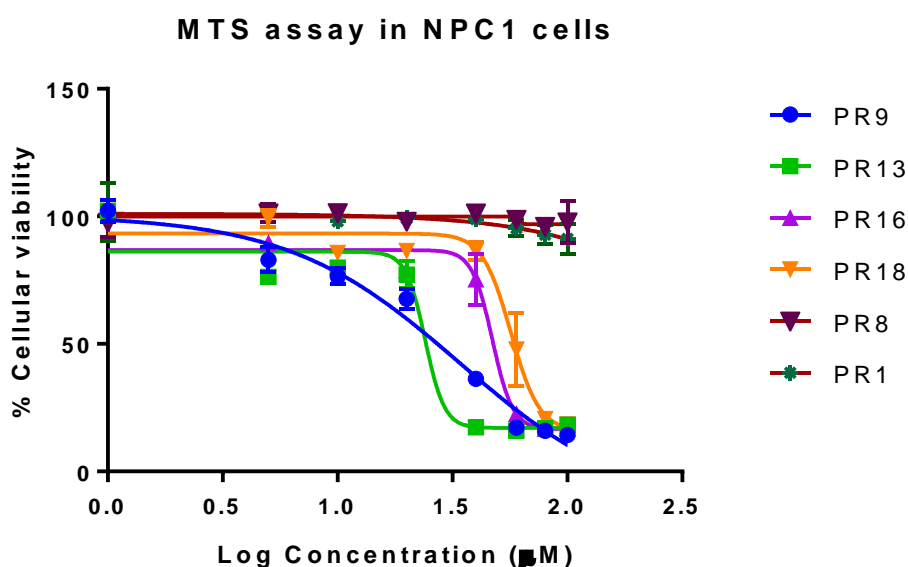


Figure 65. Cytotoxicity analysis of compounds prepared by solid phase synthesis vs solvent-assisted synthesis. NPC1-deficient cells (1500 cells/well) were plated in a 96 well plate for 36 h before treatment with varying concentrations of PRs. Cells were incubated for a further 24 h before measuring toxicity of the compounds by MTS assay according to manufacturer's protocol.

7.4 Conclusions

In conclusion, we demonstrate that polyrotaxanes prepared by solvent-assisted synthesis are capable of mobilizing trapped cholesterol from the late endosomal/lysosomal compartments of Niemann-Pick Type C1 deficient cells. The use of decaarginine endcaps helped enhanced the internalization of these compound via a HSPG mediated pathway such that they become localized in late endosomes/lysosomes where they promote cholesterol egress. Cholesterol normalization in NPC1 cells is shown to be dependent on the threading efficiency and solubility of the compounds. Rigid rod-like materials with a high number of threaded CDs show better cholesterol efflux than those with lower CD content. Incorporation of SBE- β -CD to enhance the solubility of the compounds also improves the performance of the PR toward cholesterol normalization. Although solid phase synthesis is an attractive approach for scalable production of polyrotaxanes, it likely results in cyclodextrin polymers that are more toxic than their polyrotaxane counterparts. Challenges associated with mechanochemical synthesis will need to be addressed before this method can be used to produce material for biological experiments.

REFERENCES

1. Stryer, J. M. B.; John, L. T.; Lubert, *Protein Structure and Function*. W H Freeman: 2002.
2. Crick, F. H. C.; Barnett, L.; Brenner, S.; Watts-Tobin, R. J., General Nature of the Genetic Code for Proteins. *Nature* **1961**, *192* (4809), 1227-1232.
3. Ezkurdia, I.; Juan, D.; Rodriguez, J. M.; Frankish, A.; Diekhans, M.; Harrow, J.; Vazquez, J.; Valencia, A.; Tress, M. L., Multiple evidence strands suggest that there may be as few as 19,000 human protein-coding genes. *Human molecular genetics* **2014**, *23* (22), 5866-5878.
4. Crick, F., Central Dogma of Molecular Biology. *Nature* **1970**, *227* (5258), 561-563.
5. Crick, F. H. In *On protein synthesis*, Symp Soc Exp Biol, 1958; p 8.
6. Edmonds, M., A history of poly A sequences: from formation to factors to function. In *Progress in Nucleic Acid Research and Molecular Biology*, Academic Press: 2002; Vol. 71, pp 285-389.
7. Edmonds, M.; Vaughan, M. H.; Nakazato, H., Polyadenylic Acid Sequences in the Heterogeneous Nuclear RNA and Rapidly-Labeled Polyribosomal RNA of HeLa Cells: Possible Evidence for a Precursor Relationship. *Proceedings of the National Academy of Sciences* **1971**, *68* (6), 1336.
8. Shatkin, A. J., Capping of eucaryotic mRNAs. *Cell* **1976**, *9* (4, Part 2), 645-653.
9. Banerjee, A. K., 5'-terminal cap structure in eucaryotic messenger ribonucleic acids. *Microbiological reviews* **1980**, *44* (2), 175-205.
10. Leff, S. E.; Rosenfeld, M. G.; Evans, R. M., Complex transcriptional units: Diversity in gene expression by alternative RNA processing. *Annual Review of Biochemistry* **1986**, *55* (1), 1091-1117.
11. Neumann, B.; Walter, T.; Hériché, J.-K.; Bulkescher, J.; Erfle, H.; Conrad, C.; Rogers, P.; Poser, I.; Held, M.; Liebel, U.; Cetin, C.; Sieckmann, F.; Pau, G.; Kabbe, R.; Wünsche, A.; Satagopam, V.; Schmitz, M. H. A.; Chapuis, C.; Gerlich, D. W.; Schneider, R.; Eils, R.; Huber, W.; Peters, J.-M.; Hyman, A. A.; Durbin, R.; Pepperkok, R.; Ellenberg, J., Phenotypic profiling of the human genome by time-lapse microscopy reveals cell division genes. *Nature* **2010**, *464*, 721.
12. Fire, A.; Xu, S.; Montgomery, M. K.; Kostas, S. A.; Driver, S. E.; Mello, C. C., Potent and specific genetic interference by double-stranded RNA in *Caenorhabditis elegans*. *Nature* **1998**, *391*, 806.
13. The Nobel Prize in Physiology or Medicine 2006. **2019**.
14. Gil, J.; Esteban, M., Induction of apoptosis by the dsRNA-dependent protein kinase (PKR): mechanism of action. *Apoptosis* **2000**, *5* (2), 107-114.

15. Elbashir, S. M.; Harborth, J.; Lendeckel, W.; Yalcin, A.; Weber, K.; Tuschl, T., Duplexes of 21-nucleotide RNAs mediate RNA interference in cultured mammalian cells. *Nature* **2001**, *411* (6836), 494-498.
16. Schmidt, C., RNAi momentum fizzles as pharma shifts priorities. *Nature Biotechnology* **2011**, *29*, 93.
17. Mullard, A., FDA approves landmark RNAi drug. *Nature Reviews Drug Discovery* **2018**, *17*, 613.
18. Safety, Pharmacokinetics and Preliminary Anti-Tumor Activity of Intravenous TKM-080301 in Subjects With Advanced Hepatocellular Carcinoma.
<https://ClinicalTrials.gov/show/NCT02191878>.
19. El Dika, I.; Lim, H. Y.; Yong, W. P.; Lin, C. C.; Yoon, J. H.; Modiano, M.; Freilich, B.; Choi, H. J.; Chao, T. Y.; Kelley, R. K.; Brown, J.; Knox, J.; Ryoo, B. Y.; Yau, T.; Abou- Alfa, G. K., An Open- Label, Multicenter, Phase I, Dose Escalation Study with Phase II Expansion Cohort to Determine the Safety, Pharmacokinetics, and Preliminary Antitumor Activity of Intravenous TKM- 080301 in Subjects with Advanced Hepatocellular Carcinoma. *The Oncologist* **2018**.
20. Taberero, J.; Shapiro, G. I.; LoRusso, P. M.; Cervantes, A.; Schwartz, G. K.; Weiss, G. J.; Paz-Ares, L.; Cho, D. C.; Infante, J. R.; Alsina, M.; Gounder, M. M.; Falzone, R.; Harrop, J.; White, A. C. S.; Toudjarska, I.; Bumcrot, D.; Meyers, R. E.; Hinkle, G.; Svrzikapa, N.; Hutabarat, R. M.; Clausen, V. A.; Cehelsky, J.; Nochur, S. V.; Gamba-Vitalo, C.; Vaishnav, A. K.; Sah, D. W. Y.; Gollob, J. A.; Burris, H. A., First-in-Humans Trial of an RNA Interference Therapeutic Targeting VEGF and KSP in Cancer Patients with Liver Involvement. *Cancer Discovery* **2013**, *3* (4), 406-417.
21. Dose Escalation Trial to Evaluate the Safety, Tolerability, Pharmacokinetics and Pharmacodynamics of Intravenous ALN-VSP02 In Patients With Advanced Solid Tumors With Liver Involvement. <https://ClinicalTrials.gov/show/NCT00882180>.
22. Aleku, M.; Schulz, P.; Keil, O.; Santel, A.; Schaeper, U.; Dieckhoff, B.; Janke, O.; Endruschat, J.; Durieux, B.; Röder, N.; Löffler, K.; Lange, C.; Fechtner, M.; Möpert, K.; Fisch, G.; Dames, S.; Arnold, W.; Jochims, K.; Giese, K.; Wiedenmann, B.; Scholz, A.; Kaufmann, J., Atu027, a Liposomal Small Interfering RNA Formulation Targeting Protein Kinase N3, Inhibits Cancer Progression. *Cancer Research* **2008**, *68* (23), 9788-9798.
23. Graupera, M.; Guillermet-Guibert, J.; Foukas, L. C.; Phng, L.-K.; Cain, R. J.; Salpekar, A.; Pearce, W.; Meek, S.; Millan, J.; Cutillas, P. R., Angiogenesis selectively requires the p110 α isoform of PI3K to control endothelial cell migration. *Nature* **2008**, *453* (7195), 662.
24. Leenders, F.; Möpert, K.; Schmiedeknecht, A.; Santel, A.; Czauderna, F.; Aleku, M.; Penschuck, S.; Dames, S.; Sternberger, M.; Röhl, T., PKN3 is required for malignant prostate cell growth downstream of activated PI 3- kinase. *The EMBO journal* **2004**, *23* (16), 3303-3313.
25. Strumberg, D.; Schultheis, B.; Traugott, U.; Vank, C.; Santel, A.; Keil, O.; Giese, K.; Kaufmann, J.; Drevs, J., First-in-human phase I study of Atu027, a liposomal small interfering RNA formulation, targeting protein kinase N3 (PKN3) in patients with advanced solid tumors. *Journal of Clinical Oncology* **2011**, *29* (15_suppl), 3057-3057.

26. Atu027 Plus Gemcitabine in Advanced or Metastatic Pancreatic Cancer (Atu027-I-02). <https://ClinicalTrials.gov/show/NCT01808638>.
27. Schultheis, B.; Strumberg, D.; Kuhlmann, J.; Wolf, M.; Link, K.; Seufferlein, T.; Kaufmann, J.; Gebhardt, F.; Bruyniks, N.; Pelzer, U., A phase Ib/IIa study of combination therapy with gemcitabine and Atu027 in patients with locally advanced or metastatic pancreatic adenocarcinoma. *Journal of Clinical Oncology* **2016**, *34* (4_suppl), 385-385.
28. Aagaard, L.; Rossi, J. J., RNAi therapeutics: principles, prospects and challenges. *Advanced drug delivery reviews* **2007**, *59* (2-3), 75-86.
29. Elbashir, S. M.; Harborth, J.; Weber, K.; Tuschl, T., Analysis of gene function in somatic mammalian cells using small interfering RNAs. *Methods* **2002**, *26* (2), 199-213.
30. Omi, K.; Tokunaga, K.; Hohjoh, H., Long-lasting RNAi activity in mammalian neurons. *FEBS Letters* **2004**, *558* (1-3), 89-95.
31. Yang, S.; Tutton, S.; Pierce, E.; Yoon, K., Specific double-stranded RNA interference in undifferentiated mouse embryonic stem cells. *Molecular and Cellular Biology* **2001**, *21* (22), 7807-7816.
32. Paddison, P. J.; Caudy, A. A.; Bernstein, E.; Hannon, G. J.; Conklin, D. S., Short hairpin RNAs (shRNAs) induce sequence-specific silencing in mammalian cells. *Genes & development* **2002**, *16* (8), 948-958.
33. Barve, M.; Wang, Z.; Kumar, P.; Jay, C. M.; Luo, X.; Bedell, C.; Mennel, R. G.; Wallraven, G.; Brunicaudi, F. C.; Senzer, N.; Nemunaitis, J.; Rao, D. D., Phase 1 Trial of Bi-shRNA STMN1 BIV in Refractory Cancer. *Molecular therapy : the journal of the American Society of Gene Therapy* **2015**, *23* (6), 1123-1130.
34. Niethammer, P.; Kronja, I.; Kandels-Lewis, S.; Rybina, S.; Bastiaens, P.; Karsenti, E., Discrete states of a protein interaction network govern interphase and mitotic microtubule dynamics. *PLoS biology* **2007**, *5* (2), e29.
35. Belletti, B.; Baldassarre, G., Stathmin: a protein with many tasks. New biomarker and potential target in cancer. *Expert opinion on therapeutic targets* **2011**, *15* (11), 1249-1266.
36. Collins, C. J.; McCauliff, L. A.; Hyun, S.-H.; Zhang, Z.; Paul, L. N.; Kulkarni, A.; Zick, K.; Wirth, M.; Storch, J.; Thompson, D. H., Synthesis, Characterization, and Evaluation of Pluronic-Based beta-Cyclodextrin Polyrotaxanes for Mobilization of Accumulated Cholesterol from Niemann-Pick Type C Fibroblasts. *Biochemistry* **2013**, *52* (19), 3242-3253.
37. Lee, R. C.; Feinbaum, R. L.; Ambros, V., The *C. elegans* heterochronic gene *lin-4* encodes small RNAs with antisense complementarity to *lin-14*. *Cell* **1993**, *75* (5), 843-854.
38. Bader, A. G., miR-34 - a microRNA replacement therapy is headed to the clinic. *Frontiers in genetics* **2012**, *3*, 120-120.

39. Beg, M. S.; Brenner, A. J.; Sachdev, J.; Borad, M.; Kang, Y. K.; Stoudemire, J.; Smith, S.; Bader, A. G.; Kim, S.; Hong, D. S., Phase I study of MRX34, a liposomal miR-34a mimic, administered twice weekly in patients with advanced solid tumors. *Investigational new drugs* **2017**, *35* (2), 180-188.
40. Davidson, C. D.; Ali, N. F.; Micsenyi, M. C.; Stephney, G.; Renault, S.; Dobrenis, K.; Ory, D. S.; Vanier, M. T.; Walkley, S. U., Chronic Cyclodextrin Treatment of Murine Niemann-Pick C Disease Ameliorates Neuronal Cholesterol and Glycosphingolipid Storage and Disease Progression. *Plos One* **2009**, *4* (9).
41. Chakraborty, C.; Sharma, A. R.; Sharma, G.; Doss, C. G. P.; Lee, S.-S., Therapeutic miRNA and siRNA: Moving from Bench to Clinic as Next Generation Medicine. *Molecular therapy. Nucleic acids* **2017**, *8*, 132-143.
42. Wang, W.; Liu, Y.; Guo, J.; He, H.; Mi, X.; Chen, C.; Xie, J.; Wang, S.; Wu, P.; Cao, F.; Bai, L.; Si, Q.; Xiang, R.; Luo, Y., miR-100 maintains phenotype of tumor-associated macrophages by targeting mTOR to promote tumor metastasis via Stat5a/IL-1ra pathway in mouse breast cancer. *Oncogenesis* **2018**, *7* (12), 97.
43. Malhotra, M.; Sekar, T. V.; Ananta, J. S.; Devulapally, R.; Afjei, R.; Babikir, H. A.; Paulmurugan, R.; Massoud, T. F., Targeted nanoparticle delivery of therapeutic antisense microRNAs presensitizes glioblastoma cells to lower effective doses of temozolomide in vitro and in a mouse model. *Oncotarget* **2018**, *9* (30), 21478-21494.
44. Ebert, M. S.; Neilson, J. R.; Sharp, P. A., MicroRNA sponges: competitive inhibitors of small RNAs in mammalian cells. *Nature Methods* **2007**, *4*, 721.
45. Liu, X.; Abraham, J. M.; Cheng, Y.; Wang, Z.; Wang, Z.; Zhang, G.; Ashktorab, H.; Smoot, D. T.; Cole, R. N.; Boronina, T. N.; DeVine, L. R.; Talbot, C. C., Jr.; Liu, Z.; Meltzer, S. J., Synthetic Circular RNA Functions as a miR-21 Sponge to Suppress Gastric Carcinoma Cell Proliferation. *Molecular Therapy - Nucleic Acids* **2018**, *13*, 312-321.
46. Blencowe, B. J., Alternative Splicing: New Insights from Global Analyses. *Cell* **2006**, *126* (1), 37-47.
47. Wang, Z.; Burge, C. B., Splicing regulation: from a parts list of regulatory elements to an integrated splicing code. *RNA (New York, N.Y.)* **2008**, *14* (5), 802-813.
48. Martinez-Montiel, N.; Rosas-Murrieta, N. H.; Anaya Ruiz, M.; Monjaraz-Guzman, E.; Martinez-Contreras, R., Alternative Splicing as a Target for Cancer Treatment. *International Journal of Molecular Sciences* **2018**, *19* (2), 545.
49. Aartsma-Rus, A., FDA Approval of Nusinersen for Spinal Muscular Atrophy Makes 2016 the Year of Splice Modulating Oligonucleotides. *Nucleic Acid Therapeutics* **2017**, *27* (2), 67-69.
50. Aartsma-Rus, A.; Krieg, A. M., FDA Approves Eteplirsen for Duchenne Muscular Dystrophy: The Next Chapter in the Eteplirsen Saga. *Nucleic acid therapeutics* **2017**, *27* (1), 1-3.
51. Maimon, A.; Mogilevsky, M.; Shilo, A.; Golan-Gerstl, R.; Obiedat, A.; Ben-Hur, V.; Lebenthal-Loinger, I.; Stein, I.; Reich, R.; Beenstock, J., Mnk2 alternative splicing modulates the p38-MAPK pathway and impacts Ras-induced transformation. *Cell Reports* **2014**, *7* (2), 501-513.

52. Mogilevsky, A.; Mogilevsky, M.; Karni, R.; Yavin, E.; Shimshon, O.; Keshet, E.; Kumar, S.; Heyd, F., Modulation of MKNK2 alternative splicing by splice-switching oligonucleotides as a novel approach for glioblastoma treatment. *Nucleic Acids Research* **2018**, *46* (21), 11396-11404.
53. Amodio, N.; Stamato, M. A.; Juli, G.; Morelli, E.; Fulciniti, M.; Manzoni, M.; Taiana, E.; Agnelli, L.; Cantafio, M. E. G.; Romeo, E.; Raimondi, L.; Caracciolo, D.; Zuccalà, V.; Rossi, M.; Neri, A.; Munshi, N. C.; Tagliaferri, P.; Tassone, P., Drugging the lncRNA MALAT1 via LNA gapmeR ASO inhibits gene expression of proteasome subunits and triggers anti-multiple myeloma activity. *Leukemia* **2018**, *32* (9), 1948-1957.
54. Ronchetti, D.; Agnelli, L.; Taiana, E.; Galletti, S.; Manzoni, M.; Todoerti, K.; Musto, P.; Strozzi, F.; Neri, A., Distinct lncRNA transcriptional fingerprints characterize progressive stages of multiple myeloma. *Oncotarget* **2016**, *7* (12), 14814-14830.
55. Miyake, H.; Chi, K. N.; Gleave, M. E., Antisense TRPM-2 oligodeoxynucleotides chemosensitize human androgen-independent PC-3 prostate cancer cells both in vitro and in vivo. *Clinical Cancer Research* **2000**, *6* (5), 1655-1663.
56. Liu, B. R.; Lo, S.-Y.; Liu, C.-C.; Chyan, C.-L.; Huang, Y.-W.; Aronstam, R. S.; Lee, H.-J., Endocytic Trafficking of Nanoparticles Delivered by Cell-penetrating Peptides Comprised of Nona-arginine and a Penetration Accelerating Sequence. *Plos One* **2013**, *8* (6).
57. Chi, K.; Yu, E.; Jacobs, C.; Bazov, J.; Kollmannsberger, C.; Higano, C.; Mukherjee, S.; Gleave, M.; Stewart, P.; Hotte, S., A phase I dose-escalation study of apatorsen (OGX-427), an antisense inhibitor targeting heat shock protein 27 (Hsp27), in patients with castration-resistant prostate cancer and other advanced cancers. *Annals of Oncology* **2016**, *27* (6), 1116-1122.
58. Ciocca, D. R.; Calderwood, S. K., Heat shock proteins in cancer: diagnostic, prognostic, predictive, and treatment implications. *Cell stress & chaperones* **2005**, *10* (2), 86.
59. Choueiri, T. K.; Hahn, N. M.; Werner, L.; Regan, M. M.; Rosenberg, J. E.; investigators, B.-. Borealis-2: A randomized phase II study of OGX-427 (apatorsen) plus docetaxel versus docetaxel alone in platinum-resistant metastatic urothelial cancer (mUC) (Hoosier Cancer Research Network GU12-160). *Journal of Clinical Oncology* **2017**, *35* (6_suppl), 289-289.
60. Breaker, R. R.; Joyce, G. F., A DNA enzyme that cleaves RNA. *Chemistry & Biology* **1994**, *1* (4), 223-229.
61. Cho, E.-A.; Moloney, F. J.; Cai, H.; Au-Yeung, A.; China, C.; Scolyer, R. A.; Yosufi, B.; Raftery, M. J.; Deng, J. Z.; Morton, S. W.; Hammond, P. T.; Arkenau, H.-T.; Damian, D. L.; Francis, D. J.; Chesterman, C. N.; Barnetson, R. S. C.; Halliday, G. M.; Khachigian, L. M., Safety and tolerability of an intratumorally injected DNzyme, Dz13, in patients with nodular basal-cell carcinoma: a phase 1 first-in-human trial (DISCOVER). *The Lancet* **2013**, *381* (9880), 1835-1843.
62. Shaulian, E.; Karin, M., AP-1 in cell proliferation and survival. *Oncogene* **2001**, *20*, 2390.
63. Kappelmann, M.; Bosserhoff, A.; Kuphal, S., AP-1/c-Jun transcription factors: Regulation and function in malignant melanoma. *European Journal of Cell Biology* **2014**, *93* (1), 76-81.

64. Cai, H.; Cho, E.-A.; Li, Y.; Sockler, J.; Parish, C. R.; Chong, B. H.; Edwards, J.; Dodds, T. J.; Ferguson, P. M.; Wilmott, J. S.; Scolyer, R. A.; Halliday, G. M.; Khachigian, L. M., Melanoma protective antitumor immunity activated by catalytic DNA. *Oncogene* **2018**, *37* (37), 5115-5126.
65. Hoogsteen, K., The crystal and molecular structure of a hydrogen-bonded complex between 1-methylthymine and 9-methyladenine. *Acta Crystallographica* **1963**, *16* (9), 907-916.
66. McGuffie, E. M.; Catapano, C. V., Design of a novel triple helix-forming oligodeoxyribonucleotide directed to the major promoter of the c-myc gene. *Nucleic acids research* **2002**, *30* (12), 2701-2709.
67. Boulware, S. B.; Christensen, L. A.; Thames, H.; Coghlan, L.; Vasquez, K. M.; Finch, R. A., Triplex-forming oligonucleotides targeting c-MYC potentiate the anti-tumor activity of gemcitabine in a mouse model of human cancer. *Molecular carcinogenesis* **2014**, *53* (9), 744-752.
68. Moser, H.; Dervan, P., Sequence-specific cleavage of double helical DNA by triple helix formation. *Science* **1987**, *238* (4827), 645-650.
69. Kumar, H.; Kawai, T.; Akira, S., Pathogen Recognition by the Innate Immune System. *International Reviews of Immunology* **2011**, *30* (1), 16-34.
70. Okada, M.; Kawaguchi, Y.; Okumura, H.; Kamachi, M.; Harada, A., Complex formation of cyclodextrins with poly(propylene glycol) derivatives. *Journal of Polymer Science Part a-Polymer Chemistry* **2000**, *38*, 4839-4849.
71. Ribas, A.; Medina, T.; Kummar, S.; Amin, A.; Kalbasi, A.; Drabick, J. J.; Barve, M.; Daniels, G. A.; Wong, D. J.; Schmidt, E. V.; Candia, A. F.; Coffman, R. L.; Leung, A. C. F.; Janssen, R. S., SD-101 in Combination with Pembrolizumab in Advanced Melanoma: Results of a Phase Ib, Multicenter Study. *Cancer Discovery* **2018**, *8* (10), 1250-1257.
72. Pembrolizumab in Combination With Intratumoral SD-101 Therapy. <https://ClinicalTrials.gov/show/NCT03007732>.
73. Lakhin, A. V.; Tarantul, V. Z.; Gening, L. V., Aptamers: problems, solutions and prospects. *Acta naturae* **2013**, *5* (4), 34-43.
74. Tobin, K. A., Macugen treatment for wet age-related macular degeneration. In *Insight*, 2006/07/05 ed.; 2006; Vol. 31, pp 11-4.
75. Zhou, G.; Wilson, G.; Hebbard, L.; Duan, W.; Liddle, C.; George, J.; Qiao, L., Aptamers: A promising chemical antibody for cancer therapy. *Oncotarget* **2016**, *7* (12), 13446-13463.
76. Rosenberg, J. E.; Bambury, R. M.; Van Allen, E. M.; Drabkin, H. A.; Lara, P. N., Jr.; Harzstark, A. L.; Wagle, N.; Figlin, R. A.; Smith, G. W.; Garraway, L. A.; Choueiri, T.; Erlandsson, F.; Laber, D. A., A phase II trial of AS1411 (a novel nucleolin-targeted DNA aptamer) in metastatic renal cell carcinoma. *Investigational new drugs* **2014**, *32* (1), 178-187.
77. Li, N.; Yuan, K.; Yan, F.; Huo, Y.; Zhu, T.; Liu, X.; Guo, Z.; Yao, X., PinX1 is recruited to the mitotic chromosome periphery by Nucleolin and facilitates chromosome congression. *Biochemical and Biophysical Research Communications* **2009**, *384* (1), 76-81.

78. Stuart, R. K.; Stockerl-Goldstein, K.; Cooper, M.; Devetten, M.; Herzig, R.; Medeiros, B.; Schiller, G.; Wei, A.; Acton, G.; Rizzieri, D., Randomized phase II trial of the nucleolin targeting aptamer AS1411 combined with high-dose cytarabine in relapsed/refractory acute myeloid leukemia (AML). *Journal of Clinical Oncology* **2009**, *27* (15S), 7019-7019.
79. Sen, M.; Thomas, S. M.; Kim, S.; Yeh, J. I.; Ferris, R. L.; Johnson, J. T.; Duvvuri, U.; Lee, J.; Sahu, N.; Joyce, S.; Freilino, M. L.; Shi, H.; Li, C.; Ly, D.; Rapireddy, S.; Etter, J. P.; Li, P.-K.; Wang, L.; Chiosea, S.; Seethala, R. R.; Gooding, W. E.; Chen, X.; Kaminski, N.; Pandit, K.; Johnson, D. E.; Grandis, J. R., First-in-human trial of a STAT3 decoy oligonucleotide in head and neck tumors: implications for cancer therapy. *Cancer discovery* **2012**, *2* (8), 694-705.
80. Lesnik, E. A.; Freier, S. M., Relative Thermodynamic Stability of DNA, RNA, and DNA:RNA Hybrid Duplexes: Relationship with Base Composition and Structure. *Biochemistry* **1995**, *34* (34), 10807-10815.
81. Chien, Y. H.; Davidson, N., RNA:DNA hybrids are more stable than DNA:DNA duplexes in concentrated perchlorate and trichloroacetate solutions. *Nucleic acids research* **1978**, *5* (5), 1627-1637.
82. Thibaudeau, C.; Plavec, J.; Garg, N.; Papchikhin, A.; Chattopadhyaya, J., How Does the Electronegativity of the Substituent Dictate the Strength of the Gauche Effect? *Journal of the American Chemical Society* **1994**, *116* (9), 4038-4043.
83. Plavec, J.; Thibaudeau, C.; Chattopadhyaya, J., How Does the 2'-Hydroxy Group Drive the Pseudorotational Equilibrium in Nucleoside and Nucleotide by the Tuning of the 3'-Gauche Effect? *Journal of the American Chemical Society* **1994**, *116* (15), 6558-6560.
84. Monia, B. P.; Lesnik, E. A.; Gonzalez, C.; Lima, W. F.; McGee, D.; Guinasso, C. J.; Kawasaki, A. M.; Cook, P. D.; Freier, S. M., Evaluation of 2'-modified oligonucleotides containing 2'-deoxy gaps as antisense inhibitors of gene expression. *Journal of Biological Chemistry* **1993**, *268* (19), 14514-14522.
85. Egli, M.; Minasov, G.; Tereshko, V.; Pallan, P. S.; Teplova, M.; Inamati, G. B.; Lesnik, E. A.; Owens, S. R.; Ross, B. S.; Prakash, T. P.; Manoharan, M., Probing the Influence of Stereoelectronic Effects on the Biophysical Properties of Oligonucleotides: Comprehensive Analysis of the RNA Affinity, Nuclease Resistance, and Crystal Structure of Ten 2'-O-Ribonucleic Acid Modifications. *Biochemistry* **2005**, *44* (25), 9045-9057.
86. Czauderna, F.; Fechtner, M.; Dames, S.; Aygün, H.; Klippel, A.; Pronk, G. J.; Giese, K.; Kaufmann, J., Structural variations and stabilising modifications of synthetic siRNAs in mammalian cells. *Nucleic acids research* **2003**, *31* (11), 2705-2716.
87. Allerson, C. R.; Sioufi, N.; Jarres, R.; Prakash, T. P.; Naik, N.; Berdeja, A.; Wanders, L.; Griffey, R. H.; Swayze, E. E.; Bhat, B., Fully 2'-Modified Oligonucleotide Duplexes with Improved in Vitro Potency and Stability Compared to Unmodified Small Interfering RNA. *Journal of Medicinal Chemistry* **2005**, *48* (4), 901-904.
88. Molitoris, B. A.; Dagher, P. C.; Sandoval, R. M.; Campos, S. B.; Ashush, H.; Fridman, E.; Brafman, A.; Faerman, A.; Atkinson, S. J.; Thompson, J. D.; Kalinski, H.; Skaliter, R.; Erlich, S.; Feinstein, E., siRNA targeted to p53 attenuates ischemic and cisplatin-induced acute kidney injury. *J Am Soc Nephrol* **2009**, *20* (8), 1754-1764.

89. Kawasaki, A. M.; Casper, M. D.; Freier, S. M.; Lesnik, E. A.; Zounes, M. C.; Cummins, L. L.; Gonzalez, C.; Cook, P. D., Uniformly modified 2'-deoxy-2'-fluoro-phosphorothioate oligonucleotides as nuclease-resistant antisense compounds with high affinity and specificity for RNA targets. *Journal of Medicinal Chemistry* **1993**, *36* (7), 831-841.
90. Martin-Pintado, N.; Deleavey, G. F.; Portella, G.; Campos-Olivas, R.; Orozco, M.; Damha, M. J.; González, C., Backbone FC□H...O Hydrogen Bonds in 2'F-Substituted Nucleic Acids. *Angewandte Chemie International Edition* **2013**, *52* (46), 12065-12068.
91. Pallan, P. S.; Greene, E. M.; Jicman, P. A.; Pandey, R. K.; Manoharan, M.; Rozners, E.; Egli, M., Unexpected origins of the enhanced pairing affinity of 2'-fluoro-modified RNA. *Nucleic acids research* **2011**, *39* (8), 3482-3495.
92. Gragoudas, E. S.; Adamis, A. P.; Cunningham, E. T.; Feinsod, M.; Guyer, D. R., Pegaptanib for Neovascular Age-Related Macular Degeneration. *New England Journal of Medicine* **2004**, *351* (27), 2805-2816.
93. Jones, G. D.; Lesnik, E. A.; Owens, S. R.; Risen, L. M.; Walker, R. T., Investigation of some properties of oligodeoxynucleotides containing 4'-thio-2'-deoxynucleotides: duplex hybridization and nuclease sensitivity. *Nucleic acids research* **1996**, *24* (21), 4117-4122.
94. Leydier, C.; Bellon, L.; Barascut, J.-L.; Morvan, F.; Rayner, B.; Imbach, J.-L., 4'-Thio-RNA: Synthesis of Mixed Base 4'-ThioOligoribonucleotides, Nuclease Resistance, and Base Pairing Properties with Complementary Single and Double Strand. *Antisense Research and Development* **1995**, *5* (3), 167-174.
95. Obika, S.; Nanbu, D.; Hari, Y.; Morio, K.-i.; In, Y.; Ishida, T.; Imanishi, T., Synthesis of 2'-O,4'-C-methyleneuridine and -cytidine. Novel bicyclic nucleosides having a fixed C3, -endo sugar puckering. *Tetrahedron Letters* **1997**, *38* (50), 8735-8738.
96. Wengel, J.; Petersen, M.; Frieden, M.; Koch, T., Chemistry of locked nucleic acids (LNA): Design, synthesis, and bio-physical properties. *Letters in Peptide Science* **2003**, *10* (3), 237-253.
97. Titze-de-Almeida, R.; David, C.; Titze-de-Almeida, S. S., The Race of 10 Synthetic RNAi-Based Drugs to the Pharmaceutical Market. *Pharmaceutical Research* **2017**, *34* (7), 1339-1363.
98. Eckstein, F., Phosphorothioate Oligodeoxynucleotides: What Is Their Origin and What Is Unique About Them? *Antisense and Nucleic Acid Drug Development* **2000**, *10* (2), 117-121.
99. Freier, S. M.; Altmann, K. H., The ups and downs of nucleic acid duplex stability: structure-stability studies on chemically-modified DNA:RNA duplexes. *Nucleic acids research* **1997**, *25* (22), 4429-4443.
100. Miller, C. M.; Donner, A. J.; Blank, E. E.; Egger, A. W.; Kellar, B. M.; Østergaard, M. E.; Seth, P. P.; Harris, E. N., Stabilin-1 and Stabilin-2 are specific receptors for the cellular internalization of phosphorothioate-modified antisense oligonucleotides (ASOs) in the liver. *Nucleic acids research* **2016**, *44* (6), 2782-2794.
101. Tommaso, I.; Julio Cesar, M.-M.; Beniamino, P., Phosphorothioate Oligonucleotides: Effectiveness and Toxicity. *Current Drug Targets* **2014**, *15* (7), 663-673.

102. Krieg, A. M.; Stein, C. A., Phosphorothioate Oligodeoxynucleotides: Antisense or Anti-Protein? *Antisense Research and Development* **1995**, *5* (4), 241-241.
103. Gryaznov, S.; Chen, J.-K., Oligodeoxyribonucleotide N3'.fwdarw.P5' Phosphoramidates: synthesis and Hybridization Properties. *Journal of the American Chemical Society* **1994**, *116* (7), 3143-3144.
104. Pongracz, K.; Gryaznov, S., Oligonucleotide N3'→P5' thiophosphoramidates: synthesis and properties. *Tetrahedron Letters* **1999**, *40* (43), 7661-7664.
105. Nina, M.; Fonné-Pfister, R.; Beaudegnies, R.; Chekatt, H.; Jung, P. M. J.; Murphy-Kessabi, F.; De Mesmaeker, A.; Wendeborn, S., Recognition of RNA by Amide Modified Backbone Nucleic Acids: Molecular Dynamics Simulations of DNA–RNA Hybrids in Aqueous Solution. *Journal of the American Chemical Society* **2005**, *127* (16), 6027-6038.
106. De Mesmaeker, A.; Lesueur, C.; Bévière, M.-O.; Waldner, A.; Fritsch, V.; Wolf, R. M., Amide Backbones with Conformationally Restricted Furanose Rings: Highly Improved Affinity of the Modified Oligonucleotides for Their RNA Complements. *Angewandte Chemie International Edition in English* **1996**, *35* (23- 24), 2790-2794.
107. Sanghvi, Y. S.; Swayze, E. E.; Peoc'h, D.; Bhat, B.; Dimock, S., Concept, Discovery and Development of MMI Linkage: Story of a Novel Linkage: for Antisense Constructs. *Nucleosides and Nucleotides* **1997**, *16* (7-9), 907-916.
108. Summerton, J.; Weller, D., Morpholino Antisense Oligomers: Design, Preparation, and Properties. *Antisense and Nucleic Acid Drug Development* **1997**, *7* (3), 187-195.
109. Egholm, M.; Buchardt, O.; Nielsen, P. E.; Berg, R. H., Peptide nucleic acids (PNA). Oligonucleotide analogs with an achiral peptide backbone. *Journal of the American Chemical Society* **1992**, *114* (5), 1895-1897.
110. Alter, J.; Lou, F.; Rabinowitz, A.; Yin, H.; Rosenfeld, J.; Wilton, S. D.; Partridge, T. A.; Lu, Q. L., Systemic delivery of morpholino oligonucleotide restores dystrophin expression bodywide and improves dystrophic pathology. *Nature Medicine* **2006**, *12*, 175.
111. Doyle, D. F.; Braasch, D. A.; Janowski, B. A.; Corey, D. R., Inhibition of Gene Expression Inside Cells by Peptide Nucleic Acids: Effect of mRNA Target Sequence, Mismatched Bases, and PNA Length. *Biochemistry* **2001**, *40* (1), 53-64.
112. Siwkowski, A. M.; Eldrup, A. B.; Monia, B. P.; Bennett, C. F.; Esau, C. C.; Wancewicz, E. V.; Albertshofer, K.; Malik, L.; Maier, M. A., Identification and functional validation of PNAs that inhibit murine CD40 expression by redirection of splicing. *Nucleic Acids Research* **2004**, *32* (9), 2695-2706.
113. Sazani, P.; Gemignani, F.; Kang, S.-H.; Maier, M. A.; Manoharan, M.; Persmark, M.; Bortner, D.; Kole, R., Systemically delivered antisense oligomers upregulate gene expression in mouse tissues. *Nature Biotechnology* **2002**, *20*, 1228.
114. Latest global cancer data: Cancer burden rises to 18.1 million new cases and 9.6 million cancer deaths in 2018. International Agency for Research on Cancer: 2018.

115. Siegel, R. L.; Miller, K. D.; Jemal, A., Cancer statistics, 2019. *CA: A Cancer Journal for Clinicians* **2019**, *69* (1), 7-34.
116. Bergin, J. *Genetic Modification Therapies Market Size | BCC Research*; 2018.
117. Ugalmugale, S. *Cancer Gene Therapy Market Growth | Industry Forecast Report 2024*; 2016.
118. Saraswathy, M.; Gong, S., Recent developments in the co-delivery of siRNA and small molecule anticancer drugs for cancer treatment. *Materials Today* **2014**, *17* (6), 298-306.
119. Lin, W.; Yao, N.; Li, H.; Hanson, S.; Han, W.; Wang, C.; Zhang, L., Co-Delivery of Imiquimod and Plasmid DNA via an Amphiphilic pH-Responsive Star Polymer that Forms Unimolecular Micelles in Water. *Polymers* **2016**, *8* (11).
120. Xu, Z.; Zhang, Z.; Chen, Y.; Chen, L.; Lin, L.; Li, Y., The characteristics and performance of a multifunctional nanoassembly system for the co-delivery of docetaxel and iSur-pDNA in a mouse hepatocellular carcinoma model. *Biomaterials* **2010**, *31* (5), 916-922.
121. Han, Y.; Zhang, P.; Chen, Y.; Sun, J.; Kong, F., Co-delivery of plasmid DNA and doxorubicin by solid lipid nanoparticles for lung cancer therapy. *International journal of molecular medicine* **2014**, *34* (1), 191-6.
122. Veeratterapillay, R.; Heer, R.; Johnson, M. I.; Persad, R.; Bach, C., High-risk non-muscle-invasive bladder cancer—therapy options during intravesical BCG shortage. *Current urology reports* **2016**, *17* (9), 68.
123. Botteman, M. F.; Pashos, C. L.; Redaelli, A.; Laskin, B.; Hauser, R., The health economics of bladder cancer. *Pharmacoeconomics* **2003**, *21* (18), 1315-1330.
124. Massari, F.; Santoni, M.; Ciccicarese, C.; Brunelli, M.; Conti, A.; Santini, D.; Montironi, R.; Cascinu, S.; Tortora, G., Emerging concepts on drug resistance in bladder cancer: Implications for future strategies. *Critical Reviews in Oncology/Hematology* **2015**, *96* (1), 81-90.
125. Volpe, A.; Racioppi, M.; D'Agostino, D.; D'Addressi, A.; Marangi, F.; Totaro, A.; Pinto, F.; Sacco, E.; Battaglia, S.; Chiloiro, G.; Bassi, P. F., Advanced bladder cancer: New agents and new approaches. A review. *Urologic Oncology: Seminars and Original Investigations* **2013**, *31* (1), 9-16.
126. Roh, Y.-G.; Mun, M.-H.; Jeong, M.-S.; Kim, W.-T.; Lee, S.-R.; Chung, J.-W.; Kim, S. I.; Kim, T. N.; Nam, J. K.; Leem, S.-H., Drug resistance of bladder cancer cells through activation of ABCG2 by FOXM1. *BMB reports* **2018**, *51* (2), 98-103.
127. Sonpavde, G.; Sternberg, C. N.; Rosenberg, J. E.; Hahn, N. M.; Galsky, M. D.; Vogelzang, N. J., Second-line systemic therapy and emerging drugs for metastatic transitional-cell carcinoma of the urothelium. *The lancet oncology* **2010**, *11* (9), 861-870.
128. Saika, T.; Tsushima, T.; Och, J.; Akebi, N.; Nasu, Y.; Matsumura, Y.; Ohmori, H., OVER-EXPRESSION OF METALLOTHIONEIN AND DRUG-RESISTANCE IN BLADDER CANCER. *International Journal of Urology* **1994**, *1* (2), 135-139.

129. Kunze, D.; Erdmann, K.; Froehner, M.; Wirth, M. P.; Fuessel, S., siRNA-mediated Inhibition of Antiapoptotic Genes Enhances Chemotherapy Efficacy in Bladder Cancer Cells. *Anticancer Research* **2012**, *32* (10), 4313-4318.
130. Li, X.; Wang, H.; Wang, J.; Chen, Y.; Yin, X.; Shi, G.; Li, H.; Hu, Z.; Liang, X., Emodin enhances cisplatin-induced cytotoxicity in human bladder cancer cells through ROS elevation and MRP1 downregulation. *BMC Cancer* **2016**, *16* (1), 578.
131. Dai, X.; Tan, C., Combination of microRNA therapeutics with small-molecule anticancer drugs: Mechanism of action and co-delivery nanocarriers. *Advanced Drug Delivery Reviews* **2015**, *81*, 184-197.
132. Shen, Z.; Shen, T.; Wientjes, M. G.; O'Donnell, M. A.; Au, J. L. S., Intravesical treatments of bladder cancer: review. *Pharmaceutical research* **2008**, *25* (7), 1500-1510.
133. Ariotti, N.; Hall, Thomas E.; Rae, J.; Ferguson, C.; McMahon, K.-A.; Martel, N.; Webb, Robyn E.; Webb, Richard I.; Teasdale, Rohan D.; Parton, Robert G., Modular Detection of GFP-Labeled Proteins for Rapid Screening by Electron Microscopy in Cells and Organisms. *Developmental Cell* **2015**, *35* (4), 513-525.
134. Takeuchi, H.; Yamamoto, H.; Niwa, T.; Hino, T.; Kawashima, Y., Mucoadhesion of polymer-coated liposomes to rat intestine in vitro. *Chem Pharm Bull (Tokyo)* **1994**, *42* (9), 1954-6.
135. Patnaik, S.; Gupta, K. C., Novel polyethylenimine-derived nanoparticles for in vivo gene delivery. *Expert Opinion on Drug Delivery* **2013**, *10* (2), 215-228.
136. Li, C.; Zhong, D.; Zhang, Y.; Tuo, W.; Li, N.; Wang, Q.; Liu, Z.; Xue, W., The effect of the gene carrier material polyethyleneimine on the structure and function of human red blood cells in vitro. *Journal of Materials Chemistry B* **2013**, *1* (14), 1885-1893.
137. Petersen, H.; Fechner, P. M.; Martin, A. L.; Kunath, K.; Stolnik, S.; Roberts, C. J.; Fischer, D.; Davies, M. C.; Kissel, T., Polyethylenimine-graft-Poly(ethylene glycol) Copolymers: Influence of Copolymer Block Structure on DNA Complexation and Biological Activities as Gene Delivery System. *Bioconjugate Chemistry* **2002**, *13* (4), 845-854.
138. Godbey, W. T.; Wu, K. K.; Mikos, A. G., Size matters: molecular weight affects the efficiency of poly(ethylenimine) as a gene delivery vehicle. *Journal of biomedical materials research* **1999**, *45* (3), 268-75.
139. Forrest, M. L.; Gabrielson, N.; Pack, D. W., Cyclodextrin-polyethylenimine conjugates for targeted in vitro gene delivery. *Biotechnology and Bioengineering* **2005**, *89* (4), 416-423.
140. Zhao, W.; Schorey, J. S.; Groger, R.; Allen, P. M.; Brown, E. J.; Ratliff, T. L., Characterization of the Fibronectin Binding Motif for a Unique Mycobacterial Fibronectin Attachment Protein, FAP. *Journal of Biological Chemistry* **1999**, *274* (8), 4521-4526.
141. Kulkarni, A.; VerHeul, R.; DeFrees, K.; Collins, C. J.; Schuldt, R. A.; Vlahu, A.; Thompson, D. H., Microfluidic assembly of cationic- β -cyclodextrin:hyaluronic acid-adamantane host:guest pDNA nanoparticles. *Biomaterials Science* **2013**, *1* (10), 1029-1033.

142. Wright, K. J.; Badwaik, V. D.; Samaddar, S.; Hyun, S.-H.; Glauninger, K.; Eom, T.; Thompson, D. H., Organocatalytic Synthesis and Evaluation of Polycarbonate Pendant Polymer: β -Cyclodextrin-Based Nucleic Acid Delivery Vectors. *Macromolecules* **2018**, *51* (3), 670-678.
143. Kulkarni, A.; Badwaik, V.; DeFrees, K.; Schuldt, R. A.; Gunasekera, D. S.; Powers, C.; Vlahu, A.; VerHeul, R.; Thompson, D. H., Effect of Pendant Group on pDNA Delivery by Cationic- β -Cyclodextrin:Alkyl-PVA-PEG Pendant Polymer Complexes. *Biomacromolecules* **2014**, *15* (1), 12-19.
144. Lee, Y.; Kischuk, E.; Crist, S.; Ratliff, T. L.; Thompson, D. H., Targeting and Internalization of Liposomes by Bladder Tumor Cells Using a Fibronectin Attachment Protein-Derived Peptide-Lipopolymer Conjugate. *Bioconjugate Chemistry* **2017**, *28* (5), 1481-1490.
145. Jeffs, L. B.; Palmer, L. R.; Ambegia, E. G.; Giesbrecht, C.; Ewanick, S.; MacLachlan, I., A scalable, extrusion-free method for efficient liposomal encapsulation of plasmid DNA. *Pharmaceutical research* **2005**, *22* (3), 362-372.
146. Heyes, J.; Palmer, L.; Chan, K.; Giesbrecht, C.; Jeffs, L.; MacLachlan, I., Lipid Encapsulation Enables the Effective Systemic Delivery of Polyplex Plasmid DNA. *Molecular Therapy* **2007**, *15* (4), 713-720.
147. Duan, X.; Xiao, J.; Yin, Q.; Zhang, Z.; Mao, S.; Li, Y., Amphiphilic graft copolymer based on poly(styrene-co-maleic anhydride) with low molecular weight polyethylenimine for efficient gene delivery. *International journal of nanomedicine* **2012**, *7*, 4961-4972.
148. Capretto, L.; Cheng, W.; Hill, M.; Zhang, X., Micromixing Within Microfluidic Devices. In *Microfluidics: Technologies and Applications*, Lin, B., Ed. Springer Berlin Heidelberg: Berlin, Heidelberg, 2011; pp 27-68.
149. Wong, S. H.; Ward, M. C.; Wharton, C. W., Micro T-mixer as a rapid mixing micromixer. *Sensors and Actuators B: Chemical* **2004**, *100* (3), 359-379.
150. Hoffmann, M.; Raebiger, N.; Schlueter, M.; Blazy, S.; Bothe, D.; Stemich, C.; Warnecke, A. In *Experimental and numerical investigations of T-shaped micromixers*, 11th European Conference on Mixing, Bamberg, Germany, October, Citeseer: 2003; pp 14-17.
151. Lewis, B. A.; Engelman, D. M., Lipid bilayer thickness varies linearly with acyl chain length in fluid phosphatidylcholine vesicles. *Journal of Molecular Biology* **1983**, *166* (2), 211-217.
152. Coon, B. G.; Crist, S.; González-Bonet, A. M.; Kim, H.-K.; Sowa, J.; Thompson, D. H.; Ratliff, T. L.; Aguilar, R. C., Fibronectin attachment protein from bacillus Calmette-Guerin as targeting agent for bladder tumor cells. *International journal of cancer* **2012**, *131* (3), 591-600.
153. Lai, M. Z.; Vail, W. J.; Szoka, F. C., Acid- and calcium-induced structural changes in phosphatidylethanolamine membranes stabilized by cholesteryl hemisuccinate. *Biochemistry* **1985**, *24* (7), 1654-1661.
154. Hafez, I. M.; Cullis, P. R., Cholesteryl hemisuccinate exhibits pH sensitive polymorphic phase behavior. *Biochimica et Biophysica Acta (BBA) - Biomembranes* **2000**, *1463* (1), 107-114.

155. Mooney, C.; Haslam, N. J.; Pollastri, G.; Shields, D. C., Towards the improved discovery and design of functional peptides: common features of diverse classes permit generalized prediction of bioactivity. *PLoS one* **2012**, *7* (10), e45012-e45012.
156. Mazzucchelli, L.; Burritt, J. B.; Jesaitis, A. J.; Nusrat, A.; Liang, T. W.; Gewirtz, A. T.; Schnell, F. J.; Parkos, C. A., Cell-Specific Peptide Binding by Human Neutrophils. *Blood* **1999**, *93* (5), 1738-1748.
157. Moorthy, B.; Chu, C.; Carlin, D. J., Polycyclic aromatic hydrocarbons: from metabolism to lung cancer. *Toxicological sciences : an official journal of the Society of Toxicology* **2015**, *145* (1), 5-15.
158. Huberman, E.; Selkirk, J. K.; Heidelberger, C., Metabolism of Polycyclic Aromatic Hydrocarbons in Cell Cultures. *Cancer Research* **1971**, *31* (12), 2161-2167.
159. Gomez, L.; Sebastian, V.; Irusta, S.; Ibarra, A.; Arruebo, M.; Santamaria, J., Scaled-up production of plasmonic nanoparticles using microfluidics: from metal precursors to functionalized and sterilized nanoparticles. *Lab on a Chip* **2014**, *14* (2), 325-332.
160. Bladder Cancer - Cancer Stat Facts. <https://seer.cancer.gov/statfacts/html/urinb.html>.
161. Mariotto, A. B.; Robin Yabroff, K.; Shao, Y.; Feuer, E. J.; Brown, M. L., Projections of the Cost of Cancer Care in the United States: 2010–2020. *JNCI Journal of the National Cancer Institute* **2011**, *103* (2), 117-128.
162. Truschel, S.; Wang, E.; Ruiz, W.; Leung, S.; Rojas, R.; Lavelle, J.; Zeidel, M.; Stoffer, D.; Apodaca, G., Stretch-regulated exocytosis/endocytosis in bladder umbrella cells. *Mol. Biol. Cell* **2002**, *13*, 830-846.
163. Romih, R.; Korosec, P.; de Mell, W.; Jezernik, K., Differentiation of epithelial cells in the urinary tract. *Cell Tissue Res* **2005**, *320*, 259-268.
164. Lilly, J.; Parsons, C., Bladder surface glycosaminoglycans is a human epithelial permeability barrier. *Surg. Gynecol. Obstet.* **1990**, *171*, 493-496.
165. Liang, F.; Riedel, I.; Deng, F.; Zhou, G.; Xu, C.; Wu, X.; Kong, X.; Moll, R.; Sun, T., Organization of uroplakin subunits: Transmembrane topology, pair formation and plaque composition. *Biochem. J.* **2001**, *355*, 13-18.
166. Morales, A.; Eidinger, D.; Bruce, A. W., Intracavitary Bacillus Calmette-Guerin in the treatment of superficial bladder tumors. *The Journal of urology* **1976**, *116* (2), 180-3.
167. Lamm, D. L., Long-term results of intravesical therapy for superficial bladder cancer. *The Urologic clinics of North America* **1992**, *19* (3), 573-80.
168. Sylvester, R. J.; van der Meijden, A. P. M.; Lamm, D. L., Intravesical Bacillus Calmette-Guerin Reduces the Risk of Progression in Patients with Superficial Bladder Cancer: A Meta-analysis of the Published Results of Randomized Clinical Trials. *The Journal of urology* **2002**, *168* (5), 1964-1970.

169. Sylvester, R. J.; van der Meijden, A. P.; Witjes, J. A.; Kurth, K., Bacillus calmette-guerin versus chemotherapy for the intravesical treatment of patients with carcinoma in situ of the bladder: a meta-analysis of the published results of randomized clinical trials. *The Journal of urology* **2005**, *174* (1), 86-91; discussion 91-2.
170. Bohle, A.; Bock, P. R., Intravesical bacille Calmette-Guerin versus mitomycin C in superficial bladder cancer: formal meta-analysis of comparative studies on tumor progression. *Urology* **2004**, *63* (4), 682-6; discussion 686-7.
171. Shelley, M. D.; Wilt, T. J.; Court, J.; Coles, B.; Kynaston, H.; Mason, M. D., Intravesical bacillus Calmette-Guerin is superior to mitomycin C in reducing tumour recurrence in high-risk superficial bladder cancer: a meta-analysis of randomized trials. *BJU international* **2004**, *93* (4), 485-90.
172. Bohle, A.; Jocham, D.; Bock, P. R., Intravesical bacillus Calmette-Guerin versus mitomycin C for superficial bladder cancer: a formal meta-analysis of comparative studies on recurrence and toxicity. *The Journal of urology* **2003**, *169* (1), 90-5.
173. Shelley, M. D.; Mason, M. D.; Kynaston, H., Intravesical therapy for superficial bladder cancer: a systematic review of randomised trials and meta-analyses. *Cancer treatment reviews* **2010**, *36* (3), 195-205.
174. Shang, P. F.; Kwong, J.; Wang, Z. P.; Tian, J.; Jiang, L.; Yang, K.; Yue, Z. J.; Tian, J. Q., Intravesical Bacillus Calmette-Guerin versus epirubicin for Ta and T1 bladder cancer. *The Cochrane database of systematic reviews* **2011**, (5), Cd006885.
175. Chou, R.; Selph, S.; Buckley, D. I.; Fu, R.; Griffin, J. C.; Grusing, S.; Gore, J. L., Intravesical Therapy for the Treatment of Nonmuscle Invasive Bladder Cancer: A Systematic Review and Meta-Analysis. *The Journal of urology* **2017**, *197* (5), 1189-1199.
176. Oosterlinck W, L. B., Jackse G, Malmstrom PU, Stockle M; C, a. S., EAU Recommendations 2001. "Guidelines on bladder cancer". *Prog Urol* **2002**, *12*, 1161-1163.
177. Lamm, D.; McGee, W.; K, H., Bladder cancer: Current optimal intravesical treatment. *Urol. Nurs.* **2005**, *25*, 323-326 & 331-322.
178. Morales, A.; Herr, H.; Steinberg, G.; Given, R.; Cohen, Z.; Amrhein, J.; Kamat, A. M., Efficacy and safety of MCNA in patients with nonmuscle invasive bladder cancer at high risk for recurrence and progression after failed treatment with bacillus Calmette-Guerin. *The Journal of urology* **2015**, *193* (4), 1135-43.
179. Morales, A.; Phadke, K.; Steinhoff, G., Intravesical mycobacterial cell wall-DNA complex in the treatment of carcinoma in situ of the bladder after standard intravesical therapy has failed. *The Journal of urology* **2009**, *181* (3), 1040-5.
180. Lee, Y.; Kischuk, E.; Crist, S.; Ratliff, T. L.; Thompson, D. H., Targeting and Internalization of Liposomes by Bladder Tumor Cells Using a Fibronectin Attachment Protein-Derived Peptide-Lipopolymer Conjugate. *Bioconjug Chem* **2017**, *28* (5), 1481-1490.

181. Coon, B. G.; Crist, S.; González-Bonet, A. M.; Kim, H. K.; Sowa, J.; Thompson, D. H.; Ratliff, T. L.; Aguilar, R. C., Fibronectin Attachment Protein (FAP) From Bacillus Calmette-Guerin As Targeting Agent For Bladder Tumor Cells. *Int J Cancer* **2012**, *131* (3), 591-600.
182. Simberg, D.; Weisman, S.; Talmon, Y.; Barenholz, Y., DOTAP (and other cationic lipids): chemistry, biophysics, and transfection. *Critical reviews in therapeutic drug carrier systems* **2004**, *21* (4), 257-317.
183. Du, Z.; Munye, M. M.; Tagalakis, A. D.; Manunta, M. D. I.; Hart, S. L., The Role of the Helper Lipid on the DNA Transfection Efficiency of Lipopolyplex Formulations. In *Sci Rep*, 2014; Vol. 4.
184. Bednar, J.; Woodcock, C. L., Cryoelectron microscopic analysis of nucleosomes and chromatin. In *Methods in Enzymology*, Academic Press: 1999; Vol. 304, pp 191-213.
185. Dubochet, J.; Adrian, M.; Chang, J. J.; Homo, J. C.; Lepault, J.; McDowell, A. W.; Schultz, P., Cryo-electron microscopy of vitrified specimens. *Quarterly reviews of biophysics* **1988**, *21* (2), 129-228.
186. Caracciolo, G., Clinically approved liposomal nanomedicines: lessons learned from the biomolecular corona. *Nanoscale* **2018**, *10* (9), 4167-4172.
187. Jeffs, L. B.; Palmer, L. R.; Ambegia, E. G.; Giesbrecht, C.; Ewanick, S.; MacLachlan, I., A scalable, extrusion-free method for efficient liposomal encapsulation of plasmid DNA. *Pharmaceutical research* **2005**, *22* (3), 362-72.
188. Maeki, M.; Kimura, N.; Sato, Y.; Harashima, H.; Tokeshi, M., Advances in microfluidics for lipid nanoparticles and extracellular vesicles and applications in drug delivery systems. *Advanced Drug Delivery Reviews* **2018**, *128*, 84-100.
189. Yang, X. F.; Sufen, L.; Xiaodong, R.; Huayong, Research on staggered oriented ridges static micromixers. *Sensors and Actuators B: Chemical* **2006**, *114* (2), 618-624.
190. Cullis, J. K.; Maria, M. D.; Joanne, E. M.; Sam, C.; Roy van der, M.; Jenifer, L. T.; Yuen Yi, C. T.; Pieter, R., On the Formation and Morphology of Lipid Nanoparticles Containing Ionizable Cationic Lipids and siRNA. **2018**.
191. Angelov, B.; Garamus, V. M.; Drechsler, M.; Angelova, A., Structural analysis of nanoparticulate carriers for encapsulation of macromolecular drugs. *Journal of Molecular Liquids* **2017**, *235*, 83-89.
192. Kim, B. K.; Hwang, G. B.; Seu, Y. B.; Choi, J. S.; Jin, K. S.; Doh, K. O., DOTAP/DOPE ratio and cell type determine transfection efficiency with DOTAP-liposomes. *Biochimica et biophysica acta* **2015**, *1848* (10 Pt A), 1996-2001.
193. Zhao, H.; Wang, J. C.; Sun, Q. S.; Luo, C. L.; Zhang, Q., RGD-based strategies for improving antitumor activity of paclitaxel-loaded liposomes in nude mice xenografted with human ovarian cancer. *Journal of drug targeting* **2009**, *17* (1), 10-8.

194. Dai, W.; Yang, T.; Wang, X.; Wang, J.; Zhang, X.; Zhang, Q., PHSCNK-Modified and doxorubicin-loaded liposomes as a dual targeting system to integrin-overexpressing tumor neovasculature and tumor cells. *Journal of drug targeting* **2010**, *18* (4), 254-63.
195. Sakurai, Y.; Mizumura, W.; Murata, M.; Hada, T.; Yamamoto, S.; Ito, K.; Iwasaki, K.; Katoh, T.; Goto, Y.; Takagi, A.; Kohara, M.; Suga, H.; Harashima, H., Efficient siRNA Delivery by Lipid Nanoparticles Modified with a Nonstandard Macrocyclic Peptide for EpCAM-Targeting. *Molecular pharmaceutics* **2017**, *14* (10), 3290-3298.
196. Osanai, A.; Li, S. J.; Asano, K.; Sashinami, H.; Hu, D. L.; Nakane, A., Fibronectin-binding protein, FbpA, is the adhesin responsible for pathogenesis of *Listeria monocytogenes* infection. *Microbiology and immunology* **2013**, *57* (4), 253-62.
197. Huberman, A. L.; Frank, R. C.; Cynthia, B. H. C.; Bei, X.; Eliezer, Interaction Between $\alpha 5\beta 1$ Integrin and Secreted Fibronectin Is Involved in Macrophage Differentiation of Human HL-60 Myeloid Leukemia Cells. **1999**.
198. Brunner, A.; Tzankov, A., The Role of Structural Extracellular Matrix Proteins in Urothelial Bladder Cancer (Review). In *Biomark Insights*, 2007; Vol. 2, pp 418-27.
199. Deen, S.; Ball, R. Y., Basement membrane and extracellular interstitial matrix components in bladder neoplasia--evidence of angiogenesis. *Histopathology* **1994**, *25* (5), 475-81.
200. Alitalo, K. H., T.; Vaeheri, A., Fibronectin is produced by human macrophages. In *J Exp Med*, 1980; Vol. 151, pp 602-13.
201. Viger-Gravel, J.; Schantz, A.; Pinon, A. C.; Rossini, A. J.; Schantz, S.; Emsley, L., Structure of Lipid Nanoparticles Containing siRNA or mRNA by Dynamic Nuclear Polarization-Enhanced NMR Spectroscopy. *The journal of physical chemistry. B* **2018**, *122* (7), 2073-2081.
202. Leung, A. K.; Hafez, I. M.; Baoukina, S.; Belliveau, N. M.; Zhigaltsev, I. V.; Afshinmanesh, E.; Tieleman, D. P.; Hansen, C. L.; Hope, M. J.; Cullis, P. R., Lipid Nanoparticles Containing siRNA Synthesized by Microfluidic Mixing Exhibit an Electron-Dense Nanostructured Core. *J Phys Chem C Nanomater Interfaces* **2012**, *116* (34), 18440-50.
203. Maiti, S. S.; Arun Kumar, M.; Sunil, K.; Pralay, Controlled drug delivery vehicles for cancer treatment and their performance. *Signal Transduction and Targeted Therapy* **2018**, *3* (1), 7.
204. Kaasgaard, T. L. A.; David, H. T.; Thomas, Enzyme-triggered nanomedicine: Drug release strategies in cancer therapy (Invited Review). <http://dx.doi.org/10.3109/09687688.2010.515950> **2010**.
205. Lönn, P.; Kacsinta, A. D.; Cui, X. S.; Hamil, A. S.; Kaulich, M.; Gogoi, K.; Dowdy, S. F., Enhancing Endosomal Escape for Intracellular Delivery of Macromolecular Biologic Therapeutics. In *Sci Rep*, 2016; Vol. 6.
206. Nguyen, J.; Szoka, F. C., Nucleic acid delivery: the missing pieces of the puzzle? *Acc Chem Res* **2012**, *45* (7), 1153-62.

207. Lai, M. Z.; Vail, W. J.; Szoka, F. C., Acid- and calcium-induced structural changes in phosphatidylethanolamine membranes stabilized by cholesteryl hemisuccinate. *Biochemistry* **1985**, *24* (7), 1654-61.
208. Hegele, A.; Dalpke, A.; Barth, P.; Varga, Z.; Heeg, K.; Hofmann, R.; Olbert, P., Antineoplastic effect of immunostimulatory DNA (CpG-ODN) in a murine C57-BL6/MB-49 transitional cell carcinoma model. *Anticancer Res* **2004**, *24* (4), 2225-30.
209. Mangsbo, S. M.; Ninalga, C.; Essand, M.; Loskog, A.; Totterman, T. H., CpG therapy is superior to BCG in an orthotopic bladder cancer model and generates CD4+ T-cell immunity. *Journal of immunotherapy (Hagerstown, Md. : 1997)* **2008**, *31* (1), 34-42.
210. Ninalga, C.; Loskog, A.; Klevenfeldt, M.; Essand, M.; Totterman, T. H., CpG oligonucleotide therapy cures subcutaneous and orthotopic tumors and evokes protective immunity in murine bladder cancer. *Journal of immunotherapy (Hagerstown, Md. : 1997)* **2005**, *28* (1), 20-7.
211. Olbert, P. J.; Schrader, A. J.; Simon, C.; Dalpke, A.; Barth, P.; Hofmann, R.; Hegele, A., In vitro and in vivo effects of CpG-Oligodeoxynucleotides (CpG-ODN) on murine transitional cell carcinoma and on the native murine urinary bladder wall. *Anticancer Res* **2009**, *29* (6), 2067-76.
212. Cullis, T. M. A.; Pieter, R., Drug Delivery Systems: Entering the Mainstream. **2004**.
213. Bareford, L. M.; Swaan, P. W., Endocytic mechanisms for targeted drug delivery. *Advanced Drug Delivery Reviews* **2007**, *59* (8), 748-758.
214. Kelley, W. N., A personal perspective on the early, early history of in vivo (DNA-based) gene therapy. *Hum Gene Ther* **2012**, *23* (6), 541-6.
215. Waehler, R.; Russell, S. J.; Curiel, D. T., Engineering targeted viral vectors for gene therapy. *Nat Rev Genet* **2007**, *8* (8), 573-87.
216. Mancuso, K.; Hauswirth, W. W.; Li, Q.; Connor, T. B.; Kuchenbecker, J. A.; Mauck, M. C.; Neitz, J.; Neitz, M., Gene therapy for red-green colour blindness in adult primates. *Nature* **2009**, *461* (7265), 784-7.
217. Boussif, O.; Lezoualc'h, F.; Zanta, M. A.; Mergny, M. D.; Scherman, D.; Demeneix, B.; Behr, J. P., A versatile vector for gene and oligonucleotide transfer into cells in culture and in vivo: polyethylenimine. *Proceedings of the National Academy of Sciences of the United States of America* **1995**, *92* (16), 7297-301.
218. Ryther, R. C.; Flynt, A. S.; Phillips, J. A., 3rd; Patton, J. G., siRNA therapeutics: big potential from small RNAs. *Gene therapy* **2005**, *12* (1), 5-11.
219. Liao, G.; Nayak, S.; Regueiro, J. R.; Berger, S. B.; Detre, C.; Romero, X.; de Waal Malefyt, R.; Chatila, T. A.; Herzog, R. W.; Terhorst, C., GITR engagement preferentially enhances proliferation of functionally competent CD4+CD25+FoxP3+ regulatory T cells. *International immunology* **2010**, *22* (4), 259-70.
220. Deng, Y.; Wang, C. C.; Choy, K. W.; Du, Q.; Chen, J.; Wang, Q.; Li, L.; Chung, T. K.; Tang, T., Therapeutic potentials of gene silencing by RNA interference: principles, challenges, and new strategies. *Gene* **2014**, *538* (2), 217-27.

221. Pack, D. W.; Hoffman, A. S.; Pun, S.; Stayton, P. S., Design and development of polymers for gene delivery. *Nature reviews. Drug discovery* **2005**, *4* (7), 581-93.
222. Wang, W.; Li, W.; Ma, N.; Steinhoff, G., Non-viral gene delivery methods. *Current pharmaceutical biotechnology* **2013**, *14* (1), 46-60.
223. Bondi M. L., C. E. F., Solid lipid nanoparticles for applications in gene therapy: a review of the state of the art. *Expert Opin Drug Deliv.* **2010**, *7* (7).
224. Semple, S. C.; Akinc, A.; Chen, J.; Sandhu, A. P.; Mui, B. L.; Cho, C. K.; Sah, D. W.; Stebbing, D.; Crosley, E. J.; Yaworski, E.; Hafez, I. M.; Dorkin, J. R.; Qin, J.; Lam, K.; Rajeev, K. G.; Wong, K. F.; Jeffs, L. B.; Nechev, L.; Eisenhardt, M. L.; Jayaraman, M.; Kazem, M.; Maier, M. A.; Srinivasulu, M.; Weinstein, M. J.; Chen, Q.; Alvarez, R.; Barros, S. A.; De, S.; Klimuk, S. K.; Borland, T.; Kosovrasti, V.; Cantley, W. L.; Tam, Y. K.; Manoharan, M.; Ciufolini, M. A.; Tracy, M. A.; de Fougères, A.; MacLachlan, I.; Cullis, P. R.; Madden, T. D.; Hope, M. J., Rational design of cationic lipids for siRNA delivery. *Nat Biotechnol* **2010**, *28* (2), 172-6.
225. Vachutinsky, Y.; Kataoka, K., PEG-based Polyplex Design for Gene and Nucleotide Delivery. *Isr J Chem* **2010**, *50* (2), 175-184.
226. Kawano, T.; Okuda, T.; Aoyagi, H.; Niidome, T., Long circulation of intravenously administered plasmid DNA delivered with dendritic poly(L-lysine) in the blood flow. *Journal of controlled release : official journal of the Controlled Release Society* **2004**, *99* (2), 329-37.
227. Majoros, I. J.; Williams, C. R.; Baker, J. R., Jr., Current dendrimer applications in cancer diagnosis and therapy. *Current topics in medicinal chemistry* **2008**, *8* (14), 1165-79.
228. Mintzer, M. A.; Grinstaff, M. W., Biomedical applications of dendrimers: a tutorial. *Chemical Society reviews* **2011**, *40* (1), 173-90.
229. Zhang, J.; Lynn, D. M., Multilayered Films Fabricated from Combinations of Degradable Polyamines: Tunable Erosion and Release of Anionic Polyelectrolytes. *Macromolecules* **2006**, *39* (26), 8928-8935.
230. Zhang, J.; Montanez, S. I.; Jewell, C. M.; Lynn, D. M., Multilayered films fabricated from plasmid DNA and a side-chain functionalized poly(beta-amino ester): surface-type erosion and sequential release of multiple plasmid constructs from surfaces. *Langmuir : the ACS journal of surfaces and colloids* **2007**, *23* (22), 11139-46.
231. Peng, L.; Gao, Y.; Xue, Y. N.; Huang, S. W.; Zhuo, R. X., Cytotoxicity and in vivo tissue compatibility of poly(amidoamine) with pendant aminobutyl group as a gene delivery vector. *Biomaterials* **2010**, *31* (16), 4467-76.
232. Huang, S. W.; Zhuo, R. X., Recent advances in polyphosphoester and polyphosphoramidate - Based biomaterials. *Phosphorus Sulfur* **2008**, *183* (2-3), 340-348.
233. Duceppe, N.; Tabrizian, M., Advances in using chitosan-based nanoparticles for in vitro and in vivo drug and gene delivery. *Expert Opin Drug Deliv* **2010**, *7* (10), 1191-207.
234. Lee, S. K.; Han, M. S.; Asokan, S.; Tung, C. H., Effective gene silencing by multilayered siRNA-coated gold nanoparticles. *Small* **2011**, *7* (3), 364-70.

235. Whitehead, K. A.; Langer, R.; Anderson, D. G., Knocking down barriers: advances in siRNA delivery. *Nature reviews. Drug discovery* **2009**, *8* (2), 129-38.
236. Perez-Martinez, F. C.; Guerra, J.; Posadas, I.; Cena, V., Barriers to non-viral vector-mediated gene delivery in the nervous system. *Pharm Res* **2011**, *28* (8), 1843-58.
237. Raemdonck, K.; Martens, T. F.; Braeckmans, K.; Demeester, J.; De Smedt, S. C., Polysaccharide-based nucleic acid nanoformulations. *Adv Drug Deliv Rev* **2013**, *65* (9), 1123-47.
238. Gonzalez, H.; Hwang, S. J.; Davis, M. E., New class of polymers for the delivery of macromolecular therapeutics. *Bioconjug Chem* **1999**, *10* (6), 1068-74.
239. Davis, M. E.; Brewster, M. E., Cyclodextrin-based pharmaceuticals: past, present and future. *Nature reviews. Drug discovery* **2004**, *3* (12), 1023-35.
240. Johnson, C. P.; Atwood, J. L.; Steed, J. W.; Bauer, C. B.; Rogers, R. D., Transition Metal Complexes of p-Sulfonatocalix[5]arene. *Inorganic chemistry* **1996**, *35* (9), 2602-2610.
241. Li, J.; Loh, X. J., Cyclodextrin-based supramolecular architectures: syntheses, structures, and applications for drug and gene delivery. *Adv Drug Deliv Rev* **2008**, *60* (9), 1000-17.
242. Davis, M. E., Design and development of IT-101, a cyclodextrin-containing polymer conjugate of camptothecin. *Adv Drug Deliv Rev* **2009**, *61* (13), 1189-92.
243. Eliasof, S.; Lazarus, D.; Peters, C. G.; Case, R. I.; Cole, R. O.; Hwang, J.; Schluep, T.; Chao, J.; Lin, J.; Yen, Y.; Han, H.; Wiley, D. T.; Zuckerman, J. E.; Davis, M. E., Correlating preclinical animal studies and human clinical trials of a multifunctional, polymeric nanoparticle. *Proceedings of the National Academy of Sciences of the United States of America* **2013**, *110* (37), 15127-32.
244. Ha, P. T.; Hoogmartens, J.; Van Schepdael, A., Recent advances in pharmaceutical applications of chiral capillary electrophoresis. *Journal of pharmaceutical and biomedical analysis* **2006**, *41* (1), 1-11.
245. Ortiz Mellet, C.; Garcia Fernandez, J. M.; Benito, J. M., Cyclodextrin-based gene delivery systems. *Chemical Society reviews* **2011**, *40* (3), 1586-608.
246. Li, J. J.; Zhao, F.; Li, J., Supramolecular polymers based on cyclodextrins for drug and gene delivery. *Advances in biochemical engineering/biotechnology* **2011**, *125*, 207-49.
247. Ooya, T.; Yui, N., Polyrotaxanes: Synthesis, structure, and potential in drug delivery. *Critical reviews in therapeutic drug carrier systems* **1999**, *16* (3), 289-330.
248. Wenz, G.; Han, B. H.; Muller, A., Cyclodextrin rotaxanes and polyrotaxanes. *Chem Rev* **2006**, *106* (3), 782-817.
249. Loethen, S.; Kim, J. M.; Thompson, D. H., Biomedical applications of cyclodextrin based polyrotaxanes. *Polym Rev* **2007**, *47* (3), 383-418.

250. Moon, C.; Kwon, Y. M.; Lee, W. K.; Park, Y. J.; Yang, V. C., In vitro assessment of a novel polyrotaxane-based drug delivery system integrated with a cell-penetrating peptide. *Journal of Controlled Release* **2007**, *124* (1-2), 43-50.
251. Kulkarni, R. P.; Castelino, K.; Majumdar, A.; Fraser, S. E., Intracellular Transport Dynamics of Endosomes Containing DNA Polyplexes along the Microtubule Network. In *Biophys J*, 2006; Vol. 90, pp L42-4.
252. Grosse, S.; Aron, Y.; Thevenot, G.; Monsigny, M.; Fajac, I., Cytoskeletal involvement in the cellular trafficking of plasmid/PEI derivative complexes. *Journal of controlled release : official journal of the Controlled Release Society* **2007**, *122* (1), 111-7.
253. Bai, H.; Lester, G. M.; Petishnok, L.; Dean, D., Cytoplasmic transport and nuclear import of plasmid DNA. *Biosci Rep* **2017**, *37* (6).
254. Wagner, S. B.; Sauer, T.; Carotta, S.; Cotten, M.; Saltik, M., Cell cycle dependence of gene transfer by lipoplex, polyplex and recombinant adenovirus. *Gene therapy* **2000**, *7* (5), 401.
255. Yang, C.; Li, H.; Wang, X.; Li, J., Cationic supramolecules consisting of oligoethylenimine-grafted alpha-cyclodextrins threaded on poly(ethylene oxide) for gene delivery. *Journal of biomedical materials research. Part A* **2009**, *89* (1), 13-23.
256. Harada, A.; Okada, M.; Li, J.; Kamachi, M., Preparation and Characterization of Inclusion Complexes of Poly(propylene glycol) with Cyclodextrins. *Macromolecules* **1995**, *28* (24), 8406-8411.
257. Li, J.; Yang, C.; Li, H. Z.; Wang, X.; Goh, S. H.; Ding, J. L.; Wang, D. Y.; Leong, K. W., Cationic supramolecules composed of multiple oligoethylenimine-grafted beta-cyclodextrins threaded on a polymer chain for efficient gene delivery. *Adv Mater* **2006**, *18* (22), 2969-+.
258. Yang, C.; Wang, X.; Li, H.; Goh, S. H.; Li, J., Synthesis and characterization of polyrotaxanes consisting of cationic alpha-cyclodextrins threaded on poly[(ethylene oxide)-ran-(propylene oxide)] as gene carriers. *Biomacromolecules* **2007**, *8* (11), 3365-74.
259. Yang, C.; Wang, X.; Li, H.; Tan, E.; Lim, C. T.; Li, J., Cationic polyrotaxanes as gene carriers: physicochemical properties and real-time observation of DNA complexation, and gene transfection in cancer cells. *The journal of physical chemistry. B* **2009**, *113* (22), 7903-11.
260. Li, Z. B.; Yin, H.; Zhang, Z. X.; Liu, K. L.; Li, J., Supramolecular Anchoring of DNA Polyplexes in Cyclodextrin-Based Polypseudorotaxane Hydrogels for Sustained Gene Delivery. *Biomacromolecules* **2012**, *13* (10), 3162-3172.
261. Liu, Y.; Yu, L.; Chen, Y.; Zhao, Y. L.; Yang, H., Construction and DNA condensation of cyclodextrin-based polypseudorotaxanes with anthryl grafts. *Journal of the American Chemical Society* **2007**, *129* (35), 10656-+.
262. Ke, C. F.; Hou, S.; Zhang, H. Y.; Liu, Y.; Yang, K.; Feng, X. Z., Controllable DNA condensation through cucurbit[6]uril in 2D pseudopolyrotaxanes. *Chem Commun* **2007**, (32), 3374-3376.
263. Liu, Y.; Ke, C. F.; Zhang, H. Y.; Wu, W. J.; Shi, J., Reversible 2D pseudopolyrotaxanes based on cyclodextrins and cucurbit[6]uril. *J Org Chem* **2007**, *72* (1), 280-283.

264. Tokuhisa, K.; Hamada, E.; Karinaga, R.; Shimada, N.; Takeda, Y.; Kawasaki, S.; Sakurai, K., Polyrotaxane/DNA conjugate by use of intercalation: Bridge formation between DNA double helices. *Macromolecules* **2006**, *39* (26), 9480-9485.
265. Peres, B.; Richardeau, N.; Jarroux, N.; Guegan, P.; Auvray, L., Two independent ways of preparing hypercharged hydrolyzable polyaminorotaxane. *Biomacromolecules* **2008**, *9* (7), 2007-2013.
266. Ooya, T.; Choi, H. S.; Yamashita, A.; Yui, N.; Sugaya, Y.; Kano, A.; Maruyama, A.; Akita, H.; Ito, R.; Kogure, K.; Harashima, H., Biocleavable polyrotaxane - Plasmid DNA polyplex for enhanced gene delivery. *Journal of the American Chemical Society* **2006**, *128* (12), 3852-3853.
267. Yamashita, A.; Kanda, D.; Katoono, R.; Yui, N.; Ooya, T.; Maruyama, A.; Akita, H.; Kogure, K.; Harashima, H., Supramolecular control of polyplex dissociation and cell transfection: Efficacy of amino groups and threading cyclodextrins in biocleavable polyrotaxanes. *Journal of Controlled Release* **2008**, *131* (2), 137-144.
268. Yamashita, A.; Yui, N.; Ooya, T.; Kano, A.; Maruyama, A.; Akita, H.; Kogure, K.; Harashima, H., Synthesis of a biocleavable polyrotaxane-plasmid DNA (pDNA) polyplex and its use for the rapid nonviral delivery of pDNA to cell nuclei. *Nat Protoc* **2006**, *1* (6), 2861-2869.
269. Yamada, Y.; Hashida, M.; Nomura, T.; Harashima, H.; Yamasaki, Y.; Kataoka, K.; Yamashita, A.; Katoono, R.; Yui, N., Different Mechanisms for Nanoparticle Formation between pDNA and siRNA Using Polyrotaxane as the Polycation. *Chemphyschem* **2012**, *13* (5), 1161-1165.
270. Tamura, A.; Yui, N., Cellular internalization and gene silencing of siRNA polyplexes by cytocleavable cationic polyrotaxanes with tailored rigid backbones. *Biomaterials* **2013**, *34* (10), 2480-2491.
271. Yamada, Y.; Nomura, T.; Harashima, H.; Yamashita, A.; Katoono, R.; Yui, N., Intranuclear DNA release is a determinant of transfection activity for a non-viral vector: biocleavable polyrotaxane as a supramolecularly dissociative condenser for efficient intranuclear DNA release. *Biological & pharmaceutical bulletin* **2010**, *33* (7), 1218-22.
272. Hyun, H.; Yui, N., Ligand Accessibility to Receptor Binding Sites Enhanced by Movable Polyrotaxanes. *Macromol Biosci* **2011**, *11* (6), 765-771.
273. Shaheen, S. M.; Akita, H.; Yamashita, A.; Katoono, R.; Yui, N.; Biju, V.; Ishikawa, M.; Harashima, H., Quantitative analysis of condensation/decondensation status of pDNA in the nuclear sub-domains by QD-FRET. *Nucleic Acids Research* **2011**, *39* (7), E48-U108.
274. Hu, L. Z.; Wan, N.; Ma, X. X.; Jing, Z. W.; Zhang, Y. X.; Li, C.; Zhou, S. Y.; Zhang, B. L., Enhanced gene transfection performance and biocompatibility of polyethylenimine through pseudopolyrotaxane formation with alpha-cyclodextrin. *Nanotechnology* **2017**, *28* (12), 125102.
275. Kulkarni, A.; DeFrees, K.; Schuldt, R. A.; Hyun, S. H.; Wright, K. J.; Yerneni, C. K.; VerHeul, R.; Thompson, D. H., Cationic alpha-cyclodextrin:poly(ethylene glycol) polyrotaxanes for siRNA delivery. *Molecular pharmaceutics* **2013**, *10* (4), 1299-305.

276. Kulkarni, A.; DeFrees, K.; Schuldt, R. A.; Vlahu, A.; VerHeul, R.; Hyun, S. H.; Deng, W.; Thompson, D. H., Multi-armed cationic cyclodextrin:poly(ethylene glycol) polyrotaxanes as efficient gene silencing vectors. *Integrative biology : quantitative biosciences from nano to macro* **2013**, *5* (1), 115-21.
277. Badwaik, V.; Mondjinou, Y.; Kulkarni, A.; Liu, L. J.; Demoret, A.; Thompson, D. H., Efficient pDNA Delivery Using Cationic 2-Hydroxypropyl-beta-Cyclodextrin Pluronic-Based Polyrotaxanes. *Macromol Biosci* **2016**, *16* (1), 63-73.
278. Badwaik, V. D.; Aicart, E.; Mondjinou, Y. A.; Johnson, M. A.; Bowman, V. D.; Thompson, D. H., Structure-property relationship for in vitro siRNA delivery performance of cationic 2-hydroxypropyl-beta-cyclodextrin: PEG-PPG-PEG polyrotaxane vectors. *Biomaterials* **2016**, *84*, 86-98.
279. Zhou, Y.; Wang, H.; Wang, C.; Li, Y.; Lu, W.; Chen, S.; Luo, J.; Jiang, Y.; Chen, J., Receptor-mediated, tumor-targeted gene delivery using folate-terminated polyrotaxanes. *Molecular pharmaceutics* **2012**, *9* (5), 1067-76.
280. Xu, H.-Q. S.; Yu, Q.; Rui-Quan, L.; Gang, C.; Nana, Z.; Fu, J., High-performance cationic polyrotaxanes terminated with polypeptides as promising nucleic acid delivery systems. **2018**.
281. Huang, H.; Cao, D. W.; Qin, L. H.; Tian, S. Q.; Liang, Y.; Pan, S. R.; Feng, M., Dilution-Stable PAMAM G1-Grafted Polyrotaxane Supermolecules Deliver Gene into Cells through a Caveolae-Dependent Pathway. *Molecular pharmaceutics* **2014**, *11* (7), 2323-2333.
282. Albuzat, T.; Keil, M.; Ellis, J.; Alexander, C.; Wenz, G., Transfection of luciferase DNA into various cells by cationic cyclodextrin polyrotaxanes derived from ionene-11. *Journal of Materials Chemistry* **2012**, *22* (17), 8558-8565.
283. Dandekar, P.; Jain, R.; Keil, M.; Loretz, B.; Muijs, L.; Schneider, M.; Auerbach, D.; Jung, G.; Lehr, C. M.; Wenz, G., Cellular delivery of polynucleotides by cationic cyclodextrin polyrotaxanes. *Journal of controlled release : official journal of the Controlled Release Society* **2012**, *164* (3), 387-93.
284. Davis, M. E., The First Targeted Delivery of siRNA in Humans via a Self-Assembling, Cyclodextrin Polymer-Based Nanoparticle: From Concept to Clinic. *Molecular pharmaceutics* **2009**, *6* (3), 659-668.
285. Oupicky, D., Design and development strategies of polymer materials for drug and gene delivery applications. *Advanced Drug Delivery Reviews* **2008**, *60* (9), 957-957.
286. Pack, D. W.; Hoffman, A. S.; Pun, S.; Stayton, P. S., Design and development of polymers for gene delivery. *Nature Reviews Drug Discovery* **2005**, *4* (7), 581-593.
287. Hwang, S. J.; Bellocq, N. C.; Davis, M. E., Effects of structure of beta-cyclodextrin-containing polymers on gene delivery. *Bioconjugate Chemistry* **2001**, *12* (2), 280-290.
288. Popielarski, S. R.; Mishra, S.; Davis, M. E., Structural effects of carbohydrate-containing polycations on gene delivery. 3. Cyclodextrin type and functionalization. *Bioconjugate Chemistry* **2003**, *14* (3), 672-678.

289. Reineke, T. M.; Davis, M. E., Structural effects of carbohydrate-containing polycations on gene delivery. 1. Carbohydrate size and its distance from charge centers. *Bioconjugate Chemistry* **2003**, *14* (1), 247-254.
290. Reineke, T. M.; Davis, M. E., Structural effects of carbohydrate-containing polycations on gene delivery. 2. Charge center type. *Bioconjugate Chemistry* **2003**, *14* (1), 255-261.
291. Popielarski, S. R.; Hu-Lieskovan, S.; French, S. W.; Triche, T. J.; Davis, M. E., A nanoparticle-based model delivery system to guide the rational design of gene delivery to the liver. 2. In vitro and in vivo uptake results. *Bioconjugate Chemistry* **2005**, *16* (5), 1071-1080.
292. Popielarski, S. R.; Pun, S. H.; Davis, M. E., A nanoparticle-based model delivery system to guide the rational design of gene delivery to the liver. 1. Synthesis and characterization. *Bioconjugate Chemistry* **2005**, *16* (5), 1063-1070.
293. Bellocq, N. C.; Kang, D. W.; Wang, X. H.; Jensen, G. S.; Pun, S. H.; Schluep, T.; Zepeda, M. L.; Davis, M. E., Synthetic biocompatible cyclodextrin-based constructs for local gene delivery to improve cutaneous wound healing. *Bioconjugate Chemistry* **2004**, *15* (6), 1201-1211.
294. Davis, M. E.; Zuckerman, J. E.; Choi, C. H. J.; Seligson, D.; Tolcher, A.; Alabi, C. A.; Yen, Y.; Heidel, J. D.; Ribas, A., Evidence of RNAi in humans from systemically administered siRNA via targeted nanoparticles. *Nature* **2010**, *464* (7291), 1067-U140.
295. Bartlett, D. W.; Su, H.; Hildebrandt, I. J.; Weber, W. A.; Davis, M. E., Impact of tumor-specific targeting on the biodistribution and efficacy of siRNA nanoparticles measured by multimodality in vivo imaging. *Proceedings of the National Academy of Sciences of the United States of America* **2007**, *104* (39), 15549-15554.
296. Zuckerman, J. E.; Choi, C. H. J.; Han, H.; Davis, M. E., Polycation-siRNA nanoparticles can disassemble at the kidney glomerular basement membrane. *Proceedings of the National Academy of Sciences of the United States of America* **2012**, *109* (8), 3137-3142.
297. Zuckerman, J. E.; Davis, M. E., Targeting therapeutics to the glomerulus with nanoparticles. *Adv Chronic Kidney Dis* **2013**, *20* (6), 500-7.
298. Choi, C. H.; Zuckerman, J. E.; Webster, P.; Davis, M. E., Targeting kidney mesangium by nanoparticles of defined size. *Proceedings of the National Academy of Sciences of the United States of America* **2011**, *108* (16), 6656-61.
299. Morimoto, K.; Kondo, M.; Kawahara, K.; Ushijima, H.; Tomino, Y.; Miyajima, M.; Kimura, J., Advances in Targeting Drug Delivery to Glomerular Mesangial Cells by Long Circulating Cationic Liposomes for the Treatment of Glomerulonephritis. *Pharmaceutical Research* **2007**, *24* (5), 946-954.
300. Liao, J.; Hayashi, K.; Horikoshi, S.; Ushijima, H.; Kimura, J.; Tomino, Y., Effect of Steroid-Liposome on Immunohistopathology of IgA Nephropathy in ddY Mice. *Nephron* **2001**, *89* (2), 194-200.
301. Zuckerman, J. E.; Gale, A.; Wu, P.; Ma, R.; Davis, M. E., siRNA Delivery to the Glomerular Mesangium Using Polycationic Cyclodextrin Nanoparticles Containing siRNA. *Nucleic Acid Therapeutics* **2015**, *25* (2), 53-64.

302. Rahman, M. A.; Amin, A. R. M. R.; Wang, X.; Zuckerman, J. E.; Choi, C. H. J.; Zhou, B.; Wang, D.; Nannapaneni, S.; Koenig, L.; Chen, Z.; Chen, Z. G.; Yen, Y.; Davis, M. E.; Shin, D. M., Systemic delivery of siRNA nanoparticles targeting RRM2 suppresses head and neck tumor growth. *Journal of controlled release : official journal of the Controlled Release Society* **2012**, *159* (3), 384-392.
303. Wiley, D. T.; Webster, P.; Gale, A.; Davis, M. E., Transcytosis and brain uptake of transferrin-containing nanoparticles by tuning avidity to transferrin receptor. *Proceedings of the National Academy of Sciences of the United States of America* **2013**, *110* (21), 8662-7.
304. Kulkarni, A.; Deng, W.; Hyun, S.-h.; Thompson, D. H., Development of a low toxicity, effective pDNA vector based on noncovalent assembly of bioresponsive amino- β -cyclodextrin:adamantane-poly(vinyl alcohol)-poly(ethylene glycol) transfection complexes. *Bioconjugate chemistry* **2012**, *23* (5), 933-940.
305. Kulkarni, A.; Badwaik, V.; DeFrees, K.; Schuldt, R. A.; Gunasekera, D. S.; Powers, C.; Vlahu, A.; VerHeul, R.; Thompson, D. H., Effect of Pendant Group on pDNA Delivery by Cationic- β -Cyclodextrin:Alkyl-PVA-PEG Pendant Polymer Complexes. *Biomacromolecules* **2014**, *15* (1), 12-9.
306. Kulkarni, A.; Verheul, R.; Defrees, K.; Collins, C. J.; Schuldt, R. A.; Vlahu, A.; Thompson, D. H., Microfluidic Assembly of Cationic- β -Cyclodextrin:Hyaluronic Acid-Adamantane Host:Guest pDNA Nanoparticles. *Biomaterials science* **2013**, *1* (10), 10.1039/C3BM00189J.
307. Badwaik, V.; Liu, L.; Gunasekera, D.; Kulkarni, A.; Thompson, D. H., Mechanistic Insight into Receptor-Mediated Delivery of Cationic- β -Cyclodextrin:Hyaluronic Acid-Adamantamethamidyl Host:Guest pDNA Nanoparticles to CD44+ Cells. *Molecular pharmaceutics* **2016**, *13* (3), 1176-1184.
308. Cryan, S. A.; Holohan, A.; Donohue, R.; Darcy, R.; O'Driscoll, C. M., Cell transfection with polycationic cyclodextrin vectors. *European journal of pharmaceutical sciences : official journal of the European Federation for Pharmaceutical Sciences* **2004**, *21* (5), 625-33.
309. Donohue, R.; Mazzaglia, A.; Ravoo, B. J.; Darcy, R., Cationic β -cyclodextrin bilayer vesicles. *Chem Commun* **2002**, (23), 2864-2865.
310. Cryan, S. A.; Donohue, R.; Ravoo, B. J.; Darcy, R.; O'Driscoll, C. M., Cationic cyclodextrin amphiphiles as gene delivery vectors. *Journal of Drug Delivery Science and Technology* **2004**, *14* (1), 57-62.
311. McMahon, A.; Gomez, E.; Donohue, R.; Forde, D.; Darcy, R.; O'Driscoll, C. M., Cyclodextrin gene vectors: cell trafficking and the influence of lipophilic chain length. *Journal of Drug Delivery Science and Technology* **2008**, *18* (5), 303-307.
312. McMahon, A.; O'Neill, M. J.; Gomez, E.; Donohue, R.; Forde, D.; Darcy, R.; O'Driscoll, C. M., Targeted gene delivery to hepatocytes with galactosylated amphiphilic cyclodextrins. *The Journal of pharmacy and pharmacology* **2012**, *64* (8), 1063-73.

313. Fitzgerald, K. A.; Malhotra, M.; Gooding, M.; Sallas, F.; Evans, J. C.; Darcy, R.; O'Driscoll, C. M., A novel, anisamide-targeted cyclodextrin nanoformulation for siRNA delivery to prostate cancer cells expressing the sigma-1 receptor. *International journal of pharmaceutics* **2016**, *499* (1-2), 131-145.
314. Evans, J. C.; Malhotra, M.; Sweeney, K.; Darcy, R.; Nelson, C. C.; Hollier, B. G.; O'Driscoll, C. M., Folate-targeted amphiphilic cyclodextrin nanoparticles incorporating a fusogenic peptide deliver therapeutic siRNA and inhibit the invasive capacity of 3D prostate cancer tumours. *International journal of pharmaceutics* **2017**, *532* (1), 511-518.
315. Guo, J.; Russell, E. G.; Darcy, R.; Cotter, T. G.; McKenna, S. L.; Cahill, M. R.; O'Driscoll, C. M., Antibody-Targeted Cyclodextrin-Based Nanoparticles for siRNA Delivery in the Treatment of Acute Myeloid Leukemia: Physicochemical Characteristics, in Vitro Mechanistic Studies, and ex Vivo Patient Derived Therapeutic Efficacy. *Molecular pharmaceutics* **2017**, *14* (3), 940-952.
316. Evans, J. C.; Malhotra, M.; Fitzgerald, K. A.; Guo, J.; Cronin, M. F.; Curtin, C. M.; O'Brien, F. J.; Darcy, R.; O'Driscoll, C. M., Formulation and Evaluation of Anisamide-Targeted Amphiphilic Cyclodextrin Nanoparticles To Promote Therapeutic Gene Silencing in a 3D Prostate Cancer Bone Metastases Model. *Molecular pharmaceutics* **2017**, *14* (1), 42-52.
317. Defaye, J. M. G. F.; Carmen Ortiz, M.; Sylwester, M.; Jacques, Thioureido- β -cyclodextrins as molecular carriers. **1996**.
318. Mendez-Ardoy, A.; Guilloteau, N.; Di Giorgio, C.; Vierling, P.; Santoyo-Gonzalez, F.; Ortiz Mellet, C.; Garcia Fernandez, J. M., beta-Cyclodextrin-based polycationic amphiphilic "click" clusters: effect of structural modifications in their DNA complexing and delivery properties. *J Org Chem* **2011**, *76* (15), 5882-94.
319. Diaz-Moscoso, A.; Guilloteau, N.; Bienvenu, C.; Mendez-Ardoy, A.; Blanco, J. L.; Benito, J. M.; Le Gourrierc, L.; Di Giorgio, C.; Vierling, P.; Defaye, J.; Mellet, C. O.; Fernandez, J. M., Mannosyl-coated nanocomplexes from amphiphilic cyclodextrins and pDNA for site-specific gene delivery. *Biomaterials* **2011**, *32* (29), 7263-73.
320. Martínez-Negro, M.; Caracciolo, G.; Palchetti, S.; Pozzi, D.; Capriotti, A. L.; Cavaliere, C.; Laganà, A.; Ortiz Mellet, C.; Benito, J. M.; García Fernández, J. M.; Aicart, E.; Junquera, E., Biophysics and protein corona analysis of Janus cyclodextrin-DNA nanocomplexes. Efficient cellular transfection on cancer cells. *Biochimica et Biophysica Acta (BBA) - General Subjects* **2017**, *1861* (7), 1737-1749.
321. Diaz-Moscoso, A.; Vercauteren, D.; Rejman, J.; Benito, J. M.; Ortiz Mellet, C.; De Smedt, S. C.; Fernandez, J. M., Insights in cellular uptake mechanisms of pDNA-polycationic amphiphilic cyclodextrin nanoparticles (CDplexes). *Journal of controlled release : official journal of the Controlled Release Society* **2010**, *143* (3), 318-25.
322. Gallego-Yerga, L.; Gonzalez-Alvarez, M. J.; Mayordomo, N.; Santoyo-Gonzalez, F.; Benito, J. M.; Ortiz Mellet, C.; Mendicuti, F.; Garcia Fernandez, J. M., Dynamic self-assembly of polycationic clusters based on cyclodextrins for pH-sensitive DNA nanocondensation and delivery by component design. *Chemistry (Weinheim an der Bergstrasse, Germany)* **2014**, *20* (22), 6622-7.

323. Arima, H.; Kihara, F.; Hirayama, F.; Uekama, K., Enhancement of Gene Expression by Polyamidoamine Dendrimer Conjugates with α -, β -, and γ -Cyclodextrins. *Bioconjugate Chemistry* **2001**, *12* (4), 476-484.
324. Arima, H.; Yoshimatsu, A.; Ikeda, H.; Ohyama, A.; Motoyama, K.; Higashi, T.; Tsuchiya, A.; Niidome, T.; Katayama, Y.; Hattori, K.; Takeuchi, T., Folate-PEG-Appended Dendrimer Conjugate with α -Cyclodextrin as a Novel Cancer Cell-Selective siRNA Delivery Carrier. *Molecular pharmaceutics* **2012**, *9* (9), 2591-2604.
325. Hayashi, Y.; Mori, Y.; Yamashita, S.; Motoyama, K.; Higashi, T.; Jono, H.; Ando, Y.; Arima, H., Potential Use of Lactosylated Dendrimer (G3)/ α -Cyclodextrin Conjugates as Hepatocyte-Specific siRNA Carriers for the Treatment of Familial Amyloidotic Polyneuropathy. *Molecular pharmaceutics* **2012**, *9* (6), 1645-1653.
326. Hayashi, Y.; Higashi, T.; Motoyama, K.; Jono, H.; Ando, Y.; Arima, H., In vitro and in vivo siRNA delivery to hepatocyte utilizing ternary complexation of lactosylated dendrimer/cyclodextrin conjugates, siRNA and low-molecular-weight sacran. *International Journal of Biological Macromolecules* **2018**, *107*, 1113-1121.
327. Pack, D. W.; Hoffman, A. S.; Pun, S.; Stayton, P. S., Design and Development of Polymers for Gene Delivery. *Nature Rev. Drug Disc.* **2005**, *4*, 581-593.
328. Cheng, Y.; Yumul, R. C.; Pun, S. H., Virus-inspired Polymer for Efficient In Vitro and In Vivo Gene Delivery. *Angew. Chem. Int. Ed.* **2016**, *55*, 12013-12017.
329. Dahlman, J. E.; Barnes, C.; Khan, O. F.; Thiriot, A.; Jhunjunwala, S.; Shaw, T. E.; Xing, Y. P.; Sager, H. B.; Sahay, G.; Speciner, L.; Bader, A.; Bogorad, R. L.; Yin, H.; Racie, T.; Dong, Y. Z.; Jiang, S.; Seedorf, D.; Dave, A.; Sandhu, K. S.; Webber, M. J.; Novobrantseva, T.; Ruda, V. M.; Lytton-Jean, A. K. R.; Levins, C. G.; Kalish, B.; Mudge, D. K.; Perez, M.; Abezgauz, L.; Dutta, P.; Smith, L.; Charisse, K.; Kieran, M. W.; Fitzgerald, K.; Nahrendorf, M.; Danino, D.; Tudor, R. M.; von Andrian, U. H.; Akinc, A.; Panigrahy, D.; Schroeder, A.; Kotliansky, V.; Langer, R.; Anderson, D. G., In Vivo Endothelial siRNA Delivery Using Polymeric Nanoparticles with Low Molecular Weight. *Nature Nanotech.* **2014**, *9*, 648-655.
330. McKinlay, C. J.; Vargas, J. R.; Blake, T. R.; Hardy, J. W.; Kanada, M.; Contag, C. H.; Wender, P. A.; Waymouth, R. M., Charge-altering Releasable Transporters (CARTs) for the Delivery and Release of mRNA in Living Animals. *Proc. Nat'l. Acad. Sci. U.S.A.* **2017**, E448-E456.
331. Deng, Z. J.; Morton, S. W.; Ben-Akiva, E.; Dreaden, E. C.; Shopsowitz, K. E.; Hammond, P. T., Layer-by-layer Nanoparticles for Systemic Co-delivery of an Anticancer Drug and siRNA for Potential Triple Negative Breast Cancer Treatment. *ACS Nano* **2013**, *7*, 9571-9584.
332. de Jesus, M. B.; Zuhorn, I. S., Solid Lipid Nanoparticles as Nucleic Acid Delivery System: Properties and Molecular Mechanisms. *J. Controlled Rel.* **2015**, *201*, 1-13.
333. Rinkenauer, A. C.; Schubert, S.; Traeger, A.; Schubert, U. S., The Influence of Polymer Architecture on In Vitro pDNA Transfection. *J. Mat. Chem. B* **2015**, *3*, 7477-7493.
334. Ozpolat, B.; Sood, A. K.; Lopez-Bernstein, G., Liposomal siRNA Nanocarriers for Cancer Therapy. *Adv. Drug Del. Rev.* **2014**, *66*, 110-116.

335. Ooya, T.; Choi, H.-S.; Yamashita, A.; Yui, N.; Sugaya, Y.; Kano, A.; Maruyama, A.; Akita, H.; Ito, R.; Kogure, K.; Harashima, H., Biocleavable Polyrotaxane-Plasmid DNA Polyplex for Enhanced Gene Delivery. *J. Am. Chem. Soc.* **2006**, *128*, 3852-3853.
336. Badwaik, V. D.; Aicart, E.; Mondjinou, Y. A.; Johnson, M. A.; Bowman, V. D.; Thompson, D. H., Structure-Property Relationship for siRNA Delivery Performance of Cationic 2-Hydroxypropyl--cyclodextrin: Poly(ethylene glycol)-Poly(propylene glycol)-Poly(ethylene glycol) Polyrotaxane Vectors. *Biomaterials* **2016**, *84*, 86-98.
337. Xiong, X.-B.; Binkhathlan, Z.; Molavi, O.; Lavasanifar, A., Amphiphilic Block Copolymers: Preparation and Application in Nanodrug and Gene Delivery. *Acta Biomat.* **2012**, *8*, 2017-2033.
338. Kozielski, K. L.; Green, J. J., Bioreducible Poly(beta-amino ester)s for Intracellular Delivery of siRNA. *Methods Mol. Biol.* **2016**, *1364*, 79-87.
339. Kulkarni, A.; DeFrees, K.; Hyun, S.-H.; Thompson, D. H., Pendant Polymer:Amino-beta-cyclodextrin Guest:Host Nanoparticles as Efficient Vectors for Gene Silencing. *J. Am. Chem. Soc.* **2012**, *134*, 7596-7599.
340. Mendes, L. P.; Pan, J. Y.; Torchilin, V. P., Dendrimers as Nanocarriers for Nucleic Acid and Drug Delivery in Cancer Therapy. *Molecules* **2017**, *22*, 1401.
341. Cooley, C. B.; Trantow, B. M.; Nederberg, F.; Kiesewetter, M. K.; Hedrick, J. L.; Waymouth, R. M.; Wender, P. A., Oligocarbonate Molecular Transporters: Oligomerization-based Syntheses and Cell Penetrating Studies. *J. Am. Chem. Soc.* **2009**, *131*, 16401-16403.
342. Geihe, E. I.; Cooley, C. B.; Simon, J. R.; Kiesewetter, M. K.; Edward, J. A.; Hickerson, R. P.; Kaspar, R. L.; Hedrick, J. L.; Waymouth, R. M.; Wender, P. A., Designed Guanidinium-rich Amphipathic Oligocarbonate Molecular Transporters Complex, Deliver and Release siRNA in Cells. *Proc. Nat'l. Acad. Sci. U.S.A.* **2012**, *109*, 13171-13176.
343. Dove, A. P., Organic Catalysts for Ring Opening Polymerization. *ACS Macro Lett* **2012**, *1*, 1409-1412.
344. Lohmeijer, B. G. G.; Pratt, R. C.; Leibfarth, F.; Logan, J. W.; Long, D. A.; Dove, A. P.; Nederberg, F.; Choi, J.; Wade, C.; Waymouth, R. M.; Hedrick, J. L., Guanidine and Amidine Organocatalysts for Ring Opening Polymerization of Cyclic Esters. *Macromolecules* **2006**, *39*, 8574-8583.
345. Nederberg, F.; Lohmeijer, B. G. G.; Leibfarth, F.; Pratt, R. C.; Choi, J.; Dove, A. P.; Waymouth, R. M.; Hedrick, J. L., Organocatalytic Ring Opening Polymerization of Trimethylene Carbonate. *Biomacromolecules* **2007**, *8*, 153-160.
346. Dove, A. P.; Pratt, R. C.; Lohmeijer, B. G. G.; Waymouth, R. M.; Hedrick, J. L., Thiourea-based Bifunctional Organocatalysis: Supramolecular Recognition for Living Polymerization. *J. Am. Chem. Soc.* **2005**, *127*, 13798-13799.
347. Pratt, R. C.; Lohmeijer, B. G. G.; Long, D. A.; Waymouth, R. M.; Hedrick, J. L., Triazabicyclodecene: A Simple Bifunctional Organocatalyst for Acyl Transfer and Ring Opening Polymerization of Cyclic Esters. *J. Am. Chem. Soc.* **2006**, *128*, 4556-4557.

348. Chuma, A.; Horn, H. W.; Swope, W. C.; Pratt, R. C.; Zhang, L.; Lohmeijer, B. G. G.; Wade, C. G.; Waymouth, R. M.; Hedrick, J. L.; Rice, J. E., The Reaction Mechanism for the Organocatalytic Ring Opening Polymerization of L-Lactide Using a Guanidine-based Catalyst: Hydrogen-bonded or Covalently Bound? *J. Am. Chem. Soc.* **2008**, *130*, 6749-6754.
349. Lin, B.; Waymouth, R. M., Urea Anions: Simple, Fast, and Selective Catalysts for Ring Opening Polymerizations. *J. Am. Chem. Soc.* **2017**, *139*, 1645-1652.
350. Kulkarni, A.; Badwaik, V.; DeFrees, K.; Schuldt, R. A.; Gunasekera, D. S.; Powers, C.; Vlahu, A.; VerHeul, R.; Thompson, D. H., Effect of Pendant Group on pDNA Delivery by Cationic beta-Cyclodextrin :Alkyl-PVA-PEG Pendant Polymer Complexes. *Biomacromolecules* **2014**, *15*, 12-19.
351. Rekharsky, M. V.; Inoue, Y., Complexation Thermodynamics of Cyclodextrins. *Chem. Rev.* **1998**, *98*, 1875-1917.
352. Kulkarni, A.; VerHeul, R.; DeFrees, K.; Collins, C. J.; Schuldt, R. A.; Vlahu, A.; Thompson, D. H., Microfluidic Assembly of Cationic beta-Cyclodextrin:Hyaluronic Acid-Adamantane Host:Guest pDNA Nanoparticles. *Biomater. Sci.* **2013**, *1*, 1029-1033.
353. Pratt, R. C.; Nederberg, F.; Waymouth, R. M.; Hedrick, J. L., Tagging Alcohols with Cyclic Carbonate: A Versatile Equivalent of (Meth)acrylate for Ring Opening Polymerization. *Chem. Comm.* **2008**, 114-116.
354. Kinnear, C.; Moore, T. L.; Rodriguez-Lorenzo, L.; Rothen-Rutishauser, B.; Petri-Fink, A., Form Follows Function: Nanoparticle Shape and its Implications for Nanomedicine. *Chem. Rev.* **2017**, *117*, 11476-11521.
355. Wenz, G., CYCLODEXTRINS AS BUILDING-BLOCKS FOR SUPRAMOLECULAR STRUCTURES AND FUNCTIONAL UNITS. *Angewandte Chemie-International Edition* **1994**, *33* (8), 803-822.
356. Wenz, G., Cyclodextrins as Building Blocks for Supramolecular Structures and Functional Units. *Angewandte Chemie International Edition in English* **1994**, *33* (8), 803-822.
357. Brewster, M. E.; Loftsson, T., Cyclodextrins as pharmaceutical solubilizers. *Advanced Drug Delivery Reviews* **2007**, *59* (7), 645-666.
358. Cal, K.; Centkowska, K., Use of cyclodextrins in topical formulations: Practical aspects. *European Journal of Pharmaceutics and Biopharmaceutics* **2008**, *68* (3), 467-478.
359. Loftsson, T.; Duchene, D., Cyclodextrins and their pharmaceutical applications. *International Journal of Pharmaceutics* **2007**, *329* (1-2), 1-11.
360. Davies, N. M.; Wang, G. J.; Tucker, I. G., Evaluation of a hydrocortisone/hydroxypropyl-beta-cyclodextrin solution for ocular drug delivery. *International Journal of Pharmaceutics* **1997**, *156* (2), 201-209.
361. Jambhekar, S.; Casella, R.; Maher, T., The physicochemical characteristics and bioavailability of indomethacin from beta-cyclodextrin, hydroxyethyl-beta-cyclodextrin, and hydroxypropyl-beta-cyclodextrin complexes. *International Journal of Pharmaceutics* **2004**, *270* (1-2), 149-166.

362. Kilsdonk, E. P. C.; Yancey, P. G.; Stoudt, G. W.; Bangerter, F. W.; Johnson, W. J.; Phillips, M. C.; Rothblat, G. H., CELLULAR CHOLESTEROL EFFLUX MEDIATED BY CYCLODEXTRINS. *Journal of Biological Chemistry* **1995**, *270* (29), 17250-17256.
363. Zidovetzki, R.; Levitan, I., Use of cyclodextrins to manipulate plasma membrane cholesterol content: Evidence, misconceptions and control strategies. *Biochimica Et Biophysica Acta-Biomembranes* **2007**, *1768* (6), 1311-1324.
364. Williams, R. O.; Mahaguna, V.; Sriwongjanya, M., Characterization of an inclusion complex of cholesterol and hydroxypropyl-beta-cyclodextrin. *European Journal of Pharmaceutics and Biopharmaceutics* **1998**, *46* (3), 355-360.
365. Nishijo, J.; Moriyama, S.; Shiota, S., Interactions of cholesterol with cyclodextrins in aqueous solution. *Chemical & Pharmaceutical Bulletin* **2003**, *51* (11), 1253-1257.
366. Ottinger, E. A.; Kao, M. L.; Carrillo-Carrasco, N.; Yanjanin, N.; Shankar, R. K.; Janssen, M.; Brewster, M.; Scott, I.; Xu, X.; Craddock, J.; Terse, P.; Dehdashti, S. J.; Marugan, J.; Zheng, W.; Portilla, L.; Hubbs, A.; Pavan, W. J.; Heiss, J.; Vite, C. H.; Walkley, S. U.; Ory, D. S.; Silber, S. A.; Porter, F. D.; Austin, C. P.; McKew, J. C., Collaborative Development of 2-Hydroxypropyl-beta-Cyclodextrin for the Treatment of Niemann-Pick Type C1 Disease. *Current Topics in Medicinal Chemistry* **2014**, *14* (3), 330-339.
367. Yergey, A. L.; Blank, P. S.; Cologna, S. M.; Backlund, P. S.; Porter, F. D.; Darling, A. J., Characterization of hydroxypropyl-beta-cyclodextrins used in the treatment of Niemann-Pick Disease type C1. *Plos One* **2017**, *12* (4).
368. Maarup, T. J.; Chen, A. H.; Porter, F. D.; Farhat, N. Y.; Ory, D. S.; Sidhu, R.; Jiang, X.; Dickson, P. I., Intrathecal 2-hydroxypropyl-beta-cyclodextrin in a single patient with Niemann Pick C1. *Molecular Genetics and Metabolism* **2015**, *116* (1-2), 75-79.
369. Vanier, M. T., Niemann-Pick disease type C. *Orphanet Journal of Rare Diseases* **2010**, *5*.
370. Mondjinou, Y. A.; McCauiff, L. A.; Kulkarni, A.; Paul, L.; Hyun, S.-H.; Zhang, Z.; Wu, Z.; Wirth, M.; Storch, J.; Thompson, D. H., Synthesis of 2-Hydroxypropyl-beta-cyclodextrin/Pluronic-Based Polyrotaxanes via Heterogeneous Reaction as Potential Niemann-Pick Type C Therapeutics. *Biomacromolecules* **2013**, *14* (12), 4189-4197.
371. Lopez, A. M.; Terpack, S. J.; Posey, K. S.; Liu, B.; Ramirez, C. M.; Turley, S. D., Systemic administration of 2-hydroxypropyl-beta-cyclodextrin to symptomatic Npc1-deficient mice slows cholesterol sequestration in the major organs and improves liver function. *Clinical and Experimental Pharmacology and Physiology* **2014**, *41* (10), 780-787.
372. Gould, S.; Scott, R. C., 2-hydroxypropyl-beta-cyclodextrin (HP-beta-CD): A toxicology review. *Food and Chemical Toxicology* **2005**, *43* (10), 1451-1459.
373. Muralidhar, A.; Borbon, I. A.; Esharif, D. M.; Ke, W.; Manacheril, R.; Daines, M.; Erickson, R. P., Pulmonary function and pathology in hydroxypropyl-beta-cyclodextrin-treated and untreated Npc1(-/-) mice. *Molecular Genetics and Metabolism* **2011**, *103* (2), 142-147.

374. Davidson, C. D.; Fishman, Y. I.; Puskas, I.; Szeman, J.; Sohajda, T.; McCauliff, L. A.; Sikora, J.; Storch, J.; Vanier, M. T.; Szente, L.; Walkley, S. U.; Dobrenis, K., Efficacy and ototoxicity of different cyclodextrins in Niemann-Pick C disease. *Annals of Clinical and Translational Neurology* **2016**, *3* (5), 366-380.
375. Vite, C. H.; Bage, J. H.; Swain, G. P.; Prociuk, M.; Sikora, T. U.; O'Donnell, P.; Ruane, T.; Ward, S.; Crooks, A.; Li, S.; Mauldin, E.; Stein, V.; Ory, D. S.; Kao, M. L.; Davidson, C.; Vanier, M. T.; Walkley, S. U., Intracisternal cyclodextrin ameliorates neurological dysfunction, increases survival time, and stops Purkinje cell death in feline Niemann-Pick type C1 disease. *Molecular Genetics and Metabolism* **2015**, *114* (2), S122-S122.
376. Markenstein, L.; Appelt-Menzel, A.; Metzger, M.; Wenz, G., Conjugates of methylated cyclodextrin derivatives and hydroxyethyl starch (HES): Synthesis, cytotoxicity and inclusion of anaesthetic actives. *Beilstein Journal of Organic Chemistry* **2014**, *10*, 3087-3096.
377. Purdie, L.; Alexander, C.; Spain, S. G.; Magnusson, J. P., Influence of Polymer Size on Uptake and Cytotoxicity of Doxorubicin-Loaded DNA-PEG Conjugates. *Bioconjugate Chemistry* **2016**, *27* (5), 1244-1252.
378. Duncan, R., The dawning era of polymer therapeutics. *Nature Reviews Drug Discovery* **2003**, *2* (5), 347-360.
379. Bader, H.; Ringsdorf, H.; Schmidt, B., WATERSOLUBLE POLYMERS IN MEDICINE. *Angewandte Makromolekulare Chemie* **1984**, *123* (AUG), 457-485.
380. Hoste, K.; De Winne, K.; Schacht, E., Polymeric prodrugs. *International Journal of Pharmaceutics* **2004**, *277* (1-2), 119-131.
381. Wenz, G.; Keller, B., THREADING CYCLODEXTRIN RINGS ON POLYMER-CHAINS. *Angewandte Chemie-International Edition in English* **1992**, *31* (2), 197-199.
382. Tamura, A.; Yui, N., Lysosomal-specific Cholesterol Reduction by Biocleavable Polyrotaxanes for Ameliorating Niemann-Pick Type C Disease. *Scientific Reports* **2014**, *4*.
383. Krauter, I.; Herrmann, W.; Wenz, G., Self organization of fluorescent molecular necklaces in aqueous solution. *Journal of Inclusion Phenomena and Molecular Recognition in Chemistry* **1996**, *25* (1-3), 93-96.
384. Huang, F. H.; Gibson, H. W., Polypseudorotaxanes and polyrotaxanes. *Progress in Polymer Science* **2005**, *30* (10), 982-1018.
385. Tiwari, G.; Tiwari, R.; Rai, A. K., Cyclodextrins in delivery systems: Applications. *Journal of Pharmacy and Bioallied Sciences* **2010**, *2* (2), 72-79.
386. Wenz, G.; Gruber, C.; Keller, B.; Schilli, C.; Albusat, T.; Mueller, A., Kinetics of threading alpha-cyclodextrin onto cationic and zwitterionic poly(bola-amphiphiles). *Macromolecules* **2006**, *39* (23), 8021-8026.
387. Harada, A.; Li, J.; Kamachi, M., THE MOLECULAR NECKLACE - A ROTAXANE CONTAINING MANY THREADED ALPHA-CYCLODEXTRINS. *Nature* **1992**, *356* (6367), 325-327.

388. Liu, Y.; Yang, Y. W.; Chen, Y.; Zou, H. X., Polyrotaxane with cyclodextrins as stoppers and its assembly behavior. *Macromolecules* **2005**, *38* (13), 5838-5840.
389. Meschke, C.; Buschmann, H. J.; Schollmeyer, E., Polyrotaxanes and pseudopolyrotaxanes of polyamides and cucurbituril. *Polymer* **1999**, *40* (4), 945-949.
390. Tamura, A.; Yui, N., Polyrotaxane-based systemic delivery of beta-cyclodextrins for potentiating therapeutic efficacy in a mouse model of Niemann-Pick type C disease. *Journal of Controlled Release* **2018**, *269*, 148-158.
391. Knop, K.; Hoogenboom, R.; Fischer, D.; Schubert, U. S., Poly(ethylene glycol) in Drug Delivery: Pros and Cons as Well as Potential Alternatives. *Angewandte Chemie-International Edition* **2010**, *49* (36), 6288-6308.
392. Pasut, G.; Veronese, F. M., Polymer-drug conjugation, recent achievements and general strategies. *Progress in Polymer Science* **2007**, *32* (8-9), 933-961.
393. Westheimer, F., Why nature chose phosphates. *Science* **1987**, *235* (4793), 1173-1178.
394. Herrmann, W.; Keller, B.; Wenz, G., Kinetics and thermodynamics of the inclusion of ionene-6,10 in alpha-cyclodextrin in an aqueous solution. *Macromolecules* **1997**, *30* (17), 4966-4972.
395. Richards, M.; Dahiyat, B. I.; Arm, D. M.; Brown, P. R.; Leong, K. W., EVALUATION OF POLYPHOSPHATES AND POLYPHOSPHONATES AS DEGRADABLE BIOMATERIALS. *Journal of Biomedical Materials Research* **1991**, *25* (9), 1151-1167.
396. Bogomilova, A.; Hoehn, M.; Guenther, M.; Herrmann, A.; Troev, K.; Wagner, E.; Schreiner, L., A polyphosphoester conjugate of melphalan as antitumoral agent. *European Journal of Pharmaceutical Sciences* **2013**, *50* (3-4), 410-419.
397. Liu, Z.; Wang, L.; Bao, C.; Li, X.; Cao, L.; Dai, K.; Zhu, L., Cross-Linked PEG via Degradable Phosphate Ester Bond: Synthesis, Water-Swelling, and Application as Drug Carrier. *Biomacromolecules* **2011**, *12* (6), 2389-2395.
398. Tamura, A.; Tokunaga, M.; Iwasaki, Y.; Yui, N., Spontaneous Assembly into Pseudopolyrotaxane Between Cyclodextrins and Biodegradable Polyphosphoester Ionomers. *Macromolecular Chemistry and Physics* **2014**, *215* (7), 648-653.
399. Mondjinou, Y. A.; Hyun, S.-H.; Xiong, M.; Collins, C. J.; Thong, P. L.; Thompson, D. H., Impact of Mixed beta-Cyclodextrin Ratios on Pluronic Rotaxation Efficiency and Product Solubility. *Acs Applied Materials & Interfaces* **2015**, *7* (43), 23831-23836.
400. Chang, T.-Y.; Reid, P. C.; Sugii, S.; Ohgami, N.; Cruz, J. C.; Chang, C. C. Y., Niemann-Pick Type C Disease and Intracellular Cholesterol Trafficking. *Journal of Biological Chemistry* **2005**, *280* (22), 20917-20920.
401. Froissart, R.; Guffon, N.; Vanier, M. T.; Desnick, R. J.; Maire, I., Fabry disease: D313Y is an α -galactosidase A sequence variant that causes pseudodeficient activity in plasma. *Molecular Genetics and Metabolism* **2003**, *80* (3), 307-314.
402. Vanier, M. T., Niemann-Pick disease type C. *Orphanet Journal of Rare Diseases* **2010**, *5* (1), 16.

403. Carstea, E. D.; Morris, J. A.; Coleman, K. G.; Loftus, S. K.; Zhang, D.; Cummings, C.; Gu, J.; Rosenfeld, M. A.; Pavan, W. J.; Krizman, D. B.; Nagle, J.; Polymeropoulos, M. H.; Sturley, S. L.; Ioannou, Y. A.; Higgins, M. E.; Comly, M.; Cooney, A.; Brown, A.; Kaneski, C. R.; Blanchette-Mackie, E. J.; Dwyer, N. K.; Neufeld, E. B.; Chang, T.-Y.; Liscum, L.; Strauss, J. F.; Ohno, K.; Zeigler, M.; Carmi, R.; Sokol, J.; Markie, D.; O'Neill, R. R.; van Diggelen, O. P.; Elleder, M.; Patterson, M. C.; Brady, R. O.; Vanier, M. T.; Pentchev, P. G.; Tagle, D. A., Niemann-Pick C1 Disease Gene: Homology to Mediators of Cholesterol Homeostasis. *Science* **1997**, *277* (5323), 228-231.
404. Infante, R. E.; Wang, M. L.; Radhakrishnan, A.; Kwon, H. J.; Brown, M. S.; Goldstein, J. L., NPC2 facilitates bidirectional transfer of cholesterol between NPC1 and lipid bilayers, a step in cholesterol egress from lysosomes. *Proceedings of the National Academy of Sciences* **2008**, *105* (40), 15287-15292.
405. Ramirez, C. M.; Liu, B.; Taylor, A. M.; Repa, J. J.; Burns, D. K.; Weinberg, A. G.; Turley, S. D.; Dietschy, J. M., Weekly cyclodextrin administration normalizes cholesterol metabolism in nearly every organ of the Niemann-Pick type C1 mouse and markedly prolongs life. *Pediatric research* **2010**, *68* (4), 309-15.
406. Ward, S.; O'Donnell, P.; Fernandez, S.; Vite, C. H., 2-hydroxypropyl-beta-cyclodextrin raises hearing threshold in normal cats and in cats with Niemann-Pick type C disease. *Pediatric research* **2010**, *68* (1), 52-6.
407. Ory, D. S.; Ottinger, E. A.; Farhat, N. Y.; King, K. A.; Jiang, X.; Weissfeld, L.; Berry-Kravis, E.; Davidson, C. D.; Bianconi, S.; Keener, L. A.; Rao, R.; Soldatos, A.; Sidhu, R.; Walters, K. A.; Xu, X.; Thurm, A.; Solomon, B.; Pavan, W. J.; Machielse, B. N.; Kao, M.; Silber, S. A.; McKew, J. C.; Brewer, C. C.; Vite, C. H.; Walkley, S. U.; Austin, C. P.; Porter, F. D., Intrathecal 2-hydroxypropyl- β -cyclodextrin decreases neurological disease progression in Niemann-Pick disease, type C1: a non-randomised, open-label, phase 1-2 trial. *Lancet (London, England)* **2017**, *390* (10104), 1758-1768.
408. Allen, T. M.; Cullis, P. R., Drug delivery systems: Entering the mainstream. *Science* **2004**, *303* (5665), 1818-1822.
409. Khattab, I. S.; Bandarkar, F.; Fakhree, M. A. A.; Jouyban, A., Density, viscosity, and surface tension of water+ethanol mixtures from 293 to 323K. *Korean Journal of Chemical Engineering* **2012**, *29* (6), 812-817.
410. Mondjinou, Y. A.; McCauliff, L. A.; Kulkarni, A.; Paul, L.; Hyun, S.-H.; Zhang, Z.; Wu, Z.; Wirth, M.; Storch, J.; Thompson, D. H., Synthesis of 2-Hydroxypropyl- β -cyclodextrin/Pluronic-Based Polyrotaxanes via Heterogeneous Reaction as Potential Niemann-Pick Type C Therapeutics. *Biomacromolecules* **2013**, *14* (12), 4189-4197.
411. Collins, C. J.; McCauliff, L. A.; Hyun, S. H.; Zhang, Z.; Paul, L. N.; Kulkarni, A.; Zick, K.; Wirth, M.; Storch, J.; Thompson, D. H., Synthesis, characterization, and evaluation of pluronic-based beta-cyclodextrin polyrotaxanes for mobilization of accumulated cholesterol from Niemann-Pick type C fibroblasts. *Biochemistry* **2013**, *52* (19), 3242-53.
412. Collins, C. J.; Mondjinou, Y.; Loren, B.; Torregrosa-Allen, S.; Simmons, C. J.; Elzey, B. D.; Ayat, N.; Lu, Z.-R.; Thompson, D., Influence of Molecular Structure on the In Vivo Performance of Flexible Rod Polyrotaxanes. *Biomacromolecules* **2016**, *17* (9), 2777-2786.

413. Collins, C. J.; Loren, B. P.; Alam, M. S.; Mondjinou, Y.; Skulsky, J. L.; Chaplain, C. R.; Haldar, K.; Thompson, D. H., Pluronic based β -cyclodextrin polyrotaxanes for treatment of Niemann-Pick Type C disease. **2017**, *7*, 46737.
414. Tamura, A.; Yui, N., Polyrotaxane-based systemic delivery of β -cyclodextrins for potentiating therapeutic efficacy in a mouse model of Niemann-Pick type C disease. *Journal of Controlled Release* **2018**, *269*, 148-158.
415. Egele, K.; Samaddar, S.; Schneider, N.; Thompson, D.; Wenz, G., Synthesis of the anionic hydroxypropyl- β -cyclodextrin:poly(decamethylenephosphate) polyrotaxane and evaluation of its cholesterol efflux potential in Niemann-Pick C1 cells. *Journal of Materials Chemistry B* **2019**, *7* (4), 528-537.
416. Tanaka, K.; Toda, F., Solvent-Free Organic Synthesis. *Chem Rev* **2000**, *100* (3), 1025-1074.
417. Mondjinou, Y. A.; Hyun, S.-H.; Xiong, M.; Collins, C. J.; Thong, P. L.; Thompson, D. H., Impact of Mixed β -Cyclodextrin Ratios on Pluronic Rotaxanation Efficiency and Product Solubility. *ACS Applied Materials & Interfaces* **2015**, *7* (43), 23831-23836.
418. Liu, B.; Xie, C.; Richardson, J. A.; Turley, S. D.; Dietschy, J. M., Receptor-mediated and bulk-phase endocytosis cause macrophage and cholesterol accumulation in Niemann-Pick C disease. *Journal of Lipid Research* **2007**, *48* (8), 1710-1723.
419. Vives, E.; Brodin, P.; Lebleu, B., A truncated HIV-1 Tat protein basic domain rapidly translocates through the plasma membrane and accumulates in the cell nucleus. *The Journal of biological chemistry* **1997**, *272* (25), 16010-7.
420. Schmidt, N.; Mishra, A.; Lai, G. H.; Wong, G. C. L., Arginine-rich cell-penetrating peptides. *FEBS Letters* **2010**, *584* (9), 1806-1813.
421. Madani, F.; Lindberg, S.; Langel, Ü.; Futaki, S.; Gräslund, A., Mechanisms of Cellular Uptake of Cell-Penetrating Peptides. *J Biophys* **2011**, *2011*.
422. Fuchs, S. M.; Raines, R. T., Pathway for polyarginine entry into mammalian cells. *Biochemistry* **2004**, *43* (9), 2438-2444.
423. Gonçalves, E.; Kitas, E.; Seelig, J., Binding of Oligoarginine to Membrane Lipids and Heparan Sulfate: Structural and Thermodynamic Characterization of a Cell-Penetrating Peptide. *Biochemistry* **2005**, *44* (7), 2692-2702.
424. Nakase, I.; Tanaka, G.; Futaki, S., Cell-penetrating peptides (CPPs) as a vector for the delivery of siRNAs into cells. *Molecular BioSystems* **2013**, *9* (5), 855-861.
425. Suzuki, T.; Futaki, S.; Niwa, M.; Tanaka, S.; Ueda, K.; Sugiura, Y., Possible Existence of Common Internalization Mechanisms among Arginine-rich Peptides. *Journal of Biological Chemistry* **2002**, *277* (4), 2437-2443.
426. Console, S.; Marty, C.; García-Echeverría, C.; Schwendener, R.; Ballmer-Hofer, K., Antennapedia and HIV Transactivator of Transcription (TAT) "Protein Transduction Domains" Promote Endocytosis of High Molecular Weight Cargo upon Binding to Cell Surface Glycosaminoglycans. *Journal of Biological Chemistry* **2003**, *278* (37), 35109-35114.

427. Ivaturi, S.; Wooten, C. J.; Nguyen, M. D.; Ness, G. C.; Lopez, D., Distribution of the LDL receptor within clathrin-coated pits and caveolae in rat and human liver. *Biochemical and Biophysical Research Communications* **2014**, *445* (2), 422-427.
428. Payne, C. K.; Jones, S. A.; Chen, C.; Zhuang, X., Internalization and trafficking of cell surface proteoglycans and proteoglycan-binding ligands. *Traffic (Copenhagen, Denmark)* **2007**, *8* (4), 389-401.
429. Valkó, I. E.; Billiet, H. A. H.; Frank, J.; Luyben, K. C. A. M., Effect of the degree of substitution of (2-hydroxy)propyl- β -cyclodextrin on the enantioseparation of organic acids by capillary electrophoresis. *Journal of Chromatography A* **1994**, *678* (1), 139-144.
430. Yong, C. W.; Washington, C.; Smith, W., Structural behaviour of 2-hydroxypropyl-beta-cyclodextrin in water: molecular dynamics simulation studies. *Pharm Res* **2008**, *25* (5), 1092-9.
431. Liu, X.; Wu, F.; Tian, Y.; Wu, M.; Zhou, Q.; Jiang, S.; Niu, Z., Size Dependent Cellular Uptake of Rod-like Bionanoparticles with Different Aspect Ratios. *Scientific Reports* **2016**, *6*, 24567.
432. Cheng, F.; Mani, K.; Fransson, L.-Å., Constitutive and vitamin C-induced, NO-catalyzed release of heparan sulfate from recycling glypican-1 in late endosomes. *Glycobiology* **2006**, *16* (12), 1251-1261.
433. Kanekiyo, T.; Zhang, J.; Liu, Q.; Liu, C.-C.; Zhang, L.; Bu, G., Heparan sulphate proteoglycan and the low-density lipoprotein receptor-related protein 1 constitute major pathways for neuronal amyloid-beta uptake. *The Journal of neuroscience : the official journal of the Society for Neuroscience* **2011**, *31* (5), 1644-1651.
434. Holmes, B. B.; DeVos, S. L.; Kfoury, N.; Li, M.; Jacks, R.; Yanamandra, K.; Ouidja, M. O.; Brodsky, F. M.; Marasa, J.; Bagchi, D. P.; Kotzbauer, P. T.; Miller, T. M.; Papy-Garcia, D.; Diamond, M. I., Heparan sulfate proteoglycans mediate internalization and propagation of specific proteopathic seeds. *Proceedings of the National Academy of Sciences of the United States of America* **2013**, *110* (33), E3138-E3147.
435. Hendriks, J.; Planelles, L.; de Jong-Odding, J.; Hardenberg, G.; Pals, S. T.; Hahne, M.; Spaargaren, M.; Medema, J. P., Heparan sulfate proteoglycan binding promotes APRIL-induced tumor cell proliferation. *Cell Death And Differentiation* **2005**, *12*, 637.

VITA

Shayak Samaddar, Ph.D. Candidate

West Lafayette, Indiana

Highly motivated bioanalytical chemist with research focused on formulations development of oligonucleotides and small molecules drugs for bladder cancer immunotherapy. Experienced in *in vitro* and *in vivo* characterization of developed formulations using diverse set of analytical techniques and bioassays. Managed multiple interdisciplinary projects as a part of cross-functional teams with industry and academia, while achieving goals on time.

Technical skills

- **Bio-analytical:** HPLC (Agilent 1100, 1200), MALDI TOF MS (Sciex 4800), Size-exclusion chromatography, Dynamic Light Scattering (Zetasizer Nano ZS, DynaPro II), UV/Vis/Fluorescence spectroscopy (Synergy Neo, SpectraMax M5, DTX 880) Transmission Electron Microscopy (Tecnai T20), Small Angle X-ray Scattering (SAXSpoint 2.0), Differential Scanning Calorimetry (DSC4000), High content imaging (Perkin Elmer Opera Phoenix), Confocal microscopy (Nikon A1R MP), Flow Cytometry (Beckman Coulter FC500, BD LSRFortessa), Animal imager (Spectral Ami, IVIS), Ultrasound imaging (Vevo3100)
- **Molecular Biology:** Protein quantification (BCA, Lowry and Bradford methods), ELISA, Western blot analysis, Agarose gel electrophoresis, SDS-PAGE, DNA and RNA isolation, qPCR, RT-PCR, ChIP-qPCR, Cellular assays (MTS, LDH, Migration, Tube formation)

Work experiences

Purdue University – West Lafayette, IN

PhD Candidate, Dept. of Chemistry

Oct 2014 – Present

Development of lipid-based formulations for delivery of oligonucleotides

- Formulated and optimized of peptide targeted lipid nanoparticles (LNPs) using Labtrix® Start flow reactor system for bladder cancer immunotherapy
- Characterized for size, shape, structural morphology and encapsulation of LNPs
- Evaluated immunostimulatory effect of LNPs *in vitro* in cell culture models and demonstrated its ability to suppress bladder tumors *in vivo* using a murine orthotopic bladder cancer model

Evaluation of polycarbonate pendant polymer: β -cyclodextrin based nucleic acid delivery vectors

- Developed strategies to formulate and optimized polymer-nucleic acid complex
- Characterized size, polydispersity, zeta potential, encapsulation, cytotoxicity and gene delivery efficiency of polymer library *in vitro*
- Analyzed structure-function relationship of pendant groups on complex formation and biological performance

Evaluation of polyrotaxanes as drug delivery vehicles for treatment of a rare metabolic disorder

- Evaluated toxicity profile, structure-function relationships, dose-response relationships of synthesized polyrotaxane library in primary cell culture models of Niemann-Pick Disease type C
- Studied cellular uptake and intracellular biodegradability of candidate polyrotaxane

University of Missouri - Kansas City, MO

Graduate researcher, Dept. of Pharmaceutical Sciences **Sept 2013 – May 2014**

Screening and characterization of novel Hypoxia Inducible Factor (HIF) inhibitors

- Studied and demonstrated relative inhibition of HIF dependent genes, expression of Hypoxia inducible proteins, antiangiogenic effect of inhibitors and DNA protein interactions by various cell-based assays

Harvard Medical School/Dana-Farber Cancer Institute, Boston, MA

Summer Intern, Dept. of Microbiology and Immunobiology **Jun 2013 – Aug 2013**

Formulation of albumin nanoparticle for lymphatic targeted drug delivery

- Developed and characterized albumin nanoparticles for delivery of proprietary kinase inhibitor and demonstrated its cytotoxic effects on multiple cancer cell lines
- Synthesized drug-protein conjugate and labeled them with near IR dye for *in vivo* imaging

Northeastern University, Boston, MA

Graduate Researcher, Dept. of Pharmaceutical Sciences **Jan 2012 - May 2013**

Development of enzyme based polymeric nanosensor for detection of biologically relevant analytes with a smart phone device

- Formulated polymeric nanosensors for quantification of cellular pH and oxygen concentration.

- Established and optimized enzymatic reactions and coupled it with nanosensor platform for fluorometric detection of bioanalytes like glucose, urea, creatinine, dopamine, glutamate and acetylcholine.
- Improved shelf stability of the sensor solution by screening cryoprotectants for lyophilization.

Angel Laboratories Private Limited, Kolkata, India

Analytical Chemist, Quality Control Department

Nov 2010 – May 2011

- Performed quality analysis of incoming raw materials and finished dosage forms
- Ensured process compliance with GMP protocols, record maintenance and inventory management

Education

Purdue University, West Lafayette, IN

PhD Candidate, Dept. of Chemistry

GPA: 3.84/4.00

Aug 2014 – Present

Northeastern University, Boston, MA

Master of Science, Dept. of Pharmaceutical Sciences

GPA: 3.97/4.00

Sept 2011 – May 2013

West Bengal University of Health Sciences, Kolkata, India

Bachelor of Pharmacy, Dept. of Pharmaceutical Sciences

GPA: 3.99/4.00

Sept 2006 – Aug 2010

Leadership skills

Ambassador for Bindley Bioscience Center (BBC)

Jun 2018- Present

- Represented BBC with highest level of scientific integrity and professionalism at scientific engagement events and showcased the cutting-edge technology being offered at core facilities within BBC

Supervisor for Undergraduate Organic Chemistry courses

Jan 2017- May 2018

- Led a team of teaching assistants in courses for over 200 students
- Ensured safety and productive learning experience for each lab sections
- Enforced course policies, headed weekly staff meetings and performed other administrative tasks

Mentor for Undergraduate Researchers

Oct 2016-Present

- Mentored several high-achieving undergraduate students in conducting efficient research and lead them to task completion to attain project goals in time

Honors and awards

- Bindley Bioscience Center Ambassador Travel Award
Purdue University, West Lafayette, IN

Nov 2018

- Best Poster Award
Materials Research Society Spring Meeting, Phoenix, AZ

Apr 2018

- Invited Speaker
Materials Research Society Spring Meeting, Phoenix, AZ

Apr 2018

- Center for Cancer Research Graduate Travel Award
Purdue University, West Lafayette, IN **Jan 2018**
- School of Graduate Studies Fellowship
University of Missouri, Kansas City, MO **Sept 2013**

Publications

- An implantable ultrasonically-powered micro-light-source (μ Light) for photodynamic therapy
A.Kim, J.Zhou, *S.Samaddar*, S.H. Song, D.H. Thompson, B.Ziaie
Nature Scientific Reports, 9 (1), 1395 **Feb 2019**
- Synthesis of the polyrotaxane hydroxypropyl- β -cyclodextrin: poly(decamethylenephosphate)
and evaluation of its cholesterol efflux potential in Niemann-Pick C1 Cells
K.Egele, *S.Samaddar*, N.Baudendistel, D.H.Thompson, G.Wenz
Journal of Materials Chemistry B, **7 (4)**, 528-537 **Dec 2018**
- Organocatalytic synthesis and evaluation of polycarbonate pendant polymer: β -cyclodextrin
based nucleic acid delivery vectors
K.Wright, V.D.Badwaik, *S.Samaddar*, S.H.Hyun, K.Gauninger, T.Eom, D.H.Thompson
Macromolecules, 51(3), 670–678 **Jan 2018**
- A rapid micro-molding process for fabricating polymeric biodegradable 3D structures using
hydrophobic elastomeric molds
J.Zhou, M.Ochoa, *S.Samaddar*, R.Rahimi, V.D.Badwaik, D.H.Thompson, B.Ziaie
IEEE 30th Int. Conference on Micro Electro Mechanical Systems (MEMS) **Feb 2017**
- Fluorescent sensors for the basic metabolic panel enable measurement with a smart phone
device over the physiological range
B. Awqatty, *S.Samaddar*, K. J.Cash, H. A.Clark, J. M.Dubach
Analyst, 139 (20), 5230-5238 **Aug 2014**

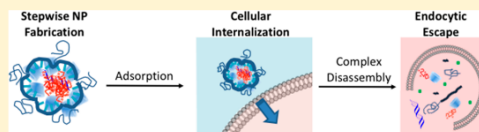
Organocatalytic Synthesis and Evaluation of Polycarbonate Pendant Polymer: β -Cyclodextrin-Based Nucleic Acid Delivery Vectors

Kyle J. Wright, Vivek D. Badwaik, Shayak Samaddar, Seok-Hee Hyun, Kristof Glauning, Taeyoon Eom, and David H. Thompson*

Department of Chemistry, Center for Cancer Research, Multi-disciplinary Cancer Research Facility, Purdue University, 1203 West State Street, West Lafayette, Indiana 47907, United States

Supporting Information

ABSTRACT: A family of mPEG-*b*-polycarbonate (mPEG-PC) diblock pendant polymers were synthesized from trimethylene carbonate and other cyclic carbonate monomers bearing hydrophobic guest ligands via organocatalytic ring-opening polymerization using 1,4,5-triazabicyclo[4.4.0]dec-5-ene catalyst or 1,8-diazabicyclo[5.4.0]undec-7-ene/thiourea cocatalyst. Diblock copolymers composed of a methoxy-poly(ethylene oxide) (mPEG) block and a polycarbonate block containing either homopolymer or mixed polycarbonates (PC) were prepared by homopolymerization or copolymerization of the cyclic carbonate monomers in the presence of mPEG2000 or mPEG5000 initiator to give materials having a tunable pendant group density along the polycarbonate backbone. Polycarbonate blocks targeting the 2.4–10 kDa range were prepared with good molecular weight control and modest polydispersities (averaging ~ 1.3). Complexation of plasmid DNA with β -cyclodextrin–polyethylenimine 2.5 kDa produced nanoparticle cores that were then coated with the mPEG-PC diblock copolymers to produce transfection complexes in the 100–250 nm size range. Stable transfection complexes prepared at N/P ratios >10 had slightly positive ζ potentials and showed comparable or modestly better transfection efficiencies in HeLa cells than the commercial transfection agent, Lipofectamine 2000. Transfection efficiencies were not dependent on polycarbonate block molecular weights. The mPEG-PC constructs displayed similar efficacy for adamantyl and cholesteryl pendants that strongly bind to β -cyclodextrin; however, slightly better performance was observed for the weakly bound pendant, benzyl. These findings suggest that pDNA release is largely mediated by hydrolysis of the ester-bound pendant ligand within the endolysosomal compartment of the cell, with desorption of the mPEG-PC layer also contributing to plasmid release and activation in the case of weak binding pendant groups. We infer from these results that mPEG-PC may be an effective degradable transfection agent for *in vivo* applications.



INTRODUCTION

There has been considerable recent interest in the development of nonviral nanoparticle-based nucleic acid delivery systems.^{1–5} These agents typically load the cargo via coacervation, physical entrapment, or covalent conjugation to alter the pharmacokinetic and pharmacodynamic properties of the nucleic acid agent.^{6–10} Amphiphilic block copolymers have been one of the most extensively studied delivery platforms owing to their synthetic accessibility, modular properties, and the variety of nanoparticle types that can be formulated using these materials.¹¹ These agents are used to effect gene delivery by transferring nucleic acids to knock in, knock out, or repair the genetic composition of target cells. Nonviral gene therapy offers the potential for improved safety, greater flexibility in accommodating large cargo, and more facile and robust design and production strategies relative to viral vectors. Nonviral vectors typically bind their nucleic acid cargo via electrostatic interactions that condense the cargo into particles, protect the cargo from degradation, and mediate cellular entry. Many different material strategies, including cationic lipids and polymers, have been proposed as nonviral gene-delivery vectors.^{6,12–14} A particularly promising class of cationic

polymers that have recently been developed for this application are the biocompatible and degradable polycarbonates (PC) bearing amidine modifications that promote nucleic acid complexation via the arginine fork motif.^{1,15,16}

In recent years, organic catalysis has become an increasingly attractive and powerful alternative for the synthesis of functional amphiphilic copolymers compared to traditional metal-based catalysis.¹⁷ Ring-opening polymerization (ROP) is the most common method for synthesis of well-defined biodegradable block copolymers. Most organocatalysts used in ROP are relatively inexpensive commercially available chemicals, generally easily purified, have long shelf lives, and are well-suited for a range of reaction conditions, solvents and monomers. Traditional metal-based catalysts generally function via the coordination–insertion mechanism as in the case of the polymerization of L-lactide by tin(II) 2-ethylhexanoate. These catalysts have generated concerns related to trace contami-

Received: October 28, 2017

Revised: December 23, 2017

Published: January 17, 2018

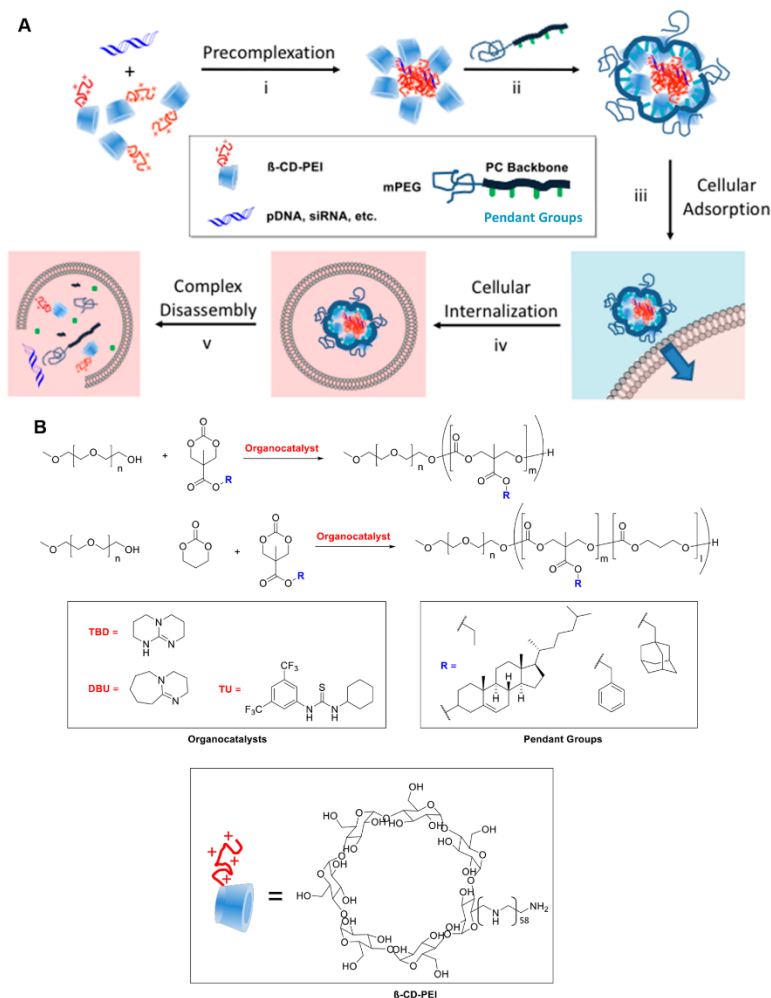


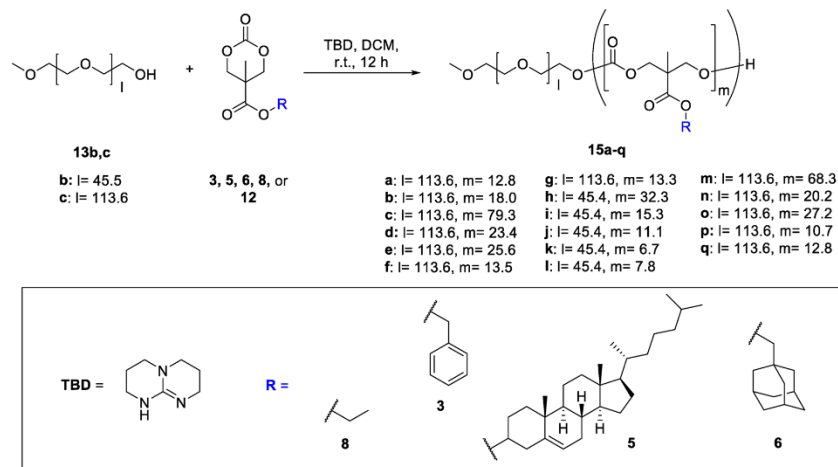
Figure 1. Conceptual diagram for polycarbonate pendant polymer-based nonviral gene delivery. (A) Polyplex formation is accomplished via (i) precomplexation of β -CD-PEI and pDNA. (ii) Polycarbonate diblock copolymers are used to coat the core β -CD-PEI:pDNA complex via host-guest interactions between the pendant groups and the surface-exposed β -CD cavities. (iii) Nanoparticles are targeted to cell surfaces via electrostatic adsorption of the slightly positively charged particles prior to endocytosis (iv). Disassembly of the transfection complexes (v) is promoted by pendant group and polycarbonate block hydrolysis, leading to endolysosomal escape of the pDNA cargo. (B) Diblock copolymer structures derived from (i) homopolymerization of cyclic carbonate monomers or (ii) copolymerization of cyclic carbonate monomers with trimethylene carbonate. The (iii) organocatalysts, (iv) pendant groups, and (v) β -cyclodextrin-poly(ethylenimine) 2.5 kDa conjugate (β -CD-PEI) are also shown.

nation of the polymer with toxic Sn-containing byproducts arising from the ROP catalyst.

Common organocatalysts for ROP include *N*-heterocyclic carbenes, organic “superbase” catalysts,^{18,19} and bifunctional catalysts. Bifunctional thiourea-amine catalysts were first applied to the polymerization of lactide.²⁰ These systems involve simultaneous activation of monomer by the thiourea (a Lewis acid) and the initiator (an alcohol) by the amine component. This strategy was applied to two-component

systems of thiourea and organic base and bifunctional thiourea-amine (TU/A) catalysts.²⁰ The most common superbase catalysts include 1,8-diazabicyclo[5.4.0]undec-7-ene (DBU), 1,4,5-triazabicyclo[4.4.0]dec-5-ene (TBD), 7-methyl-3,5,7-triazabicyclo[4.4.0]dec-5-ene (MTBD), and other phosphazene-based compounds.¹⁷ These catalysts are more active than the TU/A system, display different activities (TBD > MTBD > DBU), and have been applied for the polymerization of many different cyclic monomers.^{15,21} TBD, in particular, has

Scheme 1. Homopolymerization of Cyclic Carbonate Monomers with TBD as Organocatalyst and mPEG as Macroinitiator



been shown to exhibit very high reactivity for monomers with low ring strain or which exhibit low conversion with other catalysts. TBD functions via dual activation of the monomer and initiator in an analogous fashion to the TU/A-based catalysts. Alternatively, TBD has been shown to polymerize L-lactide via an H-bonding mechanism that does not involve acyl transfer.²² Urea anions have also recently been reported as rapid and selective ring-opening polymerization catalysts.²³

Davis and co-workers first reported a family of transfection agents based on cationic β -cyclodextrin (β -CD) main chain oligomers that utilized the β -CD cavity for noncovalent PEGylation via host-guest complexation.²⁹ Kulkarni et al. subsequently introduced a pendant polymer-based nucleic acid delivery system composed of a poly(vinyl alcohol) (PVA) main chain polymer modified with methoxypoly(ethylene oxide) (mPEG) and acid-sensitive cholesteryl benzylidene acetal linkages.^{13,24} This polymer was used in combination with amine-modified β -CD derivatives, wherein the latter were used to condense the nucleic acid cargo and the former served as a consolidating agent that created a passivating layer via host-guest complexation. These materials effectively formed transfection complexes in the 120–170 nm range by engaging multiple host-guest interactions between the cationic β -CD:nucleic acid core via individual host-guest binding affinities in the $10^{0.5}$ – 10^5 M⁻¹ range in water.²⁵ The pendant polymer concept was further applied to microfluidic assembly of transfection complexes composed of siRNA, β -CD-PEI2.5 kDa conjugate (β -CD-PEI), and hyaluronic acid (HA)-modified with adamantyl substituents.²⁶

Although these materials showed good performance, several issues related to the reproducibility of the PVA- and HA-based material syntheses, as well as limitations associated with nonbiodegradable vinylic polymers (e.g., PVA), prompted the design of a new generation of biocompatible pendant polymers that would improve on this concept by utilizing organocatalytic ROP to synthesize a library of well-defined block copolymers. This approach could allow for a more tunable synthesis and enable the incorporation of guest moieties of varying density within a biodegradable platform.

An oligocarbonate-based nonviral gene delivery system described by Hedrick, Waymouth, Wender, and co-workers^{15,16}

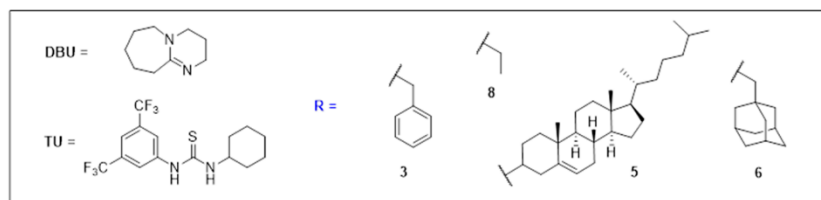
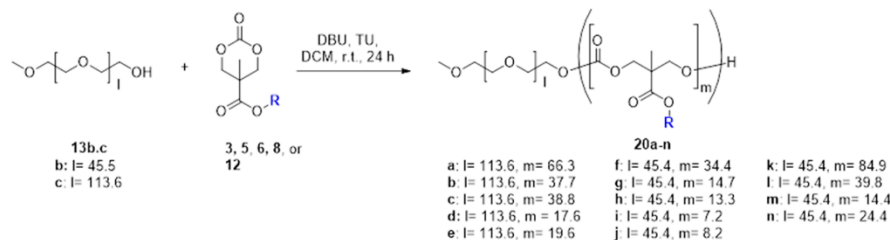
suggested an approach using a novel family of pendant polymers derived from PEG-polycarbonate diblock copolymers (Figure 1). This library of mPEG-*b*-PC diblock copolymers bearing hydrophobic pendant moieties of varying affinity for the β -CD cavity was sought to evaluate the effects of overall molecular weight, relative block length, and pendant group densities along the linear polycarbonate backbone on their transfection performance. TBD and the DBU/thiourea organocatalysts²⁰ were utilized due to their high activities and ability to generate well-defined copolymers with low polydispersity.¹⁸ Polycarbonate diblocks were chosen due to their controlled degradation rates, yielding nonacidic and nontoxic degradation byproducts within the transfected cell. In addition to homopolymerization of cyclic carbonate monomers initiated by mPEG,²⁷ copolymers where the cyclic carbonate monomer is blended with trimethylene carbonate (TMC, 12) are also included in the library to evaluate the effect of pendant group density on nanoparticle formation and efficacy of transfection complexes derived from mPEG-*b*-PC and β -CD-PEI materials.^{15,26} We found that the performance of the materials was highest for pendants having the weakest β -CD association, yielding transfection efficiencies at N:P ≥ 30 that were modestly higher than the commercial agent, Lipofectamine 2000 (L2k), as a benchmark.

EXPERIMENTAL METHODS

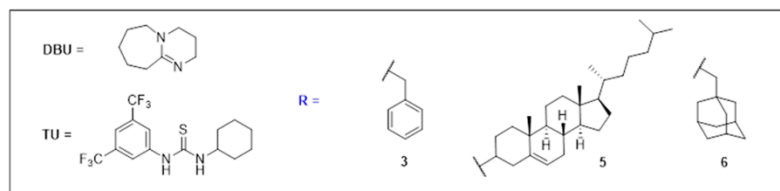
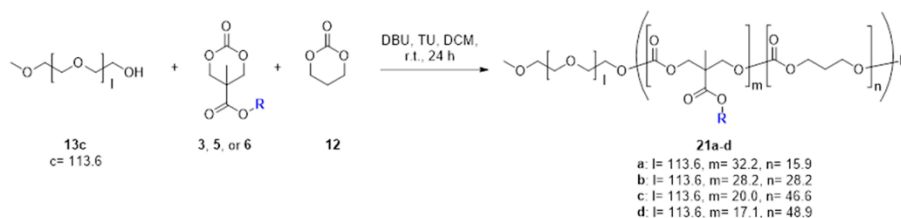
Synthesis of Cyclic Carbonate Monomers. Materials, methods and synthetic procedures for cyclic carbonate monomer synthesis are detailed in the Supporting Information.

TBD-Catalyzed mPEG-*b*-PC Pendant Diblock Copolymers (Scheme 1, 15a–q). mPEG₂₀₀₀ (13b) or mPEG₅₀₀₀ (13c) (100 mg) was added to an oven-dried 5.0 mL conical vial equipped with a magnetic spin vane and PTFE septum. Carbonate monomer (3, 5, 6, 8, or 12) (200 mg) was added, and the contents were dissolved in DCM before addition of a TBD catalyst solution (35 mg/mL in DCM; 5 mol % relative to monomer) to achieve a final monomer concentration of 1.0 M. The vials were flushed with N₂ and stirred for 12 h at 20 °C before isolation of the polymers via precipitation into

Scheme 2. Homopolymerization of Cyclic Carbonate Monomers with DBU/TU as Organocatalysts and mPEG as Macroinitiator (note: 20a, 20f, and 20k Lack the Carboxyester and Methyl Modifications in the Polycarbonate Block)



Scheme 3. Copolymerization of Cyclic Carbonate Monomers with Trimethylene Carbonate (12) Using DBU/TU as Organocatalysts and mPEG as Macroinitiator



40 mL Et₂O/5 mL iPrOH in 50 mL centrifuge tubes. The precipitate was gathered via centrifugation and dried *in vacuo* to give Compounds 15a–q as white solids. M_n was calculated by comparing the PEG methylene proton integrals with integrals from the respective monomer signals. Yield: a, 139 mg; b, 286 mg; c, 256 mg; d, 238 mg; e, 263 mg; f, 242 mg; g, 212 mg; h, 261 mg; i, 176 mg; j, 224 mg; k, 252 mg; l, 197 mg; m, 260 mg; n, 227 mg; o, 240 mg; p, 188 mg; q, 212 mg.

DBU/TU-Catalyzed-mPEG-b-PC Pendant Diblock Polymers (Scheme 2, 20a–n). An oven-dried 5.0 mL conical vial equipped with a magnetic spin vane and PTFE septum was charged with 100 mg of mPEG₂₀₀₀ (13b) or mPEG₅₀₀₀ (13c). Carbonate monomer (200 mg of 3, 5, 6, 8, or 12) was added, and the contents were dissolved in DCM. TU (19) solution (0.125 M in DCM) was added via syringe, followed by DBU solution (1.0 M in DCM). The amounts of DBU, TU, and DCM were determined by targeting 5 mol % DBU and TU

relative to total monomer concentration of 1.0 M. The vials were flushed with N₂ and stirred for 24 h at 20 °C before isolation of the polymers via precipitation into 40 mL Et₂O/5 mL iPrOH in 50 mL centrifuge tubes. The precipitate was gathered via centrifugation and dried *in vacuo* to give Compounds 20a–n as white solids. M_n was calculated by comparing the mPEG methylene proton integrals with integrals from the respective monomer signals. Yield: a, 251 mg; b, 256 mg; c, 263 mg; d, 277 mg; e, 214 mg; f, 278 mg; g, 240 mg; h, 271 mg; i, 267 mg; j, 244 mg; k, 261 mg; l, 284 mg; m, 243 mg; n, 214 mg.

DBU/TU-Catalyzed-mPEG-b-PC Pendant Diblock Copolymers (Scheme 3, 21a–d). mPEG₅₀₀₀ (13c, 150 mg, 0.03 mmol), 12, and 3 were added to an oven-dried 5.0 mL conical vial containing a magnetic spin vane and a PTFE septum. The total mass of monomers was 300 mg. The relative amounts of monomers were determined by targeting a total polycarbonate molecular weight of 10.0 kDa and ratios of 12:3 ranging from 1:2 to 4:1. DCM was added, and the solutions

Table 1. Characterization of mPEG-*b*-PC Diblock Copolymers Generated via Homopolymerization of Cyclic Carbonate Monomers Using TBD as Organocatalyst (12 h, 20 °C)

entry	R	macroinitiator	TBD (mol %)	<i>m</i> (targeted)	<i>m</i> (NMR)	% conv	PC- <i>M_n</i> , kDa (NMR)	<i>M_n</i> , kDa (GPC)	<i>M_w</i> / <i>M_n</i> (GPC)	yield (%)
1Sa	Et	mPEG ₅₀₀₀	10	53.1	12.8	24.1	2.4	12.0	1.86	46.2
1Sb	Chol	mPEG ₅₀₀₀	10	18.9	18.0	95.2	9.5	20.7	1.21	95.3
1Sc	12	mPEG ₅₀₀₀	10	98.0	79.3	80.9	8.1	11.4	1.45	85.3
1Sd	Et	mPEG ₅₀₀₀	10	53.1	23.4	44.1	4.4	17.1	1.32	79.3
1Se	Bn	mPEG ₅₀₀₀	10	40.0	25.6	64.0	6.4	15.3	1.34	87.7
1Sf	Chol	mPEG ₅₀₀₀	10	19.0	13.5	71.1	7.1	16.2	1.39	80.7
1Sg	Ad	mPEG ₅₀₀₀	10	32.4	14.3	44.1	4.4	12.1	1.28	70.7
1Sh	12	mPEG ₂₀₀₀	10	49.0	32.3	65.9	3.3	8.1	1.28	86.6
1Si	Et	mPEG ₂₀₀₀	10	26.6	15.3	57.5	2.9	7.7	1.20	58.5
1Sj	Bn	mPEG ₂₀₀₀	10	20.0	11.1	55.5	2.8	7.5	1.38	74.5
1Sk	Chol	mPEG ₂₀₀₀	10	9.5	6.7	70.5	3.5	6.4	1.38	84.0
1Sl	Ad	mPEG ₂₀₀₀	10	16.2	7.8	48.1	2.4	5.5	1.26	65.5
1Sm	12	mPEG ₅₀₀₀	5	98.0	68.3	69.7	7.0	14.2	1.26	86.7
1Sn	Et	mPEG ₅₀₀₀	5	53.1	20.2	38.0	3.8	9.6	1.34	75.5
1So	Bn	mPEG ₅₀₀₀	5	40.0	27.2	68.0	6.9	14.6	1.24	80.0
1Sp	Chol	mPEG ₅₀₀₀	5	18.9	10.7	56.6	5.7	12.9	1.28	62.7
1Sq	Ad	mPEG ₅₀₀₀	5	32.4	12.8	39.5	4.0	15.8	1.36	70.7

were stirred to dissolve the precursors. A TU solution (0.125 M in DCM) was added via syringe, followed by DBU solution (1.0 M in DCM) such that the amounts of DBU and TU gave 5 mol % DBU and TU relative to the total monomer concentration of 1.0 M. The vials were flushed with N₂ and stirred at 20 °C for 24 h before isolation of the polymers via precipitation into 40 mL Et₂O/5 mL iPrOH in 50 mL centrifuge tubes. The precipitate was gathered via centrifugation and dried *in vacuo* to give compounds 21a–d as white solids. *M_n* was calculated by comparing the mPEG methylene proton integrals with integrals from the respective monomers. Yield: a, 418 mg; b, 417 mg; c, 411 mg; d, 373 mg.

Plasmid DNA-Pendant Polymer Transfection Complex Formation. Transfection complexes were formed in a two-step manner by first adding an appropriate amount of β-CD-polyethylenimine 2.5 kDa (β-CD-PEI)²⁶ to 1 μg of pDNA (unmodified or FITC-labeled) dissolved in 30 μL of TE buffer in 1.5 mL centrifuge tubes to achieve the desired N/P ratio. mPEG-*b*-PC pendant polymer solutions (1 mM equivalent of pendant groups) were then vortex-mixed with the preassembled β-CD-PEI:pDNA complexes in water to form mPEG-*b*-PC:β-CD-PEI:pDNA polyplexes. The amount of mPEG-*b*-PC:β-CD-PEI added to pDNA varied from 1 to 3 μL to produce the desired N/P ratios of 5, 10, 20, and 30. These solutions were then incubated at 4 °C for 1 h before use in transfection experiments.

Particle Size and Zeta (ζ) Potential Measurements. The diameters, size distributions, and ζ potentials of the materials were evaluated by dynamic light scattering (DLS) using a Zetasizer Nano S (Malvern Instruments Ltd.) at 20 °C with a scattering angle of 90°. At least 40 measurements were made and averaged for each sample. The particles were diluted to 1 mL with HEPES buffer (20 mM, pH 7.4) prior to analysis.

Gel Shift Assay. The complexation ability of mPEG-*b*-PC:β-CD-PEI with pDNA was determined by low melting point 1% agarose gel electrophoresis. The agarose gels were precast in TBE buffer with GelRed dye at 1:10 000 dilution. mPEG-*b*-PC:β-CD-PEI:pDNA complexes containing 0.2 μg of pDNA at different N/P ratios were loaded onto the gel before addition of loading dye (1:5 dilution) to each well and electrophoresis at a constant voltage of 55 V for 2 h in TBE buffer. The pDNA bands were then visualized under a UV transilluminator at λ = 365 nm.

In Vitro Transfection Assay in HeLa Cells. HeLa cells were cultured in complete DMEM medium with 10% FBS. All cells were incubated at 37 °C, 5% CO₂, and 95% relative humidity at a cell density of 10 000 cells/well in a 96-well plate. After 24 h, the culture media was replaced with Opti-MEM media, with addition of mPEG-*b*-PC:β-CD-PEI:pDNA complexes containing 0.1 μg of AcGFP plasmid,

at N/P ratios of 10, 20, 30, and 60. The cells were incubated with the complexes for 24 h, after which the spent media was aspirated. Then, the cells were washed 3X with PBS, trypsinized, and analyzed by flow cytometry using a FC500 flow cytometer. The %GFP mean fluorescence intensity was calculated relative to L2k controls, considered as 100%. All treatment conditions were performed at *n* = 4.

RESULTS AND DISCUSSION

Diblock Copolymer Synthesis and Characterization.

In order to generate a library of mPEG-*b*-PC pendant polymers, a set of cyclic carbonate monomers bearing ethyl, benzyl, cholesteryl, and adamantyl esters were synthesized following a modified method that was previously reported for the synthesis of cyclic carbonates (Scheme S1).²⁷ These pendant groups were chosen because they display a broad range of β-CD affinities. Trimethylene carbonate (12) was synthesized as a spacing monomer in order to vary the pendant group density along the polycarbonate block (Scheme S2).

Initial polymerization studies focused on the synthesis of mPEG-*b*-PTMC via TBD-catalyzed ROP of 12 initiated by either mPEG₂₀₀₀ or mPEG₅₀₀₀ (Scheme S3). A molecular weight of 12.0 kDa was targeted for the polycarbonate blocks of the three diblock copolymers 14a–c. Polymerizations were carried out under N₂ at 1.0 M initial 12 concentration in DCM with 5 mol % TBD as catalyst. Polymerizations were quenched after 12 h with benzoic acid and purified via precipitation into diethyl ether. Compounds 14a–c were characterized via ¹H NMR and GPC (Table S1). *M_n* was determined based on ¹H NMR and GPC, while the percent conversion was determined from the ¹H NMR derived *M_n*. Overall, conversions were high, ranging from 94.8% to 97.5%, suggesting a near-complete conversion of monomer in all cases under these conditions. ¹H NMR was used to calculate the *M_n* via comparison of the mPEG protons with the average from protons associated with the polycarbonate block (Figure S1). *M_n* calculated from ¹H NMR all fell just below 12.0 kDa, whereas the average *M_n* calculated from GPC of the diblock copolymers in THF were consistently higher. *M_w*/*M_n* determined from GPC ranged between 1.19 and 1.23, suggesting that the diblock copolymers are relatively monodisperse.

Next, efforts were made to generate a small library of pendant mPEG-*b*-PC homopolymers using ROP of 3, 5, 6, 8,

Table 1. Characterization of mPEG-*b*-PC Diblock Copolymers Generated via Homopolymerization of Cyclic Carbonate Monomers Using TBD as Organocatalyst (12 h, 20 °C)

entry	R	macroinitiator	TBD (mol %)	<i>m</i> (targeted)	<i>m</i> (NMR)	% conv	PC- <i>M_n</i> , kDa (NMR)	<i>M_n</i> , kDa (GPC)	<i>M_w</i> / <i>M_n</i> (GPC)	yield (%)
1Sa	Et	mPEG ₅₀₀₀	10	53.1	12.8	24.1	2.4	12.0	1.86	46.2
1Sb	Chol	mPEG ₅₀₀₀	10	18.9	18.0	95.2	9.5	20.7	1.21	95.3
1Sc	12	mPEG ₅₀₀₀	10	98.0	79.3	80.9	8.1	11.4	1.45	85.3
1Sd	Et	mPEG ₅₀₀₀	10	53.1	23.4	44.1	4.4	17.1	1.32	79.3
1Se	Bn	mPEG ₅₀₀₀	10	40.0	25.6	64.0	6.4	15.3	1.34	87.7
1Sf	Chol	mPEG ₅₀₀₀	10	19.0	13.5	71.1	7.1	16.2	1.39	80.7
1Sg	Ad	mPEG ₅₀₀₀	10	32.4	14.3	44.1	4.4	12.1	1.28	70.7
1Sh	12	mPEG ₂₀₀₀	10	49.0	32.3	65.9	3.3	8.1	1.28	86.6
1Si	Et	mPEG ₂₀₀₀	10	26.6	15.3	57.5	2.9	7.7	1.20	58.5
1Sj	Bn	mPEG ₂₀₀₀	10	20.0	11.1	55.5	2.8	7.5	1.38	74.5
1Sk	Chol	mPEG ₂₀₀₀	10	9.5	6.7	70.5	3.5	6.4	1.38	84.0
1Sl	Ad	mPEG ₂₀₀₀	10	16.2	7.8	48.1	2.4	5.5	1.26	65.5
1Sm	12	mPEG ₅₀₀₀	5	98.0	68.3	69.7	7.0	14.2	1.26	86.7
1Sn	Et	mPEG ₅₀₀₀	5	53.1	20.2	38.0	3.8	9.6	1.34	75.5
1So	Bn	mPEG ₅₀₀₀	5	40.0	27.2	68.0	6.9	14.6	1.24	80.0
1Sp	Chol	mPEG ₅₀₀₀	5	18.9	10.7	56.6	5.7	12.9	1.28	62.7
1Sq	Ad	mPEG ₅₀₀₀	5	32.4	12.8	39.5	4.0	15.8	1.36	70.7

were stirred to dissolve the precursors. A TU solution (0.125 M in DCM) was added via syringe, followed by DBU solution (1.0 M in DCM) such that the amounts of DBU and TU gave 5 mol % DBU and TU relative to the total monomer concentration of 1.0 M. The vials were flushed with N₂ and stirred at 20 °C for 24 h before isolation of the polymers via precipitation into 40 mL Et₂O/5 mL iPrOH in 50 mL centrifuge tubes. The precipitate was gathered via centrifugation and dried *in vacuo* to give compounds **21a–d** as white solids. *M_n* was calculated by comparing the mPEG methylene proton integrals with integrals from the respective monomers. Yield: a, 418 mg; b, 417 mg; c, 411 mg; d, 373 mg.

Plasmid DNA-Pendant Polymer Transfection Complex Formation. Transfection complexes were formed in a two-step manner by first adding an appropriate amount of β-CD-polyethylenimine 2.5 kDa (β-CD-PEI)²⁶ to 1 μg of pDNA (unmodified or FITC-labeled) dissolved in 30 μL of TE buffer in 1.5 mL centrifuge tubes to achieve the desired N/P ratio. mPEG-*b*-PC pendant polymer solutions (1 mM equivalent of pendant groups) were then vortex-mixed with the preassembled β-CD-PEI:pDNA complexes in water to form mPEG-*b*-PC:β-CD-PEI:pDNA polyplexes. The amount of mPEG-*b*-PC:β-CD-PEI added to pDNA varied from 1 to 3 μL to produce the desired N/P ratios of 5, 10, 20, and 30. These solutions were then incubated at 4 °C for 1 h before use in transfection experiments.

Particle Size and Zeta (ζ) Potential Measurements. The diameters, size distributions, and ζ potentials of the materials were evaluated by dynamic light scattering (DLS) using a Zetasizer Nano S (Malvern Instruments Ltd.) at 20 °C with a scattering angle of 90°. At least 40 measurements were made and averaged for each sample. The particles were diluted to 1 mL with HEPES buffer (20 mM, pH 7.4) prior to analysis.

Gel Shift Assay. The complexation ability of mPEG-*b*-PC:β-CD-PEI with pDNA was determined by low melting point 1% agarose gel electrophoresis. The agarose gels were precast in TBE buffer with GelRed dye at 1:10 000 dilution. mPEG-*b*-PC:β-CD-PEI:pDNA complexes containing 0.2 μg of pDNA at different N/P ratios were loaded onto the gel before addition of loading dye (1:5 dilution) to each well and electrophoresis at a constant voltage of 55 V for 2 h in TBE buffer. The pDNA bands were then visualized under a UV transilluminator at λ = 365 nm.

In Vitro Transfection Assay in HeLa Cells. HeLa cells were cultured in complete DMEM medium with 10% FBS. All cells were incubated at 37 °C, 5% CO₂, and 95% relative humidity at a cell density of 10 000 cells/well in a 96-well plate. After 24 h, the culture media was replaced with Opti-MEM media, with addition of mPEG-*b*-PC:β-CD-PEI:pDNA complexes containing 0.1 μg of AcGFP plasmid,

at N/P ratios of 10, 20, 30, and 60. The cells were incubated with the complexes for 24 h, after which the spent media was aspirated. Then, the cells were washed 3X with PBS, trypsinized, and analyzed by flow cytometry using a FC500 flow cytometer. The %GFP mean fluorescence intensity was calculated relative to L2k controls, considered as 100%. All treatment conditions were performed at *n* = 4.

RESULTS AND DISCUSSION

Diblock Copolymer Synthesis and Characterization.

In order to generate a library of mPEG-*b*-PC pendant polymers, a set of cyclic carbonate monomers bearing ethyl, benzyl, cholesteryl, and adamantyl esters were synthesized following a modified method that was previously reported for the synthesis of cyclic carbonates (Scheme S1).²⁷ These pendant groups were chosen because they display a broad range of β-CD affinities. Trimethylene carbonate (**12**) was synthesized as a spacing monomer in order to vary the pendant group density along the polycarbonate block (Scheme S2).

Initial polymerization studies focused on the synthesis of mPEG-*b*-PTMC via TBD-catalyzed ROP of **12** initiated by either mPEG₂₀₀₀ or mPEG₅₀₀₀ (Scheme S3). A molecular weight of 12.0 kDa was targeted for the polycarbonate blocks of the three diblock copolymers **14a–c**. Polymerizations were carried out under N₂ at 1.0 M initial **12** concentration in DCM with 5 mol % TBD as catalyst. Polymerizations were quenched after 12 h with benzoic acid and purified via precipitation into diethyl ether. Compounds **14a–c** were characterized via ¹H NMR and GPC (Table S1). *M_n* was determined based on ¹H NMR and GPC, while the percent conversion was determined from the ¹H NMR derived *M_n*. Overall, conversions were high, ranging from 94.8% to 97.5%, suggesting a near-complete conversion of monomer in all cases under these conditions. ¹H NMR was used to calculate the *M_n* via comparison of the mPEG protons with the average from protons associated with the polycarbonate block (Figure S1). *M_n* calculated from ¹H NMR all fell just below 12.0 kDa, whereas the average *M_n* calculated from GPC of the diblock copolymers in THF were consistently higher. *M_w*/*M_n* determined from GPC ranged between 1.19 and 1.23, suggesting that the diblock copolymers are relatively monodisperse.

Next, efforts were made to generate a small library of pendant mPEG-*b*-PC homopolymers using ROP of **3**, **5**, **6**, **8**,

Table 3. Characterization of mPEG-*b*-PC Diblock Copolymers Generated via Copolymerization of Cyclic Carbonate Monomers with Trimethylene Carbonate Using DBU/TU as Organocatalysts (24 h, 20 °C)

entry	R	macroinitiator	TDB (mol %)	m:n (feed ratio)		m:n (NMR)		% conv	PC- M_w kDa (NMR)	M_w kDa (GPC)	M_w/M_n (GPC)	yield (%)
				m	n	m	n					
21a	12 : 1b n	mPEG ₅₀₀₀	10	2	1	32.2	15.9	96.6	9.7	16.2	1.22	92.9
21b	12 : 1b n	mPEG ₅₀₀₀	10	1	1	28.2	28.2	99.3	10.0	15.6	1.14	92.7
21c	12 : 1b n	mPEG ₅₀₀₀	10	1	2	20.0	46.6	99.1	9.7	15.9	1.20	91.3
21d	12 : 1b n	mPEG ₅₀₀₀	10	1	4	17.1	48.9	86.9	9.3	14.8	1.18	82.9

ization of cyclic carbonate monomers when using the DBU/TU cocatalyst system. In contrast, the low % conversion and high polydispersity of diblock copolymers generated using TBD catalyst may be due to side reactions associated with extended reaction times and possible transesterification of the pendant ester moieties, although no evidence of this was observed via ¹³C NMR.

Having obtained positive results for homopolymerization of carbonate monomers using the DBU/TU system, we synthesized a small library of diblock copolymers where the polycarbonate block consisted of the pendant carbonate monomers blended with **12**. The purpose of these materials was to evaluate the effect of pendant group density along the linear polycarbonate backbone on transfection performance (Scheme 3). Since the monomers are expected to show similar activities toward ROP using DBU/TU, relatively homogeneous distributions of pendant moieties in the resultant polymer were expected. If one monomer has increased reactivity, it would be expected to be present in greater proportion toward the beginning of the polycarbonate block. Copolymerizations were carried out under N₂ using 10 mol % DBU/TU in DCM and a total initial monomer concentration of 1.0 M. Reactions were allowed to proceed for 24 h before work-up. Total polycarbonate molecular weights of 10.0 kDa were targeted with various ratios of **3**:**12** (2:1, 1:1, 1:2, and 1:4) using **13c** as initiator (Table 3). ¹H NMR indicated high % conversion of monomers and good control of monomer incorporation ratios via control of monomer feed ratios. M_n calculated from ¹H NMR and GPC were in reasonable agreement. M_w/M_n as determined from GPC measurements ranged from 1.14 to 1.22, indicating the formation of relatively monodisperse copolymer.

Transfection Complex Formation. Next, select members of the homopolymer library generated via TBD-catalyzed ROP were tested for their abilities to effectively form nanoparticulate transfection complexes upon bulk mixing with β -CD-PEI^{13,26} and pDNA. β -CD-PEI and pDNA were precomplexed before addition of the diblock copolymer, yielding a layer-by-layer type of transfection complex that is stabilized by multiple host:guest interactions between the pendant groups in the polycarbonate block with the cavities of the β -CD units in a manner described by Thompson and co-workers.^{13,24}

Next, a gel retardation assay was performed to determine the ability of the mPEG-*b*-PC: β -CD-PEI-based materials to condense pDNA at various N/P ratios (Figure 2). Higher molecular weight diblock copolymers (e.g., **15e–g**) required N/P ratios >20 to effectively condense pDNA, whereas lower molecular weight diblock copolymers (e.g., **15j–l**) effectively condensed pDNA at N/P = 5, likely due to lower entanglement/steric interference of the mPEG block during the initiation of host:guest interactions between the β -CD-rich core and the polycarbonate pendant groups.

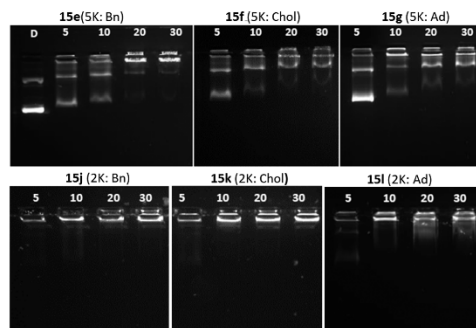


Figure 2. Gel shift analysis of transfection complexes at various N/P ratios.

Dynamic light scattering (DLS) was used to determine size and polydispersity of the transfection complexes generated using **15e–g** and **15j–l** (Figure 3). These complexes ranged

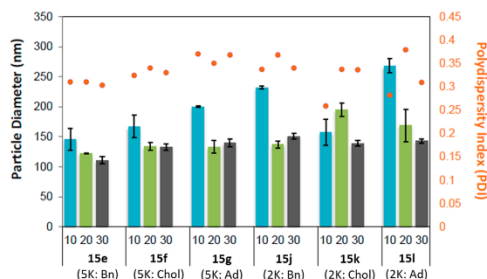


Figure 3. Size analysis of transfection complexes at various N/P ratios by DLS.

between 100 and 250 nm in diameter, a size regime that is capable of cellular internalization.²⁸ Transfection complexes formed from lower molecular weight diblock copolymers showed relatively larger sizes compared to those of higher molecular weight polymers at N/P = 10; however, they were of comparable size and polydispersity at N/P \geq 20. There was no apparent correlation observed between particle size or polydispersity and pendant group identity.

Zeta potential (ζ) analysis of transfection complexes formed by **15e–f** and **15j–l** revealed values in the range of +5–10 mV (Figure 4). These modestly positive ζ are generally preferred in order to promote internalization via electrostatic interaction of the positively charged nanoparticle surface with the negatively

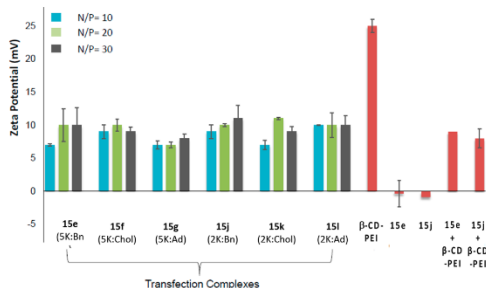


Figure 4. ζ analysis of transfection complexes at various N/P ratios.

charged cellular surface. Transfection complexes formed at N/P = 10, 20, and 30 resulted in particles with similar ζ . β -CD-PEI alone exhibited an elevated ζ = +24 mV. Copolymers 15e and 15j both exhibited a neutral ζ in solution, whereas mixtures of these copolymers with β -CD-PEI resulted in positive ζ that were lower in magnitude than β -CD-PEI. We infer from these findings that the diblock copolymers effectively screen the positive charge of β -CD-PEI both in the host:guest complex form and in the final transfection complex. Furthermore, since the β -CD-PEI:diblock copolymer complexes showed ζ similar to the transfection complexes, we conclude that the plasmid is likely not surface exposed and, thus, is likely to be protected from nuclease degradation.

Transfection Complex Performance. Transfection complexes prepared from mPEG-*b*-PC 15e, 15f, 15j, or 15l were evaluated for their transfection efficiencies in HeLa cells (Figure 5). Transfection complexes composed of benzyl-modified materials showed similar efficiency relative to L2k as benchmark (Figure 5A). Block copolymer molecular weight also seemed to have little impact on transfection efficiency, although higher N/P tended to give higher transfection efficiencies. We attribute these findings to acid-catalyzed ester hydrolysis of the pendant group and subsequent disassembly of the complex within the acidic endolysosomal compartment after internalization, yielding a plasmid complex of similar bioavailability regardless of the initial pendant group type. The modest boost in transfection performance for the benzyl derivatives is attributed to pendant exchange between the endosomal membrane and the weaker host:guest interactions of these species with the β -CD-PEI:pDNA core. When transfection efficiency is evaluated in terms of % mean fluorescence (Figure 5B), similar trends were apparent, with no clear correlation between transfection efficiency and polymer molecular weight or pendant group.

CONCLUSIONS

The pendant polymer-based gene delivery concept has shown significant potential as a novel nonviral gene delivery strategy. We sought to address material-specific limitations of previously reported pendant polymer materials by using organocatalytic ROP to develop a more well-defined new generation of degradable pendant diblock copolymers. A family of mPEG-*b*-PC pendant polymers was successfully synthesized from several novel and previously reported cyclic carbonate monomers via organocatalytic ROP using either TBD or the DBU/TU cocatalyst system. Several copolymerizations of the cyclic carbonate monomers were performed to generate materials

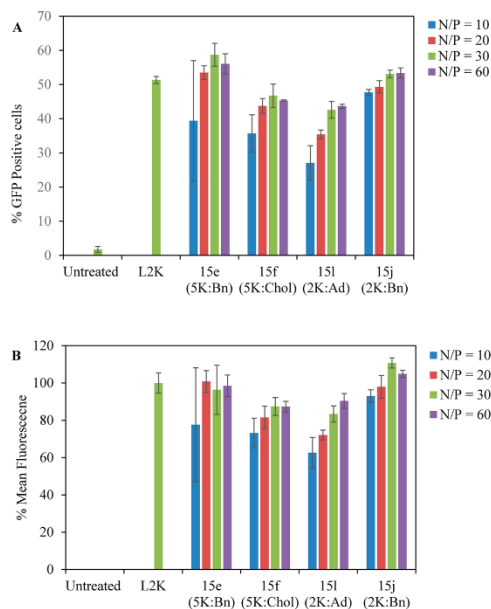


Figure 5. Transfection performance of mPEG-*b*-PC-coated polyplexes. (A) % GFP positive HeLa cells treated with transfection complexes containing AcGFP pDNA. (B) % mean fluorescence of HeLa cells treated with transfection complexes containing AcGFP pDNA.

having tunable pendant group density along the polymer backbone and polydispersities of \sim 1.3. These diblock copolymers formed nanoparticles in the 100–250 nm size range, with slightly positive ζ , when compared with β -CD-PEI and β -CD-PEI:pDNA complexes at N/P ratios >10. The favorable transfection performance of these complexes relative to Lipofectamine 2000 suggests that these materials may be useful agents for *in vivo* gene delivery applications.

ASSOCIATED CONTENT

Supporting Information

The Supporting Information is available free of charge on the ACS Publications website at DOI: 10.1021/acs.macromol.7b02293.

Descriptions of the materials, experimental methods, and NMR spectra (PDF)

AUTHOR INFORMATION

Corresponding Author

*E-mail davethom@purdue.edu (D.H.T.).

ORCID

David H. Thompson: 0000-0002-0746-1526

Author Contributions

The manuscript was written with contributions from all authors, who have given approval to the final version of the manuscript. K.J.W. synthesized and characterized all of the compounds and wrote the manuscript. K.G. and T.E. performed monomer syntheses. S.H. performed GPC analyses. V.D.B. and S.S. formulated the transfection complexes and

evaluated their *in vitro* performance. D.H.T. contributed project conception, oversight, manuscript writing, and editing.

Notes

The authors declare no competing financial interest.

ACKNOWLEDGMENTS

Support from the Purdue University Center for Cancer Research (P30 CA023168) for the Purdue NMR, Mass Spectrometry, and Flow Cytometry Shared Resources is gratefully acknowledged. Support from the Department of Chemistry is also appreciated.

REFERENCES

- Pack, D. W.; Hoffman, A. S.; Pun, S.; Stayton, P. S. Design and Development of Polymers for Gene Delivery. *Nat. Rev. Drug Discovery* **2005**, *4*, 581–593.
- Cheng, Y.; Yumul, R. C.; Pun, S. H. Virus-inspired Polymer for Efficient In Vitro and In Vivo Gene Delivery. *Angew. Chem., Int. Ed.* **2016**, *55*, 12013–12017.
- Dahlman, J. E.; Barnes, C.; Khan, O. F.; Thiriot, A.; Jhunjhunwala, S.; Shaw, T. E.; Xing, Y. P.; Sager, H. B.; Sahay, G.; Speciner, L.; Bader, A.; Bogorad, R. L.; Yin, H.; Racie, T.; Dong, Y. Z.; Jiang, S.; Seedorf, D.; Dave, A.; Sandhu, K. S.; Webber, M. J.; Novobrantseva, T.; Ruda, V. M.; Lytton-Jean, A. K. R.; Levins, C. G.; Kalish, B.; Mudge, D. K.; Perez, M.; Abezgauz, L.; Dutta, P.; Smith, L.; Charisse, K.; Kieran, M. W.; Fitzgerald, K.; Nahrendorf, M.; Danino, D.; Tuder, R. M.; von Andrian, U. H.; Aking, A.; Panigrahy, D.; Schroeder, A.; Kotliansky, V.; Langer, R.; Anderson, D. G. In Vivo Endothelial siRNA Delivery Using Polymeric Nanoparticles with Low Molecular Weight. *Nat. Nanotechnol.* **2014**, *9*, 648–655.
- McKinlay, C. J.; Vargas, J. R.; Blake, T. R.; Hardy, J. W.; Kanada, M.; Contag, C. H.; Wender, P. A.; Waymouth, R. M. Charge-altering Releasable Transporters (CARTs) for the Delivery and Release of mRNA in Living Animals. *Proc. Natl. Acad. Sci. U. S. A.* **2017**, *114*, E448–E456.
- Deng, Z. J.; Morton, S. W.; Ben-Akiva, E.; Dreaden, E. C.; Shopowitz, K. E.; Hammond, P. T. Layer-by-layer Nanoparticles for Systemic Co-delivery of an Anticancer Drug and siRNA for Potential Triple Negative Breast Cancer Treatment. *ACS Nano* **2013**, *7*, 9571–9584.
- de Jesus, M. B.; Zuhorn, I. S. Solid Lipid Nanoparticles as Nucleic Acid Delivery System: Properties and Molecular Mechanisms. *J. Controlled Release* **2015**, *201*, 1–13.
- Rinkenauer, A. C.; Schubert, S.; Traeger, A.; Schubert, U. S. The Influence of Polymer Architecture on In Vitro pDNA Transfection. *J. Mater. Chem. B* **2015**, *3*, 7477–7493.
- Ozpolat, B.; Sood, A. K.; Lopez-Berstein, G. Liposomal siRNA Nanocarriers for Cancer Therapy. *Adv. Drug Delivery Rev.* **2014**, *66*, 110–116.
- Ooya, T.; Choi, H.-S.; Yamashita, A.; Yui, N.; Sugaya, Y.; Kano, A.; Maruyama, A.; Akita, H.; Ito, R.; Kogure, K.; Harashima, H. Biocleavable Polyrotaxane-Plasmid DNA Polyplex for Enhanced Gene Delivery. *J. Am. Chem. Soc.* **2006**, *128*, 3852–3853.
- Badwaik, V. D.; Aicart, E.; Mondjinou, Y. A.; Johnson, M. A.; Bowman, V. D.; Thompson, D. H. Structure-Property Relationship for siRNA Delivery Performance of Cationic 2-Hydroxypropyl-cyclodextrin: Poly(ethylene glycol)-Poly(propylene glycol)-Poly(ethylene glycol) Polyrotaxane Vectors. *Biomaterials* **2016**, *84*, 86–98.
- Xiong, X.-B.; Binkhathlan, Z.; Molavi, O.; Lavasanifar, A. Amphiphilic Block Copolymers: Preparation and Application in Nanodrug and Gene Delivery. *Acta Biomater.* **2012**, *8*, 2017–2033.
- Kozielski, K. L.; Green, J. J. Bioreducible Poly(beta-amino ester)s for Intracellular Delivery of siRNA. *Methods Mol. Biol.* **2016**, *1364*, 79–87.
- Kulkarni, A.; DeFrees, K.; Hyun, S.-H.; Thompson, D. H. Pendant Polymer: Amino- β -cyclodextrin Guest:Host Nanoparticles as Efficient Vectors for Gene Silencing. *J. Am. Chem. Soc.* **2012**, *134*, 7596–7599.
- Mendes, L. P.; Pan, J. Y.; Torchilin, V. P. Dendrimers as Nanocarriers for Nucleic Acid and Drug Delivery in Cancer Therapy. *Molecules* **2017**, *22*, 1401.
- Cooley, C. B.; Trantow, B. M.; Nederberg, F.; Kiesewetter, M. K.; Hedrick, J. L.; Waymouth, R. M.; Wender, P. A. Oligocarbonate Molecular Transporters: Oligomerization-based Syntheses and Cell Penetrating Studies. *J. Am. Chem. Soc.* **2009**, *131*, 16401–16403.
- Geihe, E. L.; Cooley, C. B.; Simon, J. R.; Kiesewetter, M. K.; Edward, J. A.; Hickerson, R. P.; Kaspar, R. L.; Hedrick, J. L.; Waymouth, R. M.; Wender, P. A. Designed Guanidinium-rich Amphipathic Oligocarbonate Molecular Transporters Complex, Deliver and Release siRNA in Cells. *Proc. Natl. Acad. Sci. U. S. A.* **2012**, *109*, 13171–13176.
- Dove, A. P. Organic Catalysts for Ring Opening Polymerization. *ACS Macro Lett.* **2012**, *1*, 1409–1412.
- Lohmeijer, B. G. G.; Pratt, R. C.; Leibfarth, F.; Logan, J. W.; Long, D. A.; Dove, A. P.; Nederberg, F.; Choi, J.; Wade, C.; Waymouth, R. M.; Hedrick, J. L. Guanidine and Amidine Organocatalysts for Ring Opening Polymerization of Cyclic Esters. *Macromolecules* **2006**, *39*, 8574–8583.
- Nederberg, F.; Lohmeijer, B. G. G.; Leibfarth, F.; Pratt, R. C.; Choi, J.; Dove, A. P.; Waymouth, R. M.; Hedrick, J. L. Organocatalytic Ring Opening Polymerization of Trimethylene Carbonate. *Biomacromolecules* **2007**, *8*, 153–160.
- Dove, A. P.; Pratt, R. C.; Lohmeijer, B. G. G.; Waymouth, R. M.; Hedrick, J. L. Thiourea-based Bifunctional Organocatalysis: Supramolecular Recognition for Living Polymerization. *J. Am. Chem. Soc.* **2005**, *127*, 13798–13799.
- Pratt, R. C.; Lohmeijer, B. G. G.; Long, D. A.; Waymouth, R. M.; Hedrick, J. L. Triazabicyclodene: A Simple Bifunctional Organocatalyst for Acyl Transfer and Ring Opening Polymerization of Cyclic Esters. *J. Am. Chem. Soc.* **2006**, *128*, 4556–4557.
- Chuma, A.; Horn, H. W.; Swope, W. C.; Pratt, R. C.; Zhang, L.; Lohmeijer, B. G. G.; Wade, C. G.; Waymouth, R. M.; Hedrick, J. L.; Rice, J. E. The Reaction Mechanism for the Organocatalytic Ring Opening Polymerization of L-Lactide Using a Guanidine-based Catalyst: Hydrogen-bonded or Covalently Bound? *J. Am. Chem. Soc.* **2008**, *130*, 6749–6754.
- Lin, B.; Waymouth, R. M. Urea Anions: Simple, Fast, and Selective Catalysts for Ring Opening Polymerizations. *J. Am. Chem. Soc.* **2017**, *139*, 1645–1652.
- Kulkarni, A.; Badwaik, V.; DeFrees, K.; Schuldt, R. A.; Gunasekera, D. S.; Powers, C.; Vlahu, A.; VerHeul, R.; Thompson, D. H. Effect of Pendant Group on pDNA Delivery by Cationic β -Cyclodextrin-Alkyl-PVA-PEG Pendant Polymer Complexes. *Biomacromolecules* **2014**, *15*, 12–19.
- Rekharsky, M. V.; Inoue, Y. Complexation Thermodynamics of Cyclodextrins. *Chem. Rev.* **1998**, *98*, 1875–1917.
- Kulkarni, A.; VerHeul, R.; DeFrees, K.; Collins, C. J.; Schuldt, R. A.; Vlahu, A.; Thompson, D. H. Microfluidic Assembly of Cationic β -Cyclodextrin:Hyaluronic Acid-Adamantane Host:Guest pDNA Nanoparticles. *Biomater. Sci.* **2013**, *1*, 1029–1033.
- Pratt, R. C.; Nederberg, F.; Waymouth, R. M.; Hedrick, J. L. Tagging Alcohols with Cyclic Carbonate: A Versatile Equivalent of (Meth)acrylate for Ring Opening Polymerization. *Chem. Commun.* **2008**, 114–116.
- Kinnear, C.; Moore, T. L.; Rodriguez-Lorenzo, L.; Rothen-Rutishauser, B.; Petri-Fink, A. Form Follows Function: Nanoparticle Shape and its Implications for Nanomedicine. *Chem. Rev.* **2017**, *117*, 11476–11521.
- Gonzalez, H.; Hwang, S. J.; Davis, M. E. New Class of Polymers for the Delivery of Macromolecular Therapeutics. *Bioconjugate Chem.* **1999**, *10*, 1068–1074.



Cite this: *J. Mater. Chem. B*, 2019, 7, 528

Synthesis of the anionic hydroxypropyl- β -cyclodextrin:poly(decamethylenephosphate) polyrotaxane and evaluation of its cholesterol efflux potential in Niemann–Pick C1 cells†

Kerstin Egele,^a Shayak Samaddar,^b Nina Schneider,^c David Thompson *^b and Gerhard Wenz *^a

Niemann–Pick type C disease (NPC) is a lysosomal storage disease that is characterized by a progressive accumulation of unesterified cholesterol in the lysosomes leading to organ damage from cell dysfunction. Hydroxypropyl- β -cyclodextrin (HP- β -CD) is an attractive drug candidate for treating NPC, as it diminishes cholesterol accumulation in NPC cells. Systemic HP- β -CD treatment, however, is limited by rapid renal clearance. We designed a new anionic HP- β -CD polyrotaxane to act as a slow release formulation based on a polyalkylene phosphate core to improve the pharmacokinetics. The polyalkylene phosphate comprises hydrophobic decamethylene spacers linked by biodegradable anionic phosphodiester bonds. HP- β -CD was threaded onto this polymer first and α -CD afterwards to prevent burst release of the threaded HP- β -CD. Our findings show that HP- β -CD was slowly released from the water soluble polyrotaxane over a 30 days period. The polyrotaxane provided persistently diminished cholesterol levels in NPC1 cells by 20% relative to untreated cells. These results demonstrate the therapeutic potential of this novel HP- β -CD polyrotaxane for the mobilization of aberrantly stored cholesterol in NPC1 cells.

Received 8th November 2018,
Accepted 6th December 2018

DOI: 10.1039/c8tb02950d

rsc.li/materials-b

1. Introduction

Cyclodextrins (CDs) are cyclic oligomers of glucose known to complex hydrophobic or amphiphilic guest molecules in aqueous environments due to hydrophobic interactions.¹ This binding ability has been widely exploited for the solubilization of active pharmaceutical ingredients (APIs) for improvement of their bio-availability and reduction of undesirable side effects.^{2,3} Hydroxypropyl- β -CD (HP- β -CD), a highly water-soluble derivative of β -CD, is already commercially used for several drug formulations, for example for itraconazole (“Sporanox”),⁴ hydrocortisone (“Dexocort”),⁵ and indomethacin (“Indocid”).⁶ Furthermore, HP- β -CD itself can exhibit pharmacological action due to solubilization and transport of cholesterol as well as influencing the lipid rafts of cells.^{7,8} HP- β -CD forms a water-soluble 2:1 complex with cholesterol as demonstrated by solubility measurements,^{9,10} thus offering therapeutic potential for the treatment of lysosomal metabolic disorders such as

Niemann–Pick Type C (NPC),^{11–13} This rare genetic disease (incidence $\sim 1:120\,000$) leads to an accumulation of cholesterol and sphingolipids in the lysosome because of mutations in either the NPC1 or NPC2 proteins. Aberrant accumulation of cholesterol as microcrystalline deposits leads to damage of liver, spleen and brain, causing progressive degeneration of the patient.¹⁴ Administration of HP- β -CD promotes cholesterol normalization within late endosomal/lysosomal compartments to enable its metabolism and excretion.¹⁵ Subcutaneous administration of 4000 mg kg⁻¹ body weight of HP- β -CD 4 days a week produced a 72% reduction of total cholesterol content in the liver of npc^{-/-} mice after treatment for 77 d.¹⁶ Despite this success, the poor pharmacokinetics of HP- β -CD require frequent administrations that are cumbersome and potentially toxic (e.g., lung damage).^{17,18} These side effects can be mitigated by intracisternal administration; however there is still a risk of ototoxicity.^{15,19} Therefore, alternative methods for a safer administration of HP- β -CD are desirable. We report a new material for cyclodextrin delivery based on a water-soluble polyphosphate HP- β -CD polyrotaxane.

In general, polymers are attractive as potential carriers for the controlled delivery of APIs. Polymeric delivery vehicles have been employed to improve both the solubility and bioavailability of drugs to improve their efficacy and/or diminish their toxicity.^{20,21} These vehicles can improve the retention of the

^a Organic Macromolecular Chemistry, Saarland University, Saarbrücken, Germany. E-mail: gerhardwenz@icloud.com

^b Dept. of Chemistry, Purdue University, Lafayette, USA

^c BASF SE, Ludwigshafen, Germany

† Electronic supplementary information (ESI) available: SEC diagram of **1**, synthesis of **7**, Fig. S2 and S3. See DOI: 10.1039/c8tb02950d

drug in the human body due to reduced renal clearance.^{22–24} Targeting is also possible through incorporation of ligands that promote active transport into specific cells *via* receptor-mediated endocytosis.²⁵

Covalent linkage of APIs to degradable polymers produces polymeric pro-drugs that are new molecular entities, thus requiring extensive toxicity and efficacy testing.²⁶ More commonly, a strategy of physically mixing small molecules and polymeric carriers, such as PLGA or modified starch, is employed to produce vehicles with improved delivery characteristics,^{27,28} although burst release of the API due to weak intermolecular interactions is often observed for these formulations.²⁷ Polyrotaxanes, molecules where many macrocyclic rings are strung onto a polymer chain, are interesting alternative carrier entities since they are kinetically less stable than polymeric prodrugs, but by far more stable than physical mixtures due to the topological bond between the threaded rings and the polymeric backbone.^{1,29} The dissociation rate of a polyrotaxane can be controlled by the type of stopper groups attached along the polymer or at the chain ends to allow slow release of the threaded rings.^{1,30}

Polyrotaxanes have been synthesized from various ring shaped molecules, such as crown ethers, cucurbiturils and cyclodextrins.³¹ Among these macrocyclic precursors, cyclodextrins have been the most widely explored since they are produced on an industrial scale, display very low toxicity under physiological conditions, and have been widely used as excipients in FDA-approved small molecule drug formulations.^{4,32} Amphiphilic polymers are suited best for the formation of CD polyrotaxanes since CDs spontaneously thread onto hydrophobic chain segments in water driven by hydrophobic interactions.^{1,33} So far, neutral and cationic polymers like polyethylene glycol,³⁴ polypropylene glycol,^{35,36} poly(oligomethylenimine)s³⁷ and derivatives of them, as well as polyamides³⁸ and polyesters³⁹ have been complexed by CDs to form polyrotaxanes. Among them, the neutral CD polyrotaxanes show very low water solubilities and require further derivatization.¹ Rapid normalization of cholesterol levels in NPC cells⁴⁰ and the mouse model of NPC disease⁴¹ has been reported for polyrotaxanes composed from HP- β -CD (or 2-(2-hydroxyethoxy)ethyl carbamate-modified β -CD) and PEG-PPG-PEG block polymers.^{40–43} Although the PEG backbone provides modest improvements in polyrotaxane solubility, it could potentially contribute to immune responses, liver accumulation, and poor bio-degradability.^{44,45} Cationic CD polyrotaxanes are known to be highly water-soluble; however, these materials are often accompanied by significant toxicity.^{46–48} These potential shortcomings in the development of an effective CD polyrotaxane-based NPC therapy led us to explore the synthesis and performance testing of anionic polyrotaxanes derived from poly(decamethylenephosphate), a nontoxic water-soluble polymer that is degradable by hydrolysis in aqueous media. Polymeric phosphoric acid diesters are synthetic analogs of polynucleotides that are known to be degradable by nucleases to generate non-toxic byproducts.^{49–52} They can be readily prepared by oxidation of polymeric phosphorous acid diesters. The latter are typically prepared by transesterification of diphenyl phosphite with α,ω -diols.⁵⁴ Polymeric phosphodiester have already been used

as prodrugs, hydrogels and drug carriers.^{51,55,56} A pseudopolyrotaxane based on biodegradable polyphosphoester ionomers obtained by ring opening polymerization has been described by Tamura *et al.*⁵³ Polyrotaxane formation was only observed with α and γ -CD and the resulting polyrotaxanes formed precipitates in aqueous solution. No inclusion complexes were obtained with β -CD.

We herein describe for the first time the homogenous assembly of a water-soluble polyrotaxane from HP- β -CD and an anionic polymeric phosphodiester. The resulting HP- β -CD polyrotaxane displays cholesterol normalization activity in NPC cells.

2. Experimental

2.1. General

Hydroxypropyl- β -CD (HP- β -CD) with d.s. = 0.9 per glucose unit and α -CD were obtained from Wacker Chemie (Munich, Germany) and dried at 70 °C for 18 h in vacuum before use. 1,10-Decanediol, diphenylphosphite, fluorescein-isothiocyanate, toluidinylnaphthalene-2-sulfonate, Filipin III, and Triton X-100 were purchased from Sigma Aldrich (Steinheim, Germany). *N*-Chlorosuccinimide (NCS), imidazole, LiCl and solvents were purchased from commercial suppliers. Dichloromethane (DCM) was dried over P₂O₅ and distilled before use. The polyrotaxane products were purified *via* ultrafiltration in a 400 mL ultrafiltration cell from Millipore (Darmstadt, Germany); the 5 kDa regenerate cellulose membrane was obtained from Microdyn-NADIR (Wiesbaden, Germany).

NMR measurements were performed using a Bruker AVANCE Ultrashield 400 (400.2 MHz) instrument (Billerica, Massachusetts, USA).

SEC measurements were performed on a PSS Suprema Lux 30 column equipped with a RI Waters 2410 detector. The flow rate was 1 mL min⁻¹ and calibrations were performed using pullulan standards. The eluent was phosphate buffer, pH 10 with 5 vol% acetonitrile (ACN).

Fluorescence measurements were performed on a Tecan Infinite 2000 microplate reader (Crailsheim, Germany). The data were processed with Tecan i-control software version 3.4.2.0.

2.2. Synthesis

2.2.1. Poly(decamethylenephosphite) 2, 1,10-Decanediol (6.227 g, 26.5 mmol, 1.0 eq.) was added under a N₂ atmosphere to diphenylphosphite (4.619 g, 26.5 mmol, 1.0 eq.) in a vacuum distillation apparatus to remove the phenol byproduct by distillation. The mixture was initially heated over a 1 h period to 100 °C at 30 mbar and stirred 1 h at 100 °C before reducing the pressure to 0.06 mbar and stirring for an additional 1 h. Then, the reaction was heated to 150 °C over a 1 h period and stirred for an additional 1 h before raising the temperature over 1 h to 200 °C and stirring for another 1 h. The reaction was then cooled to 20 °C, giving 5.77 g (26.2 mmol, 99%) of 2 as a white waxy solid. ¹H-NMR: δ /ppm (CDCl₃, 400 MHz) = 6.78 (d, 1H, PH, ¹J_{HP} = 346 Hz), 4.04 (sh, 4H, H-1), 1.70–1.54 (sh, 4H, H-2),

1.29 (sh, 12H, H-3/4/5). ^{13}C -NMR: δ/ppm (CDCl_3 , 100 MHz) = 65.8 (C-1), 30.4 (C-2), 29.4 (C-3), 29.1 (C-4), 25.5 (C-5). ^{31}P -NMR: δ/ppm (CDCl_3 , 100 MHz) = 6.06 ppm.

2.2.2. Poly(decamethylenephosphate) 1. To a solution of **2** (5.144 g, 23.38 mmol, 1.0 eq.) in 200 mL DCM was added *N*-chlorosuccinimide (3.43 g, 25.72 mmol, 1.1 eq.). The mixture was stirred for 5 d at 20 °C to produce the polymeric phosphoryl chloride **3**. Then, a solution of imidazole (3.18 g, 46.08 mmol, 2.0 eq.) in 70 mL DCM was added dropwise over 2 h at 20 °C and the solution stirred overnight at 20 °C to generate the polymeric phosphoryl imidazolide **4**. The reaction mixture was filtered and 500 mL of a 0.05 M Na_2CO_3 solution was added to the filtrate before evaporation of the DCM. The aqueous phase was stirred overnight and then filtered. The clear filtrate was purified by ultrafiltration *via* 5 kDa polyethersulfone membrane against 2 L 0.1 M phosphate buffer containing 0.1 M LiCl and then against 2 L H_2O . After freeze drying, 2.13 g (8.85 mmol, 38%) of white fluffy solid **1** was recovered. ^1H -NMR: δ/ppm (D_2O) = 3.82 (bs, 4H, H-1), 1.62 (bs, 4H, H-2), 1.32 (sh, 12H, H-3/4/5). ^{13}C -NMR: δ/ppm (D_2O) = 66.0 (C-1), 30.3 (C-2), 29.9 (C-3), 29.3 (C-4), 25.7 (C-5). ^{31}P -NMR: δ/ppm (D_2O) = 0.60 ppm.

2.2.3. Polyrotaxane 5. α -CD (11.6 mg, 16 mmol, 1.3 eq.) and **1** (4.1 mg, 12 mmol, 1.0 eq.) were each dissolved in 1 mL D_2O . Aliquots (350 μL) of both solutions were mixed and incubated at 60 °C for 22 d. ^1H -NMR: δ/ppm (D_2O) = 5.06 (s, 0.25H, α -CD threaded), 5.05 (d, 0.75H, free α -CD) 3.99–3.57 (m, 6H, H-1 + α -CD), 1.81–1.23 (sh, 16H, H-3/4/5).

2.2.4. Polyrotaxane 6. 2-HP- β -CD (ds: 0.9, average MW 1500 g mol $^{-1}$; 29.75 g, 198 mmol, 6.0 eq.) and **1** (802 mg, 3.30 mmol, 1.0 eq.) were added stepwise to 100 mL of a 0.05 M NaCl solution to produce a clear solution. The stirred solution was heated to 40 °C for 5.5 h. Then, a solution of α -CD (3.20 g, 3.3 mmol, 1 eq.) in 30 mL H_2O was added and the mixture was stirred at 70 °C for 16 h. To separate unthreaded CD from the polyrotaxane, the solution was purified *via* ultrafiltration using a 5 kDa polyethersulfone membrane against a 0.05 M LiCl solution and H_2O in sequence before freeze drying. A white, fluffy solid (1.278 g) was recovered. ^1H -NMR: δ/ppm (D_2O) = 5.22 (s, 0.6H, HP-CD), 5.08 (s, 0.7H, HP-CD), 5.04 (s, 0.16H, α -CD), 4.12–3.41 (m, 14.3H, H-1 + α -CD + HP-CD), 1.64 (bs, 4H, H-2), 1.35 (sh, 12H, H-3/4/5), 1.16 (s, 2.8H, HP-CD).

2.2.5. FITC tagged polyrotaxane 6a. Polymer **1** (27.0 mg, 0.11 mmol, 1.0 eq.) and fluorescent CD **7** (44.0 mg, 2.8×10^{-5} mol, 0.25 eq.) (synthesis in ESI †) were dissolved in 2 mL of a 0.05 M LiCl solution and the solution was heated to 40 °C. After 1 h, HP- β -CD (500 mg, 0.33 mmol, 3.0 eq.) was added and the solution was kept at 40 °C. After 6 h, a solution of α -CD (150 mg, 0.15 mmol, 1.3 eq. in 1 mL 0.05 M LiCl) was added and the mixture was heated to 70 °C for 16 h. To separate unthreaded CD from the polyrotaxane, the solution was purified *via* ultrafiltration using a 5 kDa polyethersulfone membrane against a 0.05 M LiCl solution and H_2O in sequence before freeze drying. A yellow, fluffy solid (62 mg) was recovered. ^1H -NMR: δ/ppm (D_2O) = 8.05–6.20 (bs, 0.67H, Fluo-CD), 5.14 (s, 0.76H, HP-CD), 5.08–4.97 (sh, 1.33H, HP-CD + Fluo-CD), 4.96 (s, 0.26H,

α -CD), 4.06–3.32 (m, 22H, H-1 + α -CD + HP-CD + Fluo-CD), 1.78–1.13 (sh, 12H, H-2/3/4/5), 1.09 (s, 4H, HP-CD).

2.3. TNS assay

The assay was performed in 50 mM PBS (8 g L $^{-1}$ NaCl, pH 7.35). Polyrotaxane **6** (29.0 mg) was dissolved in 11.2 mL PBS and incubated at 37 °C. In defined intervals over a 50 d period, 1 mL samples of the solution were removed and frozen. To purify the free HP- β -CD from the polyrotaxane, 500 μL of the samples were purified by ultrafiltration using Vivaspine 2, MWCO 3000 (Sartorius, Göttingen, Germany) devices. Free HP- β -CD was collected in the filtrate. The filtrates were freeze dried and redissolved in 200 μL water. These solutions (10 μL) were mixed with 15 μL water (to reach again a salt concentration of 50 mM), 225 μL PBS, and 50 μL of a 0.72 mM TNS solution in PBS. After 30 min incubation at 20 °C, the fluorescence intensities of the samples were measured at an excitation wavelength of 366 nm and a detection wavelength of 448 nm at 27 °C.

2.4. Filipin staining of NPC1 cells

NPC1-deficient cells (Coriell Institute) were seeded in 96 well tissue culture dishes at a density of 1600 cells per well in Eagle's minimum essential medium, supplemented with 10% fetal bovine serum and 1% penicillin/streptomycin. The cells were incubated for 24 h at 37 °C in 5% CO_2 before treatment with 6 or free HP- β -CD solution in triplicate. A 100 μL solution containing 0.24 mg of **6** to give a HP- β -CD equivalent concentration of 800 μM in the cell culture media was used per well as the highest concentration. HP- β -CD equivalent concentrations of 400, 200, 100, 25, 12.5 μM and untreated control were used to evaluate the dose–response relationship of **6** in NPC1-deficient cells. α -CD (0.4 μg) and 3.4 μg polydecamethylene phosphate **1** per well (amount of **1** present in 25 μM HP- β -CD equivalent of **6**) were additional controls. After 24 h, the cells were washed with PBS and fixed using 3.7% paraformaldehyde solution. Total unesterified cholesterol content within the cells was determined by staining with 50 $\mu\text{g mL}^{-1}$ filipin III in PBS for 1.5 h. Next, the cells were washed and the nuclei were stained with a solution of 16 μM Nuclear Red DCS1 (AAT Bioquest) in PBS. Cells were imaged using the $5\times$ objective on an Opera Phenix High-Content Imaging System (Perkin Elmer). Harmony Software (v4.1, Perkin Elmer) was used to quantify the data collected from one field per well while excluding border cells. Nuclei were identified in the Cy5.5 channel and unesterified cholesterol content was evaluated using the mean filipin intensity above the background in the DAPI channel. Mean filipin intensity in treated cells were compared to that of untreated cells and expressed as % filipin stain \pm SEM. One-way ANOVA analysis was performed in GraphPad Prism (v7.03, GraphPad Software). MTS assays were performed as per manufacture's protocol to evaluate the apparent toxicities of **6** at the concentrations used.

2.5. Cellular tracking of α -CD end-capped polyrotaxanes

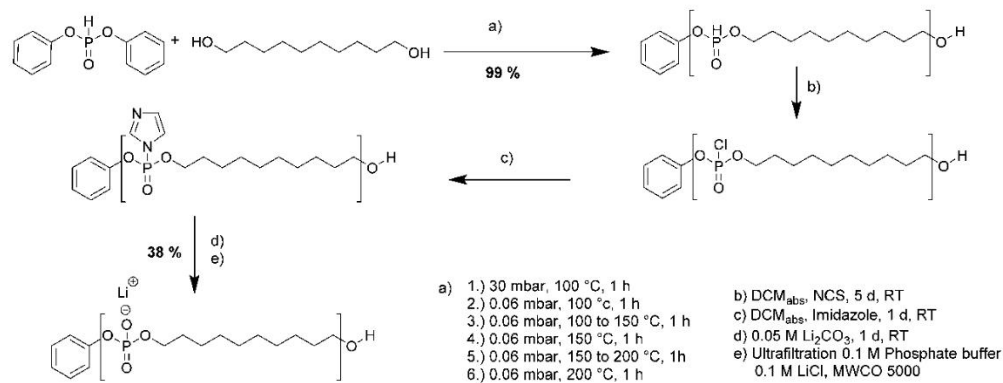
NPC1-deficient cells were treated with 25 μM CD equivalent FITC-tagged polyrotaxane **6a** in Opti-MEM media and incubated for either 4 h or 24 h at 37 °C, 5% CO_2 and 95% relative humidity.

After 24 h treatment, the polyrotaxane solution was removed and the cells washed with $1\times$ PBS to remove non-internalized polyrotaxane **6a** and incubated for another 24 h under the same conditions. For imaging, the nuclei were stained with Hoechst 33342 and the acidic endosomal and lysosomal compartments were stained with LysoTracker Red DND 99. Confocal images were acquired using a Nikon A1R multiphoton confocal microscope with a $60\times$ oil objective equipped with 405 nm, 488 nm and 561 nm

lasers for Hoechst 33342, FITC and LysoTracker Red DND 99, respectively.

2.6. FACS analysis

NPC1-deficient cells treated with $25\ \mu\text{M}$ CD equivalent FITC tagged PR **6a** in Opti-MEM media and incubated for 4 h or 24 h at $37\ ^\circ\text{C}$, 5% CO_2 and 95% relative humidity. After 24 h treatment, the PR solution was removed by aspiration and cells



Scheme 1 Synthesis of the guest polymer poly(decamethylene phosphate) **1**.

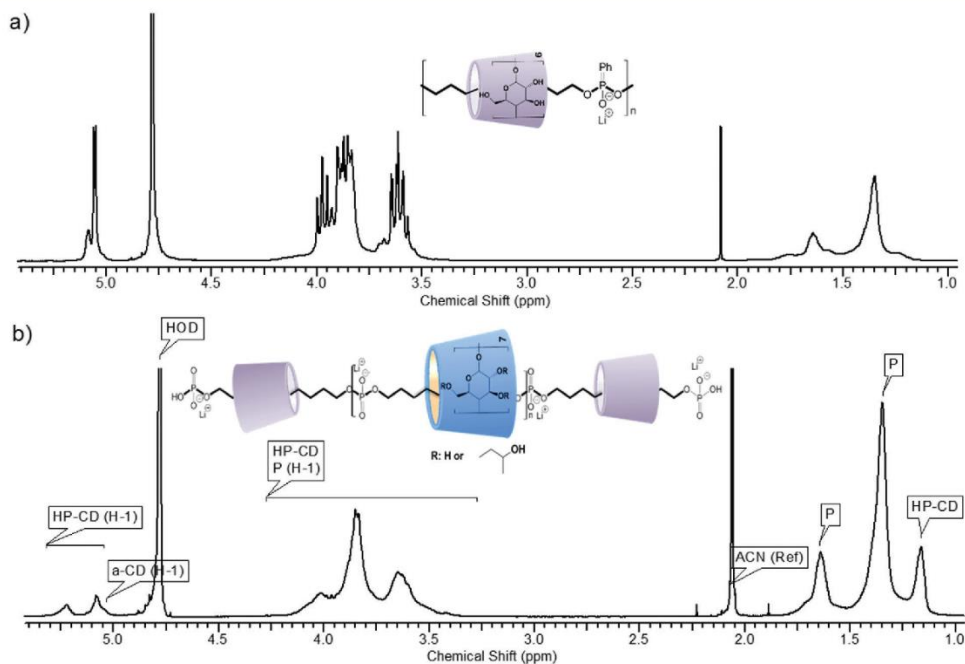


Fig. 1 ^1H NMR spectra of polyrotaxanes (a) **5** and (b) **6**.

were washed with $1 \times$ PBS to remove non-internalized PR **6a** and incubated for another 24 h under the same conditions. FACS analysis for cellular association was performed using a BD LSR Fortessa flow cytometer equipped with a 488 nm laser to quantify mean fluorescence of 5000 NPC1 cells ($n = 3$, one-way ANOVA, $***p < 0.0001$).

3. Results & discussion

3.1. Polymer synthesis

Poly(decamethylene phosphate) **1** was chosen as the guest polymer, because it is less toxic ($LC_{50} = 900 \mu\text{g mL}^{-1}$ for HEPG2 cells) than the previously used cationic polymers.⁵⁷ It was obtained through oxidation of poly(decamethylene phosphite) **2**. This was performed in three steps *via* the polymeric phosphoryl chloride **3** and polymeric phosphoryl imidazolidine **4** intermediates as shown in Scheme 1. This three step procedure was chosen to avoid the formation of pyrophosphates that are known to occur during the more direct one step oxidation with aqueous iodine.⁵⁸ Li^+ counterions appeared to be superior to Na^+ because of their positive influence on the aqueous solubility of **1**. Ultrafiltration processing of the material gave poly(decamethylenephosphate) **1** of an average molar mass of M_w 18 kDa polymer, as determined by SEC, indicating an average degree of polymerization of 76 (SEC diagram in ESI†). The solubility of the polymer in water is 110 mg mL^{-1} .

3.2. Polyrotaxane formation and stability

The spontaneous formation of polyrotaxane **5** was observable by $^1\text{H-NMR}$ spectroscopy during incubation of an aqueous solution of 8 mM **1** with 6 mM $\alpha\text{-CD}$ at 60°C (Fig. 1a). New signals at 5.06 ppm were indicative of threaded $\alpha\text{-CD}$ as observed for other ionic polymers.⁵⁹ From the integrals at 5.060 and 5.035 ppm , the occupancy y of the host $\alpha\text{-CD}$ by the polymer backbone was determined and plotted *vs.* time (Fig. 2). The very low complexation rate observed was attributed to the pronounced steric hindrance between the bulky solvated phosphate groups and

the rigid $\alpha\text{-CD}$ ring. The kinetics followed a stretched exponential time law (eqn (1)) as is typical for one-dimensional diffusion.^{60,61} The occupancy y approaches a limiting value of $y_\infty = 48.5\%$ for infinite complexation time t and a time constant τ of 2.9 d .

The equilibrium constant K was calculated from y_∞ according to eqn (2), with the total molar concentration of cyclodextrin $[\text{CD}]_0$, the molar ratio of total concentrations of guest repeats *vs.* host x , and the occupancy of cyclodextrin y defined as the molar ratio of occupied cyclodextrin *vs.* total cyclodextrin. The result, $K = 200 \text{ M}^{-1}$, was in reasonable agreement with the binding constants of other guest polymers with decamethylene binding sites.⁵⁹

$$y = y_\infty \left(1 - e^{-\sqrt{t/\tau}}\right) \quad (1)$$

$$K = \frac{y_\infty}{[\text{CD}]_0(x - y_\infty)(1 - y_\infty)} \quad (2)$$

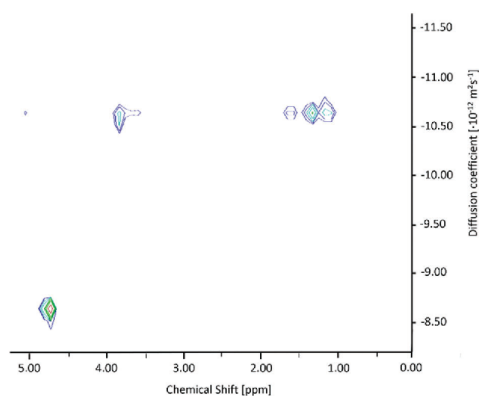


Fig. 3 DOSY NMR spectrum of polyrotaxane **6** in D_2O , signal at 4.8 ppm due to HOD.

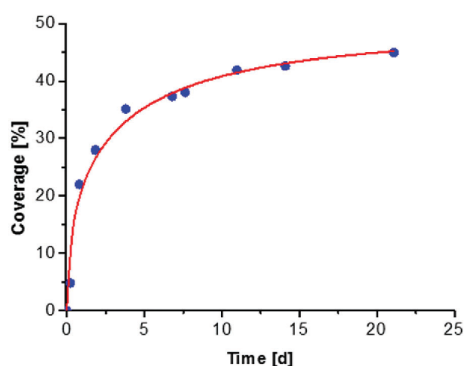


Fig. 2 Complexation kinetics of $\alpha\text{-CD}$ with guest polymer **1** at 60°C . The data were fitted with eqn (1), where $y_\infty = 48.5\%$ and $\tau = 2.9 \text{ d}$.

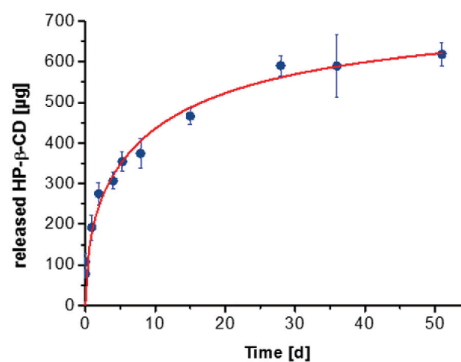


Fig. 4 Release of HP- β -CD from 2.59 mg polyrotaxane **6** in dissolved in 1 mL PBS over 50 d . The data were fitted with eqn (1), wherein $y_\infty = 697 \mu\text{g}$ and $\tau = 10.5 \text{ d}$.

Although steric hindrance between the bulky phosphate groups and the α -CD cavity impedes the rotaxation process (e.g., polyrotaxane formation takes more than a week), the resulting polyrotaxane is kinetically stable and survives extended dialysis. Conversely, HP- β -CD does not form stable complexes with the polymer since steric hindrance of the phosphate groups is negligible due to the larger internal diameter of β -CD cavity (0.65 nm) compared to the α -CD cavity (0.44 nm).⁶² Nevertheless, HP- β -CD polyrotaxanes are obtainable after subsequent incorporation of α -CD as a supramolecular stopper on the chain ends. Assembly of polyrotaxanes through subsequent threading of large and small rings was already shown to be practicable as reported previously.^{57,63} The HP- β -CD polyrotaxane **6** could be isolated in nearly quantitative yield after sequential threading of HP- β -CD and α -CD onto polyphosphate **1** and removal of excess α -CD and HP- β -CD by ultrafiltration. The solubility of **6** in water is 160 mg mL⁻¹. The composition of **6**, determined by the ¹H-NMR (Fig. 1b), indicated HP- β -CD and α -CD coverages of 18% and 3%, respectively. Consequently, 18% of repeating units of the polymer (14 in total) are complexed by HP- β -CD and the polyphosphate chain **1** is stoppered by around 2 to 3 α -CD rings situated at the chain ends. The proposed polyrotaxane structure was confirmed by the DOSY spectrum, shown in Fig. 3, where the signals of all constituents appear in one line at the same low diffusion coefficient $D = 1.55 \times 10^{-11} \text{ m}^2 \text{ s}^{-1}$.

Since polyrotaxane **6** was designed for slow release of HP- β -CD into aqueous media, its dissociation was investigated in a biological buffer. For this purpose, solutions of the polyrotaxane **6** were incubated in PBS at 37 °C for 50 d and the liberation of free HP- β -CD was followed by TNS assay. Tolidinylnaphthalene-2-sulfonate (TNS) is very useful for the detection of β -CD derivatives because it forms strongly fluorescing complexes whereas fluorescence of the free dye is negligible.^{64,65} Polyrotaxane **6** was removed by ultrafiltration from the analyte prior to this determination to avoid any

interference of the fluorescence probe with the polymer. As shown in Fig. 4, HP- β -CD was slowly released from the polyrotaxane over a 30 d period. Only 50% of the threaded rings were liberated because of the limited dilution of the system; release *in vivo* would be more complete due to the larger volume of dilution.

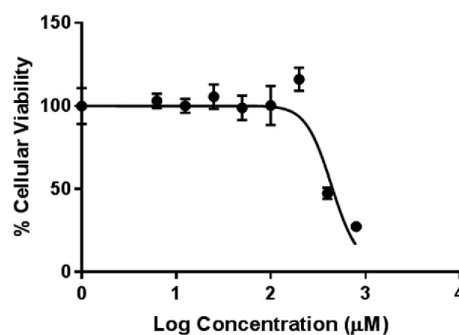


Fig. 6 Cytotoxicity of **6** evaluated *via* MTS assay after 24 h exposure to NPC1-deficient cells, concentration plotted in μM of HP- β -CD equivalents.

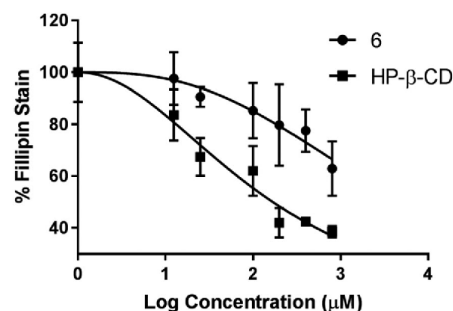


Fig. 7 Dose-response curve in NPC1 cells after a single 24 h treatment with **6** and HP- β -CD.

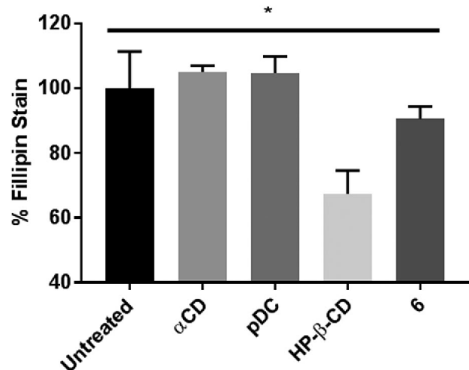


Fig. 5 Filipin staining of primary fibroblasts after treatment with α -CD, poly(decamethylenephosphate) **1**, HP- β -CD and **6** for 24 h (25 μM equivalent HP- β -CD dose, filipin was used at 50 $\mu\text{g mL}^{-1}$).

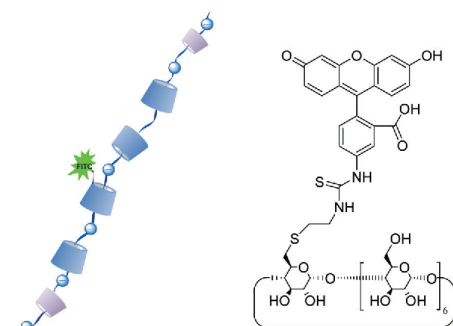


Fig. 8 Structures of FTIC-tagged polyrotaxane **6a** and the fluorescent CD-derivative **7**.

3.3. Biological evaluation of **6** in NPC1-deficient cells

The therapeutic potential of polyrotaxane **6** was evaluated in primary NPC1 fibroblasts. In brief, NPC1-deficient cells (1600 cells per well in 96-well plates) were incubated with **6** for 24 h at 37 °C with different equivalent concentrations of free HP- β -CD in the cell media. The cells were then rinsed, fixed, stained with filipin, and the relative degree of cholesterol accumulation in the treated cells compared with untreated controls. Filipin staining correlates with the relative cholesterol accumulation in cells. A significant decrease in filipin staining ($\sim 10\%$) was observed in treated NPC1 cells relative to untreated cells upon incubation for 24 h with a single dose of

polyrotaxane **6** at an equivalent HP- β -CD concentration of 25 μM (*i.e.*, polyrotaxane **6** concentration = 25 μM HP- β -CD-14 HP- β -CD/PR = 1.825 μM **6**). Additionally, treatment monomeric α -CD (at a concentration present in 1.825 μM **6**) did not result in any cholesterol efflux (Fig. 5 and Fig. S2, ESI[†]). This is most likely because the hydrophobic cavity of α -CD is too small of accommodate cholesterol molecule as reported by Davidson *et al.*⁶⁶ Increasing the concentration of **6** results in enhanced cholesterol efflux with about 20% and 40% decrease in filipin staining at 200 μM and 800 μM HP- β -CD equivalent concentrations, respectively. The observed smaller effect of polyrotaxane **6** compared to free HP- β -CD was attributed to the slow release of the

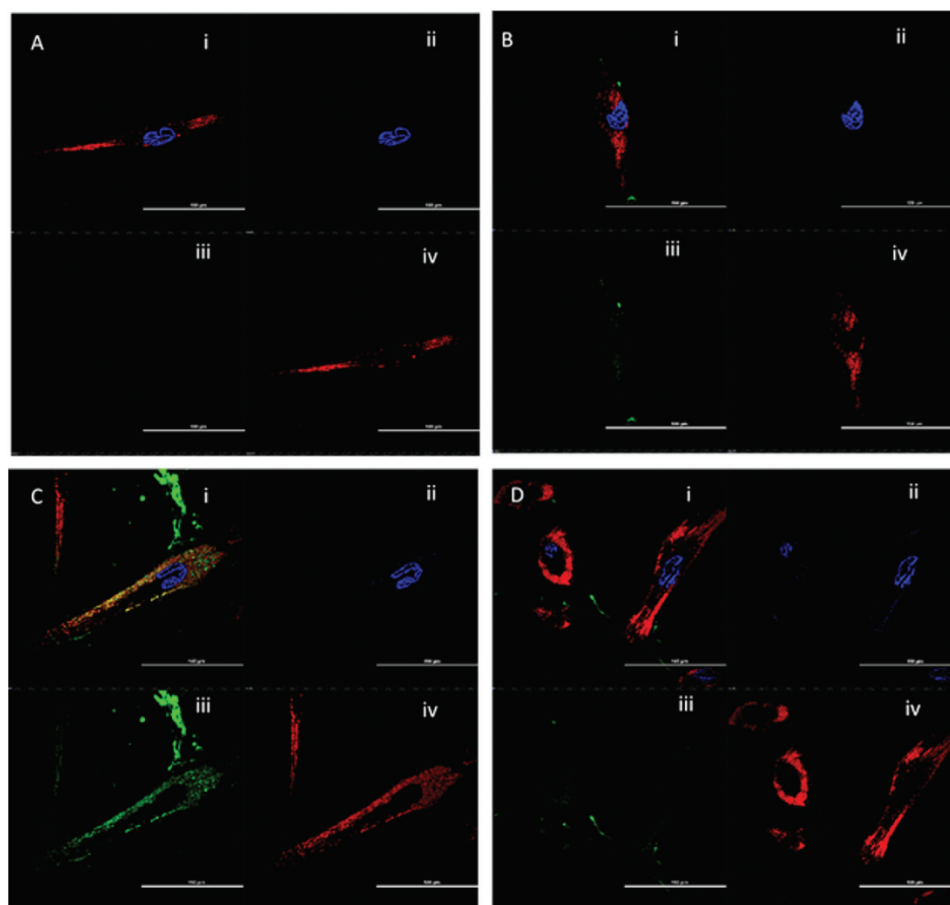


Fig. 9 NPC1-deficient cells treated with 25 μM CD-equivalent FITC tagged polyrotaxane **6a** in Opti-MEM media. (A) Untreated cells, (B) 4 h **6a** treatment (C) 24 h **6a** treatment, and (D) C + 24 h post-treatment. (i) All fluorescence channel; (ii) DAPI channel; (iii) fluorescein channel, and (iv) LysoTracker channel. Localization within acidic endosomes/lysosome (red, stained with LysoTracker) peaked at 24 h after addition of **6a**, after which the cells were washed to remove **6a** and incubated for another 24 h in complete MEM media. Confocal images acquired 24 h post treatment show a decrease in the FITC signal indicating either release of cyclodextrins into the cytoplasm where it is diluted below detectable levels, or fluorescein degradation within them. The scale bar = 100 μm .

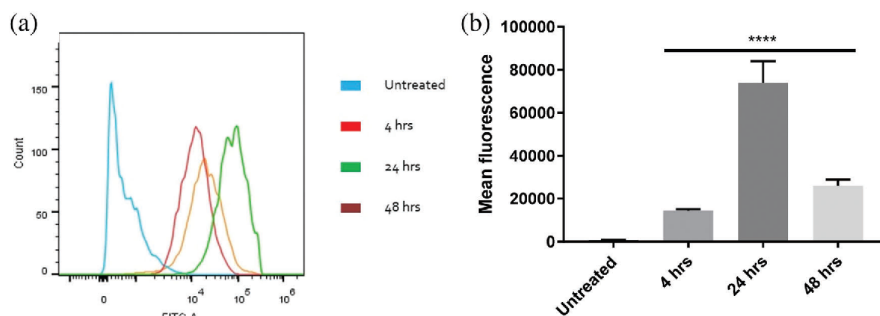


Fig. 10 (a) Histogram plot for FITC intensity distribution among NPC1-deficient cell population. (b) Cellular association of polyrotaxane **6a** with NPC1-deficient cells.

threaded rings leading to a much lower bioavailability of the polyrotaxane-borne HP- β -CD. A cytotoxicity profile evaluation of **6** using MTS assay (Fig. 6), however, reveals a sharp increase in toxicity of **6** above 200 μ M HP- β -CD equivalent dose. This acute toxicity of the polyrotaxane might be caused by a surfactant effect of the amphiphilic polyphosphate backbone. Nevertheless, its degradation products (phosphoric acid and 1,10-decanediol) only show low toxicities.

We infer from these findings that **6** is dethreaded after internalization by the cells to release the HP- β -CD payload to effectively mobilize the aberrantly stored cholesterol deposits in NPC1-deficient cells as previously reported by Collins *et al.*⁶⁷ Although monomeric dose of HP- β -CD performs better in cholesterol efflux from the cells after a single 24 hours treatment in comparison of **6** (Fig. 7), the potential of **6** as a long circulating and slow HP- β -CD releasing platform makes them an attractive candidate for NPC therapeutics.

3.4. Cellular tracking of α -CD end-capped polyrotaxanes

A FITC tagged polyrotaxane **6a** was prepared for cellular tracking studies by co-threading a small amount of fluorescein-labeled β -CD **7** (shown in Fig. 8 synthesis described in ESI†) with HP- β -CD and subsequently stoppered by α -CD.

NPC1-deficient cells begin to internalize polyrotaxane **6a** within 4 h, however, the polyrotaxane appears only within non-acidic vesicles (*i.e.*, compartments that are not stained by LysoTracker). These are most likely to be endosomes at an earlier stage of maturation.^{68,69} Extensive association of the polyrotaxane with the extracellular matrix of NPC1-deficient cells was also observed (Fig S3, ESI†). Significant cellular uptake and localization within the acidic late endosomal/lysosomal compartment was observed after 24 h of treatment (Fig. 9C).

Next, the non-internalized polyrotaxane was removed and cells were washed to prevent further uptake of **6a** before incubating for another 24 h to monitor the cellular fate of the already internalized polyrotaxane (Fig. 9D). The latter images show decreased fluorescein signal intensity indicating that the cyclodextrins escape the endosomal/lysosomal compartments within the cell leading to high dilution of the fluorophore.

3.5. FACS analysis of cellular association of α -CD end-capped polyrotaxane with NPC1-deficient cells

As suggested by our confocal data, NPC1-deficient cells show cellular association by 4 h. Mean fluorescence intensities peaked at 24 h after treatment. The cells were washed to remove non-internalized PR and prevent further uptake of PR before incubating for another 24 h to monitor the cellular fate of the already internalized PR. This is referred to as the 48 h time-point. The 48 h time point images show decreased mean FITC intensity, indicating that all cells internalize the PR. The data also suggest that the PR are capable of escaping from the endosomal/lysosomal compartments of the cell or are degraded within them (Fig. 10).

4. Conclusion

A new HP- β -CD polyrotaxane containing a decamethylenephosphate core has been synthesized and its cholesterol normalization capacity evaluated in NPC1-deficient cells. The degree of polymerization in preparation of the decamethylenephosphate polymeric precursor was determined to be 76. The degree of α -CD threading to produce **5** was estimated to be 48.5% after 2.9 d, whereas the HP- β -CD coverage was 18% and α -CD endcapping was approximately 3% in polyrotaxane **6**. Reduction in filipin staining, indicative of cholesterol depletion, was found to be approximately 20% at a polyrotaxane concentration of 0.3 g L^{-1} after 24 h incubation, similar in magnitude to the reductions observed by Mondjinou *et al.*⁷⁰ with mixed HP- β -CD:SBE- β -CD Pluronic polyrotaxanes that were used in 6 h exposures to NPC1 cells. Taken together, the findings suggest that polyrotaxane **6** may be a useful tool for the delivery of HP- β -CD as a therapeutic payload for normalizing cholesterol levels in Niemann-Pick Type C cells. The main advantages of our system is the simple release of HP- β -CD from the polymer by slippage⁷¹ and the expected slow renal clearance due to the high molecular weight of the polyrotaxane **6** of around 35 kDa. There is no need for any cleaving enzymes to release the drug in the cells.

Conflicts of interest

There are no conflicts to declare.

Acknowledgements

We thank Josef Zapp for assistance in NMR spectroscopy and Blandine Bossmann for GPC measurements. The support of NIH P30 CA023168 is also gratefully acknowledged.

References

- G. Wenz, *Angew. Chem., Int. Ed. Engl.*, 1994, **33**, 803–822.
- M. E. Brewster and T. Loftsson, *Adv. Drug Delivery Rev.*, 2007, **59**, 645–666.
- K. Cal and K. Centkowska, *Eur. J. Pharm. Biopharm.*, 2008, **68**, 467–478.
- T. Loftsson and D. Duchene, *Int. J. Pharm.*, 2007, **329**, 1–11.
- N. M. Davies, G. Wang and I. G. Tucker, *Int. J. Pharm.*, 1997, **156**, 201–209.
- S. Jambhekar, R. Casella and T. Maher, *Int. J. Pharm.*, 2004, **270**, 149–166.
- E. P. C. Kilsdonk, P. G. Yancey, G. W. Stoudt, F. W. Bangerter, W. J. Johnson, M. C. Phillips and G. H. Rothblat, *J. Biol. Chem.*, 1995, **270**, 17250–17256.
- R. Zidovetzki and I. Levitan, *Biochim. Biophys. Acta, Biomembr.*, 2007, **1768**, 1311–1324.
- R. O. Williams, V. Mahaguna and M. Sriwongjanya, *Eur. J. Pharm. Biopharm.*, 1998, **46**, 355–360.
- J. Nishijo, S. Moriyama and S. Shiota, *Chem. Pharm. Bull.*, 2003, **51**, 1253–1257.
- E. Ottinger, M. Kao, N. Carrillo-Carrasco, N. Yanjanin, R. Shankar, M. Janssen, M. Brewster, I. Scott, X. Xu, J. Craddock, P. Terse, S. Dehdashti, J. Marugan, W. Zheng, L. Portilla, A. Hubbs, W. Pavan, J. Heiss, C. H. Vite, S. Walkley, D. Ory, S. Silber, F. Porter, C. Austin and J. McKew, *Curr. Top. Med. Chem.*, 2014, **14**, 330–339.
- A. L. Yergey, P. S. Blank, S. M. Cologna, P. S. Backlund, D. Porter and A. J. Darling, *PLoS One*, 2017, **12**, e0175478.
- T. J. Maarup, A. H. Chen, F. D. Porter, N. Y. Farhat, D. S. Ory, R. Sidhu, X. Jiang and P. I. Dickson, *Mol. Genet. Metab.*, 2015, **116**, 75–79.
- M. T. Vanier, *Orphanet J. Rare Dis.*, 2010, **5**, 16.
- C. D. Davidson, N. F. Ali, M. C. Micsenyi, G. Stephney, S. Renault, K. Dobrenis, D. S. Ory, M. T. Vanier and S. U. Walkley, *PLoS One*, 2009, **4**, e6951.
- A. M. Lopez, S. J. Terpack, K. S. Posey, B. Liu, C. M. Ramirez and S. D. Turley, *Clin. Exp. Pharmacol. Physiol.*, 2014, **41**, 780–787.
- S. Gould and R. C. Scott, *Food Chem. Toxicol.*, 2005, **43**, 1451–1459.
- A. Muralidhar, I. A. Borbon, D. M. Esharif, W. Ke, R. Manacheril, M. Daines and R. P. Erickson, *Mol. Genet. Metab.*, 2011, **103**, 142–147.
- C. H. Vite, J. H. Bagel, G. P. Swain, M. Prociuk, T. U. Sikora, V. M. Stein, P. O'Donnell, T. Ruane, S. Ward, A. Crooks, S. Li, E. Mauldin, S. Stellar, M. De Meulder, M. L. Kao, D. S. Ory, C. Davidson, M. T. Vanier and S. U. Walkley, *Mol. Genet. Metab.*, 2015, **7**, 122.
- L. Markenstein, A. Appelt-Menzel, M. Metzger and G. Wenz, *Beilstein J. Org. Chem.*, 2014, **10**, 3087–3096.
- L. Purdie, C. Alexander, S. G. Spain and J. P. Magnusson, *Bioconjugate Chem.*, 2016, **27**, 1244–1252.
- N. Zander, W. Eichner, H. Conradt, F. Hackett, K. Langer, M. Orlando and R. Frank, *PCT Int. Appl.*, 2005, 230.
- R. Duncan, *Nat. Rev. Drug Discovery*, 2003, **2**, 347–360.
- T. M. Allen and P. R. Cullis, *Science*, 2004, **303**, 1818–1822.
- H. Bader, H. Ringsdorf and B. Schmidt, *Angew. Makromol. Chem.*, 1984, **123**, 457–485.
- K. Hoste, K. De Winne and E. Schacht, *Int. J. Pharm.*, 2004, **277**, 119–131.
- I. Bala and S. Haribaran, *Evolution*, 2004, **22**, 387–422.
- G. S. El-Feky, M. El-Rafie, M. El-Sheikh, M. E. El-Naggar and A. Hebeish, *J. Nanomed. Nanotechnol.*, 2015, **06**, 1–8.
- A. Tamura and N. Yui, *Chem. Commun.*, 2014, **50**, 13433–13446.
- I. Krauter, W. Herrmann and G. Wenz, *J. Inclusion Phenom. Mol. Recognit. Chem.*, 1996, **25**, 93–96.
- F. Huang and H. W. Gibson, *Prog. Polym. Sci.*, 2005, **30**, 982–1018.
- G. Tiwari, R. Tiwari and A. Rai, *J. Pharm. BioAllied Sci.*, 2010, **2**, 72.
- G. Wenz and B. Keller, *Am. Chem. Soc., Div. Polym. Chem.*, 1993, **34**, 62–64.
- A. Harada, J. Li and M. Kamachi, *Nature*, 1992, **356**, 325–327.
- M. Okada, Y. Kawaguchi, H. Okumura, M. Kamachi and A. Harada, *J. Polym. Sci., Part A: Polym. Chem.*, 2000, **38**, 4839–4849.
- Y. Liu, Y. W. Yang, Y. Chen and H. X. Zou, *Macromolecules*, 2005, **38**, 5838–5840.
- G. Wenz and B. Keller, *Angew. Chem., Int. Ed. Engl.*, 1992, **31**, 197–199.
- C. Meschke, H. J. Buschmann and E. Schollmeyer, *Polymer*, 1999, **40**, 945–949.
- H. Iguchi, S. Uchida, Y. Koyama and T. Takata, *ACS Macro Lett.*, 2013, **2**, 527–530.
- Y. A. Mondjinou, L. A. McCauliff, A. Kulkarni, L. Paul, S.-H. Hyun, Z. Zhang, Z. Wu, M. Wirth, J. Storch and D. H. Thompson, *Biomacromolecules*, 2013, **14**, 4189–4197.
- A. Tamura and N. Yui, *Sci. Rep.*, 2014, **4**, 4356.
- C. J. Collins, B. P. Loren, M. S. Alam, Y. Mondjinou, J. L. Skulsky, C. R. Chaplain, K. Haldar and D. H. Thompson, *Sci. Rep.*, 2017, **7**, 46737.
- A. Tamura and N. Yui, *J. Controlled Release*, 2018, **269**, 148–158.
- K. Knop, R. Hoogenboom, D. Fischer and U. S. Schubert, *Angew. Chem., Int. Ed.*, 2010, **49**, 6288–6308.
- G. Pasut and F. M. Veronese, *Prog. Polym. Sci.*, 2007, **32**, 933–961.
- T. Ooya, H. S. Choi, A. Yamashita, N. Yui, Y. Sugaya, A. Kano, A. Maruyama, H. Akita, R. Ito, K. Kogure and H. Harashima, *J. Am. Chem. Soc.*, 2006, **128**, 3852–3853.

- 47 C. O. Mellet, J. M. G. Fernández and J. M. Benito, *Chem. Soc. Rev.*, 2011, **40**, 1586–1608.
- 48 T. Albuzat, M. Keil, J. Ellis, C. Alexander and G. Wenz, *J. Mater. Chem.*, 2012, **22**, 8558–8565.
- 49 F. H. Westheimer, *Science*, 1987, **235**, 1173–1178.
- 50 C. Schultz, *Bioorg. Med. Chem.*, 2003, **11**, 885–898.
- 51 M. Richards, B. I. Dahiyat, D. M. Arm, P. R. Brown and K. W. Leong, *J. Biomed. Mater. Res.*, 1991, **25**, 1151–1167.
- 52 J. Baran and S. Penczek, *Macromolecules*, 1995, **28**, 5167–5176.
- 53 A. Tamura, M. Tokunaga, Y. Iwasaki and N. Yui, *Macromol. Chem. Phys.*, 2014, **215**, 648–653.
- 54 J. Pretula, K. Kaluzynski, R. Szymanski and S. Penczek, *Macromolecules*, 1997, **30**, 8172–8176.
- 55 A. Bogomilova, M. Höhn, M. Günther, A. Herrmann, K. Troev, E. Wagner and L. Schreiner, *Eur. J. Pharm. Sci.*, 2013, **50**, 410–419.
- 56 Z. Liu, L. Wang, C. Bao, X. Li, L. Cao, K. Dai and L. Zhu, *Biomacromolecules*, 2011, **12**, 2389–2395.
- 57 P. Dandekar, R. Jain, M. Keil, B. Loretz, M. Koch, G. Wenz and C.-M. Lehr, *J. Mater. Chem. B*, 2015, **3**, 2590–2598.
- 58 S. M. Gryaznov and R. L. Letsinger, *J. Am. Chem. Soc.*, 1991, **113**, 5876–5877.
- 59 W. Herrmann, B. Keller and G. Wenz, *Macromolecules*, 1997, **30**, 4966–4972.
- 60 G. Wenz, *Adv. Polym. Sci.*, 2009, **222**, 1–54.
- 61 G. Wenz, C. Gruber, B. Keller, C. Schilli, T. Albuzat and A. Müller, *Macromolecules*, 2006, **39**, 8021–8026.
- 62 A. Müller and G. Wenz, *Chem. – Eur. J.*, 2007, **13**, 2218–2223.
- 63 G. Wenz, I. Kräuter, E. Sackmann, G. Wenz and I. Kra, *J. Polym. Sci., Part A: Polym. Chem.*, 2009, **47**, 6223–6230.
- 64 H. Kondo, H. Nakatani and K. Hiromi, *J. Biochem.*, 1976, **79**, 393–405.
- 65 D. J. Jobe, R. E. Verrall, R. Palepu and V. Reinsborough, *J. Phys. Chem.*, 1988, **92**, 3582–3586.
- 66 C. D. Davidson, Y. I. Fishman, I. Puskás, J. Szemán, T. Sohajda, L. A. McCauliff, J. Sikora, J. Storch, M. T. Vanier, L. Szente, S. U. Walkley and K. Dobrenis, *Ann. Clin. Transl. Neurol.*, 2016, **3**, 366–380.
- 67 C. J. Collins, L. A. McCauliff, S.-H. Hyun, Z. Zhang, L. N. Paul, A. Kulkarni, K. Zick, M. Wirth, J. Storch and D. H. Thompson, *Biochemistry*, 2013, **52**, 3242–3253.
- 68 B. R. Liu, S. Y. Lo, C. C. Liu, C. L. Chyan, Y. W. Huang, R. S. Aronstam and H. J. Lee, *PLoS One*, 2013, **8**, e67100.
- 69 N. B. Yapici, Y. Bi, P. Li, X. Chen, X. Yan, S. R. Mandalapu, M. Faucett, S. Jockusch, J. Ju, K. M. Gibson, W. J. Pavan and L. Bi, *Sci. Rep.*, 2015, **5**, 1–8.
- 70 Y. A. Mondjinou, S.-H. H. Hyun, M. Xiong, C. J. Collins, P. L. Thong and D. H. Thompson, *ACS Appl. Mater. Interfaces*, 2015, **7**, 23831–23836.
- 71 S. a. Nepogodiev and J. F. Stoddart, *J. Am. Chem. Soc.*, 1998, **98**, 1959–1976.